Performance Based Seismic Assessment of Masonry Infilled Steel Frame Structures

A DISSERTATION SUBMITTED TO
THE DEPARMENT OF CIVIL, ENVIRONMENTAL & GEOMATIC ENGINEERING
OF UNIVERSITY COLLEGE LONDON
IN PARTIAL FULFILLMENT OF THE REQUIREMENTS
FOR THE DEGREE OF DOCTOR OF PHILOSOPHY

Arash Nassirpour

May 2018

Abstract

Steel framed structures constitute a considerable proportion of residential and commercial structures in earthquake prone regions. In such structures, typically, masonry infills are implemented as walls and partitions. However, in common practice, the influence of the infill panels on the performance and resistance of the building is mostly ignored, not just at the design stage, but also during assessment. Despite the possible strength enhancement that infill panels can bring to the structure for modest earthquakes, they may put the building at high risk of heavy damage if their impact is overlooked, and the interaction not properly designed, as seen in the 2003 Bam earthquake and many other destructive seismic events.

Following the performance-based seismic assessment methodology, the dissertation focuses on evaluating the seismic performance of existing masonry infilled steel frames. The seismic response of several building typologies, designed according to common practice, is assessed through nonlinear dynamic methods. Detailed three-dimensional numerical models of selected index buildings are developed, capable of simulating the impact of masonry infill walls along other critical elements such as the beam-column connections, according to available empirical and experimental data. In order to measure the seismic vulnerability, along with possible losses and life cycle costs, analytical fragility functions are derived for the structures, while considering the hazard characteristics of the location under study. The derived fragility functions will help enrich the limited library of existing function dedicated to both bare and infilled steel structures. The outcome is of great importance for insurance valuation, as well as managing disasters and performing strengthening if necessary.

Impact Statement

Earthquake engineering, as a multi-disciplinary branch of engineering, beside its direct impact on the design and resistance of physical structures, it has a great influence on the social, economic, political, and cultural environment. This study investigates different aspects of earthquake engineering, which can be directly and in-directly relate to the mentioned fields.

This study tends to advocate comprehensive and realistic measures for reducing the harmful effects of earthquakes. The finding of this study can assist governments, agencies, owners, investors and insurers in gaining a better understanding of the actual behavior of the studied structures under real earthquake excitation and its potential consequences on the society. Furthermore, the outcomes can be utilised to have a more realistic prediction of the potential structural and non-structural damage expected under various scenarios of earthquake at any location of the world. Accordingly, strategies can be introduced for managing disasters and planning the relief operations.

University College London
Department of Civil, Environmental & Geomatic Engineering

THESIS DECLARATION FORM

I confirm that the work presented in this thesis is my own. Where information has been derived from other sources, I confirm that this has been indicated in the thesis.

Signature:

Name: **Arash Nassirpour**

Date: **8 May 2018**

Acknowledgement

I owe a great many thanks to a great many people who helped and supported me during this research project.

I would like to express my deep and sincere gratitude to my research advisor, Prof Dina D'Ayala, for her amazing guidance and patience throughout this journey. Without her motivation and overwhelming support, the completion of this project would have been a distant reality. It was a great privilege and honour to work and study under your supervision. Thanks for believing in me.

My special thanks go to a good friend and a great man, Dr Carmine Galasso. Thanks for your encouragement and continues support. SCOSSO was an amazing experience, thank you for letting me to be a part of it. Your guidance throughout my research as well as my career have been invaluable. I owe you big time.

I express my sincere thanks to Prof Tiziana Rossetto for her continued support throughout my time at UCL. It all started from your reference letter. I'm sure EPICentre will continue its success under your leadership.

Special thanks to Dr Khaleghian and all the engineers who supported this research with their expertise and resources.

I am grateful to all of those with whom I have had the pleasure to work during this and other projects. I would like to say thanks to all my friends and colleagues at CEGE, particularly members of room 221 and GM16, Alexandra, Dr Sascha, Dr Rui, Dr Aris, Dr Pierre, Dr Athanasios, Dr Carina, Dr Viviana, Dr Natalie, Atiyeh, Palak, Omar, Chen, Biao, Ivy, David, Rohit, Oriana, Silvia, Nuria, Champ, Alessandra, Martha, Leonel, Giulia, Victor, Loan and Dr Pepper. You guys rock and I'm so sorry for all the nonsense I bothered you with during lunch times. I wish you all happiness and success. Valentina, I was just forgetting about you! Thanks for all the good times and world class gossips. I wish all your dreams come true ASAP.

To Amirhossein (SAM) and Stelios, who always helped, motivated and supported me, no matter what. I'm so lucky to have you guys as friends.

To the Iranian gang, Mehrayin, Dr Hossein, Dr Ramtin, Dr Amin and Omid, thanks for making this an enjoyable journey. I don't think I will ever forget the adventures we had together in America.

To Dr Shahryar, Babak and Hossein (the very tall one), who are amazing friends. To Zahra, your energy, passion and the way you see life has always inspired me. Keep being amazing. To Banafshe, the little explorer, I learnt a lot from you and thanks for your unstoppable motivation.

Nobody has been more important to me in the pursuit of this project than my family. I would like to thank my mother and father, for their unconditional love and guidance in whatever I pursue. I continue to feel grateful to have them in my life. Special thanks to my Aunt, who always supported me spiritually. Most importantly, I wish to thank my sister and brother-in-law, whom advice and love have helped more than they will ever know. You have always been great friends and housemates. Thank you.

Arash Nassirpour
University College London
May 2018

Table of Contents

List of Figures

List of Tables

List of Symbols

A_{strut}	Total Area of Diagonal Struts
DM	Damage Measure
d_m	Diagonal Length of Equivalent Strut
DR	Damage Ratio
DV	Decision Variables
EDP	Engineering Demand Parameter
E_f	Elastic Modulus of Frame (Column)
E_{inf}	Elastic Modulus of Masonry Infill
E_{strut}	Strain Energy from Compression in Equivalent Diagonal Strut
f_1	Fundamental Frequency of Vibration
F_{cr}	Maximum Strength at Beginning of Crushing
f_u	Tensile Strength
f_y	Yield Stress
G	Shear Modulus
H	Structural Height
h_{col}	Frame Column Height
h_{frame}	Frame Member Height
h_{inf}	Masonry Infill Height
I_{col}	Column's Second Moment of Inertia
IM	Intensity Measure
K_0	Initial Stiffness
l	Length of Beams Measured on Centre of Column (Beam Span)
l_i	Masonry Infill Length
m	Mass
m^*	Equivalent Mass
MDR	Mean Damage Ratio
M_w	Moment Magnitude
PGA	Peak Ground Acceleration
R	Reduction Factor
S	Soil Factor
S_a	Spectral Acceleration
S_d	Spectral Displacement
T_1	Fundamental Period of Vibration
t_{inf}	Masonry Infill Thickness
V_b	Base Shear
w	Effective Width of the Diagonal Strut
β	Dispersion
γ	Specific Weight

Γ	Transformation Factor
θ	Angle of Frame's Diagonal in Relation to Horizon
θ	Relative Rotation (M_{rad})
λ	Ratio of Masonry Infill Stiffness to the Stiffness of Surrounding Frame
λ	Mean Annual Probability of Exceedance
μ	Ductility Factor
μ	Mean
ν	Poisson Ratio
φ	Mode Shape
$\Phi()$	Cumulative Distribution Function

Chapter 1 Introduction

1.1. Problem Description

Steel frames with unreinforced masonry infill walls constitute a considerable proportion of residential and commercial structures in earthquake prone regions such as Middle East and New Zealand (JICA, 2000; Uma & Bradley, 2010) (Figure 1.1). Factors such as ease of construction, cost-performance efficiency, isolation features, architectural attractiveness and high strength-to-weight ratio of the steel frame have led to widespread use of masonry infill panels as interior and exterior walls.

Figure 1.1 - Samples of masonry infilled steel frame projects under construction in Iran

In common seismic design practice, the influence of the infill panels on the performance and capacity of the building is mostly ignored by the designers. Identified as non-structural elements, their contribution is simply considered as permanent loading on the supporting beams. However, when subjected to seismic excitation, unreinforced masonry infills tend to interact with their surrounding frame as some sort of composite material. As the earthquake shaking increases, the infill panels tend to partially separate from the frame, while maintaining their influence on the structural system. This phenomenon clearly alters the behaviour of the structure as intended by the designer. As structural elements, infill walls impact the dynamic response of the structure by shifting the natural frequency and altering the stiffness, damping

and overall structural strength, which in return may improve the lateral capacity of the system (El-Dakhakhni et al., 2004; Moghaddam & Dowling, 1987).

Despite possible performance enhancement for low magnitude earthquakes, infill panels may put the structure at high risk of heavy damage if their impact is overlooked. For instance, ignoring the stiffness increase is not always conservative as higher seismic acceleration is attracted by stiffer buildings, which may overload certain structural elements. On the other hand, infill walls are made of brittle materials that typically loose capacity for modest deformation. The combined effect of high stiffness and brittleness has a negative implication on the seismic performance of the bounding frames. In cases where the infill panel is overstressed and fails partially or entirely, the forces previously attracted and carried by the stiff infill panels will suddenly be transferred to the surrounding frame, resulting in pre-mature failure of the frame elements due to large shear loads (Ellul & D'Ayala, 2012). Additionally, any alteration in the stiffness distribution, due to the positioning of the wall, may alter the structure's fundamental period of vibration and in cases increase the chance of torsional effects. Therefore, simply considering the structure as a bare frame and neglecting the participation of infill walls throughout design and assessment stages may lead to unpredicted vulnerability and is hazardous (Asteris et al., 2011).

The frames, surrounding the infill panels, are mainly built with either reinforced concrete (RC) or structural steel members. A good number of studies have focused on the performance of infilled RC frames under gravity and lateral loading, while cases looking at infilled steel frame are relatively limited (Tasnimi & Mohebkhah, 2011). Typically, when subjected to earthquake loading, steel frames are considered as robust and safer structures in contrast to reinforced concrete frames, mainly due to their higher ductility and lower strength-to-weight ratio. However, evidence of recent earthquakes has shown poor structural performance in steel frames with masonry infills. Cases of moderate to heavy damage and collapse have been reported in surveys conducted after 1990 Manjil-Rudbar (M_w 7.4), 2003 Bam (M_w 6.6), 2012 Ahar-Varzaghan (M_w 6.4) and the recent 2017 Iran-Iraq (Kermanshah) (M_w 7.3) earthquakes (Mahen & Grove, 1990; Manafpour, 2003; Miyajima et al., 2012; Yekrangnia et al., 2017). Investigating the reasons of observed structural damage and collapse, it is evident that the masonry infill panels and the detailing of the frame connections were the main triggering elements, particularly in cases leading to soft-storey failure. Figure 1.2 to Figure 1.5, present examples of damage observed in steel framed structures with masonry infill panels.

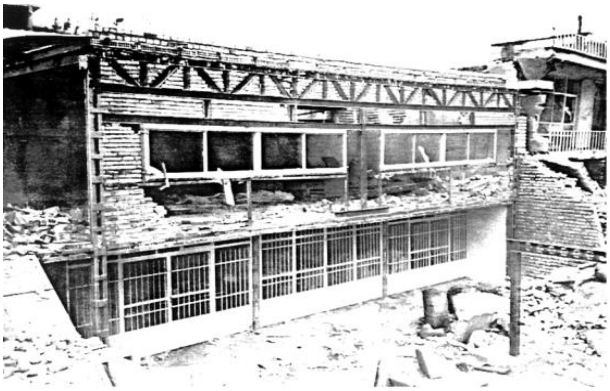

Figure 1.2 – Case of heavy damage due to failure of infill panels in the steel frame, observed during 1990 Manjil earthquake (Mahen & Grove, 1990)

Figure 1.3 - Cases of heavy damage and collapse due to connection and masonry infill wall failure, observed during 2003 Bam earthquake (Manafpour, 2003)

Figure 1.4 – Soft storey failure of masonry infilled steel frame, observed during 2003 Bam earthquake (Manafpour, 2003)

Figure 1.5 – Collapsed steel building in Sar-pole-zahab, observed during 2017 Iran-Iraq earthquake

The reluctance in considering the effect of masonry infill can be blamed on two key issues. First is the inadequate knowledge on the resultant composite behaviour of the frame and the infill panels. This is mainly due to the inherent uncertainty associated with the numerous parameters that the behaviour of infills depends on, such as the materials' mechanical property and the construction detailing. As seen from illustrations in Figure 1.2 to Figure 1.5 these structures undergo a large amount of non-linear deformation, in part owing to material non-linearity (e.g. cracking and crushing of the masonry, yielding of steel frame) and in part owing to geometric non-linearity (e.g. P-Δ effect). Therefore, to capture the extent of the interaction between frame and infill and quantify realistically their response to seismic shaking, masonry infilled steel frame structures cannot be simply modelled as linear elastic systems. Furthermore, the cyclic degradation of stiffness and strength should be considered, particularly in low- to mid-rise structures (i.e. short period structures), in which the hysteresis loops and energy dissipation capacity have a strong influence on the structural response. The second issue is the lack of practical method to predict the stiffness, strength and potential failure mechanism of the entire system for design and analysis purposes. Neglecting the influence of masonry infills in the current design practice can lead to uneconomical design of the frame, since the lateral stiffness and strength demand of the system can be largely reduced (El-Dakhakhni et al., 2003). On the other hand, throughout the performance assessment of existing infilled frames, simply considering the buildings as bare frames will lead to imprecise evaluation of the buildings' response to various levels of seismic excitation.

The substantial socio-economic consequences of recent earthquakes highlight the need for proper seismic risk assessment as a basis for efficient decision making on mitigation actions and disaster planning. Furthermore, the performance of structures designed following the code provisions cannot be explicitly quantified in the design process during major earthquakes, but rather assumed to be sufficient as the standards specified by the code are met. To this end, in recent years, the field of structural engineering has moved from traditional Load and Resistance Factor Design (LRFD), toward implementation of probabilistic methods, introduced as part of Performance-Based Earthquake Engineering (PBEE) framework (FEMA-P-58, 2012). PBEE aims to advance the seismic risk decision-making by means of scientific assessment and design methods, which express the expected results in metrics that can be understood by the stakeholders (Krawinkler & Miranda, 2004).

As an essential component of PBEE approach, Performance-Based Seismic Assessment (PBSA) anticipates the behaviour of the structure in such details that seismic risk can be evaluated and if required strengthening measures be recommended. For this matter, Pacific Earthquake Engineering Research Centre (PEER) developed a framework for PBEE, which considers uncertainties in the seismic hazard and structural response, and enables the

quantification of the seismic performance of new and existing buildings. In simple terms, PBSA is articulated in four stages, which follow a logical progression of steps to transfer information from one process to another that can be studied and resolved in a rigorous and consistent manner (Fajfar & Krawinkler, 2004). The output of each stage is obtained as probability of exceedance of its variable conditioned on the probability of exceedance of the variable of the previous stage. The initial step describes the prominent features of the ground motion hazard of the region under study in probilistic terms. The outcome is defined in terms of probable ground motion Intensity Measure (IM) given a return period (e.g. peak ground acceleration, spectral acceleration). In the next step, the structural behaviour is measured in response to the applied ground motion by conducting numerical analysis of the buildings and recording the Engineering Demand Parameters (EDP), expressed as their probability of occurrence given an assigned IM (e.g. displacement, drift, inter-storey drift). The obtained EDP values are then related to different Damage Measures (DM), which portray the physical conditions of the structure and its components subjected to the imposed demands (e.g. light, moderate or severe damage). Typically, reference is made to discrete damage states or thresholds, with a given probability of occurrence conditioned to the selected EDP value. Finally, the process ends by estimating the Decision Variables (DV), which translate the damage into economic and social metrics that can be understood by stakeholders for decision marking (e.g. monetary losses such as repair cost and casualty rate), also regarded as socio-economic vulnerability. These also are expressed as probability of exceeding a given loss, conditioned to the structure being in a given damage state. This probabilistic framework underlying the methodology allows to explicitly propagate the uncertainties throughout the process, both aleatory (due to inherent randomness) and epistemic (due to limited knowledge). The probabilistic expressions of the PBEE methodology components (i.e. IM, EDP, DM, and DV) can be integrated by the total probability theorem, expressed as the mean annual frequency of exceedance of a DV (Eq. 1.1) (Deierlein et al., 2003):

$$\lambda(DV) = \iiint G(DV|DM) \mid dG(DM|EDP) \mid dG(EDP|IM) \mid d\lambda(IM) \qquad (1.1)$$

in which $\lambda(IM)$ represents the mean annual frequencies of exceedance for a specific intensity measure. The intermediate terms $G(A|B)$ are complementary cumulative distribution functions (CCDF) for the framework components EDP, DM, and DV. $\lambda(DV)$ is the probabilistic description of the performance metrics, indicating the mean annual frequency (Y) that the direct economic loss will exceed X percent of the structure's replacement cost ($Y = \lambda(Loss > X\%\, replacement\ cost)$).

Both demand parameters (EDP) and damage measures (DM) are highly sensitive to the structure's characteristics and the implementation of the analysis methods, particularly in cases where the building responds in a highly non-linear manner with potentially mixed-ductility responses (D'Ayala et al., 2015). Hence, considering the complexity of the masonry infilled steel frame buildings, treating them as simple bare frame structures under seismic excitation will lead to unrealistic predictions of the actual structural response and introduces numerous uncertainties to the components of PBSA.

A widely practical approach to evaluate the performance of buildings subjected to seismic loading is through fragility functions for predefined damage limit states (i.e. $G(EDP|IM)$) (Shinozuka et al., 2000). As an important component of PBSA, fragility functions provide a probabilistic representation of the building's damage potential due to seismic hazard of varying intensities and can be translated into vulnerability function to measure the losses. As each variable obtained through PBSA influences the outcome of the next stages, the authenticity of obtained structural response and consequently the fragility functions are crucial in evaluating the vulnerability of the structure. Therefore, assessing the performance of a masonry infilled steel frame through simplified models, while neglect the impact of the infill panels will lead to unrealistic estimation of losses and impractical disaster planning. So far, only a limited number of studies have investigated the fragility and vulnerability of masonry infilled steel frames, despite the considerable presence of such structures in earthquake-prone regions worldwide. However, the existing research have mainly focused on simplified analysis methods and basic two-dimensional models of individual index buildings intended to represent an entire population (HAZUS, 2003; Kiani et al., 2016).

The overall aim of this research project is to characterise the vulnerability of masonry infilled steel frame structures through performance based seismic assessment approach. The project tends to compare the performance and expected losses of real case bare and infilled steel frames under different earthquake scenarios. Therefore, a population of buildings are selected and modelled following the data obtained on exposure, the prevalent material properties, design code and construction practice employed in the studied region. The structural seismic response obtained through advanced analytical methods will be utilised to derive analytical fragility functions for bare and infilled steel frames. The derived functions cover a vast collection of low- to mid-rise buildings with distinctive characteristics. The obtained fragility functions give the opportunity of evaluating the vulnerability at large scales, rather than concentrating on a particular case with unique characteristics. Moreover, the fragility functions are employed to investigate the influence of infill panels on the life cycle cost of a real structure with various levels of construction quality.

Advances in computational power and the development of models that can more accurately reproduce the behaviour of structural components have made such assessments possible. The derived fragility and vulnerability functions can be used to estimate the losses associated with the structural performance and can be implemented in tools such as PACT (2012), SP3 (2017) and OpenQuake (2017).

1.2. Thesis Structure

This thesis seeks to evaluate the vulnerability of infilled steel framed structures through performance based assessment. Chapter 1 discusses the backgrounds and motivations for this research project, as well as the overall organisation of the thesis. This dissertation is organised into eight additional chapters as follows:

Chapter 2 reviews the research dedicated to performance assessment of bare and infilled steel framed structures through fragility and vulnerability functions. This allows identifying the existing shortcomings and possible solutions in the assessment approach of the considered structures. Furthermore, various methods proposed for simulating the behaviour of infill panels are discussed, while highlighting their strengths and weaknesses. Hence, the best modelling approach can be implemented for simulating the infill behaviour under seismic loading. Understanding the limitations and their reasoning, conclusions are drawn in order to define and support the research scope.

Chapter 3 outlines the main aims and objectives of this research study, by highlighting the existing issues and inadequacies discussed in the literature review. A framework is proposed as the methodology to address the defined objectives. The methodology defines steps for implementing simplified and advanced vulnerability assessment methods to a population of buildings with various characteristics, following the PBEE approaches. Different stages of the methodology are discussed in the coming chapters by focusing on specific case studies and index buildings.

Chapter 4 introduces a highly seismic region as the case study and accordingly a number of index buildings are defined based on the most common structural characteristics observed. A number of index buildings will be based on existing structures, while others need to be designed. Therefore, a section is dedicated to the structural design process and explaining the assumptions following the relevant provisions of the region under study.

Chapter 5 discusses various aspects of the numerical modelling and analysis methods to estimate the seismic response of the index buildings. The methods utilised for simulating different elements of the buildings, such as the masonry infill panel and beam-column connections, are explain thoroughly as well as the calibration process of the analytical models

with experimental outcomes. Furthermore, the impact of different structural elements and arrangements on the global behaviour of the system are investigated to make sure the models are as realistic as possible.

Chapter 6 investigates the differences of simplified and advanced methods of seismic performance evaluation by focusing on a real case building. The structural response and fragility functions of bare and infilled steel frame are obtained through each of the applied methods to understand the shortcomings and assess the accuracy and feasibility of each method. The chapter discusses various aspects such as the ground motion selection, definition of damage states and thresholds, as well as the fragility curve fitting techniques. The selected procedure has been implemented to evaluate the seismic performance of the index buildings and derive the analytical fragility functions. The outcomes give the opportunity to estimate the expected damage and losses, which play a vital role in mitigation strategies and both pre- and post- disaster decision making.

Chapter 7 presents the implementation of PBSA stages to assess the vulnerability of a real case infilled steel frame building, while considering variations in its construction quality. The assessment is conducted based on the latest probabilistic seismic hazard of the region and possible exposure scenarios, rather than focusing on a single unique case. The obtained vulnerabilities are compared to the one of an identical bare frame. Moreover, to have a better perspective of the infilled and bare frame performance, the life cycle cost of the studied buildings is evaluated and compared. The results indicate a substantial difference in terms of structural seismic performance and subsequently the economic losses.

Chapter 8 presents the summary and major conclusions of this work. It describes the limitations of the present study and provides recommendations for future research directions.

Chapter 2 Literature Review

2.1. Introduction

This chapter presents an overview of studies conducted on fragility assessment and seismic performance of bare and infilled steel framed structures through empirical and analytical approaches. Initially, the concepts behind seismic fragility functions and its derivation methods are discussed. Subsequently, the fragility functions generated for steel structures with various characteristics are collected, while identifying their limitation and shortcomings.

Additionally, a comprehensive discussion is provided on the empirical and analytical studies conducted to understand the dynamic response of framed structures with infill panels during the last half a century. The proposed numerical simulation techniques, looking at either local or global behaviour of the infilled frames are reviewed, while recognising their advantages and necessities. The focus is mainly kept on steel infilled frames, although the studies conducted on reinforced concrete infilled frames are also reflected on, whenever deemed relevant.

For ease of reading and reference, any additional studies, relevant to other sections of this research are presented along its associated discussion, in the following chapters.

2.2. Structural Seismic Fragility & Vulnerability Assessment

The performance of a building, subjected to seismic excitation depends on many factors, including the structure's configuration and proportions, its dynamic aspects, the hysteretic characteristics of the elements and joints, the type of non-structural components, the quality of the materials and workmanship, adequacy of maintenance, the site conditions, and the intensity and dynamic features of the earthquake motion experienced. Therefore, predicting the seismic response of a structure is generally a complex and timely procedure. In addition, due to the inherent lack of knowledge in the precise definition of the structure's characteristics and the existing variability in the nature of the future ground shakings, estimation of seismic performance involves significant uncertainty. The uncertainties associated with a random factor, such as the characteristics of the earthquake are acknowledged as aleatory

uncertainties. On the contrary, the uncertainty sources related to our incomplete knowledge are known as epistemic and can be potentially reduced. For instance, in case of epistemic uncertainties, the structural properties may differ from those assumed during the design stage or may alter significantly during an earthquake event (e.g. sudden fracture of joints). These stated uncertainties may be reduced by conducting further experimental studies or using more sophisticated numerical models and methods of analysis. Consequently, to have the most realistic predictions of structural response, both the aleatory and epistemic uncertainties should be accounted for in the seismic performance evaluation (Fajfar & Krawinkler, 2004; Peruš et al., 2008).

Fragility and vulnerability functions are practical tools for evaluating the seismic performance and probability of structural damage and losses under distinct levels of seismic loading. These functions constitute as key elements for seismic risk assessment and are able to reflect the stated uncertainties to certain extent. In case of seismic excitation, given the earthquake's intensity measure (IM), the fragility functions evaluate the probability that the resultant seismic demand exerted on the structure, exceeds the capacity of the building (Porter, 2017).

$$Fragility = P[Demand > Capacity|IM] \tag{2.1}$$

On the other hand, vulnerability functions, often referred to as damage or loss functions, measure the probability of social or economic losses by relating the level of ground shaking with the damage ratios, which correlate the cost of repair to the cost of demolition and replacement of the structures (Porter et al., 2012). The main aim of a loss function is to estimate the seismic hazard at all sites of interest and to convolve this hazard with the fragility functions of the exposed building stock such that the damage distribution of the building stock and losses can be predicted (Calvi & Pinho, 2006). Hence, fragility functions play a vital role in evaluating the seismic vulnerability, not only because of their obvious physical consequences, but because it is the potential aspect for which the engineering research can intervene, improve and even control seismic behaviour of the existing buildings, reducing the level of vulnerability and consequently the level of physical damage, life loss and economical loss. Development of vulnerability studies, particularly at large scales such as urban centres, can lead to recognition of building stock deficiencies and reduction of seismic risk.

The following section discusses the fragility functions derived for steel structures through different methods. A thorough discussion on vulnerability assessment can be found in Chapter 7 of this study.

2.3. Fragility Functions Derivation Methods

The common methods followed to develop fragility functions are mainly classified as empirical, analytical, judgmental-based (expert opinion) or as a combination of the mentioned methods, known as hybrid (Porter, 2017).

The empirical methods are based on surveys conducted after earthquake events and the observation of actual damage and performance of assets. Hence, they provide the most desirable fragilities from a risk management point of view and are highly credible. However, this method can only provide the best estimates for fragility functions if sufficient and reliable post-earthquake damage data are available, which is seldom realistic. Another drawback is the lack of recorded data for high levels of ground shaking, in which more structural damage and losses are expected. Moreover, a considerable portion of existing building typologies such as the recently built steel frames with masonry infills, have not yet experienced strong motions or very little has been observed and recorded. Furthermore, the resultant empirical functions are specific to a particular site as they are derived from specific tectonic, geotechnical conditions and the associated properties of the damaged structures (Rossetto et al., 2014a). An empirical fragility function can also be developed by fitting a function to observed data extrapolated directly from laboratory tests (Gardoni et al., 2002; Retamales & Davies, 2013; Schotanus et al., 2004). A comprehensive review on existing empirical vulnerability and fragility functions worldwide are presented in (Rossetto et al., 2014b).

The analytical fragility functions are constructed on the basis of the numerical analysis of a representative structural model, subjected to various forms of earthquake excitation (Casotto et al., 2015). The accuracy and uncertainty of analytical methods varies depending on the model specifications (e.g. 2D or 3D) and simulated loading (e.g. static or dynamic). Unlike the empirical method, in case of analytical fragility functions at least in theory, all necessary data can be determined. For instance, the desired intensity level at which the analysis is performed, the number of analyses and the class of assets under investigation can all be quantified according to the requirements (Calvi & Pinho, 2006). Hence, the analytical method provides insight where the empirical and expert methods might struggle. For instance, analytical fragilities can be developed for building types, which have not yet experienced strong motion or the shaking was not strong enough to cause life threatening damage. Analyses can result in a reduced bias and increased reliability of the fragility estimates for different structures compared to expert opinion by identifying the source of damage and the effect of building details such as soft-storey condition (Rossetto & Elnashai, 2003). As mentioned, the precision of the derived fragility curves relies heavily on the complexity and accuracy of the applied analysis method (Silva et al., 2014). For example, the seismic input can be represented

by a simplified response spectrum in case of static methods or an acceleration time-history of a real earthquake for the dynamic methods. Therefore, the method can be time-consuming and computationally expensive, while one might argue its credibility against empirical methods.

Judgmental-based fragility curves are developed in response to experts' opinion and experience. Where empirical data are lacking, and analytical methods may be too costly, expert opinion are employed to derive fragility functions. Hence, they can be versatile, efficient and relatively fast to derive. However, in addition to the uncertainties inherent to any estimation of damage due to the variability in actual building performance, there are the uncertainties related to the opinion of the experts and their reliability can be questioned due to their dependency on the experiences of the experts consulted. ATC-13 (1985) compiles a large number of judgment-based damage functions for 40 classes of buildings found in state of California-USA, including moment resisting steel buildings. However, the suggested damage probability matrices are difficult to calibrate or modify in order to incorporate new data or technologies. It is also a challenge to extend ATC-13 to other building types and other regions, as well as to individual building characteristics (Lang, 2002). To overcome this issue, Ventura et al., (2005) determined modification factors that can be applied to ATC-13 (1985) and generate fragility curves applicable to structures located outside California.

Combining the mentioned methods, one can develop hybrid fragility functions. For instance, following a hybrid method and by employing the empirical observations and some analytical evaluation according to the American code provisions, HAZUS (2003) has developed fragility curves for certain types of structures based on a very simplified representation of the structural behaviour. Utilising equivalent nonlinear single-degree of freedom oscillators to represent different building classes, HAZUS estimates the values for the structure's yield and ultimate strength, which could only best suit the American buildings, similar to ATC-13 (1985). HAZUS considers four possible seismic design levels: high-code, moderate-code, low-code and pre-code, the latter referring to buildings without any seismic design. For each building type and design level, the parameters defining the building capacity, typical drift ratios and spectral displacements at the threshold of the different structural damage states are given. The fragility curves are then computed for the entire building based on a capacity-demand spectrum method in four qualitative damage states (i.e. slight, moderate, extensive, complete), similar to ATC-40 (1996). The intense simplification in defining the structures' capacity and implementing elastic design spectrum instead of real earthquake records reduces the reliability of the fragility functions proposed by HAZUS. The variability in seismic demand is accounted for without explicit consideration of the influence of structural parameters, such as damping, period and yield strength level.

SEAOC Vision 2000 (1995) and ATC-40 (1996) along with FEMA-356 (2000) define the first generation of performance-based design approaches, based on the assumption that the building should reach a specific desired performance. However, none have addressed the estimation of losses in terms of casualties, repair costs and occupancy interruption, which are particularly decisive parameters for decision makers on selecting the appropriate performance objectives for a project. The ATC-58 (2012) project was initiated to address these issues. The majority of proposed fragility functions in ATC-58, which are component specific, are derived from post-earthquake observations or laboratory experiments, while some are based on structural analysis and some are derived from expert opinion.

2.4. Fragility Function for Steel Structures

Despite the considerable number of studies investigating the seismic response and fragility functions of reinforced concrete (RC) structure through different methods (Al Mamun & Saatcioglu, 2017; Brunesi et al., 2015; Erberik, 2008; Kwon & Elnashai, 2006; Liel & Lynch, 2012; McCrum et al., 2016; Pitilakis, 2010; Rossetto et al., 2016; Rossetto & Elnashai, 2005; Borele & Datta, 2015; Borzi et al., 2008; Kappos et al., 2006; Sattar & Liel, 2010; Vona, 2014), only a limited number of studies have focused on generating fragility function for steel structures. This is directly related to the popularity and exposure of RC structures with and without infills in seismically active areas. Evidence of pass earthquake events have reported the poor performance of such structures, including recent events such as the 1999 Kocaeli (Izmit) earthquake (M_w 7.6) (Aschheim et al., 2000), 2009 L'Aquila earthquake (M_w 6.3) (Ricci et al., 2011), 2011 Van earthquake (M_w 7.1) (Bayraktar et al., 2013), 2012 Emilia earthquake (M_w 6.1) (Ioannou et al., 2012) and 2015 Gorkha earthquake in Nepal (M_w 7.3) (Brando et al., 2015).

Furthermore, the general belief that steel structures are robust structures and have high resistance against extreme lateral loading, implies that fewer research have looked at their seismic fragility and vulnerability. Nonetheless, destructive earthquakes, particularly the 1994 Northridge earthquake in California (M_w 6.7), the 1995 Hanshin-Awaji (Kobe) earthquake in Japan (M_w 6.9), the 1999 Chi-Chi earthquake in Taiwan (M_w 7.7), 2001 Gujarat (Bhuj) earthquake in India (M_w 7.7) and 2003 Bam earthquake in Iran (M_w 6.6) inflicted various levels of damage upon a large number of low- to medium-rise steel framed structures (FEMA-350, 2000; Manafpour, 2003; Yamazaki & Murao, 2000; Yoshimura & Kuroki, 1999). In all cases, the observed structural damage was primarily caused by insufficient lateral load capacity, poor detailing of connections and failure of masonry infill panels, which in return refers to lack of applicable design provisions, insufficient enforcement and poor quality of construction. The inadequacy in fragility functions of steel structures, impacts the

vulnerability estimation process and consequently the risk assessment, early damage forecasting, disaster preparedness and insurance policies (Silva et al., 2014; Strasser et al., 2008). Furthermore, fragility functions offer an insight to the seismic performance of building types, which can be utilised for mitigation and strengthening measures.

Majority of studies investigating the seismic fragility and vulnerability of bare and infilled steel structures are collected and discussed in this section. The studies are presented in a chronological order in Table 2.1, along with a summary including information such as the applicable region, applied design code, structural system and the characteristics of their fragility functions (e.g. analysis type, intensity measure, engineering demand parameter, damage states). The following will discuss the findings of the summarised studies, discussing their features and identifying the existing shortcomings.

Table 2.1 - Fragility function developed for steel structures

#	Study	Application	Design Code	Structure Type	Structure Features	Analysis Type	Demand Parameter	Intensity Measure	Damage States
1	Song and Ellingwood (1999)	California - USA	1980 City of Los Angeles Building Code	MRF	4 & 13 storey	2D NLTHA	MIDR	$S_a(T_1)$	Service.; First yielding; Impaired function; Incipient collapse
2	Yamazaki and Murao (2000)	Japan	Japan Seismic Design Code (1970; 1980; 1990)	Steel Struct.	Various Heights & Plans	Empiric. Obsrv.	Observed Damage Level	PGV	Heavy + Moderate Damage; Heavy Damage
3	HAZUS (2003)	USA	Various Codes (Pre, Low, Mid, High)	MRF & CBF & Steel Frame + Infill	Various Heights	Empiric. Obsrv. & Analytic.	MIDR	$S_d(T_1)$	Slight Moderate Extensive Complete
4	Cherng (2001)	Taiwan	Taiwan Seismic Design Code	MRF & CBF	Six models with ranging heights: 69m – 103m	2D NLTHA	MIDR	$S_d(T_1)$	HAZUS (2003); VISION 2000
5	Cortés-Areizaga et al. (2006)	Puerto Rico	UBC (1990); IBC (2000)	MRF	91 models low- mid- high-rise	2D IDA	MIDR	PGA	FEMA-351
6	Kinali and Ellingwood (2007)	Central and Eastern USA	US National Building Code (1993)	MRF & CBF	3, 4 & 6 storey	2D IDA	MIDR	$S_a(T_1)$	FEMA-273
7	Ellinwood et al. (2007)	Central America	US National Building Code (1993)	MRF	2 & 3 storey	IDA	MIDR	$S_a(T_1)$	FEMA-273; FEMA-356; HAZUS (2003)

Table 2.1 - Fragility function developed for steel structures (continued)

#	Study	Application	Design Code	Structure Type	Structure Features	Analysis Type	Demand Parameter	Intensity Measure	Damage States
8	Li and Ellingwood (2008)	California - USA	UBC (1994)	MRF	9 & 20 storey	2D NLTHA	MIDR	$S_a(T_1)$	FEMA-273
9	Badpay and Arbabi (2008)	California - USA	NEHRP (1997)	CBF & BRB	3 storey	2D NTHA	MIDR	$S_a(T_1)$	FEMA-273; FEMA-356
10	Uma and Bradley (2010)	New Zealand	NZS 4203 (1992); NZS 3101 (1995)	MRF & EBF	low- mid-high-rise	2D	Displace Capacity at Yield	$S_d(T_1)$	HAZUS (2003)
11	Kazantzi et al. (2011)	Europe	EC8	MRF	5 storey	2D NLTHA	MIDA	$S_a(T_1)$	FEMA-356
12	Muto and Krishnan (2011)	California -USA	UBC (1982); UBC (1997)	MRF	20 storey	3D IDA	MIDR	PGV	FEMA-356
13	Majd et al. (2012)	Iran	ISIR Standard No. 2800 (3rd ed.) (2007); UBC (1997)	CBF	3, 5 & 7 storey; regular in plan and elevation	3D NLTHA	MIDR; axial plastic; deformation of bracing elements"	PGA	FEMA-356
14	Güneyisi (2012)	California -USA	SEAOC (1999)	MRF & CBF	3 & 8 storey	2D NLTHA	MIDR	$S_a(T_1)$	Negl. (0.5%); Light (1.5%); Moderate (>2.5%); Severe (>3.8%)
15	Petruzzelli et al. (2012)	Italy	1971; 1991	Portal Frame	Industrial building	2D & 3D IDA	peak transient roof drift ratio	$S_a(T_1)$	FEMA-356
16	Kazemi et al. (2013)	Iran	ISIR Standard No. 2800 (3rd ed.) (2007)	MRF+ RC walls	5 storey irregular plan	3D IDA	MIDR	$S_a(T_1)$	FEMA-356
17	Sarokolaei et al. (2013)	Iran	ISIR Standard No. 2800 (3rd ed.) (2007)	CBF	3, 8 & 12 storey	3D IDA	MIDR	PGA	Yielding; Collapse
18	Tirca et al. (2013)	Canada	NBCC (1980)	CBF	3 & 6 storey	2D IDA	MIDR	$S_a(T_1)$	Joint fail; Building Collapse
19	Gomez (2014)	Canada	CSA (1969; 1984;2009) NRCC (1965; 1980; 2010)	MRF	6 storey	2D	MIDR	$S_a(T_1)$	FEMA-356
20	Farsangi et al. (2014)	Iran	ISIR Standard No. 2800 (1988; 1999; 2007); AISC (2005)	MRF	2 storey	2D IDA	MIDR	PGA	FEMA-356

Table 2.1 - Fragility function developed for steel structures (continued)

#	Study	Application	Design Code	Structure Type	Structure Features	Analysis Type	Demand Parameter	Intensity Measure	Damage States
21	Mathiasson and Medina (2014)	California	ASCE 7-10 (2013)	MRF	20 storey	2D IDA	MIDR	$S_a(T_1)$	Collapse
22	Kazantzi et al. (2014)	California	IBC (2003); AISC (2005)	MRF	4 storey	2D IDA	MIDR	$S_a(T_1)$	local damage & local failure based on storey-level response
23	Nazri and Saruddin (2015)	Malaysia	EC 3 & 8	MRF	3 & 6 storey	2D IDA	Drift ratio	PGA	FEMA-273
24	Kiani et al. (2016)	Iran	ISIR Standard No. 2800 (3rd ed.) (2007)	MRF+ Infill; CBF; CBF+ Infill	3 & 5 storey	2D IDA	MIDR	$S_a(T_1)$	FEMA-356; FEMA-350; HAZUS (2003)
25	Asgarian and Ordoubadi (2016)	Iran	ISIR Standard No. 2800 (3rd ed.) (2007)	MRF & SMRF	5 storey	2D IDA	MIDR	$S_a(T_1)$	FEMA-350
26	Mai et al. (2017)	Swiss	EC8	MRF	3 storey	2D MSA	MIDR	PGA & $S_a(T_1)$	FEMA-356; Eurocode 8
27	Liu and Zhang (2017)	Korea	AISC (2005; 2010)	MRF	9 storey	2D NLTHA	-	$S_d(T_1)$; $S_a(T_1)$ & Wave Energy	HAZUS (2003)

Building Type:
MRF: Moment Resisting Frame
SMRF: Special Moment Resisting Frame
CBF: Concentric Braced Frame
EBF: Eccentric Braced Frame
BRB: Buckling Restrained Brace
Analysis Type:
NLTHA: Nonlinear Time History Analysis
IDA: Incremental Dynamic Analysis
MSA: Multiple-Stripe Analysis
Demand Parameter:
MIDR: Maximum Inter-Storey Drift Ratio
MIDA: Maximum Inter-Storey Drift Angle
Intensity measure:
PGA: Peak Ground Acceleration
PGV: Peak Ground Velocity
$S_a(T_1)$: Spectral Acceleration at fundamental period
$S_d(T_1)$: Spectral Displacement at fundamental period
Damage States:
FEMA-273 (1997); FEMA-350 (2000); FEMA-356 (2000):
Immediate Occupancy (IO), Life Safety (LS), Collapse Prevention (CP).
HAZUS (1997; 2003); VISION2000 SEAOC (1995): Slight, Moderate, Extensive, Complete.
BS EN 1998-3 (2005): Limited Damage (LD)[20% in 50 years], Significant Damage (SD)[10% in 50 years], Near Collapse (NC)[2% in 50 years].

Referring to Table 2.1, it is evident that due to the existing shortcoming in observed and empirical damage data for steel frames, majority of developed fragility functions are through analytical methods. These include nonlinear dynamic analysis on two- or three- dimensional models, with distinct levels of detailing ranging from equivalent SDoF oscillator (Kazantzi et

al. 2011) to detailed 3D simulations of the considered structures (Sarokolayi et al. 2013). Except for the HAZUS (2003) guidelines, the majority of studies replicated a real case structure, commonly found in the region under study, which can be considered as representative of a class of buildings, i.e. an index building.

Out of the 27 listed studies, about 30% are dedicated to California-USA with specific reference to the 1994 Northridge earthquake. Hence, the majority of these studies have developed fragilities for high-rise (+8 storey) buildings constructed in various periods (1980s to 2014). In contrast, 22% of studies looked at common mid-rise (3-8 storey) steel buildings in Iran. These include moment resisting frames (MRF) and concentric braced frames (CBF), all designed following different versions of the Iranian seismic provisions, known as "ISIR Standard No. 2800" (BHRC, 2007), which in turn is an adaptation of UBC (1997). An interesting observation is that majority of these studies follow the recommendations of FEMA-273 (1997) or its updated version FEMA-356 (2000) for defining their damage states and corresponding threshold values.

Analytical fragility curves have also been developed for other seismic prone regions such as New Zealand, Canada, Taiwan, Switzerland and Korea. Similarly, these studies adopted the damage states given in HAZUS (2003) and FEMA-356 (2000) guidelines, which are primarily defined for construction practice and material characteristics of America. Although one can argue that the design provisions utilised in almost all of these regions are modified and localised versions of the American standards (e.g. UBC-97, AISC-10, IBC-03) and share a great number of similarities, this might not be true in terms of material availability and construction practices.

In terms of the intensity measure, spectral acceleration at the fundamental period of the structure ($S_a(T_1)$) (64%) and peak ground acceleration (PGA) (24%) are the most common ones, mainly due to the available information on the seismic hazard of the regions under study. In case of the engineering demand parameter, most studies have measured the structural seismic response in terms of maximum inter-storey drift (MIDR) (76%), while comparing the obtained values against the recommended threshold ranges in guidelines such as FEMA-356 (2000) and HAZUS (2003).

Besides HAZUS, which only considers pre- and low-code steel frames with unreinforced masonry infill walls, the only study considering the effect of masonry infill walls is Kiani et al. (2016). The main focus of this study is on saddle connections, a specific type of semi-rigid connections, commonly used in steel frames due to its low construction cost and relative simplicity of assembly. The key lateral load resisting system of such buildings is either masonry infill walls, concentric braces (CBF) or a combination of both. In the past two major

earthquakes of Iran, the 1990 Manjil-Rudbar and 2003 Bam earthquakes, the performance of these steel frames was unsatisfactory and many cases resulted in heavy damage and total collapse (Mahen & Grove, 1990; Manafpour, 2003). The study follows a probabilistic framework to assess the fragility of 3 and 5 storey index buildings. Utilising the 44 real ground motions recommended in ATC-63 (FEMA P-695, 2009), two-dimensional models of the buildings' side frames (3-bay with typical span length of 5.0m) were analysed through Incremental Dynamic Analysis (IDA). Using hysteresis obtained through experimental studies carried out by Moghadam and Aalaee (2003), the connection spring were calibrated to represent the actual behaviour of the saddle connections. Moreover, to simulate the behaviour of infill panels, the recommendations of FEMA-356 (2000) were followed, in which the masonry panel is replicated by two compression struts. The cyclic behaviour of struts was based on a modified Ibarra-Medina-Krawinkler deterioration model (Ibarra et al., 2005) with pinched hysteretic response (Figure 2.1). The parameters required to define the hysteresis response where taken according to Crisafulli (1997). Different aspects of infill modelling will be discussed thoroughly in section 2.5.2.

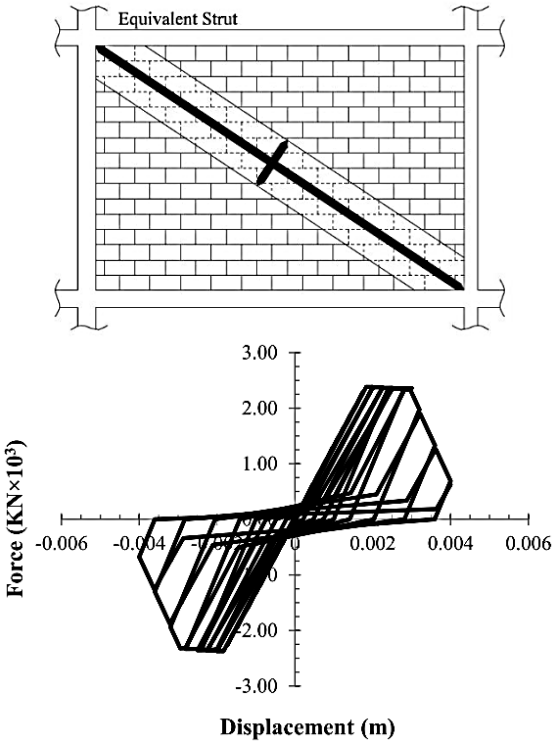

Figure 2.1 – The equivalent strut model utilised for simulating the infill walls and the hysteresis behaviour of the masonry material (Kiani et al., 2016)

Comparing the performance of the considered buildings, the study concluded that the infill walls provide strength and stiffness merely at the very early stage of response prior to their failure. Frames with infill walls were very vulnerable and not capable of resisting strong shakings due to the premature failure of the panels, which resulted in sudden strength and stiffness degradation. The swift rise and fall observed in the structure's capacity, stiffness and

ductility, as a result of infill panels being added to the bare steel frame, led to a completely different structural system. Hence, a significantly altered seismic performance was obtained, which consequently influenced the estimated damage states, fragility and vulnerability functions (Figure 2.2). Therefore, evaluating the actual seismic performance of steel frames with masonry infills, referring and relying on data originally generated for bare MRF or CBF steel frames, would be inaccurate and in cases dangerous.

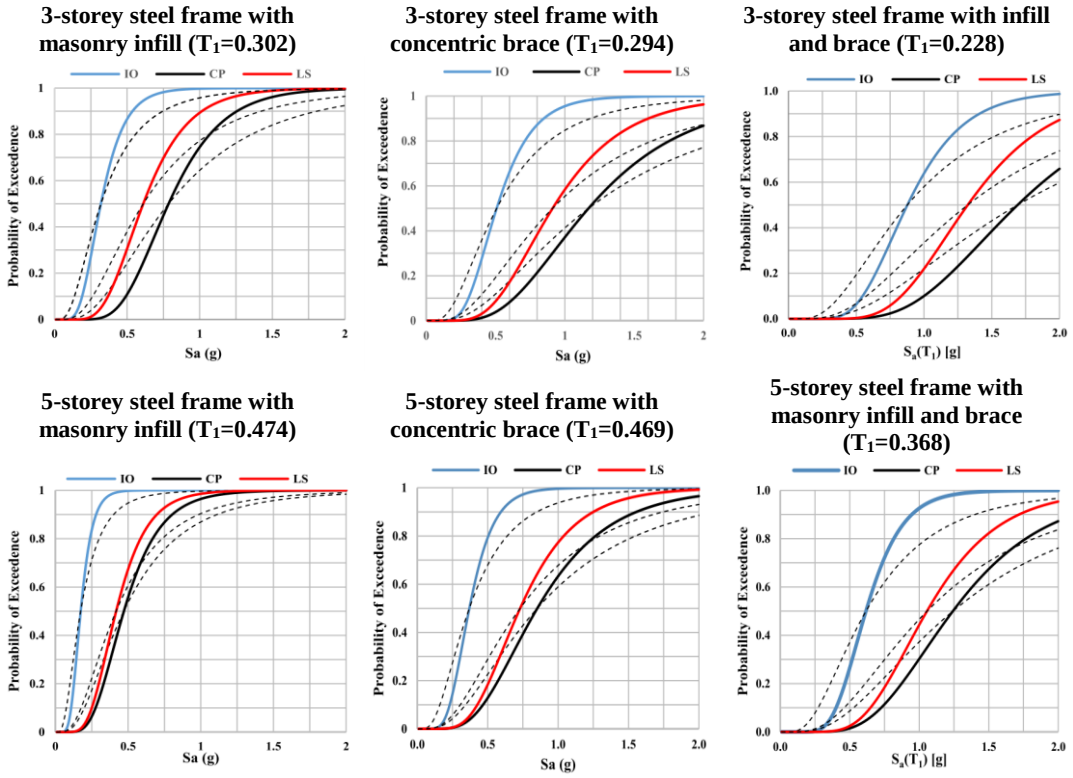

Figure 2.2 – Fragility curves derived by Kiani et al. (2016)
Continues line: β_{TOT} ($\beta_{TOT} = \sqrt{\beta_{RTR}^2 + \beta_{DR}^2 + \beta_{TD}^2 + \beta_{MDL}^2}$), where β_{RTR} is record-to-record uncertainty, β_{DR} is design requirements-related uncertainty, β_{TD} is rest data-related uncertainty and β_{MDL} modelling uncertainty. β_{RTR}, β_{RTR}, β_{RTR} values are assumed 0.35 (Fair), 0.35 (Fair) and 0.2 (Good) according to ATC-63
Dashed line: β_{RTR} obtained from IDA results.

Moreover, majority of studies dealing with the performance of infilled steel frames are experimental and have mainly concentrated on dynamic behaviour of scaled single storey – single bay cases, due to existing limitations in full scale testing (Cardone & Perrone, 2015; Flanagan & Bennett, 2001; Moghaddam & Dowling, 1987; Tasnimi & Mohebkhah, 2011). The limited number of analytical ones, focused mainly on verifying and calibrating the proposed infill models against the experimental observations. A thorough discussion on conducted experiments and techniques proposed for modelling the masonry infill panels are provided in the following section.

2.5. Behaviour and Analysis of Masonry Infilled Frames - State of the Art

As stated in Chapter 1, the present common practice treats the masonry infill as a non-structural element and solely designs the surrounding frame for gravity and lateral loading. An argument for ignoring the effect of the infills is that typically these walls do not offer much displacement capacity and during significant lateral demands, the infill wall would disintegrate, whereas the original lateral load-resisting system acts as intended in the design assumptions and processes. This assumption is not true as the pioneering work of Holmes (1961), Polyakov (1956) and Stafford-Smith (1962) has proven that the presence of masonry infill panels can significantly alter the stiffness, strength and energy dissipation of the structural system. Accordingly, infill panels continue to govern the overall response of buildings even after the initial cracks appear on the masonry walls (Murty & Nagar, 1996), while, the bounding frames can provide the structure with some ductility, particularly under lateral loading exerted from wind and earthquake (Mohyeddin-Kermani et al., 2008; Wibowo et al., 2008).

It is worth noticing that before the publication of advanced regulations and guidelines such as ASCE/SEI 41-13 (2013), ATC-58 (2012) and FEMA-356 (2000), the majority of surrounding frames did not meet sufficient detailing requirements to enter plastic behaviour. None the less, in past minor to medium earthquakes, infilled frames have shown an acceptable behaviour. This is mainly due to the friction between the frame and infill, the plasticity of the frame sections and the damping of infills after shear cracks (Crisafulli, 1997). However, in severe earthquakes, due to the crushing failure of infill parts and widening of the cracks, the panel becomes unstable against the lateral loads and cannot dissipate energy and absorb the earthquake force (Crisafulli, 1997).

On the other hand, ignoring the impact of infill panels is understandable when considering the complexity of the resulting system and lack of applicable design guidelines. However, a very few codes recommend isolating the masonry infill from the frame such that the extended stiffness does not play a role on the global behaviour of the system (NZS 4230, 2004; SNIP-II-7-81, 1996). On the contrary, some codes and guidelines prefer to take advantage of the resultant features such as the high initial stiffness, cost-effectiveness and ease in construction, such as the BS EN 1998-1-3 (2004), Nepal's code (NBC-201, 1994) and FEMA-306 (1999). The structural interaction between the two components (i.e. frame and wall panel) produces a composite structure with a unique behaviour, as each element contributes in carrying a share of the applied loads. The frame, while directly bearing a portion of the lateral and gravity load, primarily serves to distribute the applied load onto the infilled wall (Asteris, 2003). The way in which this distribution occurs, influences the stiffness response of the composite structure.

Meanwhile, the contribution of the frame to the overall stiffness depends upon its deformed shape, which in turn is determined by the reaction of the wall. At the same time, the response of the infill in terms of stiffness, strength and failure mode are affected by the stress state in the infill. This stress state is a function of the distribution of the load from the bounding frame. Therefore, inherently, the infilled frame structure is indeterminate. The issue is that simplified design and assessment approaches, in which the contribution of infills is dismissed, cannot predict the actual response of the resultant composite structure and the level at which the damage in the infill wall occurs. As a result, the global and local effects of these stiff and brittle elements coupled with the primary lateral load-resisting system may be miscalculated. The consequential overall change of structural behaviour, such as the shift in the natural frequency of the structure and the increases in shear demand on the columns, each has sufficient potential to change the failure mechanism of the entire system, which in return influences the vulnerability assessment (El-Dakhakhni et al., 2004; Kaushik et al., 2006).

On one side, by not taking advantage of the infill's inherent large in-plane stiffness, the design might not be so economical, as the lateral resistance is assumed to be taken up by other elements and the contribution of the infill is ignored. Additionally, interruption of the infill walls in height can cause over-strengthening of some floors and introduce soft-storey mechanism in floors without infills, which is highly undesirable from the earthquake resistance point of view, since all the necessary inelastic deformation is concentrated over just one floor height rather than over the entire height of the building (Mehrabi & Shing, 2003). The panels may also enforce pre-mature failure of the frame elements by exerting large amounts of shear loads to the surrounding frame (D'Ayala et al., 2009).

Therefore, as the masonry infills may have negative impact on the global response of a building, understanding the actual behaviour of frame-wall interaction is of immense importance for seismic analysis and fragility assessment and neglecting their effect may be unsafe (Asteris et al., 2011; Fardis, 2009). However, as stated earlier, the composite behaviour of infilled frames is a complex statically indeterminate problem. Thus, masonry infills have received much attention in the past sixty years and extensive number of studies have investigated their dynamic behaviour and various methods have been proposed for designing, assessing and simulating them.

The effort conducted on the masonry infilled frames can be categorised into two general approaches, the experimental investigations and the analytical ones. The data from the experimental tests are generally used to evaluate the theoretical methods, calibrate the analytical models or to update the design and assessment approaches proposed for such structural systems. The analytical studies are generally classified according to their modelling

approach, as macro and micro methods. The most important aspects and findings regarding each of the mentioned approaches are discussed in more details in the following sections.

2.5.1. Experimental Investigations

There is a fair, though heterogeneous volume of experimental data obtained through physical tests and observations on steel and reinforced concrete frames infilled with distinct types of masonry and mortar material. The assessed specimens include a range of different scales and comprise of both in-plane and out-of-plane. However, the majority of these studies have focused on the behaviour of single-frame single-bay unreinforced masonry infilled frames under monotonic or cyclic lateral loading. This is mainly due to existing limitations and restriction facing experimental studies. A comprehensive review of these studies can be found in Moghaddam & Dowling (1987), Calvi & Santini (1996), Mehrabi et al. (1996) and FARDIS et al. (1999), mainly for the case of reinforced concrete frames. Discussions on studies looking at cases with multi-storey multi-bays with both steel and reinforced concrete frames are provided in Gergely et al. (1993), Liauw and Kwan (1985), Mosalam et al. (1998).

In general, the experimental studies focus on issues relating to the stiffness of the bounding frames and the masonry walls, alteration in capacity and ductility, damage patterns and possible failure mechanisms, along with the influence of openings' positioning and size. The initial tests conducted on full- or small- scale infilled frames indicated the rise of stiffness and strength in comparison to the bare frame (Polyakov, 1956; Wallace & Krawinkler, 1985). The studies also concluded that the energy dissipation of infilled frame is much larger than that of the bare frame, while the ductility is much less when compared to a bare frame (Mehrabi et al., 1996). Accordingly, the maximum resistances of the tested strong frames were increased by the weak (hollow) and strong (solid) infills by factors of 1.4 and 3.2, respectively. Furthermore, the maximum load resistance of a weak frame-weak panel tested specimen was about 1.5 times that of a bare frame, while the resistance of a weak frame-strong panel specimen was about 2.3 times.

According to experimental observations, the nonlinear response of the infilled frame subjected to lateral loading can be defined in four general stages. Initially, the infill and its surrounding frame behave like a cantilever beam as a unified system with a relatively high initial stiffness, until the first propagation of cracks at the perimeters of the wall appears at relatively low horizontal loading. As the lateral load increase and the cracks start to propagate, a braced frame mechanism develops, in which the wall starts acting like a compressive strut. Further increase in lateral forces results in step-like cracks to appear on the vertical and horizontal mortar joints following different patterns. Consequently, the lateral stiffness decreases due to the initiation of cracks and the loss of contact between the panel and the frame at the tension

corners. The failure of the structural system occurs due to several possible combinations of simple mechanisms of failure that form in both the surrounding frame and the masonry panel. The element deterioration continues until strength and stiffness of the entire system decays significantly and fails.

A number of studies have investigated the possible failure mechanisms of the masonry infilled frames in more details. Predicting the failure mechanisms of the masonry infilled frames is a complex procedure due to the high number of parameters involved in the seismic response of the structure such as the material property, configuration, relative stiffness of the frame to the infill, detailing, etc. As a result, the experiments show a wide variety of failure modes which are usually complex and are a combination of different modes. For instance, quasi-static cyclic loading on infilled frames have demonstrated that the stronger masonry blocks lead to mortar cracking, while weaker blocks experience corner crushing as an early sign of damage (Flanagan et al., 1991; Mosalam et al., 1998). In more flexible frames, crushing occurs at the loaded corners, while for stiffer frames, crushing is more randomly distributed and remote from the loaded corners. The experimental outcomes have also pointed out that the performance of frame depends largely on the masonry infill typology, aspect ratio and the distribution of panels (Angel et al., 1994; Colangelo, 2005; Yorulmaz & Sozen, 1968). For instance, solid bricks indicated an improved response in comparison to the hollow masonry bricks, in terms of strength and stiffness. The structural behaviour also demonstrated a significant sensitivity against the structural characteristics such as number of bays, number of storeys, plan and elevation irregularity. Although, findings of Mosalam et al. (1998) and Negro and Verzeletti (1996) have shown that the behaviour of multi-storey and multi-bay infilled frames are approximately similar to that observed for a single-storey single-bay infilled frame, in multi-storey structures, the inelastic deformation concentrates mainly in the first storey, which may trigger a soft-storey failure mechanism. Furthermore, the full-scale tests of Dawe and Seah (1989) on steel frames with solid bricks and concrete block infills concluded that the failure modes and cracking patterns of full scale specimens were similar to those of small-scale specimens.

The stated failure mechanism of masonry infill panels is the defining concept behind the proposed analytical models. Hence, it is essential to understand how the damage propagates in infill panels and the structural system, from the elastic stage towards the ultimate capacity and collapse.

Mehrabi et al. (1996) has identified 24 different in-plane failure mechanisms for infilled frames. Provided that the frame has sufficient strength, the in-plane failure of the masonry

infill panels without opening can be narrowed down into five possible modes as follows (Al-Chaar et al., 2002; Mosalam & Günay, 2012; Shing & Mehrabi, 2002):

1) Flexural, in which frame and infill act as an integral flexural element
   [it occurs at low load level where the separation of infill and frame does not occur, very rare]

2) Horizontal sliding crack at mid-height of infill
   [this can cause a short column mechanism in the surrounding frame members]

3) Diagonal cracks propagate from one loaded corner to the other, also referred to as the diagonal strut failure
   [a distinct diagonal strut mechanism with two separate parallel cracks which is often accompanied by corner or centre crushing]

4) Horizontal slip
   [mainly due to weak mortar, resulting in a ductile behaviour, if the shear failure of the column can be avoided]

5) Corner crushing
   [it may lead to plastic hinges or shear failure in the frame member]

The stated failure modes are categorised and illustrated in Figure 2.3 and Figure 2.4. There is a consensus that the corner-crushing, sliding-shear along with diagonal strut failure are of practical importance and most common failure observation (El-Dakhakhni et al., 2003).

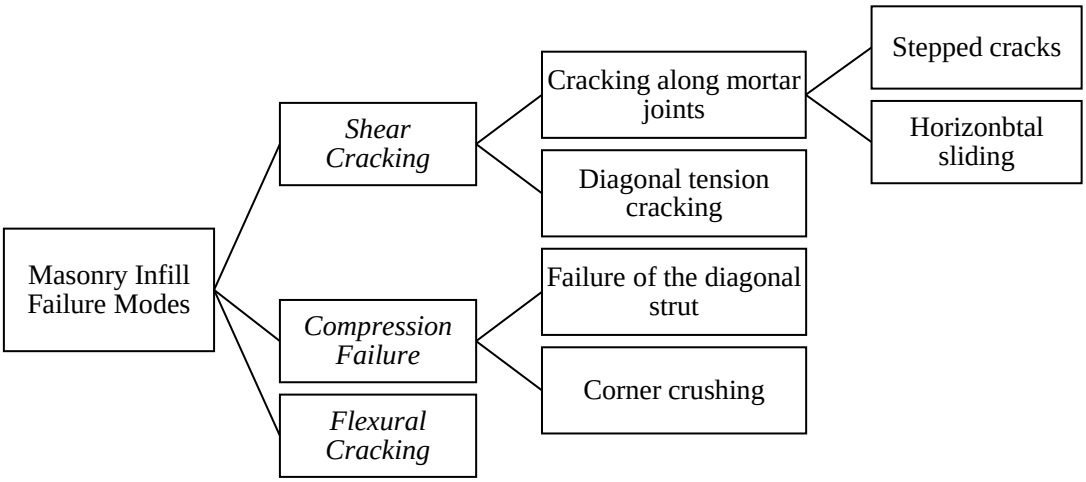

Figure 2.3 – Categorisation of common masonry infill failure modes

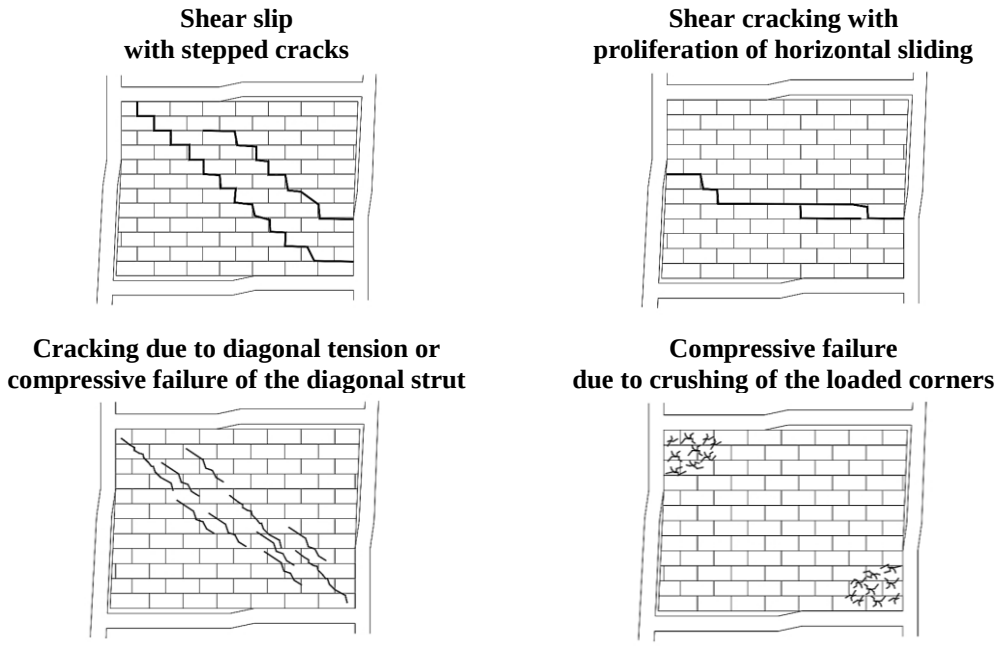

Figure 2.4 – Crack propagation due to common masonry infill in-plane failure modes

The cracking in infills can be divided into two categories; tension cracking and shear cracking. Tension cracking through the brick occurs occasionally when the mortar is extremely strong and therefore, shear sliding cannot occur along the existing bed and face joints. Also, complete failure does not occur as the infill is able to carry additional load after the propagation of cracks. On the other hand, shear sliding along the mortar joints is the predominant mode of cracking in the majority of onsite observed cases. Hence, the shear capacity associated to the horizontal sliding mechanism is often assumed as the ultimate limit state for the evaluation of the shear strength of the infill panel (BS EN 1998, 2004; NZS 4230, 2004).

The out-of-plane failure of infilled walls have also reported in post-earthquake reports, especially in case of double leaf walls and reinforced concrete frame. Braga et al. (2011) and Furtado et al. (2015) have reported out-of-plane failure observation after 2009 L'Aquila (M_w 6.3) and 2015 Gorkha (M_w 7.8) earthquakes. Out-of-plane resistance of infill panels has been studied experimentally by (Angel et al., 1994; Dawe & Seah, 1989a; R. D. Flanagan & Bennett, 1999). The effects of height-to-thickness ratio, combined in-plane and out-of-plane loading and the effect of prior damage due to in-plane loading were investigated. The results of all the tests showed that an infill panel that is not isolated by gaps from the frame can develop enough out-of-plane resistance so as not to require any ties or anchors to the frame.

Experimental studies indicate a different behaviour and far more complex failure mode among infilled frames with openings than the ones with solid panels. The size and in particular the location of the opening influences the overall behaviour of the structural system according to observations of Asteris et al. (2011). Moreover, in infills with openings, the cracks started

propagating at the corners of the openings. Infilled frames with symmetrical window openings, for instance, yielded nearly the same resistance as those without openings, while infilled frames with door openings had about 20% reduction in their shear resistance. In case of opening, plastic hinges may appear in columns, while there may be a combination of compressive failure and crushing of the infill. A different behaviour of the infill in the region between the opening (door/window) and the column in tension is observed when compared to the region between the opening and the column in compression. It was further observed that infilled frames with openings, although having a lower shear resistance, exhibited more ductile behaviour than those with solid infills (Mosalam et al., 1997). However, the experimental investigation conducted by Tasnimi and Mohebkhah (2011) showed that infilled frames with openings experienced pier diagonal tension or toe crushing failure and have smaller ductility factors than those frames with solid infill. Figure 2.5, illustrates the observed failure modes and cracking patterns for each case of the four considered arrangements according to the location and size of the opening.

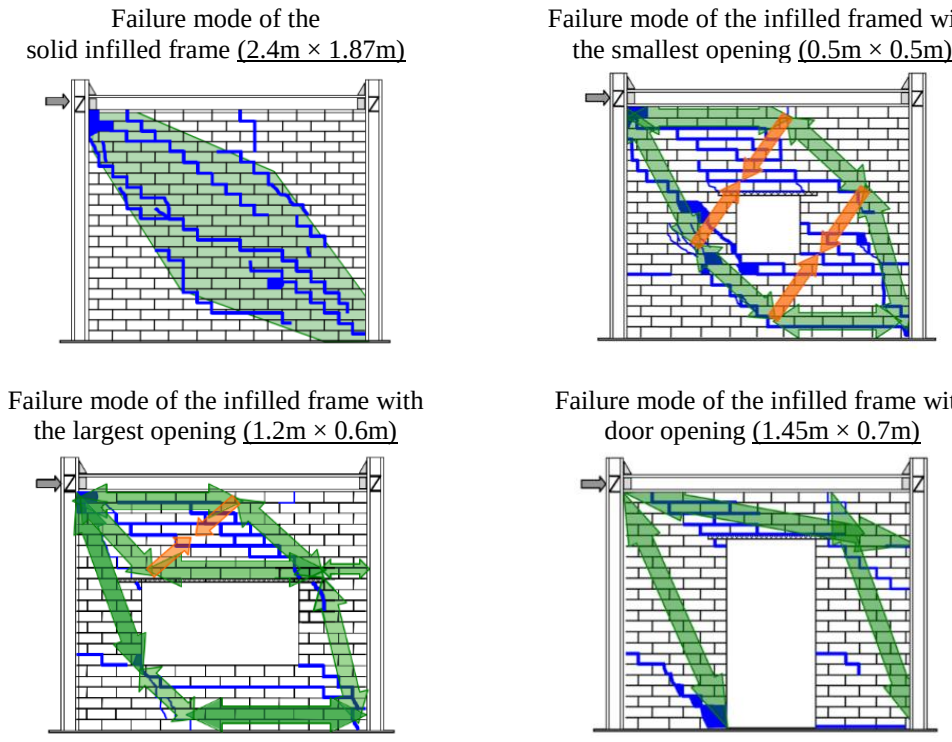

Figure 2.5 - Failure mode cases observed for each experimental sample (Tasnimi & Mohebkhah, 2011)

Another aspect of failure can be associated with the unbalanced distribution of infill walls within the frame, which may lead to structural configuration issues and failure modes such as weak or soft storey and torsional effects (Dolšek & Fajfar, 2001). The weak or soft storey occurs when comparatively fewer or no infill panel are located in one storey, particularly at the ground level, intended for commercial space or parking areas, when compared to the

others. During a seismic event, the deformation and damage tend to concentrate in the storey with less concentration of infill panels due to lower stiffness and strength. Even in instances when solid infill walls extend the full height of the building, in case they have the same strength, earthquake forces will generally be the largest in the bottom storey. These forces will tend to cause infill walls to fail, leading to the formation of a weak and soft storey. Infill walls can also induce torsion in instances when sides of a structure have solid infill walls, while other sides have either infill walls with openings or no wall is present, mainly due to architectural or usage purposes. The resultant stiffness imbalance may cause the building to twist, while increasing the deformation demands on the frame members in the more open sides.

Furthermore, different failure mechanisms can develop in the surrounding frame due to the properties of structural components, frame and infill panels, and the interaction between them (Crisafulli, 1997). Figure 2.6, illustrates the common failure modes observed in the surrounding frame under lateral loading.

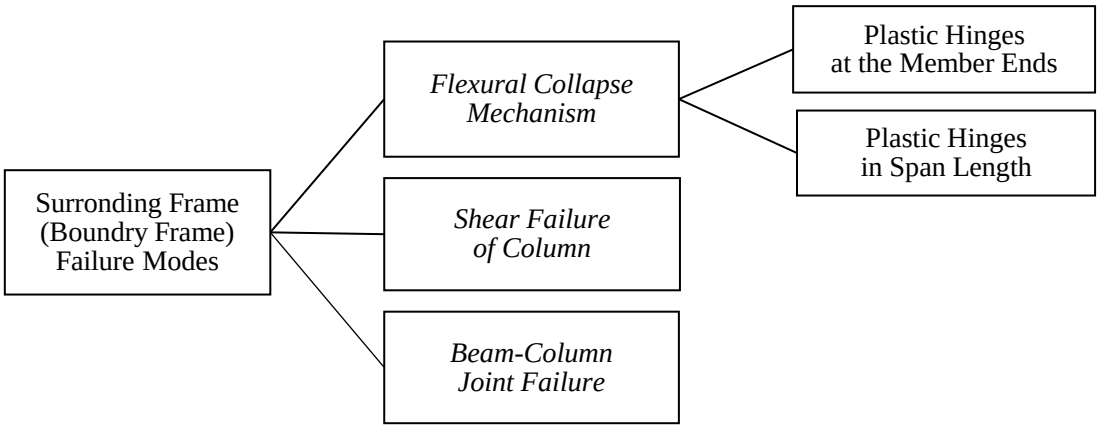

Figure 2.6 – Common failure modes of the surrounding simple frame

Beside identifying the most common failure mechanism of the infilled frame system, the experimental studies investigated the alteration in stiffness and strength of the infilled frames and also their degradation upon load reversals (Asteris, 2003; El-Dakhakhni, 2002; Mehrabi et al., 1996; Mohebkhah & Tasnimi, 2012). They concluded that the stiffness and failure mode of infilled frames depend upon the frame-to-wall stiffness ratio, frame-to-wall interface conditions and the material characteristics of the components. Less influential factors that affect the strength and stiffness degradation are the percentage of opening in the panels, type of loading, number of bays and number of storeys.

As a large number of parameters directly affect the behaviour of the infilled frame, it is difficult to thoroughly compare the output of different experimental campaigns and draw qualitative conclusions. One of the critical factors contributing to the non-linear behaviour of

infilled frames is the inherent material non-linearity. In general, defining accurate material properties is difficult, especially for masonry panels, which usually are composed of more than one component. Additionally, the effect of geometric non-linearity should not be ignored, particularly when the structure is allowed to undergo large horizontal displacements. Therefore, when evaluating the performance of infilled frames, all aspects of material and geometric nonlinearity should be considered. In conclusion, for each constitutive component of the system, the most important parameters affecting the response can be summarised as follows;

- Masonry Infill Panel:
    - Compressive strength of masonry,
    - Shear strength of masonry,
    - Cracking strength of the masonry,
    - Crushing strength of masonry,
    - Stiffness and strength degradation.
- Surrounding Frame:
    - Yielding of steel frame,
    - Cracking of concrete frame,
    - Yielding of reinforcing bars,
    - Local bond slip,
    - Flexural capacity of the surrounding frame,
    - Axial capacity of the surrounding frame,
    - In case of braced steel frames, the local buckling of braces can,
    - Shear capacity of the surrounding frame.
- Panel-Frame Interaction:
    - Relative stiffness of the masonry panel to that of the surrounding frame,
    - Variation of contact length,
    - Degradation of bond-friction mechanism.
    - In case of braced steel frames, the interaction of brace members and the masonry panel should be considered.

Since most experimental investigations are performed using static, quasi-static or pseudo-dynamic loading, it is not clear how accurately the data can represent the actual dynamic performance of the infilled frame system under real earthquake loading. Indeed, so far, very limited number of experimental studies have looked at full scale multi-storey buildings under dynamic loadings. For instance, Stavridis et al. (2012) conducted a shake table test on a two-thirds-scale model of an exterior frame of a prototype structure representing the 1920s RC construction in California. Furthermore, Buonopane et al. (1999) performed an experimental test on a half-scale double bay-two storey configuration albeit with different material and geometric configuration (aspect ratio 1:1.24). The specimens were exposed to pseudo-dynamic excitation, while investigating their failure mechanism and formation of diagonal struts. Hence, crucial factors such as the damping characteristics of the infill panels or the

resultant torsional effects have not been captured by existing studies. The existing limitations along with the substantial cost of experimental tests have restricted studies to simplified test specimens with finite number of storeys and bays, which are not a suitable representative of the actual three-dimensional structures.

2.5.2. Analytical Investigations

Analytical investigations on infilled frames initiated as early as 1955, when Whitney et al. (1955) studied the stiffness and ultimate strength of infilled frames by assuming the system as a vertical cantilever. Subsequent developments have resulted in four methods of analysis:

- Stress function method (e.g. Polyakov 1956; Liauw 1972)
- Equivalent diagonal strut method (e.g. Holmes 1961; Stafford-Smith 1962; Liauw & Lee 1977)
- Equivalent frame method (e.g. Liauw 1972; Liauw & Lee 1977)
- Finite or Discrete element method (e.g. Tasnimi & Mohebkhah 2011; D'Ayala et al. 2009)

Contingent on the preferred analytical method and the level of detailing required, the modelling techniques can be divided into two main groups, namely the local (micro) and the simplified (macro) approach. In micro or localised models, the wall panels consisting of the masonry units and the mortar are usually treated as two separate element types, while their interface might also be modelled as an additional element, representing the friction between the two materials. The interaction between masonry brick along the joints as well as the frame-infill panel interaction is accounted for through established finite element and distinct/discrete element methods. In contrast, the macro or simplified models consider the units, mortar and their interface as a homogeneous anisotropic material and replicate the structural response based on a physically reasonable representation of the infilled frame's structural behaviour, observed during empirical investigations (Lourenço, 2002).

The main difference between macro model and micro model is that the macro model decouple the failure modes from the geometry and layout of the component materials, representing its effect on the behaviour of the infill as spatially homogeneous, while the micro model is able to account for the localised phenomena and to follow in detail the sequence of failures leading to the panel cracking or crushing (Lourenço, 2002). Therefore, each method is implemented depending on the focus of the study. For instance, in cases where the interaction of units and mortar are of importance the micro model should be employed, while for evaluating the global response of the entire structure the macro models might be more suitable, if appropriately calibrated. The following sections review the studies dedicated to each of the mentioned modelling approaches. As this research study intends to investigate the overall behaviour and

performance of existing structures as a whole, the main focus will be on the proposed macro model approaches and their general specifications.

2.5.2.1. Micro-models

In case of micro modelling, finite element methods (FEM) and distinct/discrete element methods (DEM) are established, in which the frames are usually modelled by plane or beam elements, infills by plane elements and the interface by one-dimensional linear elements. The micro models are able to consider the interaction between masonry brick along the joints as well as the frame-infill panel interaction. Since mortar joint may be the weakest elements in a masonry wall, micro-modelling can be considered to be the most exact simulation approach for the masonry infills. The mortar joints can be modelled as typical continuum solid elements or zero length joint elements where the interface model is implemented (Koutromanos et al., 2011). In general, the micro-modelling method can give the most detailed picture of the local stress and deformation states in each mortar and brick elements, which allows close tracking of the crack propagation in the infill wall.

Using FEM, Mallick and Garg (1971), produced elements capable of calculating the elastic stiffness of single-storey single-bay infilled frame, while taking into account the slip between frame and panel. Liauw and Kwan (1985) used simple bar type elements to replicate the interface, to account for separation and slip. In this study, the infill panel was assumed to be isotropic before cracking and anisotropic after cracking.

Asteris (2008) has proposed a criterion to describe the frame-infill separation under lateral loading. The study suggests that the infill/frame contact lengths and the contact stresses should be estimated as an integral part of the solution, and cannot be simply assumed in an ad hoc way. Initially, the model assumed that the infill finite elements are linked to the surrounding frame just in correspondence of the ends of the compressed diagonal of the infill. As the nodal forces, displacements and stresses at the element extremities are computed, a check is carried out to verify if the infill panel points are overlapped to the surrounding frame. If there is overlapping, new links between infill and frame are added in the neighbourhood of the previously linked points and the procedure is repeated. The acceptability of the new deformed configuration is checked by verifying the absence of tensile stresses in the links at the panel–frame interface. If this condition is satisfied, the obtained deformed configuration is correct, otherwise the tensile links are suppressed and the procedure is repeated.

Lotfi and Shing (1991) investigated the efficiency of a homogenous smeared-crack model to capture the response of a reinforced masonry wall. In the smeared-crack model, the un-cracked material is considered as an isotropic material and the cracked material is replicated with a nonlinear orthotropic constitutive model. The smeared-crack model accurately captured the

flexural failure of the wall. However, the model failed to simulate the brittle shear behaviour of the wall coming from the diagonal cracking for lightly reinforced wall panels. Instead of using a homogenous approach, Lotfi and Shing (1994) developed a nonlinear interface constitutive model in combination with their smeared crack model for masonry brick, to capture the combined normal and shear stress and the dilatancy observed in the experiments. Mehrabi and Shing (1997) developed a constitutive model for the mortar joints in masonry infill panels. The model considered the nonlinear hardening behaviour of the interface, the reversal shear dilatancy in cyclic loading and the contraction of the interface under shear sliding due to the loss of asperities.

Stavridis and Shing (2010) developed a complex nonlinear finite element model for RC frames with masonry infill, combining the smeared (for masonry units) and discrete crack (for mortar joints) approaches to compensate for the weaknesses of the smeared crack model to capture the brittle shear failure of the masonry mortar joints and RC frame. The new element was used to model the behaviour of concrete, brick, and mortar.

An advantage of micro models is their ability in simulating details such as openings in the infill panel, and the resulting localised stress field, and the influence of different connection arrangements between the frame members and the wall, provided that adequate constitutive models are used. The presence of openings can aggravate the interactive effect of in-plane and out-of-plane loading (Yuen et al., 2016).

Mohebkhah et al. (2008) investigated the nonlinear in-plane behaviour of masonry infilled steel frames with openings. Two-dimensional discrete element models, at a semi-detailed level was adopted in which the joint is modelled as an interface with zero thickness. The blocks are considered fully deformable, thus allowing deformation to occur both in the blocks and joints and a better simulation of crack propagation and sliding in the joints. The study investigated the effect of opening size and position on the lateral stiffness, ductility and collapse load. In contrast to typical continuum FEM, the discrete elements are treated as rigid bodies, while complex and non-smooth boundary surfaces can be defined for each element.

D'Ayala et al. (2009) studied the influence of various parameters on the masonry infill-concrete frame interaction and looked through the shear failure of RC column by providing a more realistic model for the lateral load redistribution between the infill and the frame. The results of two different numerical models in ALGOR v.19 and DRAIN3DX were compared with experimental data of Al-Chaar et al. (2002). The study highlighted that to have a reliable failure pattern and load capacity prediction for infilled frames, it is essential to have an accurate simulation of the shear capacity in the columns. Furthermore, simulating the behaviour of infilled frame with a more generic tool than the equivalent strut method, is critical

to the correct interpretation of the load paths through the composite structure. The study predicts the system's behaviour by a relatively simple redistribution procedure based on relative pre- and post-cracking stiffness of columns, frame and infill. Moreover, the maximum shear locations for a single-bay, single-storey infilled frame was identified at the top of tension column and bottom of compression column (D'Ayala et al., 2009).

Ellul and D'Ayala (2012) assessed the performance of low engineered masonry infilled reinforced concrete frames. A finite element model was used for RC frame and a meso-modelling approach was developed for the masonry infill, while a spring element simulated the interaction between them. In the meso-model, the infill panel is treated as a homogenous material where the interface between brick and mortar is smeared into a continuum. This means that there is no distinction between individual masonry units and mortar joints. Hence, horizontal sliding along bed joints cannot be simulated. This type of failure is very rare and happens when the frame-panel interaction is minimum. In contrast to the diagonal strut methods, which rely solely on calibration, the proposed modelling technique did not require significant calibration to agree with the experimental response and gives better local failure predictions (Ellul & D'Ayala, 2012). The model is capable of identifying the onset of shear failure in the columns. Geometric nonlinearities were not included in modelling the infill panels, which limited the analysis to small deformation. It was assumed that masonry is not able to sustain large deformations without undergoing severe damage. The effect of different infill configuration was studied by considering different distribution of infills (changing stiffness distribution and soft storey at different floors), openings (ratio 0.13 and 0.19) and infill geometrical characteristics. It was concluded that the presence of infill panels is not always damaging but nor is always beneficial. In general, by introducing the infill the deformation capacity reduced by 10%, while the overall lateral strength increased by over 50%. Likewise, the initial stiffness increased up to 3.7 times the one of bare frame. The study argues that the presence of infill at top storeys improves the capacity and slightly increase the stiffness and, in contrast to the field observation, the higher mode effects, which would impose a higher demand on the upper floor, were not reproduced and remained unscathed in these parts. However, omitting the infill panels at mid-height clearly increased the vulnerability by decreasing the deformation capacity up to 40%.

Introducing a combined discrete-finite element method (DFEM), Yuen and Kuang (2015) studied the seismic response and failure mechanisms of infilled RC-frame structures with and without opening. The analysis indicated that the degrees of continuity and regularity of the infill panels crucially affect the seismic performance of structures. As long as out-of-plane collapse of infills does not occur, full-height and continuous-infill panels can enhance the overall stability and energy dissipation of frame structures. In contrast, discontinuous infills

can inflict serious damage localised at the points of discontinuity in the frame members. Furthermore, the analysis revealed that the columns of infilled frame structures suffer much greater damage than the adjacent connecting beam members. Hence, the capacity design concept of strong column–weak beam may not always be applicable to infilled frames due to the effect of infills on the bare frame.

Table 2.2, summarizes the chronological improvements in micro modelling of masonry infilled frames. An agreement exists among different researchers on modelling the brick units using the smeared crack. However, simulating the response of the mortar joint is more challenging than the one of the brick due to its highly nonlinear and brittle behaviour. This has motivated many researchers to improve the modelling of the mortar joint and simulate it as interface between bricks.

Table 2.2 – Micro models proposed for modelling infilled frame and masonry units

Author	**Model Capability**	**Structural System**	**Modelling Type**	**Brick Model**
Lotfi and Shing (1991)	Captures the flexural response of masonry wall	Wall	Homogeneous	-
Lotfi and Shing (1994)	Captures the flexural response of masonry wall	Wall	Simplified Micro-modelling	Smeared crack
Mehrabi and Shing (1997)	Simulates cracking, crushing, and sliding of masonry panel for cyclic and monotonic response	Infilled RC Frame	Simplified Micro-modelling	Smeared crack
Lourenço et al. (1998)	Simulates cracking, crushing, sliding, and collapse load of the masonry wall for monotonic response	Wall	Simplified Micro-modelling	-
Lourenço-de-Oliveira et al. (2004)	Improves the 1997 model to capture the cyclic behaviour of masonry wall	Wall	Simplified Micro-modelling	Smeared crack
Stavridis and Shing (2010)	Combining the smeared and discrete crack approaches to compensate for the weaknesses of the smeared crack model to capture the brittle shear failure of masonry infill	Infilled RC Frame	Simplified Micro-modelling	Smeared crack
Koutromanos et al. (2011)	Enhance the 2009 model to capture the cyclic behaviour of the masonry wall in dynamic tests	Infilled RC Frame	Simplified Micro-modelling	Smeared crack
Ellul and D'Ayala (2012)	Simulated the shear failure in the columns, while infill panel is treated as a homogenous material	Infilled RC Frame	Meso-modelling	-

Although micro-models can simulate the structural behaviour with great details, they are computationally intensive, making them difficult to apply in the analysis of structures with large number of bays and storeys. This drawback of micro-models can be resolved by implementing macro models.

2.5.2.2. Macro Modelling

The macro modelling approach is mainly based on a physical understanding of the infill panel's behaviour and its contribution to the overall response of the structure, obtained through empirical and experimental observations. The macro model takes advantage of the accuracy of the micro model, yet is computationally efficient for use in seismic performance assessments requiring repeated nonlinear dynamic analyses. In contrast to micro models, in which the wall components are modelled as separate elements, the macro model simulates the behaviour of the wall by using different type of springs and as an entirety. Mortar joints and masonry units are recognized together, considering their collective mechanical and physical properties, to obtain more simplified solution especially for large scaled models. Hence, macro modelling is not fully capable of identifying the failure mechanism of the frame and wall-frame interaction (Albayrak et al., 2017).

The earliest comprehensive research dedicated to identifying the difference between bare and infilled frame can be attributed to Polyakov (1956). The experimental observation on infilled steel frame indicated that the stress transmission between infill and frame elements only occurs in the compression zone based on elastic theory. According to Polyakov (1956), an estimated 20-30% of the perimeter of the infill panel will be in contact with the frame (top of the windward column and bottom of the leeward column) after the initial bond between the panel and frame is lost. Following this empirical observation, in which the frame rests (leans) on the compressive diagonal of the infill when subjected to lateral loading, Polyakov proposed the idea of *Equivalent Diagonal Strut* for modelling the infilled frames (Figure 2.7). This analogy was justified by observation of the phenomenon of slip and separation between the frame and infill, except in the proximity of the two compression corners at early stages of the lateral loading. More recent full scale experimental studies by El-Dakhakhni et al. (2004) and Moghaddam (2004) also proved the formation of the compression struts at different force levels. The bearing of the frame on the infill determining the compressive diagonal, produces an interactive force between these two elements and consequently increases the global stiffness.

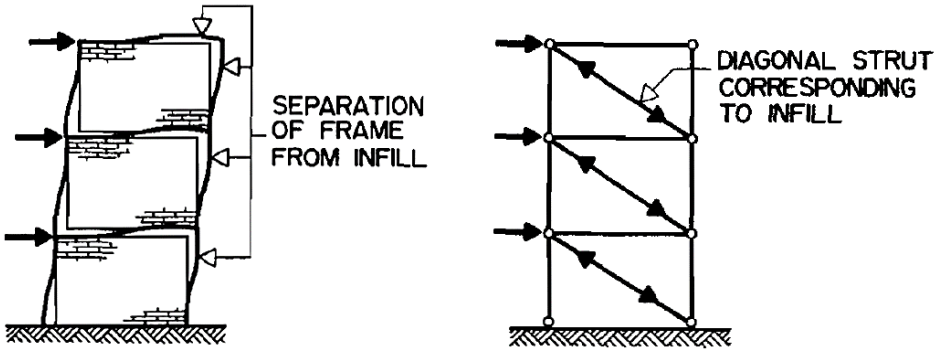

Figure 2.7 - Behaviour of infilled frame under lateral loading
and its analogous structural representation (Polyakov, 1956)

Therefore, as discussed earlier in section 2.4, the first simplified analogy for the analysis of infilled-frame was to consider the masonry infill panel equivalent to a concentric compressive bracing strut, connecting the top of the windward column to the bottom of the leeward column (Figure 2.8). The ends of the strut are considered pinned, so that only axial forces are transmitted through it. The strut ends are typically assumed to coincide with the intersection of the centrelines of the frame members, therefore the resultant strut length is usually longer than the infill diagonal, although this difference is insignificant. Following this analogy, the analysis of a complex composite structure would downgrade to the analysis of a simple braced frame (Mohyeddin et al., 2017).

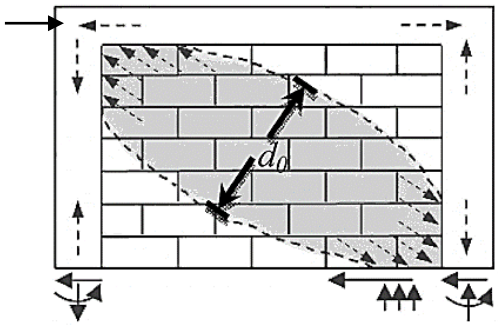

Figure 2.8 - Internal actions in an infill-frame under lateral loading
and formation of a compressive diagonal strut (Mohyeddin et al., 2017)

The equivalent diagonal strut model is accepted as a simple and rational way to describe the influence of the masonry infills on the global behaviour of the structure (Siamak, 2013). Owing to its simplicity, the strut model is proposed as a design approach of infilled frames by several codes, including NZS 4230 (2004), EN 1998 (2004), ASCE/SEI 41-06 (2007) and CSA S304 (2014).

Since the introduction of the equivalent strut a considerable number of experimental, theoretical and numerical studies have focused on various aspects of the problem of determining its characteristics, such as geometry, location, cross sectional area and number of struts, and their evolution for different levels of loading and drift. Furthermore, the type of

masonry material, scale of the specimens, infill-frame aspect ratio, the amount of gap between infill panel and frame, perforation in the panels, ductility of the surrounding frame, number of storeys and the number of bays have been the focus of different studies such as Crisafulli and Carr (2007), Mainstone (1971) and Stafford-Smith (1966). Each of the stated features and their impact on the modelling of the strut are discussed in this section.

In the early developments of macro modelling, Holmes (1961) proposed a linear equivalent compressive strut model for estimating the maximum strength, stiffness, and deflection of infill panels at failure. The proposed strut has an effective width (w) equal to 1/3 of the diagonal length of the rectangular steel frame and can only carry compressive forces with no tensile strength. Holmes (1961) assumed a constant width for the equivalent strut based on observation of small scale monotonic tests on masonry infilled steel frames. Failure of the strut was defined based on the ultimate strain and compressive strength of the infill material.

The total cross-sectional area of the strut (A_{strut}) is normally calculated as the product of its equivalent width (w) and the nominal thickness of the masonry infill panel (t_{inf}) (Eq. 2.2). Hence, the calculated value of the effective width significantly influences the initial stiffness, structure's natural frequency, ultimate strength of the strut and the force-displacement response of infill-frame and should be estimated according to the actual characteristics of the infill panel.

$$A_{strut} = w \times t_{inf} \tag{2.2}$$

Stafford-Smith (1966) concluded that the stiffness of the diagonal strut and the strength of an infill panel depend not only on its dimensions and physical properties but also on its length of contact with its surrounding frame (Figure 2.9). Also, it is primarily the flexural stiffness of the column and not that of the top beam, that influences the stiffness of the infilled frame, which has been consecutively confirmed by experimental and analytical studies (Brzev et al., 2009; Papia et al., 2003). Therefore, the stiffness and strength of an infilled frame are different from the simple sum of the two component structures.

To calculate the equivalent width of the strut (w), Stafford-Smith et al. (1969) considered the contact length between the frame and the infill in its deformed configuration (α) (Eq. 2.3). The contact length was expressed as a function of a non-dimensional parameter (λ), which expresses the relative stiffness of the infill panel to that of the frame when subjected to lateral loading (Eq. 2.4). Accordingly, as the strut-width increases the lateral stiffness of infilled frames increases. By doing so, the width of the equivalent strut decreases as the loading increases, which account for reduction of stiffness and variation of the Young's modulus (E_{inf}) of the infill panel with increased cracking.

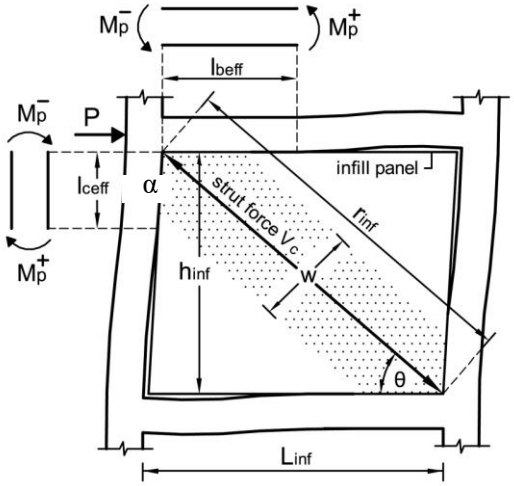

Figure 2.9 - Deformations of infill and frame after separation (Moretti et al., 2014)

$$w = 0.58\,(\frac{1}{h_{col}})^{-0.455}.(\lambda\, h_{inf})^{-0.335} d_{inf}\left(\frac{1}{h_{col}}\right)^{0.064} \tag{2.3}$$

$$\lambda = \sqrt[4]{\frac{E_{inf}\, t_{inf}\, \sin 2\theta}{4\, E_f\, I_{col}\, h_{inf}}} \tag{2.4}$$

Where d_{inf} is the diagonal length, E_{inf}, t_{inf} and h_{inf} are the elastic modulus, thickness, and height of the infill, E_f is the elastic modulus of the frame, I_{col} is the moment of inertia of the columns and h_{col} is the height of the frame. θ is the slope of the infill diagonal to the horizontal axis accounting for the effect of height-to-length aspect ratio.

Based on experimental observation on RC frame with brick infills, Mainstone (1971) proposed a semi empirical relation for estimating the width of the equivalent compressive strut (w), following the proposed relative stiffness (λ) and including the diagonal length of the masonry infill (d_{inf}) (Eq. 2.5). The proposed equation is recommended in guidelines such as FEMA 274 (1997), FEMA 306 (1998), FEMA 356 (2000) and the Turkish Seismic Code (2007).

$$w = 0.175\,(\lambda\, h_{col})^{-0.4}\, d_{inf} \tag{2.5}$$

Alternative formulations for evaluating the equivalent strut width have been recommended according to empirical and analytical work on different materials and arrangements, such as (Decanini & Fantin, 1986; Flanagan & Bennett, 2001; Liauw & Kwan, 1985; Saneinejad & Hobbs, 1995). The existing diversion in the proposed expressions, yields to unequal estimations of the strut's cross-sectional area for the same system, by as much as 2.5 times difference (Mohyeddin et al., 2017). Adoption of different values of strut width and layouts (e.g. number and positioning), leads to considerably altered stiffness and consequently

different overall response of the infilled frame (Crisafulli et al., 2000; Moretti et al., 2014; Papia et al., 2003).

Furthermore, when comparing the estimated values to experimental outcomes, overestimation or underestimation of the behaviour is observed. Hence, there is no clear conclusion on which function is the most applicable one. The only common agreement is that the strut width decreases as the stiffness parameter (λ) increase (i.e. contact length decreases). Therefore, none of the proposed equations have been thoroughly accepted in any national design code worldwide. However, as mentioned previously guidelines such as FEMA 306 (1999), ASCE/SEI 41-06 (2007) and CSA S304 (2014) have recognised the equivalent strut method as an acceptable approach for evaluating the contribution of the infill walls and have proposed values for the width and the stiffness ratio. Table 2.3, summarises the formulation proposed for estimating the equivalent width of the strut by different studies and guidelines.

Table 2.3 – Proposed equations for estimating the width of equivalent strut

Study / Guideline	Year	Equivalent width formulation
Holmes	1961	$w = 0.333\, d_{inf}$
Stafford-Smith & Carter	1969	$w = 0.58\,(\frac{1}{h_{col}})^{-0.455}.(\lambda\, h_{inf})^{-0.335} d_{inf}\left(\frac{1}{h_{col}}\right)^{0.064}$
Mainstone & Weeks	1970	$w = 0.16\,(\lambda\, h_{col})^{-0.3}\, d_{inf}$
Mainstone – FEMA 273 (1997) – FEMA 306 (1998) – FEMA 356 (2000) – ASCE/SEI 41-06 (2007) – Turkish Earthquake Code [TDY] (2007)	1971	$w = 0.175\,(\lambda\, h_{col})^{-0.3}\, d_{inf}$ if $\lambda\, h_{col} < 5$ $w = 0.175\,(\lambda\, h_{col})^{-0.4}\, d_{inf}$ if $\lambda\, h_{col} > 5$
Hendry	1981	$w = \frac{1}{2}\sqrt{\alpha_h^2 + \alpha_l^2}$ $\alpha_h = \frac{\pi}{2}(\frac{4E_f I_c h}{E_m t_e sin2\theta})^{1/4}$ $\alpha_L = \pi(\frac{4E_f I_b h}{E_m t_e sin2\theta})^{1/4}$
Liauw & Kwan	1984	$w = \frac{0.86\, h_{inf}\, \mathrm{Cos}\,\theta}{\sqrt{\lambda\, h_{col}}}$
Tassios	1984	$w = 0.20\, sin\theta \sqrt{\frac{E_c A_c}{G_i A_i}}\, d_{inf}$ (if $1 < \frac{E_c A_c}{G_i A_i} < 5$)
Decanni & Fantin	1986	$w = \left(\frac{0.748}{\lambda H} + 0.085\right) d$ if $\lambda H \leq 7.85$ uncracked $w = \left(\frac{0.393}{\lambda H} + 0.130\right) d$ if $\lambda H > 7.85$ uncracked $w = \left(\frac{0.707}{\lambda H} + 0.010\right) d$ if $\lambda H \leq 7.85$ cracked $w = \left(\frac{0.470}{\lambda H} + 0.040\right) d$ if $\lambda H > 7.85$ cracked
Moghaddam and Dowling	1988	$w = d_{inf}/6$
Bazan & Meli	1990	$w = (0.35 + 0.22\beta)h$ $\beta = \frac{E_{fr}\, A_{fr}}{G_{inf}\, A_{inf}}$
Paulay & Priestley NZS-4230 (2004)	1992	$w = 0.25\, d_{inf}$
Durrani & Luo	1994	$w = 0.32\,\sqrt{Sin2\theta}\left(\frac{h_{col}^4 E_i t_i}{m E_f I_{col} h_i}\right)^{-0.1}\mathrm{Sin}\,2\theta$

Table 2.3 – Proposed equations for estimating the width of equivalent strut (continued)

Study / Guideline	Year	Equivalent width formulation
Flanagan & Bennet	1999	$w = \frac{\pi}{C\ \lambda\ Cos\theta}$
Al-Chaar	2002	$w = 0.0835 C_{AC} d \left(1 + \frac{2.574}{\lambda H}\right)$ for $l/h \geq 1.5$ $w = 0.1106 d \left(1 + \frac{6.027}{\lambda H}\right)$ for $l/h \geq 1.0$ C_{AC} is the multiplication factor, accounting for the aspect ratio, $C_{AC} = -0.3905 \left(\frac{l}{h}\right) + 1.7829$
Tucker C.	2007	$w = 0.25\ (\lambda\ h_{col})^{-1.15}\ d_m$
Masonry Standards Joint Committee (MSJC)	2011	$w = \frac{0.3}{\lambda\ Cos\theta}$
Turgay *et al.*	2014	$w = 0.18\ (\lambda\ h_{col})^{-0.25}\ d_m$
CSA S304	2014	$w = \sqrt{\alpha_h^2 + \alpha_L^2}$ $\alpha_h = \frac{\pi}{2} \left(\frac{4 E_f I_c h}{E_m t_e sin2\theta}\right)^{1/4}$ $\alpha_L = \pi \left(\frac{4 E_f I_b h}{E_m t_e sin2\theta}\right)^{1/4}$

In general, the expressions used in the majority of studies and codes for estimating the equivalent strut width refers to the infill panels not fully connected to the frame. These values have been derived empirically and from experimental research on unreinforced masonry infills in both steel and RC frames. In case of reinforced infilled, in which a strong connection exists between the frame and the infill, the overall stiffness of the infilled frame is underestimated when the equivalent width is calculated according to the above provisions (Moretti et al., 2014).

The equivalent width is only valid prior to separation of the infill from the frame. According to Paulay & Priestley (1992), the separation is expected to occur at 50% of the lateral shear resistance of the infilled frame. As the separation occurs, the stiffness of the system degrades and this should be taken into account by reducing the strut's effective width. Hence, models in which the strut width is constant cannot precisely predict the stiffness of the system under increasing lateral loading.

On the other hand, Poliakov's model assumed that the diagonal struts are only active when they are under compression. A compressive only strut is feasible on the basis that the bond strength at the panel-frame interface and the tensile strength of the masonry infill are very low. Thus, the tensile forces can be transferred through the intersection between panel and frame only for small levels of seismic excitation. Therefore, Flanagan (1994) suggested a refined model using tension-compression truss members instead of diagonal compressive struts. These truss members will have half of the equivalent strut area in each diagonal direction, while the model is able to consider the tensile behaviour. Although this does not have a significant effect on the infill's behaviour, substantial changes are observed in the internal

forces of the surrounding frame, especially the axial forces in the columns (i.e. tensile forces decreased, whereas compression forces increased).

Regardless of which model is used, a general limitation of the strut model is in accurately estimating the shear force and bending moment exerted on the frame members. This relates to the fact that the actual contact length/area between the frame and infill panel is not represented realistically by the strut model, particularly when utilising concentric single strut (Crisafulli, 1997). To overcome this issue, a number of studies have proposed models with multiple struts (Crisafulli & Carr, 2007; El-Dakhakhni et al., 2003; Fiore et al., 2012). The proposed methods are based on a series of micro level finite element models, indicating the level and location of nonlinearity in the frame and panel. For instance, Mohyeddin et al. (2013) illustrated the formation, direction and location of principle stresses in two half scale single-storey RC frames infilled with concrete masonry units tested earlier by Mehrabi et al. (1996). The two specimens had identical overall RC frame dimensions, while the compressive strength and elastic modulus of the masonry panels differed. Looking at the compressive stresses in the two infill panels (Figure 2.10 and Figure 2.11), it is clear how the load path varied.

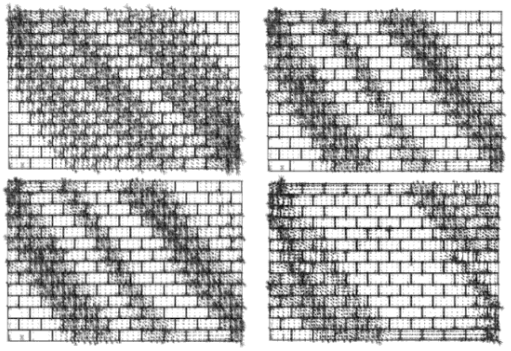

Figure 2.10 - Principle compressive stress in the infill panel with hollow clay blocks (f'm 10MPa) under monotonic lateral load, at drifts of 0.17% (top left), 0.63% (top right), 0.76% (bottom left), 1.73% (bottom right)

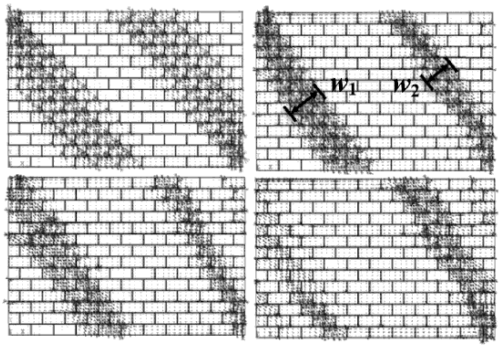

Figure 2.11 - Principle compressive stress in the infill panel with solid clay bricks (f'm 14MPa) under monotonic lateral load, at drifts of 0.17% (top left), 0.72% (top right), 1.06% (bottom left), 1.88% (bottom right)

The observed load path indicates that a single strut, connecting only the two loaded corners of the frame, is not fully capable of evaluating the bending moment and shear forces exerted on the frame members. Therefore at least two struts in diagonal directions are needed to simulate the location of potential plastic hinges and the local effects resulting from the interaction between the infill and the frame. Increasing the number of connection points of the strut to the columns or altering the location at which the diagonal strut transfers the load to the columns can improve the accuracy of the model in simulating the interaction. However, by adding to the number of struts, one may also increase the complexity and computational effort. Figure 2.12, illustrates macro models with multiple struts.

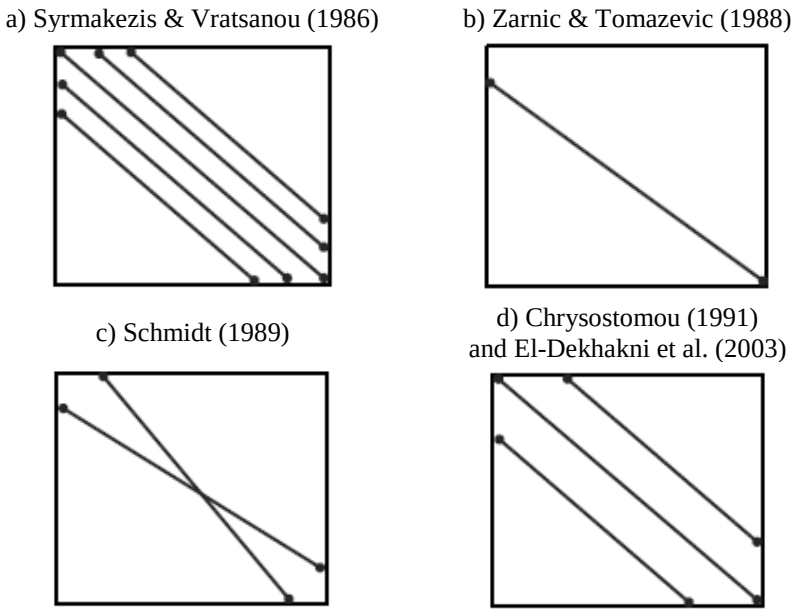

Figure 2.12 – Alternative models with off-diagonal struts to model the frame infill interaction. For clarity, struts in only one direction are shown.

To predict the accurate bending moment and shear force exerted on the frame members and also capture the corner crushing failure mechanism, (Chrysostomou et al., 1990) and (El-Dakhakhni et al., 2003) proposed models employing three non-parallel struts as shown in Figure 2.13. In this arrangement two additional off-diagonal struts where placed at the end points of the maximum field moment in the top beam and columns. The properties of the three struts are calculated by means of the principle of virtual work and it is assumed that the central strut deteriorates faster than the two outer struts. The implemented struts do not fail simultaneously, which is the case in actual infill panels, since the crushing starts at the corners and keeps propagating in the corner region leading to failure of the panel.

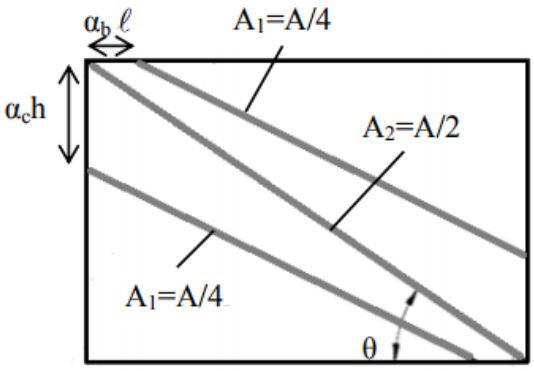

Figure 2.13 – Proposed multiple strut model by El- Dakhakhni et al. (2003)

Figure 2.14 and Figure 2.15 illustrate the load-deflection relations obtained through different experimental specimens and compares them to analytical results acquired using the triple-strut model of (El-Dakhakhni et al., 2003). An acceptable prediction of stiffness and ultimate load capacity up to failure is observed in both cases of single and double bays.

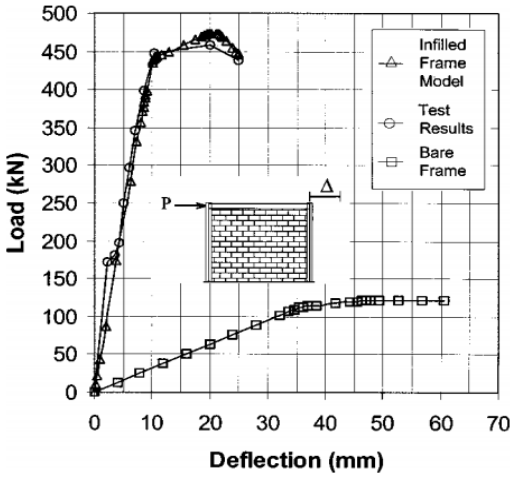

Figure 2.14 – Load-Deflection relations for single-bay specimen WC7 of Amos (1986)

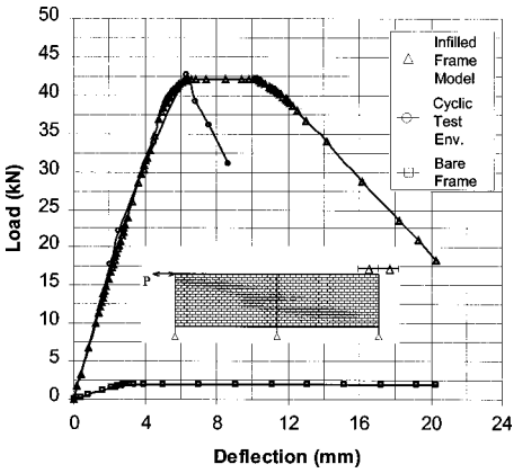

Figure 2.15 – Load-Deflection relations for double-bay specimen Q21SSB of Mosalam et al. (1997)

Besides predicting the shear forces exerted on the frame members, another aspect macro models need to reflect is the shear failure of the infill panel. Since shear failure of the masonry (shear friction and diagonal tension failure) is one of the most common type of failure observed in a masonry panel, Crisafulli and Carr (2007) has proposed a multi-spring model. The proposed model is capable of accounting for the compressive and shear behaviour of the masonry panel using two parallel struts and a shear spring in each direction. The axial forces calculated in the strut are used to evaluate the shear strength of the masonry panel. This configuration allows an adequate consideration of the lateral stiffness of the panel and of its strength, particularly when shear failure along mortar joints or diagonal tension failure are expected.

On the other hand, as the lateral displacement (drift) increases, due to alteration of load paths, the struts' width and location (contact area) should also change. Therefore, to better capture the internal actions in frame members, adaptive strut models are proposed, which can incorporate these changes on the configuration and section properties of the struts at different drift levels (Crisafulli & Carr, 2007; Smyrou et al., 2011). For instance, (Fiore et al., 2012) proposed modelling the infill panel by two non-parallel struts, the location of which is defined as a function of the aspect ratio of the infill (i.e. length/height). Empirical formulas are used to estimate the location of the struts at different storeys and later validated through finite element analysis. The model was tested against a single strut model in a 5-storey building and showed better global behaviour of the infilled frames in terms of displacements and also the local effects on frames in terms of bending moments and shear stresses.

Table 2.4, summarises the macro models proposed for simulating the impact of masonry infills.

Table 2.4 – Macro models proposed for simulating masonry infill frames

Authors	**Year**	**Number of struts in each direction**	**Purpose of the model**
Holmes	1961	1	Modelling the ultimate strength, stiffness, and deflection at failure of the infill
Stafford-Smith	1962	1	Modelling effective width of the equivalent (linear) strut
Stafford-Smith & Carter	1969	1	Modelling stiffness, ultimate strength, cracking load of the infill
Mainstone & Weeks	1970	1	Modelling stiffness and strength of the infill
Mainstone	1971	1	Modelling stiffness and strength of the infill
Klingner & Bertero	1976	1	Modelling the hysteretic response of the infill, as well as strength and stiffness of the infill
Liauw & Kwan	1984	1	Modelling stiffness and strength of the infill
Zarnic & Tomazevic	1988	1	Modelling the lateral strength and stiffness of the infill
Schmidt	1989	2	Modelling the frame-infill interaction as well as strength and stiffness of the infill
Syrmakezis & Vratsanou	1986	5	Considering the effect of the contact length on the moment distribution of the frame as well as strength and stiffness of the infill
Chrysostomou	1991	3	Modelling the frame-infill interaction as well as the hysteretic response of the infill frame under earthquake loading considering stiffness and strength degradation
El-Dakhakhni	2003	3	Modelling the frame-infill interaction as well as corner crushing failure mechanism
Crisafulli & Carr	2007	2	Modelling the frame-infill interaction as well as accounting for compressive and shear strength of the infill
Fiore et al.	2012	2	Evaluation the stresses in beams and columns. Determine the lateral stiffness of infilled frames

2.5.2.3. Masonry Cyclic Hysteresis

The discussed macro models define the arrangement of the equivalent strut and propose formulas for estimating the effective width of the strut, which in turn is applied to compute the stiffness and ultimate strength of the infill panel. However, they do not specifically define the force-displacement (stress-strain) behaviour of the strut, particularly under cyclic loading. A number of relationships have been proposed to describe the hysteretic behaviour of the infilled frame through the diagonal strut under axial and lateral loading, which are reviewed in this section. A thorough review of analytical hysteresis relationships can be found in Crisafulli et al. (2000).

As there is a high chance for the infilled frame to enter its nonlinear stage under even slight lateral loading, the hysteretic behaviour of the components should account for inelasticity. In case of non-linear analysis, the infilled frame cannot be modelled as an elasto-plastic system due to stiffness and capacity degradation that gradually occurs under cyclic loading. In general, the relationship adopted for the strut represents the global hysteretic response of the infilled frame system and not only the behaviour of the infill panel, which is represented by the diagonal strut. An important hysteretic property of structural masonry panels is the loss of stiffness and strength due to deformation beyond yield (Madan et al., 1997). Pinching of hysteresis loops due to opening and closing of masonry cracks is also a commonly observed phenomenon in masonry structural systems subjected to cyclic loading (Crisafulli, 1997; Klingner & Bertero, 1976). Moreover, due to the diversity in masonry units and mortar material and also the construction methods, the hysteretic models should be calibrated against experimental results of the specific masonry and frame under study. This also allows reducing the uncertainty related to components interaction.

One of the first attempts to produce a hysteretic behaviour for infills is by Klingner and Bertero (1976) following their experimental observations of masonry infilled RC frames. The proposed cyclic model included both stiffness and strength degradation as shown in Figure 2.16. Accordingly, the lateral strength and stiffness are essentially zero under tension, until the vertical panel cracks close and the panel returns to its un-deformed configuration.

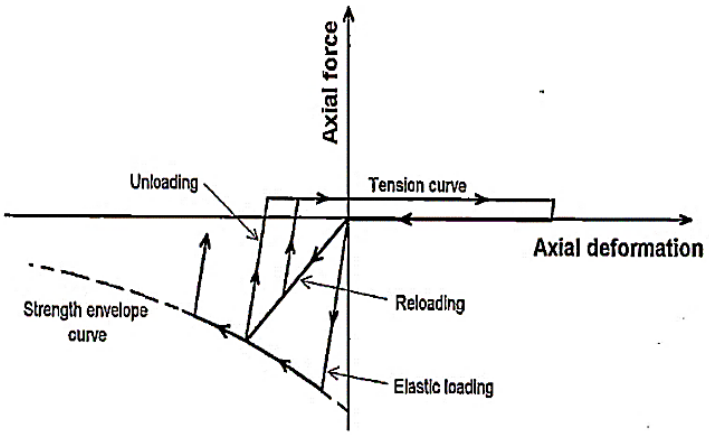

Figure 2.16 - Hysteresis behaviour of the strut model proposed by Klingner and Bertero (1976)

If the infills are modelled by equivalent struts, the pinching effect of the hysteresis response should be simulated through the nonlinear behaviour of the strut model. Calibrating the hysteresis with experimental observations, Andreaus et al. (1985) and Doudoumis and Mitsopoulou (1986) also proposed slightly altered curves for infilled RC frames with masonry material with different characteristics to those of Klingner & Bertero (1976) as shown in Figure 2.17 and Figure 2.18. All three hysteresis envelopes are similar and consider a significant effect for strength degradation.

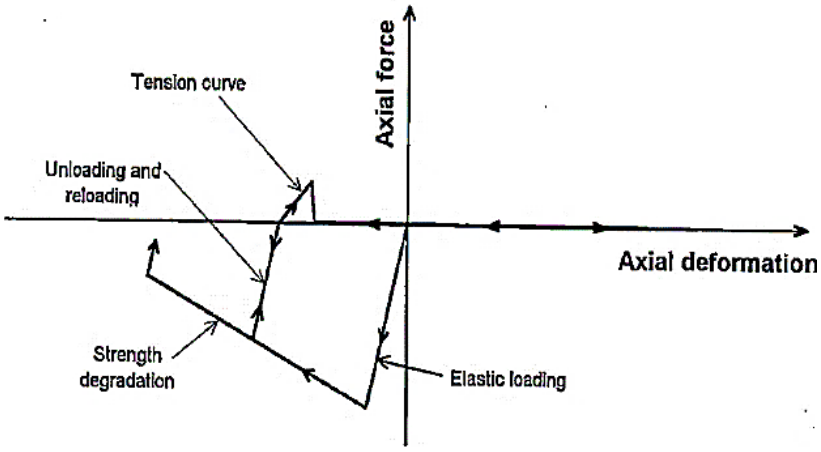

Figure 2.17 - Hysteretic behaviour of the strut model proposed by Andreaus et al. (1985)

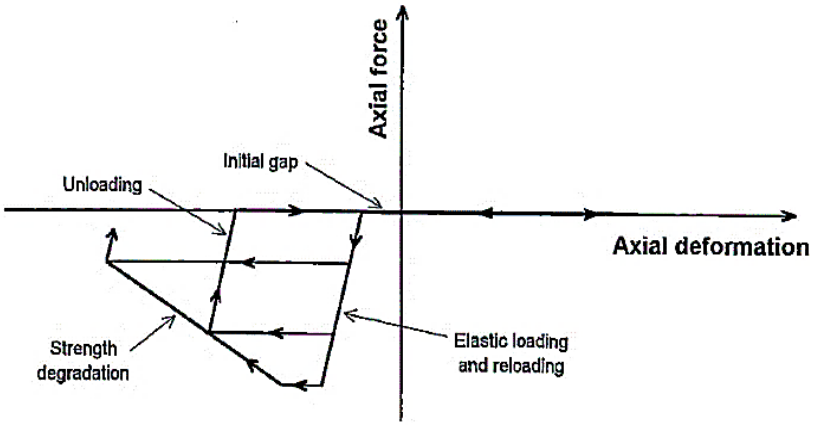

Figure 2.18 - Hysteresis behaviour of the strut model proposed by Doudoumis and Mitsopoulou (1986)

Madan et al. (1997) proposed a smooth force-deformation hysteresis model which accounts for the stiffness degradation, strength degradation and pinching by integrating three separate models (Figure 2.19). The hysteresis was implemented in a macro model composed of two equivalent diagonal struts. The model was verified and used to simulate experimental behaviour of tested masonry infill frame under quasi-static and dynamic time history. The computed force-deformation response may be used to assess the overall structure damage and its distribution to a sufficient degree of accuracy. Thus, the proposed macro-model is better suited for representing the behaviour of infills in nonlinear time history analysis of large or complex structures with multiple components particularly in cases where the focus is on evaluating the inelastic structural response.

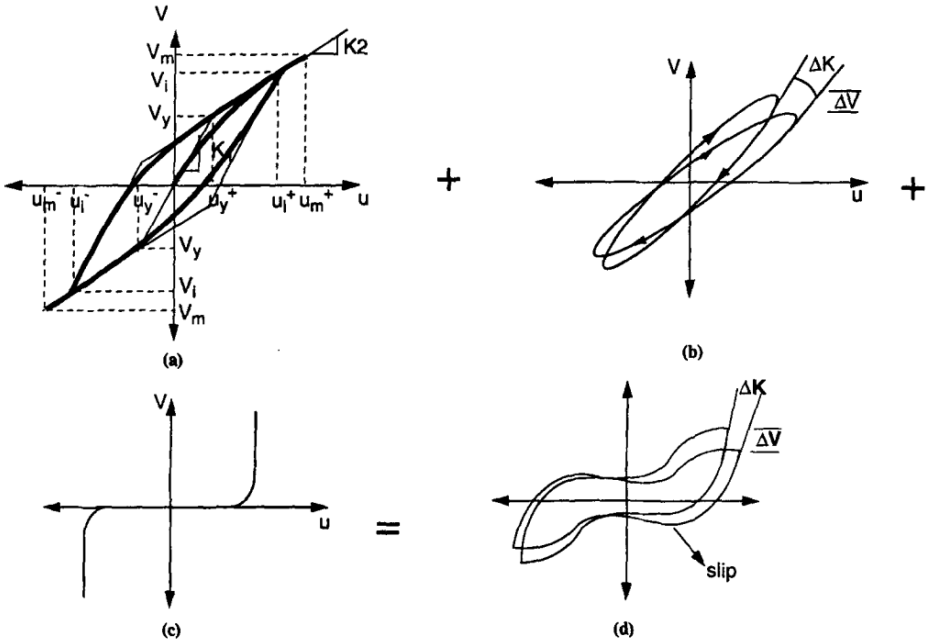

Figure 2.19 - Integrated hysteretic model for degrading pinching elements

(a) Wen-Bouc Hysteresis Model; (b) Hysteretic Model with Stiffness and Strength Degradation; (c) Slip-Lock Model; (d) Integrated Model of Madan et al. (1997)

Saneinejad and Hobbs (1995) proposed an inelastic method for analysis and design of multi-storey steel frames infilled with concrete and masonry walls. The suggested bilinear hysteresis was calibrated on a number of past experimental observation, such as Liauw and Kwan (1985), Mainstone (1971), Stafford-Smith et al. (1969), Stafford-Smith and Riddington (1978) and Wood (1978), which included the initial stiffness (K_0), the Cracking Load (F_{cr}) and the Peak Load (F_{max}) (Figure 2.20). By defining a tri-linear response for the single strut model, the post-capping branch was also included by (Dolšek & Fajfar, 2008) (Figure 2.21). An arbitrary ratio of 1:5 was assumed between the post-capping slope to the initial stiffness of the infill. In this case, the initial stiffness was estimated as a function of shear modulus and configuration of the infill panel, proposed in ECOEST-PREC 8 Report (1996). The cracking load was defined as 60% of the ultimate strength after Zarnic (1997).

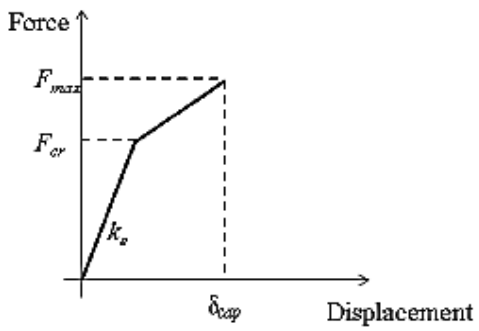

Figure 2.20 - Schematic force-displacement response of the infill strut model proposed by Saneinejad & Hobbs (1995)

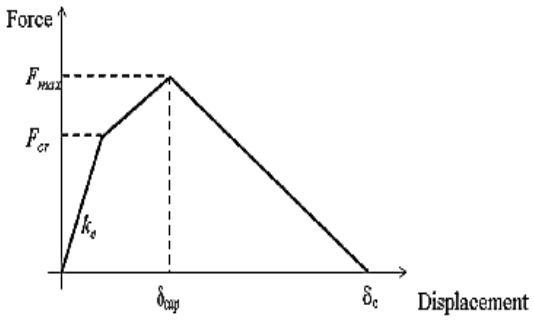

Figure 2.21 - Schematic force-displacement response of the infill strut model proposed by Dolsek & Fajfar (2008)

A compression/tension cyclic relationship was proposed by Crisafulli (1997), which, in addition to the compression envelope and its loading, unloading and reloading rules, features the effects of small inner cycles, tension softening and tension stiffening (Figure 2.22). The variation of strut's cross section is considered as a function of the axial strain experienced by the element. Hence, as the lateral load and consequently deformation increases, any loss of stiffness due to the reduction of the contact length between the frame and the wall panel can be accounted for as the strut area reduces. In addition, for evaluating the shear of infill panel, a hysteresis response is defined for the shear spring following an elasto-plastic rule with variable shear strength (Figure 2.23). This shear strength variation is controlled by a shear-friction mechanism. Hence, the shear strength is calculated considering two different stages; first, the elastic response, which happens before reaching the bond-shear strength, and secondly, the sliding, in which the strength depends on the compressive force of the struts. To avoid large shear values in the sliding stage, the shear strength is limited due to high axial forces in the struts. Moreover, the shear stiffness is assumed to be a fraction, between 50% to 75%, of the total stiffness of the masonry strut. A good agreement was achieved comparing its analytical results to the experimental outcomes, therefore, the refined model was later implemented in the computer programmes Ruaumoko (Carr, 2007) and SeismoStruct (SeismoSoft, 2014) for nonlinear dynamic analysis of infills.

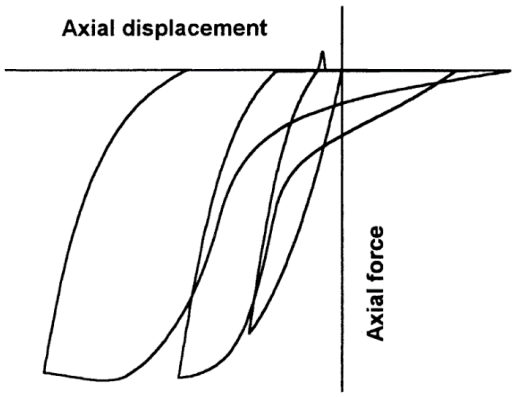

Figure 2.22 - Hysteresis curve and compressive diagonal strut for masonry infill (Crisafulli, 1997)

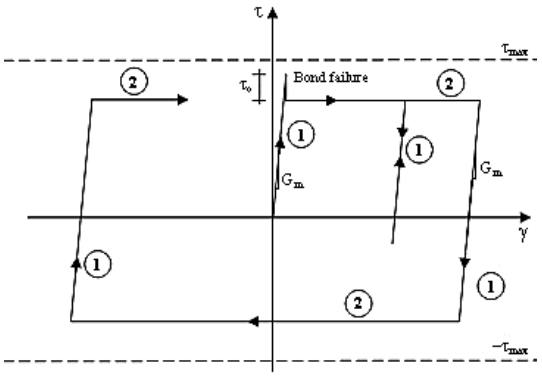

Figure 2.23 - Analytical response for cyclic shear response of mortar joints (Crisafulli, 1997)

The method by Crisafulli (1997) utilised for evaluating the horizontal shear sliding of the infill panel was initially proposed by Leuchars & Scrivener (1976), in which a friction connection was added between the two diagonal struts (Figure 2.24). This allows the model to capture the response of the infilled frame after the occurrence of inclined cracking of the infill panel that potentially may cause damage to both columns of the frame.

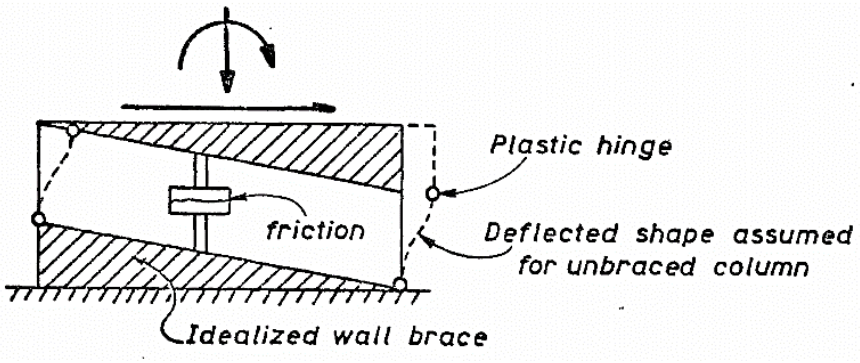

Figure 2.24 - Hypothetical model (Knee Braced Frame Concept) for describing the response of infilled frame subsequent to cracking of the wall

This concept was later modified in Crisafulli and Carr (2007) by implementing a shear spring for replicating the behaviour of the infill following the shear failure of the infill, either along mortar present at equivalent strut stiffness and its' hysteretic response is based on a simplified elastoplastic rule with variable shear strength, representing the elastic response prior to bond-shear failure and after the sliding.

As discussed, similar to other aspects of infilled frame modelling, in case of material hysteresis there are a number of options to choose from. Therefore, selecting the most applicable one can become a challenge and one should be cautious. Moreover, an important point is the calibration of existing hysteresis models to represent the actual behaviour according to the material used for construction of the infill and the frame.

2.6. Conclusions

Recognising fragility and vulnerability functions as the vital components of the performance based seismic assessment, this chapter presented an overview of studies conducted on fragility assessment and seismic performance of bare and infilled steel framed structures through empirical and analytical approaches. Although, a large number of studies have acknowledged the substantial impact of infill panels on the seismic response of framed structures, it is concluded that a very limited number of studies have considered this matter in evaluating the seismic performance and fragility of masonry infilled steel frames. Hence, majority of studies have focused solely on assessing the bare steel frames, while neglecting the infill panels. However, evaluating the vulnerability and life cycle cost of infilled steel frame structures cannot be conducted based on the performance of bare steel frames. Bearing in mind the great exposure of infilled steel frames in various regions with high seismicity, having an applicable and reliable fragility and vulnerability function is of great importance. This can be achieved through numerical simulation of the infilled steel structures and deriving analytical fragility functions.

Considering the potential failure mechanisms observed in infilled frames, different studies have proposed numerical models for simulating the response of the resultant composite system in local and global scale. Reviewing the stated studies, it is evident that replicating the infill panels through equivalent diagonal struts is an established method. Therefore, the seismic performance of infilled steel structures can be numerically assessed as long as the struts' properties are calibrated according to the experimental observations.

However, despite the maturity of the equivalent strut approach, due to the inherent complexity of the structural system and the calibration process, only a limited number of studies have investigated the seismic performance and fragility of full-scale structures and majority have mainly focused on simplified single-storey, single-bay cases. Consequently, there is a major deficiency in seismic vulnerability functions for performance assessment of existing infilled steel frame structures.

In Chapter 3, by raising the stated observations and identified shortcomings, the main objectives of this research study will be defined and accordingly a methodology is proposed to address the introduced objectives following the performance-based seismic assessment methodology.

Chapter 3 Research Scope & Methodology

3.1. Research Objectives

As discussed in Chapter 2, in contrast to reinforced concrete and masonry structures, a relatively fewer number of studies have investigated the seismic vulnerability and life cycle cost of steel framed structures (Liu et al. 2004; Park & Kim 2010). The inherent higher ductility of steel structures has contributed to the commonly held view that these buildings are generally robust and perform well under seismic excitation. However, the observed damage due to past earthquake events, such as 2003 Bam (M_w 6.6) and 2017 Iran–Iraq (M_w 7.3) earthquake, have highlighted the poor performance of low- to mid-rise steel framed structures. The recorded damage has been more intense in case of steel frames with masonry infills, to levels of moderate to heavy damage. The evidence indicates that the presence of masonry infills have actively contributed in structural failure and casualty (Mahen & Grove 1990; Manafpour 2003).

Although, masonry infilled steel frames are commonly constructed in earthquake-prone regions, only a few studies have investigated the seismic vulnerability of such structures, whereas those studies dedicated to evaluating their performance have mainly followed simplified methods with limited detailing (HAZUS, 2003; Kiani et al., 2016). Therefore, for the majority of existing masonry infilled steel frames, limited or no reliable data is accessible to predict their seismic performance and vulnerability. As a consequence of this limitation, throughout the different stages of seismic risk assessment, loss mitigation and disaster planning, the fragility and vulnerability functions derived for bare steel frames are frequently implemented instead of appropriate ones for actual infilled steel frames. This is notwithstanding the fact that, due to the nature of the masonry panels and the resultant composite system, the seismic behaviour of infilled steel frames is significantly different to that of bare steel frames, as discussed in Chapter 2. As a result of this misuse, the evaluated structural performance and associated seismic losses will be inaccurate and misleading. To overcome this shortcoming, appropriate tools and methods should be implemented to generate accurate fragility and vulnerability functions for existing infilled steel frame structures. As performance-based earthquake engineering (PBEE) is gaining more popularity among

earthquake engineers and structural designers for both design and assessment, the necessity for detailed structural models and accurate vulnerability evaluation becomes more apparent as a necessary tool for the correct implementation of PBEE.

Moreover although the concept of equivalent diagonal strut (Stafford-Smith et al., 1969) is widely accepted as a convenient representative of masonry infill panels (Jazany et al., 2013; Kiani et al., 2016; Martinelli et al., 2015), none of the proposed simulating methods have been implemented in modelling and analysing the seismic performance of full scale steel framed structures with masonry infill panels. The majority of numerical studies have particularly focused on evaluating the response of bare moment resisting or braced steel frame in two-dimensional environment and under static and dynamic loading (Asgarian & Ordoubadi, 2016; Kazantzi et al., 2014), while completely ignoring the impact of infills, mainly due to limitations in experimental studies and data calibration. Nonetheless, for an accurate evaluation of the structural performance and seismic vulnerability, it is essential to estimate the overall behaviour of the entire structure under potential earthquake shakings.

Acknowledging the mentioned shortcomings, this study aims to investigate the performance of real case infilled steel framed structures under actual seismic excitation and understand to what extent the vulnerability of such structures is influenced by the presence of infill panels when compared to bare steel frames. Accordingly, the main objectives of this research can be outlined based on a proposed performance-based seismic assessment (PBSA) methodology, following the concepts introduced by the Pacific Earthquake Engineering Research (PEER) Centre (Porter, 2003). The proposed methodology extends beyond evaluating the performance with respect to a single event scenario with a given probability of exceedance in a certain time frame and it investigates the entire life performance of the stated structure.

To this end, the key objectives of this research project are defined as follows:

1. To identify and define index buildings, representing commonly built low- to mid-rise infilled steel frame structures across a designated region, while complying to the prevalent construction arrangement, structural components, material characteristics and code provisions.
2. To develop full scale detailed numerical models of the selected index buildings to an acceptable level of accuracy by replicating the realistic response of critical structural components, such as the masonry infill panels and beam-column connections, following empirical observations and experimental studies.
3. To quantify the seismic performance of the selected infilled steel frames through simplified and advanced numerical methods, in order to understand the applicability

and validity of each method in the specific case and recommend an efficient and effective approach.

4. To define different damage limit states, while considering the impact of the resultant composite system of the infilled frame on the global behaviour of the structure and accordingly quantify distinctive damage thresholds specific to the actual performance of each index building.
5. To develop seismic fragility functions for the defined index buildings, for each of the damage states identified in point 4, by comparing the performance points obtained through state-of-the-art analytical methods, to the damage thresholds defined above.
6. To evaluate the vulnerability of a population of infilled steel frame structures, while considering the distribution of different construction qualities and the actual seismic hazard of the region under study.
7. To estimate the expected life cycle cost (LCC) of masonry infill steel frames, while representing different qualities of construction, based on the obtained analytical fragility functions and following the actual probabilistic seismic hazard assessment (PSHA) of the region under study.
8. To compare and observe the variation in structural performance, vulnerability and life cycle cost of infilled steel frames with the ones evaluated for identical bare steel frame structures, as most design codes and structural engineers presume the building to have comparable performance.

3.2. Research Methodology

The thesis objectives, as stated in Section 3.1, are addressed through a series of steps. The procedure of each step and its intended outcomes are presented in this section. Adopting the performance-based seismic assessment methodology, the applied methodology can be divided into five progressive stages as follows:

- **Defining the Index Buildings**

For this research project, Iran has been selected as the case study, since approximately the entire country is located in one of the most seismically active areas of the world (Tavakoli et al., 1999). As a result, several cities have been greatly affected in past destructive earthquake events since the beginning of the 20th century (Manafpour 2003). Moreover, a considerable number of residential, commercial and public buildings including schools and hospitals are constructed as steel frames with masonry infills. Therefore, the research outcomes can support the ongoing efforts of the country to increase its structural safety and becoming more resilient, as well as being beneficial for the disaster management plans and preparedness.

To characterise the index buildings, a number of detailed drawings of the exiting and newly designed buildings have been collected, covering an extensive population of low- to mid-rise steel framed structures. Accordingly, the most common characteristics have be identified and exploited to develop the index buildings. Investigating the typical structural typologies and characteristics based on available exposure and latest statistical data, a number of index buildings are defined following the local provisions, while representing the common construction practice, prevalent geometry and the accessible materials. The major limitation in this stage is the diversity prevailing in the structural arrangement, construction practices and material properties, which makes it difficult to define suitable index buildings. Therefore, the parameters most influential on the seismic response have been identified and combined with a focus on the most common recurring structural assemblies found in the field:

- Number of storeys; limited to low- and mid-rise structures up to 8 storeys,
- Plan geometry; simple plans defined by varying the number and dimension of bays and frames, assuming modest plan irregularity,
- Steel framing system; simple gravity frame and moment resisting frame according to the local code of practice,
- Steel frame material properties and section size, as per most common use in the region, according to literature and field observations,
- Participation of infill panels in structural response (i.e. Bare Steel Frame or Infilled Steel Frame),
- Masonry infill material properties, as per most common use in the region, according to literature and field observations,
- Types of joint connections, as per most common use in the region, according to literature and field observation.

To have a realistic representation of the masonry material, the most common masonry infills being used in the Iranian construction industry have been identified. Referring to the available literature, the outcome of experimental studies (Flanagan & Bennett, 2001; Tasnimi & Mohebkhah, 2011) are employed to calibrate the hysteresis curve of the selected macro model simulating the infill panels according to Crisafulli and Carr (2007) approach. Therefore, the calibration of masonry infills is limited to availability of experimental data, which restricts the considered infill types. However, this is an opportunity to identify the most influential factors in calibrating the infill model and their sensitivity, which can later assist the calibration process of other infill types.

A similar approach is followed for the most common beam-column connection observed in the region under study. The characteristics of the connection is simulated by adopting a

simplified response curve defining the behaviour of a link element (Leon, 1990). It should be noted that as the selected buildings are simulated in three-dimensions and considering their scale, having a link element at every beam-column connection may induce numerical convergence difficulties and increase the analysis time substantially.

The considered structural variety gives the opportunity to define index buildings representing a substantial proportion of the existing steel frame buildings of the region under study, which is a critical condition for realistic seismic risk assessment. Furthermore, this variation can assist in generating identical buildings with different qualities of construction, each representing a case of poor, typical and good quality following the existing building distribution, as proposed in the GEM Guidelines (D'Ayala et al., 2015).

This step addresses objective No. 1 as stated in 3.1 and is discussed in more detail in Chapter 4.

- **Modelling & Analysing the Index Buildings**

In order to verify the accuracy and feasibility of the modelling and the analysis procedure, as well as identifying its shortcomings, initially all steps are conducted on a single index building and later the most appropriate procedure has been implemented on the rest of the selected index buildings. To this end, focusing on the region under study, a large-scale estate development project is identified. Among the various structural arrangements observed, a representative mid-rise infilled steel frame structure is modelled and analysed in full scale through fibre-based finite element method. Accessing the detailed drawings and design calculations of the building, different aspects of the structural components are simulated, including the masonry infills, steel bracings and beam-column connections. This gives the opportunity to investigate the impact and extent of masonry infills and other structural components on the seismic response of the building while comparing the outcomes to an identical bare frame.

Owing to the recent advancements in computational power and modelling programmes, analysing the seismic behaviour of full scale structures with high details and assorted components is possible. Furthermore, utilising the available experimental data on the cyclic behaviour of various material and structural components such as beam-column connections can assist in calibrating components to generate more realistic models. However, as mentioned previously, this process relies heavily on availability and relevance of the experimental studies conducted on the structural components of interest, which in return can limit the considered variety of material characteristics and component arrangements.

Having the models set, the correlation between variation in simulating the construction detailing and the structural response are quantified by means of non-linear static (e.g. pushover) and dynamic analysis (e.g. Cloud and Multiple-stripe Analysis) of multi-degree of freedom (MDoF) systems using finite element software. The obtained seismic responses are compared to the simplified ones suggested in guidelines such as HAZUS (2003), commonly utilised in seismic risk assessment studies, to demonstrate the need for purposely generated capacity and fragility functions.

This step addresses objectives No. 2 and No. 3 as stated in 3.1, while the details and assumptions considered throughout the modelling and analysis process are discussed in Chapter 5.

- **Defining the Damage Limit States**

The seismic fragility, vulnerability and loss assessment of structures are highly sensitive to the description of the damage limit states and the employed thresholds defining different states of the building (D'Ayala et al., 2015). As discussed in Chapter 2, the structural damage states and thresholds of steel structures are commonly specified relying on pre-defined descriptions and values implied in guidelines such as FEMA 356 (2000), HAZUS (2003) and ASCE/SEI 41 (2017). These guidelines are primarily based on empirical and judgemental observations or are established using simplified numerical analysis of structures designed and constructed following the American practice and material properties. Furthermore, the suggested thresholds are intended for a wide population of buildings, categorised solely based on their height range (e.g. low-, mid- and high-rise), lateral resisting system (e.g. Moment Resisting Steel Frame, Braced Steel Frame), and code compliance. As there is no associated analysis of dispersion of these thresholds, it is impossible to determine whether they are applicable to the index buildings studied herein.

Therefore, in this study, by defining adapted damage limit states which acknowledge the influence of the masonry infill panels as well as the contribution of the steel frame, tailored damage thresholds are allocated to each of the selected index buildings. The thresholds are set based on the overall nonlinear response of the entire structural system under both seismic and gravity loadings, while considering the available experimental observations and the response of individual structural components. However, due to lack of detailed empirical observations on various damage states of infilled steel frames, validating the implemented thresholds with real case structures and under different scenarios is not totally feasible.

This step addresses objective No. 4 as stated in 3.1 and the process of defining damage states and allocating thresholds is discussed in more detail in Chapter 5 and Chapter 6.

- **Developing Analytical Seismic Fragility Functions**

Fragility functions are extensively used for multiple purposes, for instance loss estimation (Pei & van de Lindt, 2009), structural performance evaluation (Astriana et al., 2017), assessment of structural damage and collapse risk (Eads et al., 2013), design checking (DesRoches & Padgett, 2012), evaluation of the effectiveness of retrofit measures (Güneyisi & Altay, 2008), etc. To this end, the seismic performance of the selected index buildings is determined through less computationally expensive and time consuming simplified approach, such as the N2 method (Dolsek & Fajfar, 2005) and FRACAS (Rossetto et al. 2016), as well as the more time intensive advanced dynamic methods, such as Cloud Analysis (Jalayer, (2003); Baker, (2006)) and Multiple-Stripe Analysis (Jalayer & Cornell, 2009). This gives the opportunity to understand whether simplified methods are able to estimate the performance of infilled steel frames to an acceptable degree of accuracy or more advanced methods are necessary to obtain sufficient reliability of the process.

For the fragility assessment, various suites of real ground motions are selected comprising global events to account for the aleatory uncertainty due to record-to-record variability given the intensity. To make sure the selected suite is well representative of the region's hazard characteristics, each suite is compared to the code based elastic response spectra proposed for the location. Earthquake record selection for nonlinear analysis is a challenge and has been the main topic of many studies (Bommer & Aceved, 2004; Iervolino & Cornell, 2005; Katsanos et al., 2010). For this study, the ground motion suites are selected in a way that the same suite can be employed in the analysis process of all of the considered index buildings with distinct seismic characteristics.

The structural seismic performance is measured and presented in terms of the applied earthquake intensity measures (IM) and their corresponding structural response, known as engineering demand parameter (EDP). The obtained performance points are compared against different damage thresholds and the analytical fragility functions for each building is derived by utilising the most applicable regression technique proposed by different studies (Baker, 2015; Shinozuka et al., 2000).

This addresses objective No. 5 as stated in 3.1 and is discussed in detail in Chapter 6.

- **Estimating the Seismic Vulnerability & Life Cycle Cost**

Focusing on the index building define based on a real case estate-development, by modifying its structural characteristics, a number of cases with different seismic performance are generated. Each model represents a different quality of construction, while all are categorised under the same typology (D'Ayala et al., 2014). Incorporating the construction quality in the

structural vulnerability, results in a more realistic structural and non-structural loss estimation as the actual distribution of structural capacity can be evaluated. In the absence of a detailed exposure database, this is deemed a valid approach.

The seismic vulnerability and associated monetary losses of each index building and construction quality level is estimated by utilising the obtained analytical fragility functions, the latest seismic hazard data of the location under study, as well as the exposure profile of the selected index buildings. Hence, the mean damage ratio under various levels of earthquake intensities can be estimated (ASTM E-2026, 1999). The total repair cost is then projected for the earthquake intensities with different probabilities of occurrence choosing the four return periods of 75, 475, 975 and 2475 years to be consistent with the local design codes and practice. Additionally, the anticipated cost over the expected life time of the building (i.e. 50 years) is estimated through life-cycle cost analysis (LCCA) principles (Wen & Kang, 2001). The LCCA can be a good indicator of the seismic performance as it comprises both seismic hazard and the structural vulnerability over the considered life period. Different aspects of the cost analysis including the repair cost, rental loss and relocation as well as the cost of injury and fatality are incorporated in this analysis.

Associating the obtained seismic performance in terms of monetary losses and life cycle cost can assist in further understanding the impact of masonry infill panels on different structural arrangements of the steel framed buildings.

A challenge in this stage relates to the availability of detailed probabilistic seismic hazard assessment (PSHA) of the studied location, which plays a crucial role in determining realistic measures of the expected losses and life cycle cost. Another challenge is due to uncertainties involved in estimating the cost components such as the basic cost of repair, loss of content, etc.

This addresses objective No. 6 and 7 as stated in 3.1 and is discussed in detail in Chapter 7.

- **Comparing Results of Infilled Steel Frame with Bare Steel Frame**

Throughout the discussed stages, the results obtained for the infilled steel frames are compared to the outcomes of their identical bare steel frames. As the infill panels are commonly ignored in design and analysis of steel structures, it is important to measure the resultant diversity between the simplified bare frame and the cases in which the infill's impact are simulated. Various aspects of the analysis, including the nonlinear static pushover curve, damage state thresholds, performance points and their resultant fragility functions are compared and discussed. In Chapter 7 of this study, the vulnerability in terms of monetary losses and the life

cycle cost of an identical bare steel frame are assessed and compared to the infilled steel models representing different qualities of construction and distribution.

This addresses objective No. 8 as stated in 3.1 and is discussed throughout Chapters 5, 6 and 7.

The findings can be utilised to improve the assessment guidelines or to address the mitigation and strengthening issues of existing buildings if necessary. Additionally, the generated fragility functions can help enrich the limited library of existing functions dedicated to both bare and infilled steel frame buildings, which are of great importance for insurance valuation, as well as managing disasters. Moreover, this will allow improving the Global Earthquake Model (GEM) guideline on analytical vulnerability assessment, the current state of the art, as this kind of structural system has not been considered explicitly (D'Ayala et al., 2015).

3.3. Methodology Framework

The discussed methodology stages can be summarised into a roadmap, following a similar format proposed in GEM guidelines for analytical vulnerability assessment (D'Ayala et al., 2015) and the PEER methodology of performance-based seismic assessment (Porter, 2003). The Framework illustrated in Figure 3.1, gives an overview of the discussed process and demonstrates the relationship between different stages.

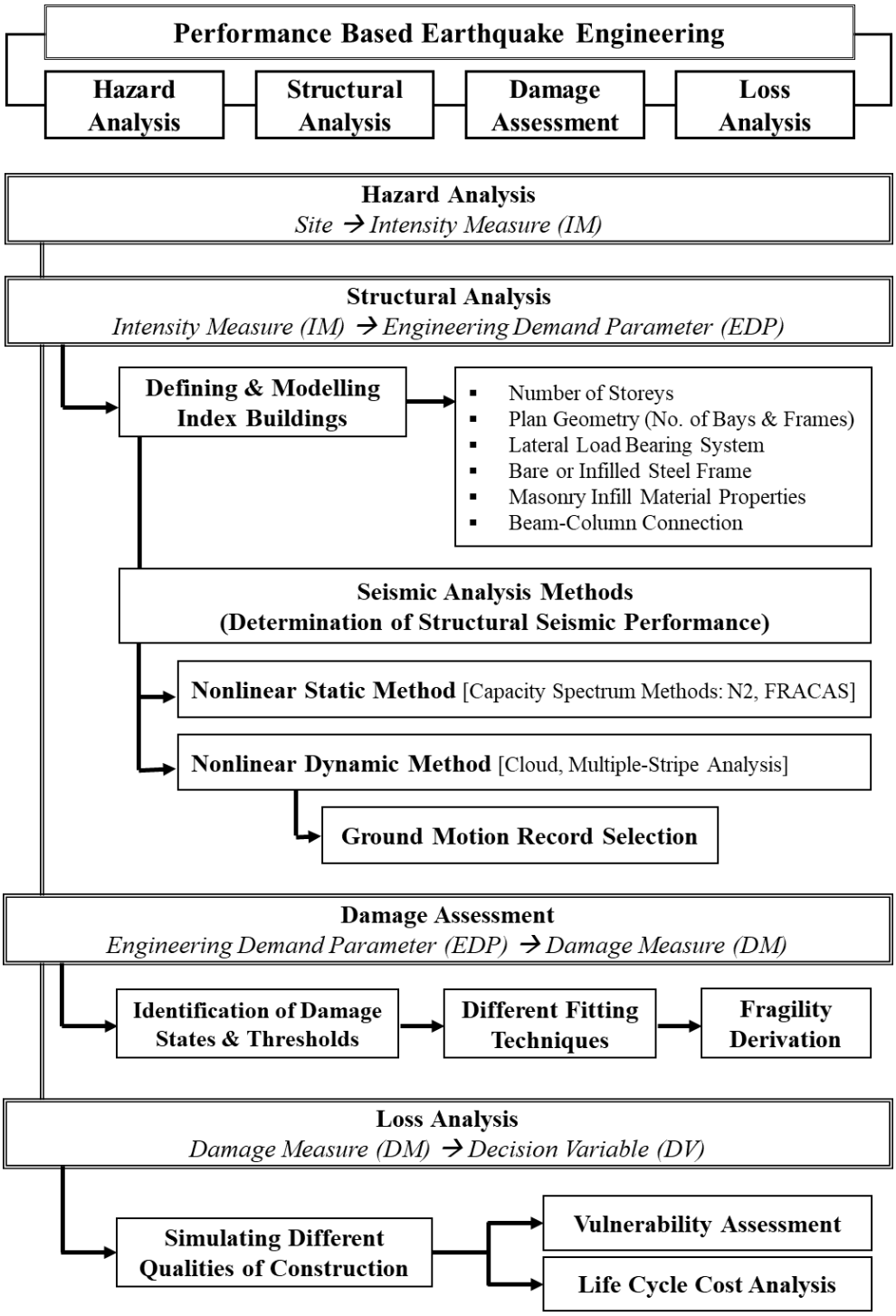

Figure 3.1 - Methodology framework

3.4. Conclusions

Identifying the existing shortcomings in seismic performance and vulnerability evaluation of infilled steel frames, the main aim of this study along with a number of objectives to be achieved are introduced. To address each of the objectives, a series of steps are proposed, for which the procedure and the intended outcomes are presented, as well as the possible challenges. Adopting the performance-based seismic assessment methodology, a framework is proposed indicating the different methods applied at each stage.

In the next chapter (Chapter 4), by referring to the seismicity of a region and the extent of its structural vulnerability, a location is selected and justified as the case study. Accordingly, a number of index buildings are introduced, representing an acceptable range of existing infilled steel frames with different arrangements and seismic characteristics. The index buildings are designed and modelled, while their seismic performance and vulnerability is assessed through different method in the subsequent chapters (Chapter 5, 6 and 7).

Chapter 4 Exposure & Index Building Definition

4.1. Introduction & Motivations

This chapter discusses the motives behind the selection process of index buildings, representing the steel framed structures of a particular region, for the seismic fragility and vulnerability assessment. The history of the region's earthquake activities will indicate the extent and the significance of its seismic hazard. Furthermore, an overview of the seismic code evolution will indicate the variation expected in the building stock. Referring to the conducted statistical studies on the region under study and available data, a number of sample low- to mid-rise residential buildings have been introduced, featuring variations of common materials, geometric arrangements, applied loadings and design approaches.

The collision among the Iranian, the Arabian and the Eurasian plates on the central part of the Alpine-Himalayan orogenic belt, makes the Iranian plateau one of the most seismically active regions of the globe. As a result, the country of Iran has been the subject of several destructive seismic events throughout its history and since 1900, at least 126'000 fatalities have been caused by earthquakes (Berberian, 2014). Table 4.1 presents the significant earthquakes recorded in Iran since 1900, including the extent of ground shaking as well as the number of estimated casualty and injury.

Table 4.1 – Earthquake events of Iran (1900-2017) (Berberian, 2014; Yekrangnia et al., 2017)

Year	Month	Day	Location / Event	Depth (km)	M_W	Casualty	Injury	Shaking*
1909	01	23	Silakor fault	-	7.3	5500	-	Severe
1923	05	25	Kajderakht,Torbat	-	5.5	2219	-	Severe
1923	06	17	Torbat-e-Heydarie	-	-	1000s	-	Moderate
1929	05	01	Kopet-Dagh	22	7.2	3257	many	Extreme
1930	05	06	Salmas	17	7.3	2514	-	Severe
1932	05	20	Torbet-Kheydariy	12	5.4	1070	-	Severe
1957	07	02	Mazandaran	17	7.1	1200	10000s	Severe
1957	12	13	Farsinaj fault	-	7.2	2000	many	Severe
1962	09	01	Buyin-Zahra	25	7.2	12225	2776	Extreme
1968	08	31	Dasht-i-Biyaz	13	7.3	15000	1000s	Extreme

Table 4.1 – Earthquake events of Iran (1900-2017) (continued)

Year	Month	Day	Location / Event	Depth (km)	M_w	Casualty	Injury	Shaking*
1972	04	10	Ghir	-	6.8	5010	1710	Extreme
1976	11	24	Muradiye	36	7.3	3900	many	Severe
1977	04	6	Naghan	33	6.0	348	200	Severe
1978	09	16	Tabas	33	7.4	18220	many	Moderate
1981	06	11	Kerman	33	6.7	3000	1000s	Extreme
1981	07	28	Kerman	33	7.1	1500	1000	Severe
1990	06	20	Manjil-Rudbar	19	7.4	40000	60000	Extreme
1997	02	28	Ardebil	10	6.1	1100	2600	Severe
1997	05	10	Qayen,Birjand	10	7.3	1572	2300	Severe
2003	12	26	Bam	10	6.6	10000s	10000s	Extreme
2005	02	22	Zarand	16	6.4	612	1411	Severe
2006	03	31	Borujerd	10	6.1	70	1418	Severe
2012	08	11	Ahar-Varzaghan	9	6.4	306	3037	Severe
2013	04	13	Saravan	82	7.7	35	117	Very Strong
2017	11	12	Iran-Iraq (Kermanshah)	19	7.3	630	8435	Severe
2017	12	20	Tehran	7	5.2	2	97	Strong

*Modified Mercalli Intensity (MMI) Scale:
V: Moderate, VI: Strong, VII: Very Strong, VIII: Severe, IX: Violent, X: Extreme

Besides being among the most seismic active regions of the world, according to the available census data (SCI, 2016), in the past forty years the major cities of Iran observed a swift population growth, followed by an uncontrolled surge in housing demand. This resulted in a substantial surge in the construction industry, making it one of the key drivers of the country's economic sector. While, in contrast to other sectors, the housing industry has been subjected to lower state controls. Thus, poor construction quality and lack of building code enforcement were just some of the inevitable consequences and eventually an amplifying factor of seismic vulnerability. It was just until the 1990 Manjil-Rudbar earthquake (M_w 7.4) in northwest Iran, during which 40'000 people lost their lives and more than 100'000 building were demolished, that the government planned to raise the people's awareness and enforce the building code in some major cities. Consequently, the proportion of none or low engineered structures have dropped considerably in the past three decades. For instance, the fraction of unreinforced masonry buildings has dropped from 90% to 23% between years 1990 and 2010, while steel and concrete buildings saw a substantial growth from 3% to 74% according to building inventory data of the Statistical Centre of Iran (SCI, 2016). According to the regional census data, in 2016 about 22% of the submitted right to build requests were registered for steel framed structures.

In recent years, motives such as governmental support of so called industrially-produced buildings, manufactured mainly off-site, with benefits such as ease and speed of erection and relatively higher quality of construction, have attracted more contractors to build steel framed structures. While the share of steel frames is about 33.1% for the entire country, in major cities, such as Tehran and Tabriz (Figure 4.1), the proportion reaches up to 64% with a steep growth forecast (SCI, 2016).

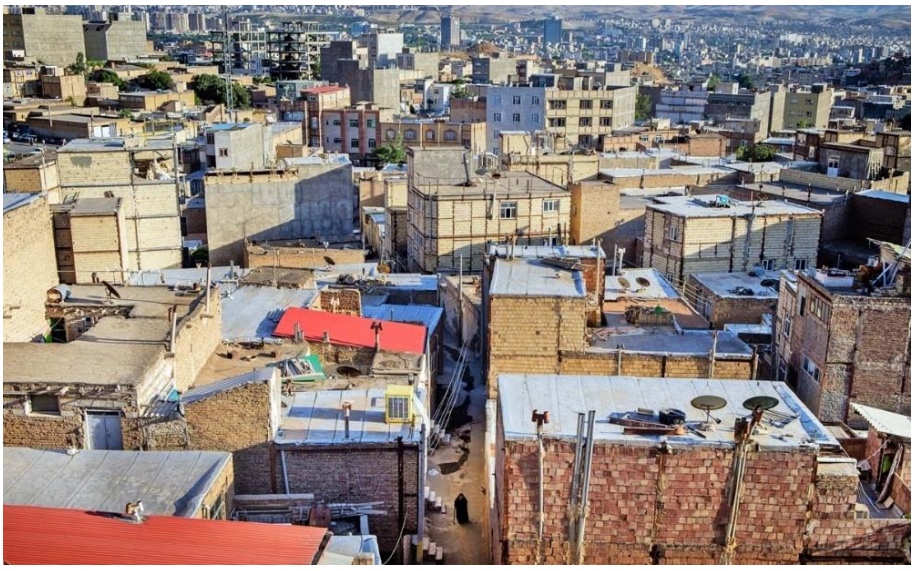

Figure 4.1 – An undeveloped district near city of Tabriz - Iran.
Majority of existing and newly designed structures are built with steel frames and masonry infills

It is evident that steel structures consist a large proportion of the prevailing and newly designed buildings in Iran. Therefore, considering the high occurrence probability of damaging seismic events in the region under study as well as the high exposure of steel framed structures, a reliable vulnerability estimation of the stated buildings is of great importance. Understanding the actual deficiencies and fragilities of the region's steel buildings can assist in refining the current design codes and mitigating the buildings if necessary. Moreover, the assessed seismic vulnerability can contribute to the country's pre- and post-disaster planning and management.

4.2. Seismic Code Evolution

A source to evaluate the performance and a reference for developing appropriate numerical models of the existing buildings is the provisions given in the local design codes. The Iranian buildings safety regulations against earthquake was first introduced in 1969. But it was in 1988 which the 1st Iranian Seismic Code 2800 (ISC) was officially established after the 1978 Tabas (M_w 7.4) and 1977 Naghan (M_w 6.0) earthquakes. However, the authorities did not enforce it for the new buildings and never required the existing buildings to be retrofitted or improved accordingly, until the 1990 Manjil-Rudbar earthquake (M_w 7.4). Years later, in 1993, serious deficiencies in seismic requirements led to the publication of the 2nd edition,

known as “Standard No. 2800”, duplicating the American Uniform Building Code of 1991 (UBC, 1991).

The 3rd edition, issued in 2007 after the 2003 Bam earthquake (M_w 6.6), was a major update to the Iranian seismic code in terms of seismic load estimation and design criteria provisions (BHRC, 2007). This code has been widely employed in design and construction of recently built reinforced concrete and steel framed structures. Generally, the provisions defined in this edition are very similar to those of AISC’s seismic provisions for structural steel buildings (AISC, 1997) and FEMA’s seismic design criteria for new moment-resisting steel frame construction (FEMA-350, 2001). The basic concepts proposed by the code can be summarised as followings:

- Minimising mortality by keeping the building stable under severe earthquake.
- Decreasing structural damage due to earthquakes with low to moderate intensities in common buildings (e.g. residential, commercial).
- Preventing structural damage due to earthquakes with low to moderate intensities in important buildings (e.g. hospitals).

The code describes a major (severe) earthquake or “Design Level Earthquake”, as the ground motion with less or equal to 10% probability of occurrence in 50 years, the service life time of the building. While, low to moderate seismic ground motions or “Service Level Earthquake” is the ground motion that has a 99.5 percent probability of not being exceeded in 50 years life time of the building. Moreover, the code recommends equivalent static and dynamic analytical procedures, including response spectrum analysis, linear and nonlinear time history for estimating the seismic demand of structures based on their regularity and importance. The equivalent static analysis is allowed for regular structures with less than 50m height or in case of irregular ones up to 18m, while all other cases should be designed using dynamic approaches.

The latest edition of the Iranian seismic code, published in November 2015, beside some minor improvements in the general provisions, the code provides detailed recommendations for nonlinear static and dynamic structural analysis approaches. Further discussion on the development and improvements of Iran seismic code are presented in Faizian and Ishiyama (2004), Keyvani Boroujeni and Sadeghazar (2008), Andisheh and Amiri (2010) and Imashi and Massumi (2011).

4.3. Defining Index Buildings

The wide variety observed in defining criteria of existing structures, such as material, design, structural and architectural integrity introduces a major complexity in evaluating the seismic performance. Buildings with diverse structural systems, age, material, arrangement, construction technique and quality makes it nearly impossible to have an authentic dataset of fragility and vulnerability functions indicating each and every one of the standing buildings. Therefore, an initial step for conducting analytical fragility derivation is to define relevant samples of the buildings population, known as index buildings, which can describe the principal characteristics of the region's building stock. An index building is a sample of a number of representative buildings, defined to signify the overall population by capturing the distribution of the most important characteristics (D'Ayala et al., 2015). These characteristics should be chosen amongst the structural properties that have the most influence on the structural response during seismic excitation.

In this study, the index buildings have been introduced based on an existing real case, as well as a number of simulated buildings, representing the most common characteristics identified among the population of typical steel framed buildings of the region under study. In case of the real building, the structural characteristics have been defined based on a mid-rise residential building, which is part of a relatively new government led campaign of large-scale estate developments in Iran. Therefore, a considerable number of such steel framed buildings with identical specifications are constructed in numerous locations throughout the country. Detailed discussion on characteristics of these buildings is presented in Chapter 5.

The rest of the index buildings are established based on the most conventional characteristics and comprising elements, identified to have effective impact on the structures' seismic response, as stated in studies and guidelines such as HAZUS (2003), D'Ayala et al. (2015) and Kiani et al. (2016). The common properties and their extent are identified by accessing the construction drawings and design documents of the existing and newly designed buildings, as well as the opinion of the local engineers and experts of the region under study. Additionally, majority of available studies conducted on the seismic performance of the regional steel frames, despite their simplifications, have acknowledged the most important structural elements to consider and their extent of impact, (e.g. Asgarian et al., 2010; Asgarian and Ordoubadi, 2016; Farsangi et al., 2014; Kazemi et al., 2013; Kiani et al., 2016; Majd et al., 2012; Sarokolayi et al., 2013). Moreover, the data collected through visual inspections of regional pre- and post-earthquake events can assist this process (e.g. Manafpour, 2003; Mehrabian and Haldar, 2005; Yekrangnia et al., 2017; Zahrai and Heidarzadeh, 2004).

Defining new index buildings based on common structural characteristics, instead of modelling a specific existing building, gives the opportunity to include a broader cohort of buildings, categorised under the same structural typology. As discussed in Chapter 2, due to the prevailing shortage in fragility and vulnerability functions, the seismic damage assessment is obliged to implement any available function with the closest structural resemblance. For instance, functions introduced in guidelines, such as HAZUS (2003) are frequently applied in Iran as long as the elevation and the lateral resistance system of the structures correspond, regardless of the evident disparity in construction practice and material. On the other hand, neglecting the fundamental factors such as the plan arrangement will increase the prevailing uncertainty and may result in imprecise conclusions. Therefore, the defined index buildings may reduce the resultant uncertainties up to certain extents by considering a larger range of structural characteristics, based on the common practice of the region under study. Overall, the typical considered properties included the following:

- Design approach,
- Strength of material,
- Number of storey,
- Storey height,
- Number of bays in each direction,
- Dimension of bays,
- Members' size and sections,
- Floor slab properties,
- Connection types,
- Contribution of masonry infill panels,
- Loading type and values,
- Loading combinations.

Considering the variation domain for each of the mentioned properties, the most common values, range, arrangements and characteristics have been identified and employed to define the new index buildings. Accordingly, 33 index buildings have been introduced, ranging from 2 to 8 storeys, including bare and infilled frames. Three of the index buildings are defined after the mentioned real case, two of which are infilled frame with two different masonry materials and one represents a bare frame. In general, the defined index buildings represent well the stock of low- to mid-rise steel frame structures with distinctive seismic performance, either existing or currently being built in Iran, as well as other countries in the Middle-East.

Regarding the structural system, the index buildings were designed as simple gravity frames (SGF) or moment resisting frame (MRF). The SGF buildings are designed without accounting

for the lateral load effect, these can represent the existing low or non-engineered buildings. The MRF structures are designs following the provisions of the regional code and the common practice, representing the engineered buildings. Considering the age of existing steel structures in the region, majority of them can be categorised as engineered buildings (SCI, 2016). Furthermore, given the boom in the construction industry, it makes sense to study the seismic fragility and vulnerability of the future building stock. The influence of steel bracings has only been considered for the structure designed after a real case building. The impact of concentric bracings on the modal characteristics, strength, stiffness and ductility of the structure are discussed in detail by introducing different hypothesis and arrangements on the real case building in Chapter 5. The main reason of this demonstration is to have a better understanding of the masonry infill panels' effect, as infill panels replicate a similar mechanism to braces through the seismic numerical analysis.

Although the focus of this study is on low- and mid-rise structures, an 8-storey building with typical characteristics has also been designed and analysed. According to HAZUS (2003) an 8-storey structure represents a semi-high-rise while, FEMA 351 (2000) considers an 8-storey steel frame as mid-rise and any building with 12 storeys or more is categorised as high-rise. On the other hand, the Iranian seismic code (BHRC, 2007) considers building with 15 storey and more or exceeding 50 metres in height as high-rise. This arrangement of structure is not as common as the other cases considered, especially for the case of bare gravity frame, which does not comply with the design codes and was mainly included for comparison reasons.

Two types of frequently used masonry infill material are utilised in this study, the Solid Clay Bricks (SCB) and Hollow Clay Blocks (HCB). For each of the masonry infill panels, a case of solid panel and one with central window opening is considered. The structural properties of each masonry material are further discussed in Chapters 5 and 6, as the calibrated process of the designated infill numerical models with the experimental observations are discussed in more details.

It should be noted that during the design stage, the intention was to keep a consistency in the general arrangement of the structures. For instance, the positioning of infills, either solid or with window opening, as well as the slabs' load distribution are kept the same in structures with identical plan and different number of storeys. A schematic of the general arrangement of the defined index buildings in three dimensions is show in Figure 4.2.

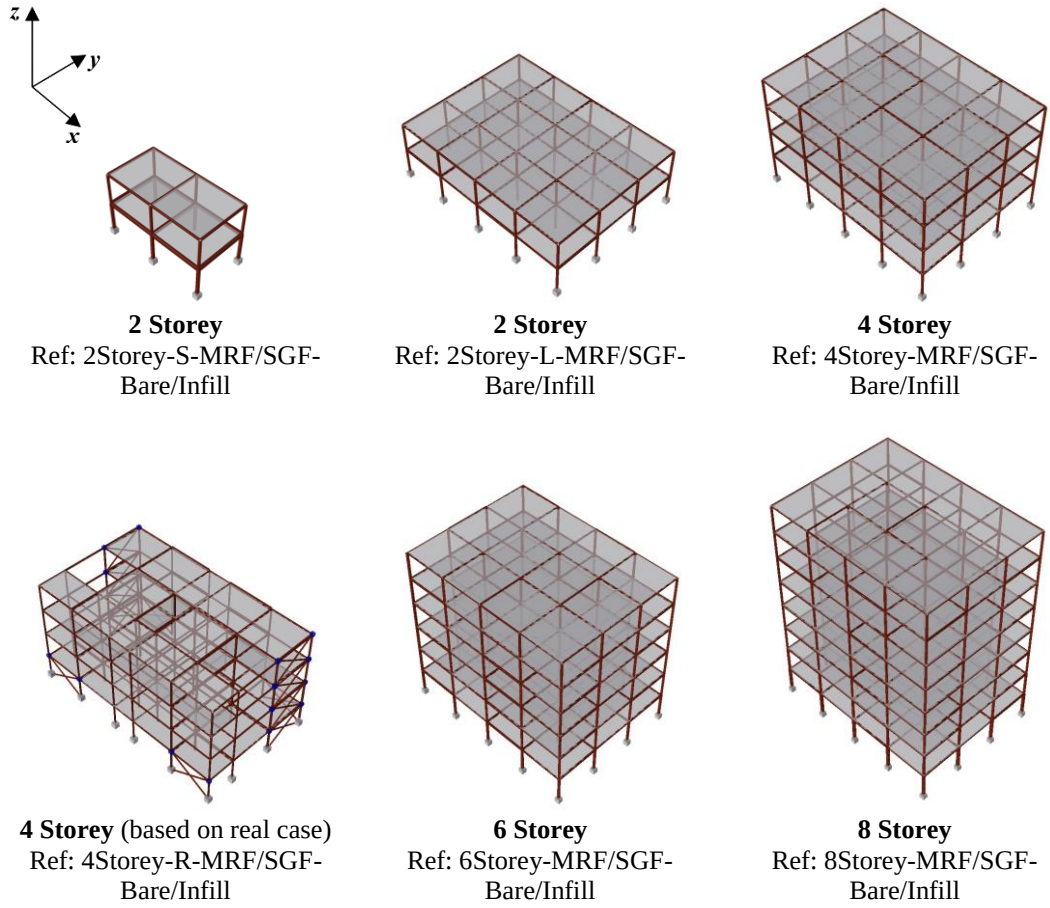

2 Storey
Ref: 2Storey-S-MRF/SGF-Bare/Infill

2 Storey
Ref: 2Storey-L-MRF/SGF-Bare/Infill

4 Storey
Ref: 4Storey-MRF/SGF-Bare/Infill

4 Storey (based on real case)
Ref: 4Storey-R-MRF/SGF-Bare/Infill

6 Storey
Ref: 6Storey-MRF/SGF-Bare/Infill

8 Storey
Ref: 8Storey-MRF/SGF-Bare/Infill

Figure 4.2 – General arrangment of defined index buildings

The general characteristics of the defined index buildings are presented in Table 4.2, including the number and dimensions of storeys and bays, as well as the structural system and the masonry material used for the infill panels. It should be noted that none of the define index buildings have elevator or staircase cores made of reinforced concrete shear walls.

Table 4.2 – General characteristics of the selected index buildings

#	No. of Storey	Structural System*	Infill Material	Bay No. X-dir.	Bay Size X-dir. (m)	Bay No. Y-dir.	Bay Size Y-dir. (m)	Floor Height (m)
1	2	MRF	-	2	5.0	1	5.0	3.5
2	2	SGF	-	2	5.0	1	5.0	3.5
3	2	MRF	Solid Clay Brick	2	5.0	1	5.0	3.5
4	2	SGF	Solid Clay Brick	2	5.0	1	5.0	3.5
5	2	MRF	Hollow Clay Block	2	5.0	1	5.0	3.5
6	2	SGF	Hollow Clay Block	2	5.0	1	5.0	3.5
7	2	MRF	-	4	5.5	3	5.5	3.5
8	2	SGF	-	4	5.5	3	5.5	3.5
9	2	MRF	Solid Clay Brick	4	5.5	3	5.5	3.5
10	2	SGF	Solid Clay Brick	4	5.5	3	5.5	3.5
11	2	MRF	Hollow Clay Block	4	5.5	3	5.5	3.5
12	2	SGF	Hollow Clay Block	4	5.5	3	5.5	3.5

Table 4.2 – General characteristics of the selected index buildings (continued)

#	No. of Storey	Structural System*	Infill Material	Bay No. X-dir.	Bay Size X-dir. (m)	Bay No. Y-dir.	Bay Size Y-dir. (m)	Floor Height (m)
13	4	MRF	-	4	5.5	3	5.5	3.5
14	4	SGF	-	4	5.5	3	5.5	3.5
15	4	MRF	Solid Clay Brick	4	5.5	3	5.5	3.5
16	4	SGF	Solid Clay Brick	4	5.5	3	5.5	3.5
17	4	MRF	Hollow Clay Block	4	5.5	3	5.5	3.5
18	4	SGF	Hollow Clay Block	4	5.5	3	5.5	3.5
19	4	MRF	-	5	varies	3	varies	varies
20	4	MRF	Solid Clay Brick	5	varies	3	varies	varies
21	4	MRF	Hollow Clay Block	5	varies	3	varies	varies
22	6	MRF	-	4	5.5	3	5.5	3.5
23	6	SGF	-	4	5.5	3	5.5	3.5
24	6	MRF	Solid Clay Brick	4	5.5	3	5.5	3.5
25	6	SGF	Solid Clay Brick	4	5.5	3	5.5	3.5
26	6	MRF	Hollow Clay Block	4	5.5	3	5.5	3.5
27	6	SGF	Hollow Clay Block	4	5.5	3	5.5	3.5
28	8	MRF	-	4	5.5	3	5.5	3.5
29	8	SGF	-	4	5.5	3	5.5	3.5
30	8	MRF	Solid Clay Brick	4	5.5	3	5.5	3.5
31	8	SGF	Solid Clay Brick	4	5.5	3	5.5	3.5
32	8	MRF	Hollow Clay Block	4	5.5	3	5.5	3.5
33	8	SGF	Hollow Clay Block	4	5.5	3	5.5	3.5

[+] MRF: Moment Resisting Frame; SGF: Simple Gravity Frame

The index buildings are classification according to the suggested categories of HAZUS (2003) and GEM Building Taxonomy v.2.0 (Brzev et al., 2013) (Table 4.3). Both HAZUS and GEM taxonomy identify buildings according to their structural material and lateral force resisting system, while GEM taxonomy considers more defining elements with higher detailing. Further discussion on the design stages and structural characteristics of each index building is presented in the next section (4.4).

Table 4.3 – Index buildings typology

#	Index Building Reference	HAZUS Typology*	GEM Typology[+]
1	2 Storey - S - MRF - Bare	S1H Low-Rise	S/LFM+DUC/HEX:2/PLFR
2	2 Storey - S - SGF - Bare	S1L Low-Rise	S/LFM+DNO/HEX:2/PLFR
3	2 Storey - S - MRF - Infill SCB	S5H Low-Rise	S/LFINF+DUC/HEX:2/PLFR
4	2 Storey - S - SGF - Infill SCB	S5L Low-Rise	S/LFINF+DNO/HEX:2/PLFR
5	2 Storey - S - MRF - Infill HCB	S5H Low-Rise	S/LFINF+DUC/HEX:2/PLFR
6	2 Storey - S - SGF - Infill HCB	S5L Low-Rise	S/LFINF+DNO/HEX:2/PLFR
7	2 Storey - L - MRF - Bare	S1H Low-Rise	S/LFM+DUC/HEX:2/PLFR
8	2 Storey - L - SGF - Bare	S1L Low-Rise	S/LFM+DNO/HEX:2/PLFR
9	2 Storey - L - MRF - Infill SCB	S5H Low-Rise	S/LFINF+DUC/HEX:2/PLFR
10	2 Storey - L - SGF - Infill SCB	S5L Low-Rise	S/LFINF+DNO/HEX:2/PLFR
11	2 Storey - L - MRF - Infill HCB	S5H Low-Rise	S/LFINF+DUC/HEX:2/PLFR
12	2 Storey - L - SGF - Infill HCB	S5L Low-Rise	S/LFINF+DNO/HEX:2/PLFR
13	4 Storey - MRF - Bare	S1H Mid-Rise	S/LFM+DUC/HEX:4/PLFR
14	4 Storey - SGF - Bare	S1L Mid-Rise	S/LFM+DNO/HEX:4/PLFR
15	4 Storey - MRF - Infill SCB	S5H Mid-Rise	S/LFINF+DUC/HEX:4/PLFR
16	4 Storey - SGF - Infill SCB	S5L Mid-Rise	S/LFINF+DNO/HEX:4/PLFR
17	4 Storey - MRF - Infill HCB	S5H Mid-Rise	S/LFINF+DUC/HEX:4/PLFR
18	4 Storey - SGF - Infill HCB	S5L Mid-Rise	S/LFINF+DNO/HEX:4/PLFR

Table 4.3 – Index buildings typology (continued)

#	Index Building Reference	HAZUS Typology*	GEM Typology+
19	4 Storey - R - MRF - Bare	S1+S2H Mid-Rise	S/LH+DUC/HEX:4/PLFR
20	4 Storey - R - MRF - Infill SCB	S5H Mid-Rise	S/LH+LFINF+DUC/HEX:4/PLFR
21	4 Storey - R - MRF - Infill HCB	S5H Mid-Rise	S/LH+LFINF+DUC/HEX:4/PLFR
22	6 Storey - MRF - Bare	S1H Mid-Rise	S/LFM+DUC/HEX:6/PLFR
23	6 Storey - SGF - Bare	S1L Mid-Rise	S/LFM+DNO/HEX:6/PLFR
24	6 Storey - MRF - Infill SCB	S5H Mid-Rise	S/LFINF+DUC/HEX:6/PLFR
25	6 Storey - SGF - Infill SCB	S5L Mid-Rise	S/LFINF+DNO/HEX:6/PLFR
26	6 Storey - MRF - Infill HCB	S5H Mid-Rise	S/LFINF+DUC/HEX:6/PLFR
27	6 Storey - SGF - Infill HCB	S5L Mid-Rise	S/LFINF+DNO/HEX:6/PLFR
28	8 Storey - MRF - Bare	S1H High-Rise	S/LFM+DUC/HEX:8/PLFR
29	8 Storey - SGF - Bare	S1L High-Rise	S/LFM+DNO/HEX:8/PLFR
30	8 Storey - MRF - Infill SCB	S5H High-Rise	S/LFINF+DUC/HEX:8/PLFR
31	8 Storey - SGF - Infill SCB	S5L High-Rise	S/LFINF+DNO/HEX:8/PLFR
32	8 Storey - MRF - Infill HCB	S5H High-Rise	S/LFINF+DUC/HEX:8/PLFR
33	8 Storey - SGF - Infill HCB	S5L High-Rise	S/LFINF+DNO/HEX:8/PLFR

* S1: steel moment frame; S2: steel brace frame; S5: steel frame with unreinforced masonry infill walls
L: low-code, M: moderate-code, H: high-code.
High-Code, Moderate-Code, Low-Code and Pre-Code buildings are based on modern code (e.g., 1976 Uniform Building Code, 1985 NEHRP Provisions, or later editions of these model codes)
Low-Rise: 1-3 storeys, Mid-Rise: 4-7 storeys, High-Rise: 8+ storeys
+ Material: S-Steel. Lateral load-resisting system: LFM-Moment frame; LFINF-Infilled frame; LH-Hybrid system
System ductility: DUC-Ductile; DNO-Non-ductile. Height: HEX. Shape of building plan: PLFR-Rectangular, solid

4.4. Design Assumptions & Input

As stated previously, despite the selected real case study (i.e. 4 Storey - R – MRF), the rest of the introduced index buildings are not defined based on a specific existing structure. Therefore, these index buildings need to be designed initially, as they are composed of a combination of common structural properties. Throughout the structural design process, the aim was to have the assumptions and inputs concurring with the common practices and standards of the region under study. Hence, the most frequently used design software package in Iran, ETABS v.2015 (Computers & Structures Inc., 2016), approved by the Building & Housing Research Centre of Iran (BHRC), has been employed to design each of the index buildings. The following discusses the key assumptions and features implemented at different stages of the design.

The general structural design has been conducted according to part 6: Minimum Design Loads for Buildings (3rd edition) (INBC, 2013a) and part 10: Steel Structures (4th edition) (INBC, 2013b) of the Iranian National Building Code. Both stated parts of the national code are generally based on the provisions of ASCE/SEI 7-10 (2013) and ANSI/AISC 360-10 (2010) respectively. The seismic requirements and actions are established following the provisions of Iranian seismic code, "Standard No. 2800" or "ISIRI-2800" (3rd edition) (BHRC, 2007), as majority of existing buildings have been designed accordingly and has identical requirements to the recently published code (4th edition).

The beams and columns have been modelled as one-dimensional frame elements. This assumption holds well for elements whose biggest cross-section dimension is at least four times smaller than the length of the element. A set of typical steel beam and column sections have been characterised for the program in order to automatically select the most appropriate ones. The steel sections, I-section with parallel flanges (IPE) and square hollow sections (SHS), are identified according to common practice and availability. Data extracted from regional steel manufacturers and official import datasets accessed through the Statistical Centre of Iran (SCI) and Tehran Chamber of Commerce and Industries (TCCIM) have assisted in this selection process. It is important to note that the typical columns are composed of two parallel flange channel (PFC) sections, welded together to form a box section, however due to limitations in numerical simulation, SHS sections with similar geometric properties are employed. The steel mechanical properties are defined according to DIN EN 10025-1 (2004), for steel grade S235, an efficient and economical option, frequently used in construction of residential and commercial buildings (Table 4.4). The list of typical steel profiles for beams and columns are presented in Table 4.5 and Table 4.6 respectively.

Table 4.4 - Mechanical properties of steel material (S235)

Properties	**Value**
Minimum Yield Stress (f_y)	24 kgf/mm^2
Minimum Tensile Strength (f_u)	36 kgf/mm^2
Elastic Modulus (E)	20389.02 kgf/mm^2
Shear Modulus (G)	7841.93 kgf/mm^2
Poisson's ratio (v)	0.3
Coefficient of Thermal Expansion (A)	0.0000117 1/C
Weight per Unit Volume (γ)	7833.4 kgf/m^3

Table 4.5 – Typical IPE beam steel sections with parallel flanges (hot formed) [DIN 1025-5:1994] Mechanical properties according to regional manufacturers: Esfahan Steel Co. (ESCO), Iran National Steel Industrial Group (INSIG), Khuzestan Steel Co. (KSC), Esfahan Mobarakeh Steel Co. (MSC)

Section Ref.	**Mass per Unit Length**	**Height**	**Width**	**Thickness of Web**	**Thickness of Flange**	**Root Radius**	**Area**	**Second Moment of Area (y-y axis)**	**Elastic Section Modulus (y-y axis)**	**Second Moment of Area (z-z axis)**	**Elastic Section Modulus (z-z axis)**
	γ	h	b	t_w	t_f	r	A	I_y	W_y	I_z	W_z
	kg/m	*mm*	*mm*	*mm*	*mm*	*mm*	*cm^2*	*cm^4*	*cm^3*	*cm^4*	*cm^3*
IPE 120	10.4	120	64	4.4	6.3	7	13.2	317.8	52.96	27.67	8.646
IPE 140	12.9	140	73	4.7	6.9	7	16.4	541.2	77.32	44.92	12.31
IPE 160	15.8	160	82	5	7.4	9	20.1	869.3	108.7	68.31	16.66
IPE 180	18.8	180	91	5.3	8	9	23.9	1317	146.3	100.9	22.16
IPE 200	22.4	200	100	5.6	8.5	12	28.5	1943	194.3	142.4	28.47
IPE 220	26.2	220	110	5.9	9.2	12	33.4	2772	252	204.9	37.25
IPE 240	30.7	240	120	6.2	9.8	15	39.1	3892	324.3	283.6	47.27
IPE 270	36.1	270	135	6.6	10.2	15	45.9	5790	428.9	419.9	62.2
IPE 300	42.2	300	150	7.1	10.7	15	53.8	8356	557.1	603.8	80.5

Table 4.5 - Typical IPE beam steel sections with parallel flanges (hot formed) (continued)

Section Ref.	Mass per Unit Length	Height	Width	Thickness of Web	Thickness of Flange	Root Radius	Area	Second Moment of Area (y-y axis)	Elastic Section Modulus (y-y axis)	Second Moment of Area (z-z axis)	Elastic Section Modulus (z-z axis)
	γ	h	b	t_w	t_f	r	A	I_y	W_y	I_z	W_z
IPE 330	*kg/m*	*mm*	*mm*	*mm*	*mm*	*mm*	cm^2	cm^4	cm^3	cm^4	cm^3
IPE 360	57.1	360	170	8	12.7	18	72.7	16270	903.6	1043	122.8
IPE 400	66.3	400	180	8.6	13.5	21	84.5	23130	1156	1318	146.4
IPE 450	77.6	450	190	9.4	14.6	21	98.8	33740	1500	1676	176.4
IPE 500	90.7	500	200	10.2	16	21	115.5	48200	1928	2142	214.2
IPE 550	105.5	550	210	11.1	17.2	24	134.4	67120	2441	2668	254.1
IPE 600	122.4	600	220	12	19	24	156.0	92080	3069	3387	307.9

Table 4.6 – Typical structural steel square hollow sections (hot formed) [DIN EN 10210-1:2006] Mechanical properties according to regional manufacturers: Esfahan Steel Co. (ESCO), Iran National Steel Industrial Group (INSIG), Khuzestan Steel Co. (KSC), Esfahan Mobarakeh Steel Co. (MSC)

Section Ref.	Side Dimension	Thickness	Mass Per Unit Length	Cross-Sectional Area	Second Moment of Area	Elastic Section Modulus	Torsional Inertia Constant
	b	t	γ	A	I	W_{el}	I_t
	mm	*mm*	*kg/m*	cm^2	cm^4	cm^3	cm^4
200×12.0	200	12.0	69.60	88.70	5171	517	8208
200×12.5	200	12.5	72.30	92.10	5336	534	8491
200×16.0	200	16.0	90.30	115.00	6394	639	10340
220×12.5	220	12.5	80.10	102.00	7254	659	11480
220×16.0	220	16.0	100.00	128.00	8749	795	14050
250×12.0	250	12.0	88.50	113.00	10556	844	16567
250×16.0	250	16.0	115.00	147.00	13270	1061	21140
260×16.0	260	16.0	120.00	153.00	15060	1159	23940
300×16.0	300	16.0	141.00	179.00	23850	1590	37620
320×16.0	320	16.0	152.00	193.00	29650	1853	46010
350×16.0	350	16.0	166.00	211.00	38940	2225	60990
400×20.0	400	20.0	235.00	300.00	71540	3577	112500

A rigid diaphragm assumption is applied for all levels. This is to ensure that the earthquake loads are transferred according to the stiffness of each member and not based on their tributary area (Naeim & Boppana, 2000). Furthermore, one-way composite floor slabs are implemented with a chess-like load distribution. The slab comprises of lightly reinforced concrete cast with a depth of 100 mm, on top of profiled steel deck and supporting steel joists, as shown in Figure 4.3 and Figure 4.4.

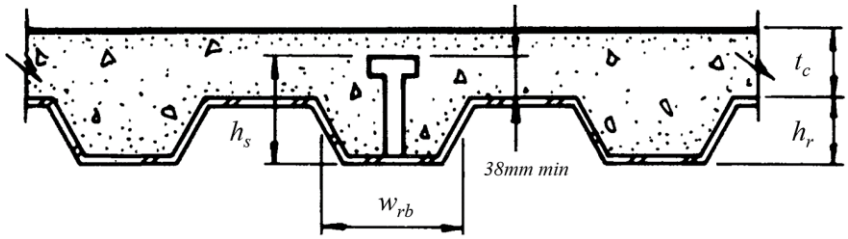

Figure 4.3 - Filled deck properties for the slab

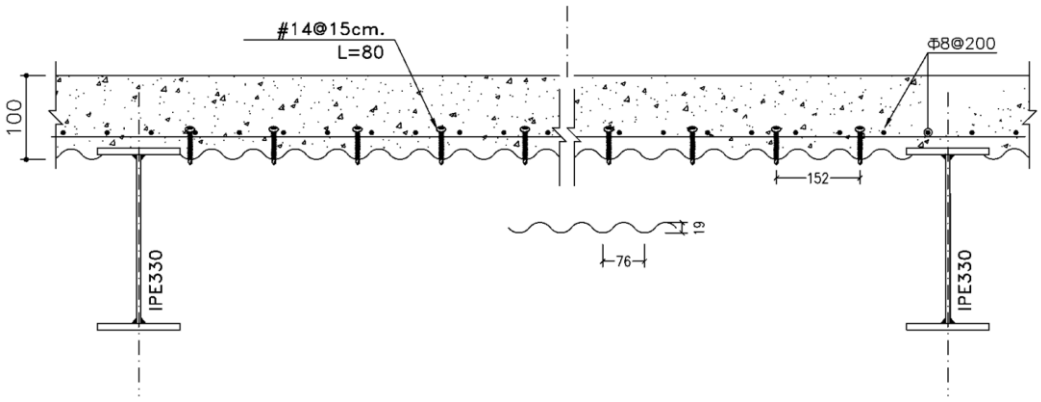

Figure 4.4 – Typical slab reinforcement and arrangement of the metal deck (Scale: 1/10)

Table 4.7 and Table 4.8 present the main properties of the slab comprising components.

Table 4.7 – Mechanical properties of concrete material (C25/30)

Properties	Value
Specific Concrete Compressive Strength (f'_c)	2.1 kgf/mm^2
Elastic Modulus (E)	2531.05 kgf/mm^2
Shear Modulus (G)	1054.6 kgf/mm^2
Poisson's Ratio (v)	0.2
Coefficient of Thermal Expansion (A)	0.0000099 1/C
Weight per Unit Volume (γ)	2500 kgf/m^3

Table 4.8 – Mechanical properties of the composite filled deck

Properties	Value
Slab Material	C25/30
Deck Material	S235
Slab Depth (t_c)	87.5 mm
Rib Depth (h_r)	75 mm
Rib Width Top (w_{rt})	175 mm
Rib Width Bottom (w_{rb})	125 mm
Rib Spacing (s_r)	300 mm
Deck Shear Thickness	1.0 mm
Deck Unit Weight	11.22 kgf/m^2
Shear Stud Diameter	19 mm
Shear Stud Height (h_s)	150 mm
Shear Stud Tensile Strength (F_u)	40.79 kgf/mm^2

The beam-column connections are designed by the program to resist shear and moment through major axis, according to AISC 360-10. In order to avoid the interference of the secondary beams of the deck (joists) with the principal beams, the beam-beam connection will be designed as pinned. A rigid base is assumed by restraining the translation and rotation of bottom joints in all global directions.

Five load patterns are considered, namely the dead load (self-weight of beams, columns and braces), cladding load, partition load, live load (imposed) and the seismic load (EQ). The applied load types and their allocated values are presented in Table 4.9. The values are

assigned based on the minimum design loading suggested in part 6 of INBC (2013a) [3-3-2-6]. Following the common design approach, the contribution of infill panels has been included as permanent loading on the beams. Moreover, the effect of loads due to wind, snow and flood have been neglected in the applied loading combinations for simplicity. It should be noted that in design of simple gravity frames no lateral loading is considered in any form, hence the structure is solely design for vertical loading.

Table 4.9 – Applied permanenet and imposed loads (INBC, 2013a)

Element	Load Type	Load Value
Floor Slab	Imposed (Live)	200 kgf/m^2
	Partitions	170 kgf/m^2
Roof	Imposed (Live)	150 kgf/m^2
Beam	Claddings	10 – 12 kgf/m

The ISIRI-2800 (3rd and 4th edition) approach for designing regular structures is based on the equivalent static force, similar to majority of current seismic design codes of practice, such as ASCE-7-16 (2016), IBC (2015), EN 1998-1 (2004). This approach is fundamentally based on the determination of storey shear strength and stiffness characteristics of the structural system through utilising the design compatible spectrum lateral force patterns (Ganjavi & Amiri, 2018). Although, during considerable earthquake intensities, the structural elements are expected to experience significant levels of inelasticity, the code-specific seismic design force patterns are basically established according to dynamic response of elastic structural systems. The lateral seismic force for regular buildings up to 50-metre-high may be obtained by the equivalent static analysis method, in which the base shear (V) is obtained from equation 4.1.

$$V = C.W \tag{4.1}$$

where W is the effective weight of the building defined as the total dead load and a percentage of the imposed load and C is the seismic response coefficient defined below.

$$C = \frac{ABI}{R} \tag{4.2}$$

where A is the function of design baseline acceleration (ratio of seismic acceleration to gravity acceleration, g), B is the reflection coefficient of the building determined from the design response spectrum, I is the importance factor and R is the response modification factor. The minimum value of V is $V_{min} = 0.1AIW$. From importance of function perspective, ISIRI-2800 (2013) divides buildings in four groups and defines the importance factor for very high importance buildings as 1.4, for high importance buildings as 1.2, for average important buildings as 1.0, and for lesser importance buildings as 0.8. All residential, office and commercial buildings fall in to the moderate importance group. The response modification factor or building behaviour factor, R, represents the global characteristics of the structure

such as ductility, redundancy and the inherent over-strength capacity, determined in accordance with the type of lateral-force-resisting system. The code suggests a value of R=7 for intermediate steel moment-resisting frame and R=5 for ordinary steel moment-resisting frame.

The evaluated design base shear (V) is linearly distribution (triangular shape) through the height of the structure (F_i) as follows:

$$F_i = (V - F_t)\frac{W_i h_i}{\sum_{j=1}^{n} W_j h_j} \tag{4.3}$$

where W_i is the seismic weight of level i out of n stories, that is equal to the dead load plus a percentage of the imposed load at that level, as well as half of the weight of walls and columns located immediately above and below this level. h_i is the height of the story of level i out of n stories. F_t is a concentrated force at the top level in case of long period structures ($T_1 > 0.7s$) and is determined from the following formula:

$$F_t = 0.07TV \ < 0.25V \tag{4.4}$$

The design storey drift is obtained by multiplying the lateral deflections at the floor level resulted from elastic analysis under design base shear, by 0.7R factor ($\Delta_{Mi}=0.7R\Delta_{Wi}$), after applying P-Δ effects. ISIR-2800 (2013) limits the design story drift for structures with period less than 0.7 seconds to 0.025 times the floor height and for structures with period greater than or equal to 0.7 seconds to 0.020 times the floor height.

The building response factor, B, is estimated according to the code-based response spectrum of ISIR-2800 (2013) (Figure 4.5). Accordingly, the evaluated design base shear is distributed linearly along the building's height according to the first deformation mode of the structure in both orthogonal directions. For this study, 100 percent of the seismic load in one direction is considered along with 30 percent of the seismic load in the orthogonal direction. The defined index buildings are classified as regular in both plan and elevation [1-8-1, ISIR-2800] and according to their function, all are categorised as buildings with "moderate importance" [1-7, ISIR-2800]. All index buildings are assumed to be located on a semi-compact soil condition (type II of ISIRI-2800, 375 m/s < $V_{S,30}$ < 750 m/s), corresponding to site class C (very dense soil and soft rock) of NEHRP (FEMA P-1050, 2015) and ASCE 7-16 (2016). The uppermost value of the code's design base acceleration, 0.35g has been implemented to derive the code-based response spectrum [2-3-2, ISIR-2800]. An accidental eccentricity of 5 percent is considered at any floor level for each direction of the earthquake force [2-3-10-3, ISIR-2800]. This accounts for possible variations in mass and stiffness distributions and also the forces

due to the torsional component of the earthquake. The building response spectrum is defined through the factor B, based on the following formulation (Eq. 4.5 to 4.7) [2-3-4, ISIR-2800]:

$$B = 1 + S(\frac{T}{T_0}) \qquad 0 \leq T \leq T_0 \qquad (4.5)$$

$$B = S + 1 \qquad T_0 \leq T \leq T_s \qquad (4.6)$$

$$B = (S + 1)(\frac{T_s}{T})^{2/3} \qquad T \geq T_s \qquad (4.7)$$

where T is the fundamental period of vibration of the structure in the direction under consideration. ETABS estimates the building period in two different ways. The first method is the one based on the provisions of ISIRI-2800 code [2-3-6, ISIR-2800] according to the height and structural system of the building. The obtained period is called T_A and the method is discussed in more details in section 4.5. The second method is when the program evaluates the period of the mode (T_{mode}) based on the largest participation factor in the direction that loads are being calculated (X or Y) based on the eigenvalue analysis. The building's period that the program choses to determine the building response factor (B) and subsequently the base shear (V), is chosen depending on the seismic zonation of the location under study. Hence, if the building is located in a zone with very high (I) level of relative seismic hazard then:

- If $T_{mode} \leq 1.30T_A$, then $T = T_{mode}$.
- If $T_{mode} > 1.30T_A$, then $T = T_A$.

For all other seismic zones (i.e. high (II), intermediate (III) and low (IV) levels of relative seismic hazard), the period is selected accordingly:

- If $T_{mode} \leq 1.40T_A$, then $T = T_{mode}$.
- If $T_{mode} > 1.40T_A$, then $T = T_A$.

Furthermore, a damping ratio of 0.05 is applied for the response spectrum, while T_0, T_s and S are determined from the soil profile type and level of seismicity as shown in Table 4.10.

Table 4.10 – Code-based response spectrum defining properties [2-3-5, ISIR-2800]

Criteria	Value
Design base acceleration (Zone 1 – Very high level of relative seismic hazard)	0.35g
Soil profile (S) (Soil profile type: II)	1.5
T_0 (determined according to soil profile type and level of seismicity)	0.1
T_S (determined according to soil profile type and level of seismicity)	0.5

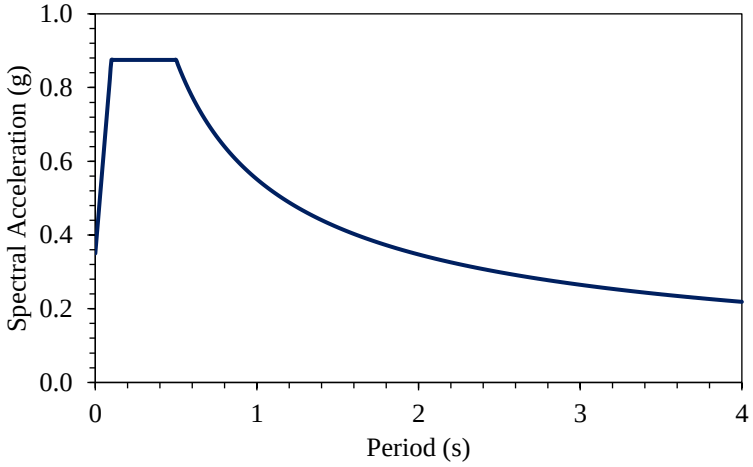

Figure 4.5 – Code-based response spectrum (ISIR-2800, 2007)

A number of load combinations are defined and applied for designing the index buildings following the limit state design (LSD) approach, while satisfying both ultimate limit state (ULS) and the serviceability limit state (SLS) principles proposed in INBC (2013b) and ISIR-2800 (2007) (Table 4.11).

Table 4.11 – Load combinations applied for structural design [1-13-9, ISIR-2800]

Design Component	**Load Combinations**
Steel Frame (Gravity Design)	1) 1.4Dead + 1.4Partition + 1.4Cladding (Strength check) 2) 1.4Dead + 1.6Live+ 1.4Partition + 1.4Cladding (Strength check) 3) Dead + Partition + Cladding (Deflection check) 4) Dead + Live + Partition + Cladding (Deflection check) 5) Dead + 0.75Live + Partition + Cladding (Deflection check)
Steel Frame (Seismic Design)	1) 1.4Dead + 1.4Partition + 1.4Cladding (Strength check) 2) 1.4Dead + 1.6Live+ 1.4Partition + 1.4Cladding (Strength check) 3) 1.2Dead + 0.5Live + 1.2Partition + 1.2Cladding ± EQ_x ± 0.3EQ_y (Strength check) 4) 1.2Dead + 0.5Live + 1.2Partition + 1.2Cladding ± EQ_y ± 0.3EQ_x (Strength check) 5) 0.9Dead + 0.9Partition + 0.9Cladding ± EQ_x ± 0.3EQ_y (Strength check) 6) 0.9Dead + 0.9Partition + 0.9Cladding ± EQ_y ± 0.3EQ_x (Strength check) 7) Dead + Partition + Cladding (Deflection check) 8) Dead + 0.75Live + Partition + Cladding (Deflection check) 9) 0.6Dead + 0.6Partition + 0.6Cladding ± 0.7EQ (Deflection check) 10) Dead + 0.75Live + Partition + Cladding ± EQ (Deflection check)
Composite Beam Design	1) 1.2Dead (Construction check) 2) 1.2Dead + 1.2Partition + 1.2Cladding (Strength check) 3) 1.2Dead + 1.6Live+ 1.2Partition + 1.2Cladding (Strength check) 4) Dead + Partition + Cladding (Deflection check) 5) Dead + Live + Partition + Cladding (Deflection check)

Once the loading combinations are set, ETABS designs the structural sections according to demand and capacity of each structural element, while following the concepts of capacity design. In simple terms, capacity design is a design process in which it is decided which objects within a structural system will be permitted to yield (ductile components) and which objects will remain elastic (brittle components). The ductile components are designed with sufficient deformation capacity such that they may satisfy displacement-based demand-capacity ratio, while the brittle components are designed to achieve sufficient strength levels such that they may satisfy strength-based demand-capacity ratio. Accordingly, the sum of column flexure strengths at a joint should be more than the sum of beam flexure strengths in order to avoid strong beam-weak column phenomena.

4.5. Index Buildings' Fundamental Period of Vibration

The fundamental period of vibration (T_1) is estimated through eigenvalue analysis to establish a perspective for the dynamic behaviour of the selected index buildings. Additionally, the initial periods are also calculated based on the empirical formulation of the regional code for designing steel structures (Eq. 4.8) [2-3-6, ISIR-2800] (Table 4.12). Accordingly, in case the infill walls impose restraint on the frame's displacements, T_1 should be estimated as 80 percent of the value calculated for the bare steel frame.

$$T_1 = 0.08H^{3/4} \tag{4.8}$$

where H is the height of the building in meters, measured from the base level.

Table 4.12 – Index buildings' code-based and actual fundamental period of vibration

No.	Reference	HAZUS Category	Total Height (m)	Code-Based T_1 (s)	Calculated T_1 (s)	Percentage Error
1	2 Storey - L -MRF - Bare	S1H Low-Rise	7.00	0.34	0.78	56%
2	2 Storey - L -SGF - Bare	S1L Low-Rise	7.00	0.34	0.80	57%
3	2 Storey - L -MRF - Infill SCB	S5H Low-Rise	7.00	0.28	0.30	8%
4	2 Storey - L -SGF - Infill SCB	S5L Low-Rise	7.00	0.28	0.32	14%
5	2 Storey - L -MRF - Infill HCB	S5H Low-Rise	7.00	0.28	0.30	8%
6	2 Storey - L -SGF - Infill HCB	S5L Low-Rise	7.00	0.28	0.32	14%
7	2 Storey - S - MRF - Bare	S1H Low-Rise	7.00	0.34	0.40	14%
8	2 Storey - S - SGF - Bare	S1L Low-Rise	7.00	0.34	0.68	49%
9	2 Storey - S - MRF - Infill SCB	S5H Low-Rise	7.00	0.28	0.24	-17%
10	2 Storey - S - SGF - Infill SCB	S5L Low-Rise	7.00	0.28	0.27	-2%

Table 4.12 – Index buildings' code-based and actual fundamental period of vibration (continued)

No.	Reference	HAZUS Category	Total Height (m)	Code-Based T_1 (s)	Calculated T_1 (s)	Percentage Error
11	2 Storey - S - MRF - Infill HCB	S5H Low-Rise	7.00	0.28	0.21	-28%
12	2 Storey - S - SGF - Infill HCB	S5L Low-Rise	7.00	0.28	0.25	-12%
13	4 Storey - MRF - Bare	S1H Mid-Rise	14.00	0.58	1.46	60%
14	4 Storey - SGF - Bare	S1L Mid-Rise	14.00	0.58	1.84	69%
15	4 Storey - MRF - Infill SCB	S5H Mid-Rise	14.00	0.46	0.68	32%
16	4 Storey - SGF - Infill SCB	S5L Mid-Rise	14.00	0.46	0.72	36%
17	4 Storey - MRF - Infill HCB	S5H Mid-Rise	14.00	0.46	0.70	34%
18	4 Storey - SGF - Infill HCB	S5L Mid-Rise	14.00	0.46	0.74	37%
19	4 Storey - R - MRF - Bare	S1+S2M Mid-Rise	12.58	0.53	1.33	60%
20	4 Storey - R - MRF - Infill SCB	S5M Mid-Rise	12.58	0.43	0.41	3%
21	4 Storey - R - MRF - Infill HCB	S5M Mid-Rise	12.58	0.43	0.44	7%
22	6 Storey - MRF - Bare	S1H Mid-Rise	21.00	0.78	1.96	60%
23	6 Storey - SGF - Bare	S1L Mid-Rise	21.00	0.78	2.70	71%
24	6 Storey - MRF - Infill SCB	S5H Mid-Rise	21.00	0.63	0.98	36%
25	6 Storey - SGF - Infill SCB	S5L Mid-Rise	21.00	0.63	1.02	38%
26	6 Storey - MRF - Infill HCB	S5H Mid-Rise	21.00	0.63	0.96	35%
27	6 Storey - SGF - Infill HCB	S5L Mid-Rise	21.00	0.63	1.00	37%
28	8 Storey - MRF - Bare	S1H High-Rise	28.00	0.97	3.50	72%
29	8 Storey - SGF - Bare	S1L High-Rise	28.00	0.97	3.60	73%
30	8 Storey - MRF - Infill SCB	S5H High-Rise	28.00	0.78	1.40	44%
31	8 Storey - SGF - Infill SCB	S5L High-Rise	28.00	0.78	1.36	43%
32	8 Storey - MRF - Infill HCB	S5H High-Rise	28.00	0.78	1.38	44%
33	8 Storey - SGF - Infill HCB	S5L High-Rise	28.00	0.78	1.34	42%

Figure 4.6, shows a comparison between the actual fundamental period of the index buildings and the ones obtained through the ISIR-2800 (2007) formulations which are meant to be conservative. In general, it can be concluded that the code underestimates the actual initial period in majority of cases. The divergence is at maximum for more flexible, less stiff bare framed index buildings, in both case of SGF and MRF. On the contrary, the code's prediction of T_1 for the case of low-rise infilled frames are in good agreement with the actual initial periods. However, as the number of storeys raises from 4 to 8, the observed disparity increases. For the mid-rise index buildings, the underestimation of initial periods can be considered conservative as a higher spectral acceleration may be implemented for the structural design.

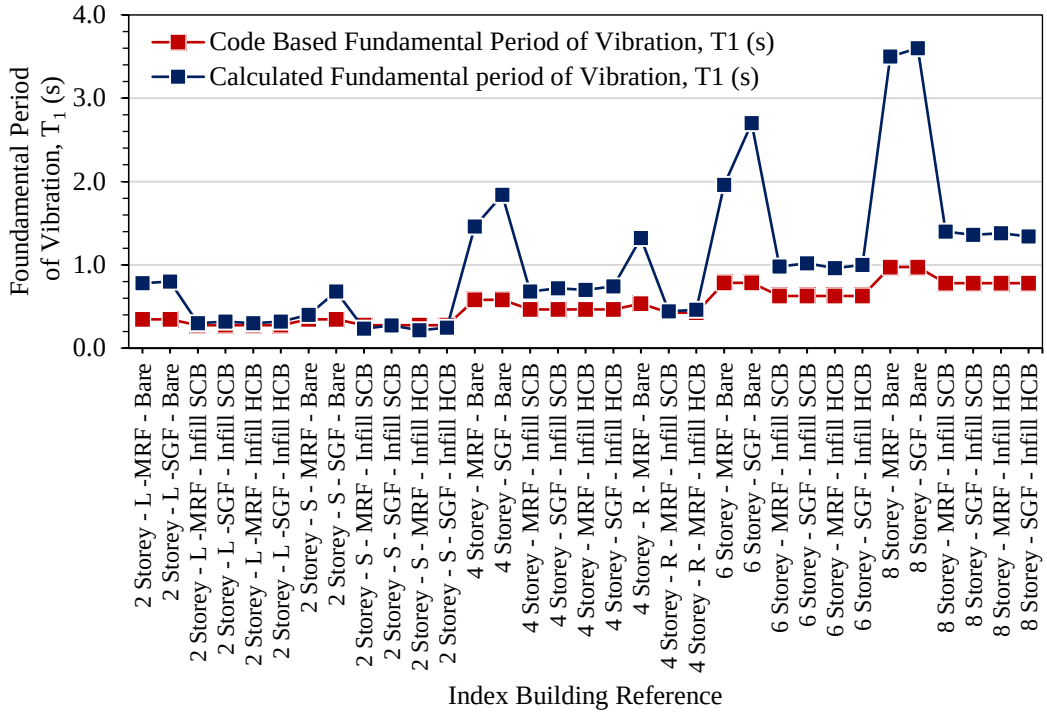

Figure 4.6 - Contrast of index buildings and code-based fundamental period of vibration

Moreover, comparing the initial periods of the defined index buildings against the ones of HAZUS sample buildings, a good agreement is observed particularly in case of infilled frames with different elevations (Figure 4.7). On the contrary, HAZUS buildings have lower initial periods in comparison to the defined bare steel frames.

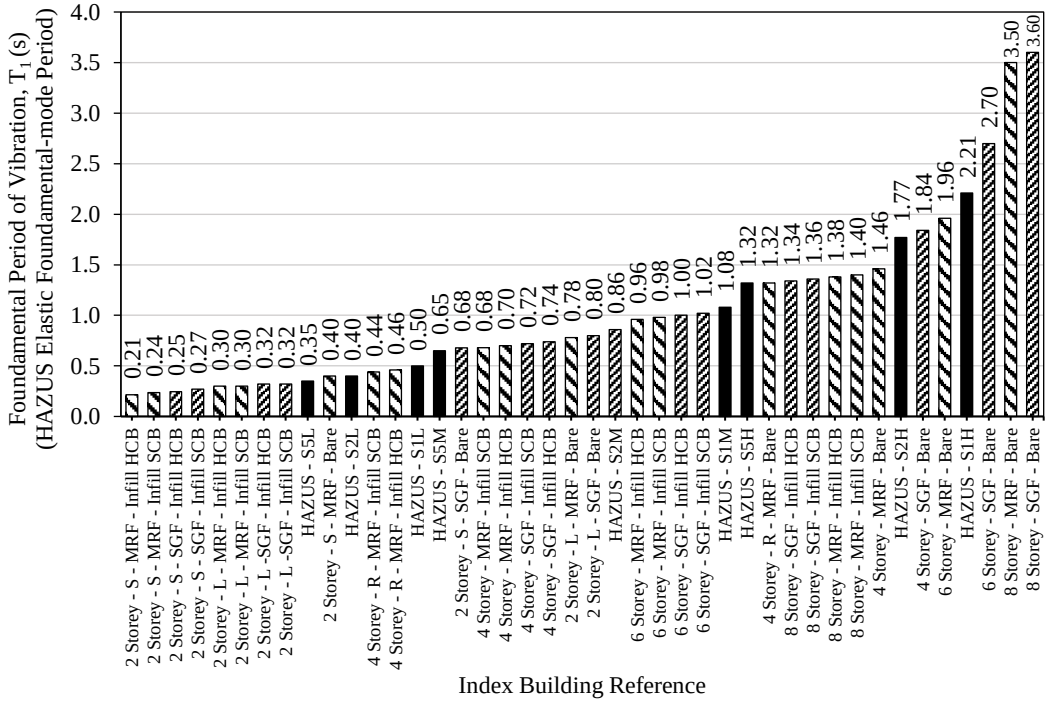

Figure 4.7 - Comparison of index buildings' fundamental period of vibration versus HAZUS steel buildings

The fundamental period of structure plays a critical role in evaluating the seismic demand at different stages of the vulnerability assessment. For instance, in case the fragility and vulnerability functions are presented in terms of spectral accelerating at the initial period $S_a(T_1)$, any over- or under-estimation of T_1 may result in imprecise seismic performance and heavily impact the estimated losses.

4.6. Conclusions

This chapter discussed the motives behind the selected index buildings for seismic fragility and vulnerability assessment. Iran has been proposed as a suitable case study for this research project, due to its high seismicity and the considerable number of existing low- to mid-rise steel structures. The evidence of past seismic events, such as 1990 Manjil-Rudbar and 2003 Bam earthquakes, have highlighted the vulnerability of existing steel structures and the need for further assessment. Furthermore, the increasing trend of constructing steel frames in recent years, indicated a need for seismic fragility and vulnerability function of recently built structures as well as the existing ones.

Investigating the most common and influential structural arrangement, characteristics, design approach and material in steel structures, 33 index buildings have been defined and designed. The design assumption and inputs are discussed in detail according to the local design codes and common practice. The introduced index buildings tend to represent a considerable proportion of existing and newly designed low- to mid-rise residential steel structures in the region under study. Comparing the estimated fundamental period of vibration of the index buildings, it is clear that the selected buildings comprise a large cohort of structures with diverse seismic response. Alongside, the proposed buildings, a number of index buildings have been defined according to a typical building designed for large-scale estate developments, distributed throughout the country.

The following chapters (Chapter 5 and 6) will discuss the various phases of numerical structural modelling and the steps involved in deriving analytical seismic fragility functions. The estimated seismic performance and consequently the fragility functions of the proposed structures will be of great importance for further vulnerability assessment and seismic loss estimation.

Chapter 5 Numerical Modelling & Seismic Analysis

5.1. Introduction

Having a set of index buildings defined in Chapter 4, this chapter discusses the numerical structural modelling and relevant assumptions considered in the simulation process of the stated steel framed structures. The influence of various structural components on the seismic response are identified by investigating a common steel building. The selected index building represents a mid-rise residential structure, characterised based on a real case designs of a government led campaign of large-scale estate developments near Tehran, a mega-city in Iran acknowledged for its high seismicity. The reasons behind this selection are discussed in detail, followed by a comprehensive discussion on the characteristics of the index building. The global performance of the structure is studied by introducing a number of different arrangements with various structural components such as the type of beam-column connection and masonry infill panels. To understand the extent of the resultant structural behaviour, the models are analysed through both nonlinear static and nonlinear dynamic analysis.

5.2. Selection of Case Study

In 2011, the government of Iran offered real estate developers free land in return of building affordable residential units to cover a part of the country's house shortage. The project is expected to provide more than 2 million dwellings in 31 provinces throughout the country by the end of year 2019. These designated buildings are mainly mid-rise with similar plans and are designed according to provision of the Iranian seismic code, "Standard No. 2800" or "ISIRI-2800" (BHRC, 2007). Approximately, one third of the expected 600'000 units are steel framed with masonry infill panels. Figure 5.1, shows the major construction sites of the project overlaid on the seismic hazard map of the country. Accordingly, it is evident that the majority of the mentioned sites are situated in areas with moderate to high seismicity, exposing a considerable population to seismic hazard.

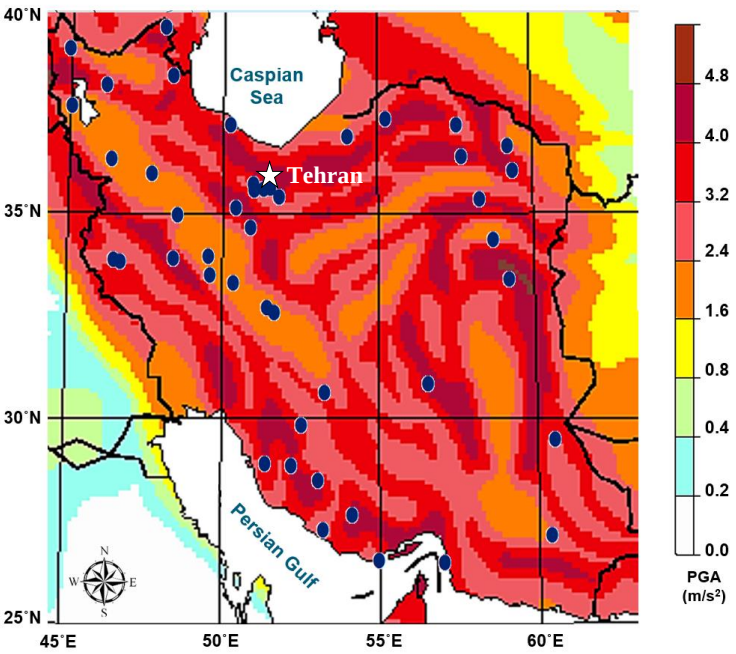

Figure 5.1 - Location of the project sites overlaid on the seismic hazard map of Iran. Peak Ground Acceleration (m/s^2) with 10% probability of exceedance in 50 year (Tavakoli et al., 1999)

According to the preliminary post-earthquake reports of the 2017 Iran-Iraq earthquake (M_w 7.3), throughout the province of Kermanshah, as a result of the severe ground shaking (MMI: VIII) 14 blocks of the stated buildings collapse and the external infill walls of 34 blocks have failed completely (Yekrangnia et al., 2017). The reports state that 40% of the damaged buildings were steel frame. Hence, assessing the seismic performance and vulnerability of these buildings is of great importance.

Representing the discussed residential buildings, a four-storey infilled steel frame has been selected according to a typical real-case building design, near Tehran (35.65°N 50.90°E). Besides having a typical design among the stated mass residential development, the implemented construction method, material characteristics and the building arrangement are frequent practice in the country and the middle-east region (e.g. Iran, Turkey and the Gulf countries). Therefore, the observed seismic performance and the obtained vulnerability function can be generalised to a wide extent of regional structures with shared or similar characteristics.

5.3. General Characteristics of the Case Study

The mega-capital city of Tehran (35.70°N 51.41°E), a highly-urbanised city with a population of over eight million, is one of the most densely populated capitals of the world (SCI, 2016). It covers an area of 1274 km^2 with a population density of 10’367 person/km^2 at the southern foot of the central Alborz mountains. The Tehran and its neighbouring Alborz province, are

home to more than 15 million people, i.e., about one-fifth of the 80 million population of Iran. It is the political and economic capital of Iran and the most populous city in western-Asia, with an unplanned growing rate of more than 20% during the last 20 years. The fault system around the region of Tehran consists of nine active faults, as shown in Figure 5.2. The majority of the identified ones are thrust fault and generally stretch in a northwest-southeast or east-west direction perpendicular to the regional tectonic compression (Wang & Taheri, 2014).

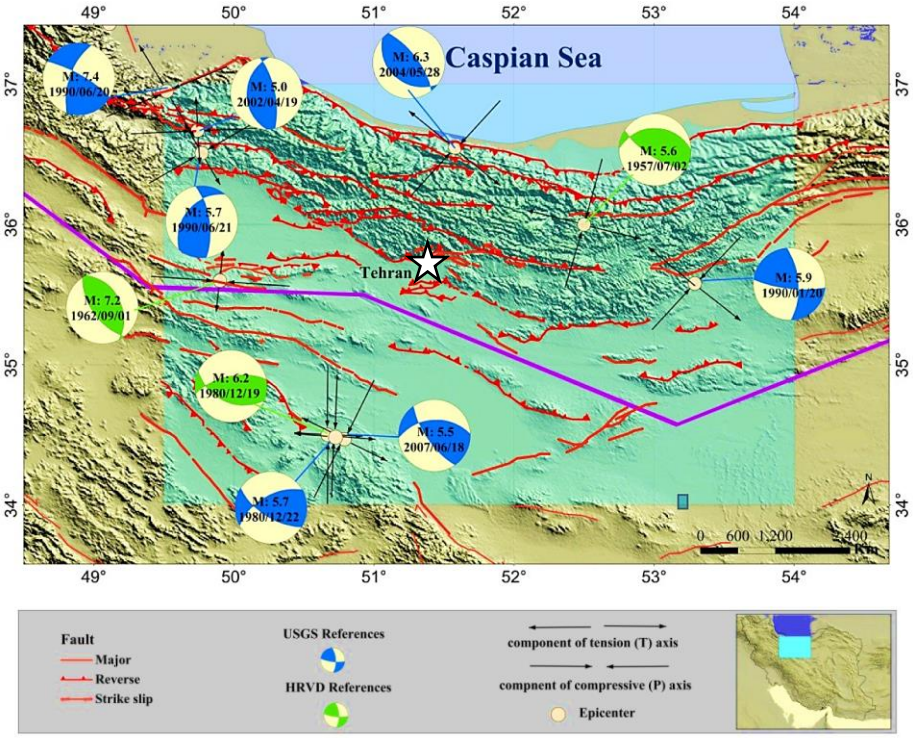

Figure 5.2 – Fault system around the region of Tehran and seismic activity of the region. Thick line indicates the border of seismotectonic provinces (Abdi et al., 2013)

The most prominent strong grounds shakings experience in Tehran are listed as follows (Ambraseys & Melville, 1982):

- 4th century BC (M_w 7.6, MMI=X)
- 855 AD (M_w 7.1, MMI=VIII)
- 958 AD (M_w 7.7, MMI=X)
- 1177 AD (M_w 7.2, MMI=VIII)
- 1830 AD (M_w 7.1, MMI=VIII)

The city has not experienced a damaging earthquake since 1830, which killed 45’000. However, the existence of faults such the North of Tehran fault, Mosha fault, North and South of Rey fault, which are known to be active are a clear evidence of the great seismicity of the region and a possibility of an earthquake occurrence with moment magnitude greater than seven. The regional probabilistic seismic hazard studies indicate seismic events capable of

generating a peak ground acceleration (PGA) of 0.50g to 0.55g with a return period of 475-years (i.e. 10% probability of exceedance in 50-year life time of the structure) (Gholipour et al., 2008). Any destruction in this rapidly growing and important mega-city will have severe effects on the whole country.

According to the Tehran municipality database, in 1996, out of 1,484,138 residential units in Tehran, the total number of steel buildings was 604,363 (41%) and reinforced concrete buildings were only 169,9602 (11%) (TMD, 2017). The distribution of steel structures continued its growth and according to the Tehran municipality database, by the year 2006, around 63.8% of the city's buildings were constructed with steel material (Figure 5.3).

Residential Steel Structures in Tehran (1996)

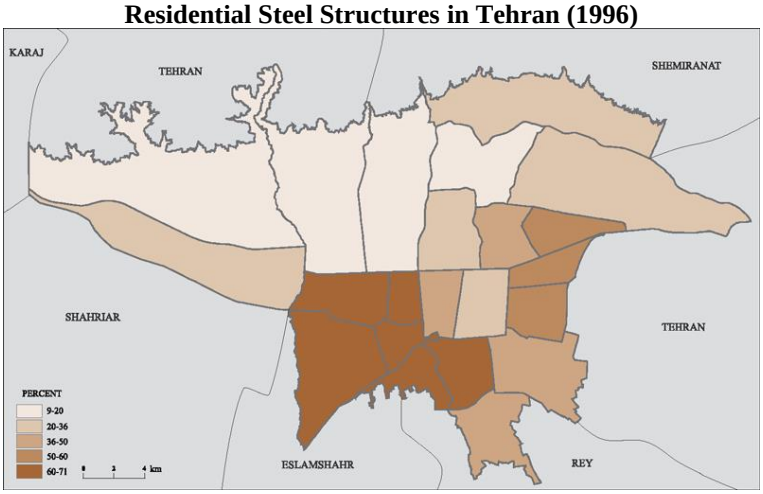

Residential Steel Structures in Tehran (2006)

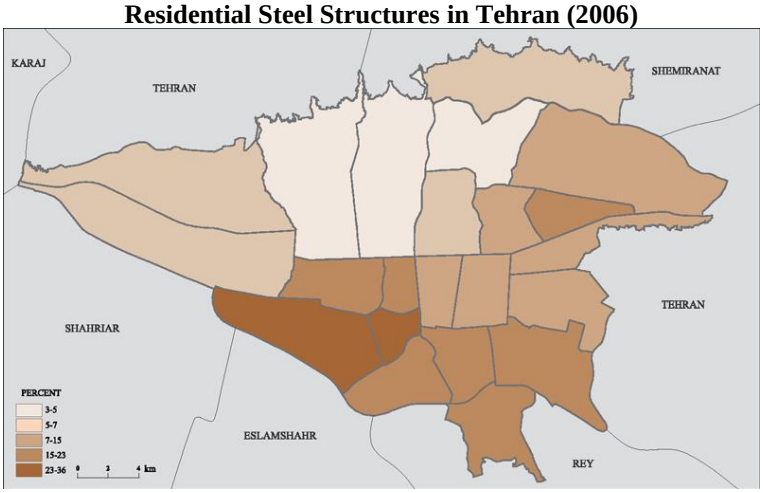

Figure 5.3 - Distribution of residential units with metal frame and brick wall (TMD, 2017)

Regarding the age of the buildings, based on the acquired statistics, 22% of the buildings in Tehran are 20 years old and 21% of the buildings are five years old or less (Figure 5.4). In a ten-year period between 1996 and 2006, the amount of buildings older than 30 years have dropped from 50% to below 20%. This drop in structural age is mainly due to the movement

toward demolishing older and low engineered buildings and replacing them with new and durable buildings with a service life of 50 years according to the local code (BHRC, 2007).

Residential units with 20 years old in Tehran (2006)

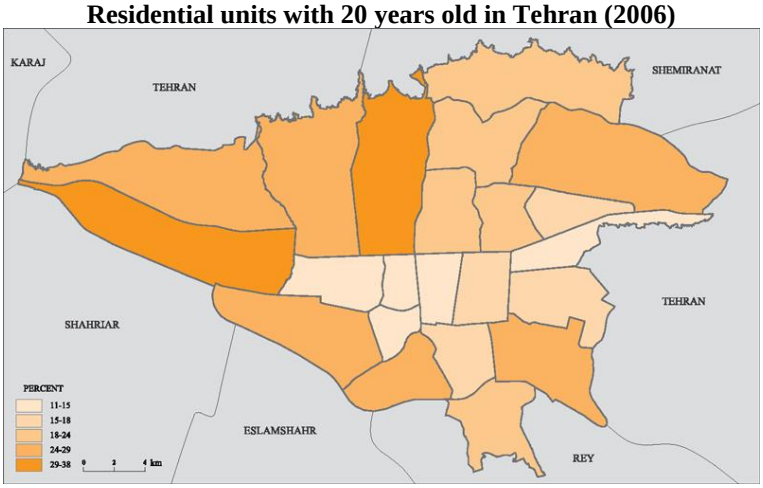

Residential units with 10 years old and less in Tehran (2006)

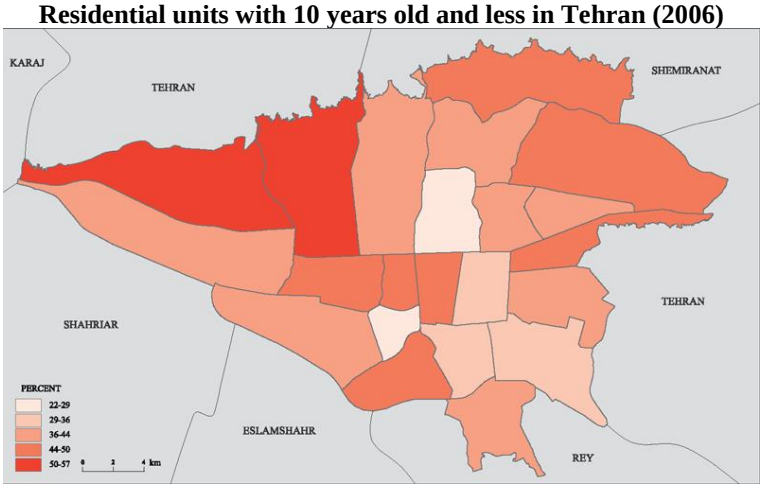

Residential units with 5 years old and less in Tehran (2006)

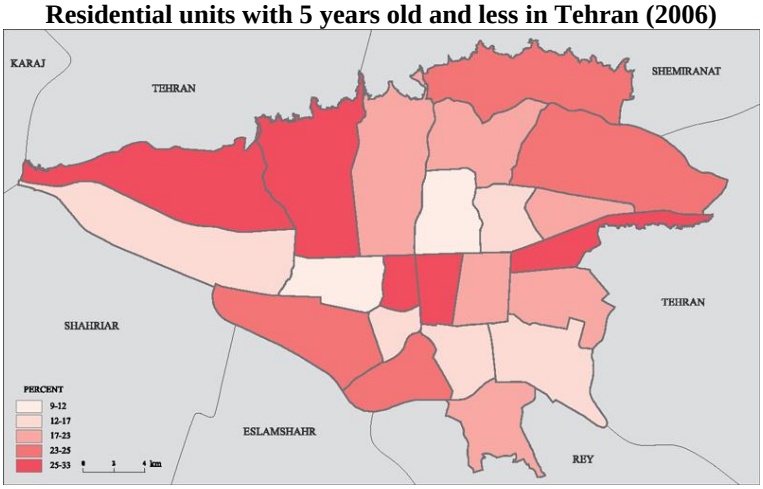

Figure 5.4 – Structural age of buildings in Tehran (TMD, 2017)

5.4. General Characteristics of the Index Building

As discussed in Chapter 4, although the current Iranian seismic design code, ISIRI-2800 (4th edition) (BHRC, 2007) has been recently updated, the discussed index building was originally designed following the 3rd edition of ISIRI-2800 (BHRC, 2007). According to the code, Tehran is categorised as zone 1 with very high level of seismic hazard, hence the design base acceleration employed for designing the building is 0.35g, which is the highest value given in the code. The geology of the location indicated a semi-compact soil condition (type II of ISIRI-2800, 360 m/s < $V_{S,30}$ < 800 m/s), corresponding to site class C (very dense soil and soft rock) of NEHRP (FEMA P-1050, 2015) and ASCE 7-16 (2016). A general view of the index building is shown in Figure 5.5 and Figure 5.6.

Figure 5.5 - Side view of the index building
(No stair case elevator core is built for the Index building)

Figure 5.6 - Bracing positioning at longitudinal and transvers direction of the index building

The structural plans of the building are illustrated in Figure 5.7 and Figure 5.8, indicating the location and dimensions of the beams (IPE), columns (HEB) and cross bracings. The column sections are given in

Table 5.1 and the beam sections are shown along elements on the plan. The properties of the steel sections are given in Table 5.2. The cross bracings are hollow square section with cross sectional size of 120mm and thickness of 6.3mms. The building is a dual-system structure, consisting of 5-bays in its longitudinal direction (x-direction) and 3-bays in its transversal direction (y-direction). The lateral resisting system consists of concentric cross bracings in its transversal direction for all storeys and moment resisting frame in its longitudinal direction. Additionally, cross bracings are located at the ground level, dedicated as parking space, on both directions as indicated in the plan. The building can be categorised as asymmetrical, due to presence of bracings on all floors in the transverse direction, while the braces are only present at the ground floor of the longitudinal direction. Therefore, some torsional effects are anticipated, however, the building does not include any staircase and elevator core or shear walls. It should be noted that the majority of the buildings constructed as part of this building scheme do not have elevators. In case the elevator or the staircases are supported by shear walls and the surrounding walls are connected to the floor slabs, then the structural lateral resisting system will be altered and other modelling approaches should be followed. The steel frames are infilled with masonry panels, composed of solid clay bricks and mortar in both form of solid and panels with window opening.

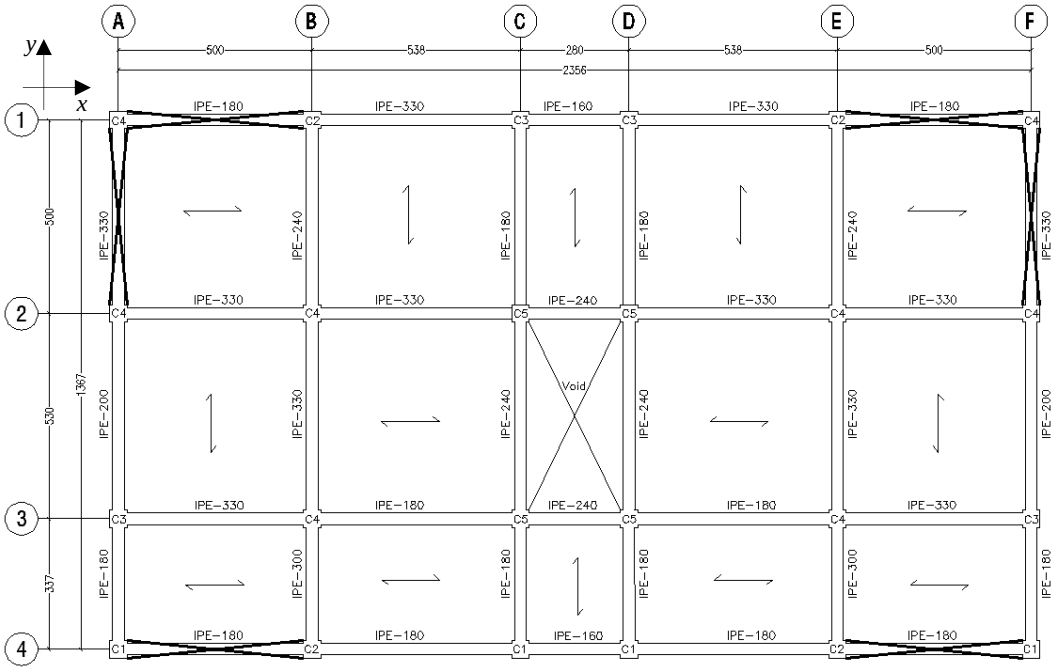

Figure 5.7 - 1st floor plan of the index building (units in centimetre)
IPE: European steel I-beam withparallel flange surfaces

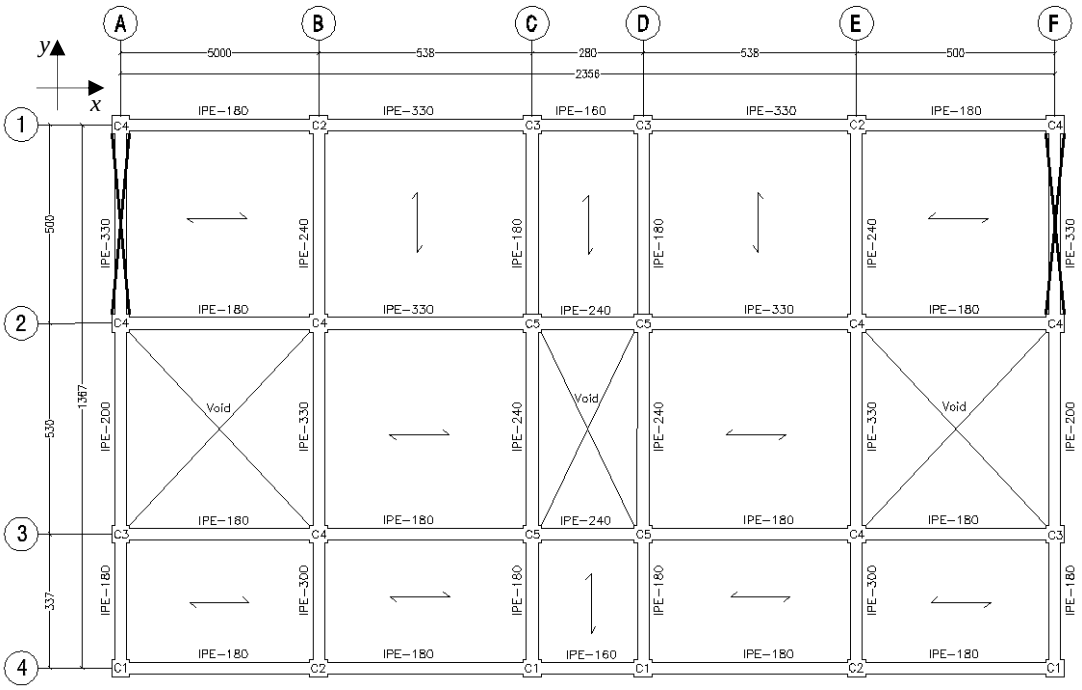

Figure 5.8 - 2nd, 3rd and 4th floor plans of the index building (units in centimetre)
IPE: European steel I-beam with parallel flange surfaces

Table 5.1 - Column sections of the index building

Storeys	Columns Ref.	C1	C2	C3	C4	C5
	4th Floor	HEB-140	HEB-140	HEB-120	HEB-160	HEB-160
	3rd Floor	HEB-140	HEB-140	HEB-120	HEB-160	HEB-160
	2nd Floor	HEB-140	HEB-140	HEB-140	HEB-180	HEB-160
	1st Floor	HEB-140	HEB-160	HEB-140	HEB-180	HEB-160

HEB: European wide flange beams with parallel flange surfaces and approximate equal width and depth

Table 5.2 - Properties of steel sections used

Section Ref.	**A** Cross Sectional Area (cm^2)	**I_{x-x}** Moment of Inertia around major axis (cm^4)	**I_{y-y}** Moment of Inertia around minor axis (cm^4)	**$W_{pl,x}$** Plastic Modulus (cm^3)	**I_T** Torsional (cm^4)
IPE-160	20.1	869	68.3	124	3.6
IPE-180	23.9	1320	101	166	4.8
IPE-200	28.5	1940	142	221	7.0
IPE-240	39.1	3890	284	367	12.9
IPE-300	53.8	8360	604	628	20.2
IPE-330	62.6	11770	788	804	28.3
HEB-120	34.0	864	318	165	13.9
HEB-140	43.0	1510	550	245	20.1
HEB-160	54.3	2490	889	354	31.4
HEB-180	65.3	3830	1360	481	42.3

In addition to the dead load, an imposed load of 200 kgf/m^2 and 150 kgf/m^2 is considered for the floors and the flat roof (4th floor) respectively. The permanent loading consists of floor finishing, joists and metal decks with 0.15-metre-thick concrete slab and is estimated equal to 350 kgf/m^2 for all floors and 370 kgf/m^2 for the roof. The employed structural material and construction practice signify a typical-quality structure. The following section discusses the numerical simulation methods and their differences.

5.5. Characteristics of the Numerical Model

During severe earthquakes a selective of structural elements are supposed to yield or buckle. Hence, both geometric and material nonlinearity should be taken into account while modelling the structures. Using finite element method based on uniaxial elements is a way to face the matter.

The inelastic structural component models are differentiated based on the way plasticity is distributed through the members' cross section and along its length (Deierlein et al., 2010). Accordingly, concentrated plasticity and distributed plasticity methods are introduced as illustrated in Figure 5.9. Two widely used methods to model the nonlinear behaviour of structural components are plastic hinge modelling (concentrated plasticity) and fibre element modelling (distributed plasticity).

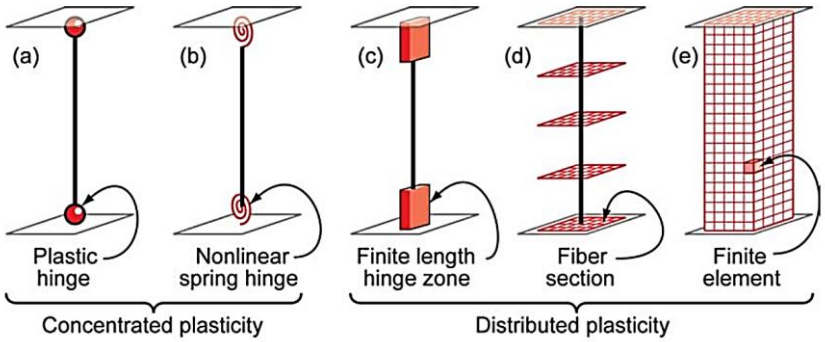

Figure 5.9 – Different numerical models for considering inelasticity (Deierlein et al., 2010)

The structural elements of a building subjected to seismic excitation are mostly stressed at their connections. Where major forces are located at both ends of the elements, the distribution of moment can be assumed linearly, while the shear forces are constant. Therefore, in concentrated plasticity, the plastic deformations are "lumped" at the extremities of a linear-elastic structural element (Clough & Benuska, 1967; Giberson, 1967). A fixed point or predetermined length, typically the plastic hinge length, is determined to be the region in which all inelastic action is concentrated, while elastic properties are assigned to the remainder of the element. The lumped plasticity approach is advantageous due to its simplicity, reduced computational effort and better numerical stability. Moreover, the hinge/spring models may be better suited to capture the nonlinear degradation of the member, through calibration with test data on moment-rotations and hysteresis curves. However, the concentrated methods have limitations since inelastic flexural deformation are assumed to be concentrated at a hinge with predefined and constant length, which cannot fully capture the spread of plasticity.

Distributed plasticity beam–column elements allow plastic hinges to form at any location along the member and offer a more accurate description of the inelastic behaviour (Deierlein et al., 2010). In this case, the inelasticity is monitored in terms of stresses and strains, thus accounting for both flexure and axial force interaction. It consists of a discretization of the cross section into a finite number of axial springs acting in parallel, by considering the Euler-Bernoulli beam theory (Ceresa et al., 2007). Accordingly, the sectional stress-strain state of beam-column elements is obtained through the integration of the nonlinear uniaxial material response of the individual fibres in which the section has been subdivided, fully accounting for the spread of inelasticity along the member length and across the section depth. The number of integration sections and section fibres used in equilibrium computations carried out at each of the element's integrations needs to be defined. Commonly, the single-material sections will usually be adequately represented by 100 fibres with 5 integration sections to capture the hardening.

The section stiffness is computed with the tangent stiffness of each fibre material, its area of influence and its coordinates on the cross section. In contrast to lumped plasticity, the main shortcoming of distributed plasticity elements is that they require more computing resources. They can be easily applied to sections consisting of different material, while avoiding the prior process of calibrating the moment–curvature of members. Moreover, there is no need of introducing any element hysteretic response, as it is implicitly defined by the material constitutive models. However, it should be noted that the hysteresis only works for normal forces and do not consider the shear stresses. Though, the elements are highly sensitive to the implemented material behaviour and thus need to be calibrated with experimental results. The gradual spreading of inelasticity, in fibre models, over the cross section and the element height leads to a smoother transition between elastic and inelastic element response in respect to the lumped plasticity model.

Distributed inelasticity frame elements can be implemented with two different finite elements (FE) formulations, the classical displacement-based (DB) ones and the more recent force-based (FB) formulations. The primary advantage of force-based elements is that it requires a single beam–column element per member to simulate its material nonlinear response. This is in contrary to displacement-based elements, in which a denser mesh at the sections is required where the inelastic deformations are expected to develop.

For this study, the fibre based finite element (FE) software SeismoStruct (v.7.0.1) (SeismoSoft, 2014) is utilised to simulate the nonlinear behaviour of the selected index buildings. The software is capable of predicting large displacement behaviour of space frames under static and dynamic loadings, taking into consideration the geometric non-linearities and

material inelasticity. Large displacements/rotations and large independent deformations relative to the frame element's chord (P-Δ) are considered through the employment of a total co-rotational formulation developed and implemented by Correia & Virtuoso (2006). Another important aspect in simulating the buildings is the choice of representing the building in three- or two-dimensional environment. In the case of structures that are not regular in plan, the torsional effects are often ignored if the structure is considered in two dimensions, which can lead to imprecise results (D'Ayala et al., 2015).

5.6. Modelling Parameters

The developed models consist of numerous parameters, defining the mechanical, geometrical and empirical characteristics of the structure. In this section some of the most critical modelling assumptions and structural characteristics are presented in greater detail.

5.6.1. Steel Members

Force-based beam–column element, consisting of 100 fibre elements, have been selected to model beams, columns and braces. The steel materials are modelled using the cyclic response assuming a uniaxial stress-strain behaviour with kinematic strain hardening, simulated following Menegotto-Pinto steel model (Menegotto & Pinto, 1973). The original model was improved by introducing isotropic strain hardening (Filippou et al., 1983). The model is widely used to simulate the dynamic response of steel members discretized by means of fibres and subjected to normal stresses (Ariyaratana & Fahnestock, 2011; Atlayan & Charney, 2014; Salawdeh & Goggins, 2013).

The properties are allocated according to the original design details as S235 [St 37] (f_{yk}=235 MPa, E=2.1×10^5 MPa, G=7.7×10^4 MPa, ν=0.3, γ=78 kN/m^3). This is the most common steel material used for the residential construction practices in the region under study. The concentric steel braces are modelled as moment-released elements at both ends (i.e. perfectly pinned) and behave as axial members. The hysteretic response of concentric braces is characterized by the buckling in compression, the yielding in tension, moderate hardening and significant pinching when the deformation reverses (D'Aniello et al., 2012). In this study, the cross-section behaviour is reproduced by means of the fibre approach, assigning a uniaxial stress-strain relationship at each fibre following the Menegotto-Pinto steel model (Menegotto & Pinto, 1973). Hence, the in-plane and out-of-plane buckling of the braces are accounted for through the introduced material nonlinearity, particularly the buckling strain (ε_{ult}). Each brace cross-section was divided into a mesh of 100 fibres, while 5 integration points has been considered in each element. It should be noted that some phenomena such as the local buckling of the braces or the low-cycle fatigue effects are beyond the scope of this study.

5.6.2. Masonry Infill panels

As discussed in Chapter 2, the presence of masonry infill panels can substantially alter the response of the structure both globally and locally, and hence assuming a simple elastoplastic system can considerably reduce the reliability of the analysis outcome. This is particularly relevant for mid-rise buildings, characterised by short periods and subjected to substantial stiffness and strength degradation in the post yielding regime, so that the shape of the hysteresis loops and the corresponding energy dissipation capacity have a strong influence on the evolution of damage. Ignoring the mechanical properties associated with the infilled frame such as strength, stiffness and ductility can lead to substantial inaccuracy in the structural analyses. Subjected to seismic excitation, the panels tend to interact with their bounding frames and attract lateral loads, which may result in failure mechanisms, totally different from the bare frame.

In this study, the contribution of infill panels has been considered using the nonlinear macro model proposed by Crisafulli & Carr (2007). A thorough discussion on reasons behind selecting this model and the issues raised by the infill simulation is provided in Appendix-A. The model is capable of considering the most common failure modes identified by Shing & Mehrabi (2002) as the compressive failure, toe crushing and flexural cracking. The adopted model is also capable of simulating the shear behaviour when bond failure occurs along the mortar joints. The model is based on a four-node panel element, which is connected to the frame at the beam-column joints. The panel is represented by six strut members, accounting for the compressive and shear forces separately. Each diagonal direction features two parallel struts to carry axial loads across two opposite diagonal corners and a third one to carry the shear from the top to the bottom of the panel as shown in Figure 5.10. The variation of the stiffness and the axial strength of the masonry struts can be controlled. The shear strut only acts across the diagonal which is in compression and its activation is a function of the lateral deformation of the panel. The axial load struts follow a hysteresis model proposed by Crisafulli 1997, while the shear strut utilises a bilinear hysteresis rule, as illustrated in Appendix-A. It should be noted that in case of frames in which concentric steel braces and infill panels are present, the interaction between the two members cannot be replicated through the selected macro model. However, the summative stiffness and strength are simulated, whereby the contribution of the concentric braces dominates the response. The interaction can be evaluated through FEM and micro modelling, however this investigation is beyond the scope of this study. Moreover, except for the real building selected as case study, the defined index buildings are all moment resisting frame or simple gravity frames with no braces.

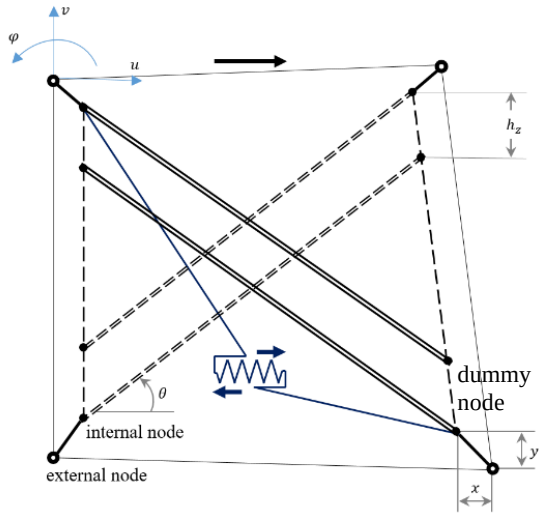

Figure 5.10 – Multi-strut model for infill panels, indicating the truss mechanism and shear spring

As shown in Figure 5.10, the four internal nodes account for the actual points of contact between the frame and the infill panel, indicating the width and height of the surrounding columns and beams. The four dummy nodes are a mean to measure the contact length between the frame and the infill panel. All internal forces are transferred to the external nodes where the panel element is connected to the frame members and the gravity load is absorbed by the surrounding frame.

This configuration allows an adequate consideration of the lateral stiffness and strength of masonry panels and is able to capture shear failure along the mortar joints or diagonal tension failure or crushing of the panel toe (Crisafulli, 1997). The shear friction failure and debonding of the mortar-brick interface are captured by the shear spring. This mechanism happens after a stepped cracking pattern or in case the horizontal sliding along the mortar joint occurs. The diagonal tensile failure of panel units ensues due to a combination of compressive and shear stresses in the masonry panel. The corner crushing can occur in case of rather weak infills surrounded by a frame with weak joints and strong members, resulting in local failure of masonry units at the end of diagonal compression struts (i.e. the loaded corners).

A limitation of the implemented infill model is that the direct transfer of shear forces from the panel along the axis of the columns and beam are not accounted for, since the strut elements are connected to the beam-column joints of the frame. Therefore, the model does not have the capacity of simulating potential shear failure developed in the columns, even though it can account for the eccentricity of the struts. However, while this has been reported to be a critical issue in weak concrete frames (D'Ayala et al., 2009; Mehrabi et al., 1996), limited cases of shear failure in the steel frame have been observed and in most cases the infill panel fails before the steel frame due to its lower shear capacity (Moghaddam, 2004).

Post-earthquake investigations conducted by Manafpour (2003) and Personeni & Pilato (2008) on the 2003 Bam earthquake has reported cases of out-of-plane failure of masonry panels in case of both reinforced concrete and steel framed structures. As discussed in Chapter 2, out-of-plane failure is among the common failure types of masonry panels and hence it should be accounted for in the modelling. In the present work, the employed macro model cannot adequately evaluate the extent of this failure type. The model accounts for the out–of–plane failure of the panel by considering a failure drift limit in the direction normal to the infill plane. The drift is introduced as a percentage of the storey height and once the panel, not the frame, reaches the allocated out-of-plane drift value, it will no longer contribute to the structural resistance nor the stiffness. The allocated drift limit value for each of the considered infill panels are presented in Table 5.4. According to the experimental observations of Flanagan & Bennett (1999), steel framed infilled panels have an acceptable out-of-plane stability under both inertial (uniform) loads and imposed drift loads. This is primarily due to arching or the development of in-plane membrane forces due to the type of masonry material and mortar.

Beside the parameters employed to define the hysteresis behaviour, in order to fully characterise this type of element, a number of items need to be defined such as the panel thickness and the volumetric weight of the panel. The initial strut area ($A1$), representing the stiffness, is defined as the product of the panel thickness and the equivalent width of the strut (b_w). The equivalent strut width is measured based on experimental data and analytical results, varying between 10% and 25% of the diagonal of the infill panel (d_m). A summary of numerous empirical expressions with varying degree of complexity can be found in the work of (Smyrou et al., 2011). Furthermore, due to cracking of the infill panel, the contact length between the frame and the infill decreases as the lateral and consequently the axial displacement increases, affecting thus the area of equivalent strut, initially taken as $A1$. Hence, a second value is introduced for the strut area as a percentage of the initial strut area. In this case, it is assumed that the area varies linearly as a function of the axial strain (ε_m) and the two strains, between which the area reduction takes place, are defined as input parameters of the masonry hysteresis model. A link element can be implemented between the frame and the infill panel nodes, taking into account the fact that the infill panels are commonly not rigidly connected to the surrounding frame.

Moreover, the equivalent contact length (h_z) (vertical separation between struts) is defined as a percentage of the vertical height of the panel, accounting for the contact length (z) between the frame and the infill panel.

$$h_z = 0.5\ \pi\ \lambda^{-1} \tag{5.1}$$

$$\lambda = h \sqrt[4]{\frac{E_m t_w \sin(2\theta)}{4 E_{col} I_{col} h_w}} \tag{5.2}$$

where λ is the dimensionless relative stiffness parameter proposed by Stafford-Smith (1966), E_m is the elastic modulus of the masonry, t_w is the thickness of the panel, θ is the angle of diagonal strut with respect to the beam, $E_{col}I_{col}$ is the bending stiffness of the column and h_w represents the height of the infill panel. In order to replicate the presence of the openings in the infill panels, the strut area ($A1$) should be decreased, which in return will reduce the panel's stiffness. This strut area reduction is conducted in proportion to the area of the opening with respect to the panel.

The shear behaviour is represented according to a bond-friction model, in which the model assumes that the behaviour of mortar joints is linear elastic till reaching the shear strength. At reaching the shear strength, the bond between mortar and brick is broken and the cracks start propagating in the affected region. Hence, one part of the infill panel slides with respect to the other, at this point only the friction mechanism remains and the bond strength has no influence.

To replicate the response of the panel, the infill model characteristics have been calibrated with the outcome of the pseudo-dynamic tests on masonry infill panels built with the identical materials used in the construction of the index building. Two types of infill panels have been considered, a solid clay brick (SCB) and a hollow clay block (HCB), both commonly used as the primary material for walls.

The first infill panel consists of 219×110×66mm solid clay brick (SCB) units, placed in running bond with Portland cement type I and sand mortar. Experimental tests conducted by Tasnimi & Mohebkhah (2011) on the behaviour of matching brick-infilled steel frame with and without opening have been utilised for this process. Following the actual plan of the building, the location of solid infill panels and the ones with window opening have been set and positioned in the model accordingly. Only one type of infill panel with window opening (centred 1.2m × 0.6m) has been implemented in the numerical model for all arrangements, due to deficiency of experimental observations. The average prism compressive strength (f'_m) for each arrangement of the infill panel has been evaluated following ASTM C1314-10 (2010) and ASTM C10-07 (2007). Accordingly, for full solid infill panel, the prism compressive strength is 7.4 MPa and for the ones with window opening, located at its centre is equal to 8.5 MPa. Properties of the masonry infill panels and its components are presented in Table 5.3.

Table 5.3 - Properties of the masonry infill panel and its components (Mohebkhah, 2007)

Characteristics	**Brick**	**Mortar**	**Brickwork**	
			Solid Panel	**with Opening**
Compression strength (MPa)	12.6	10.1	7.4	8.5
Tensile strength (MPa)	0.48	0.5	0.12	0.12
Young's Modulus (MPa)	8442	1000	5194	5985
Cohesion (MPa)	3.64	0.48	-	-
Internal friction angle (degree)	30	36	-	-

The single-storey, single-bay moment–resistant steel frame used in the physical testing has been simulate in SeismoStruct (v.7.0.6) (SeismoSoft, 2014), making sure the hysteresis behaviour simulates the test observations. The frame was fabricated using IPE140 sections (A=16.4 cm^2, I_{xx}=541 cm^4, d=14, b_f =7.3, t_f =0.69, t_w =0.47 cm). In-plane cyclic loading, identical to the displacement-history of the experiment, was applied at the top corner of the frame surrounding the infill panel. A full solid infill and one with window opening located at its centre (ratio ≈ 20%) have been calibrated with the experimental observations. This was followed by a sensitivity study, whereby the relative importance of each parameter necessary to calibrate the model was evaluated. Further discussion on the calibration process and the sensitivity of the model parameters are presented in Appendix-A. For both case of solid panel and panel with opening, the calibration outcomes in terms of base shear and top displacement are shown in Figure 5.11. In case of the solid infill panel, the calibrated numerical model has a good agreement with the experimental observation in both hysteresis and envelope curve. In case of the panel with window opening, a slight disparity can be observed in the softening part as the model overestimates the experimental results. As discussed in Chapter 2, this disagreement is mainly due to the limitation of the infill macro models and the concept of equivalent diagonal struts in accounting for the panel openings (Yuen et al., 2016).

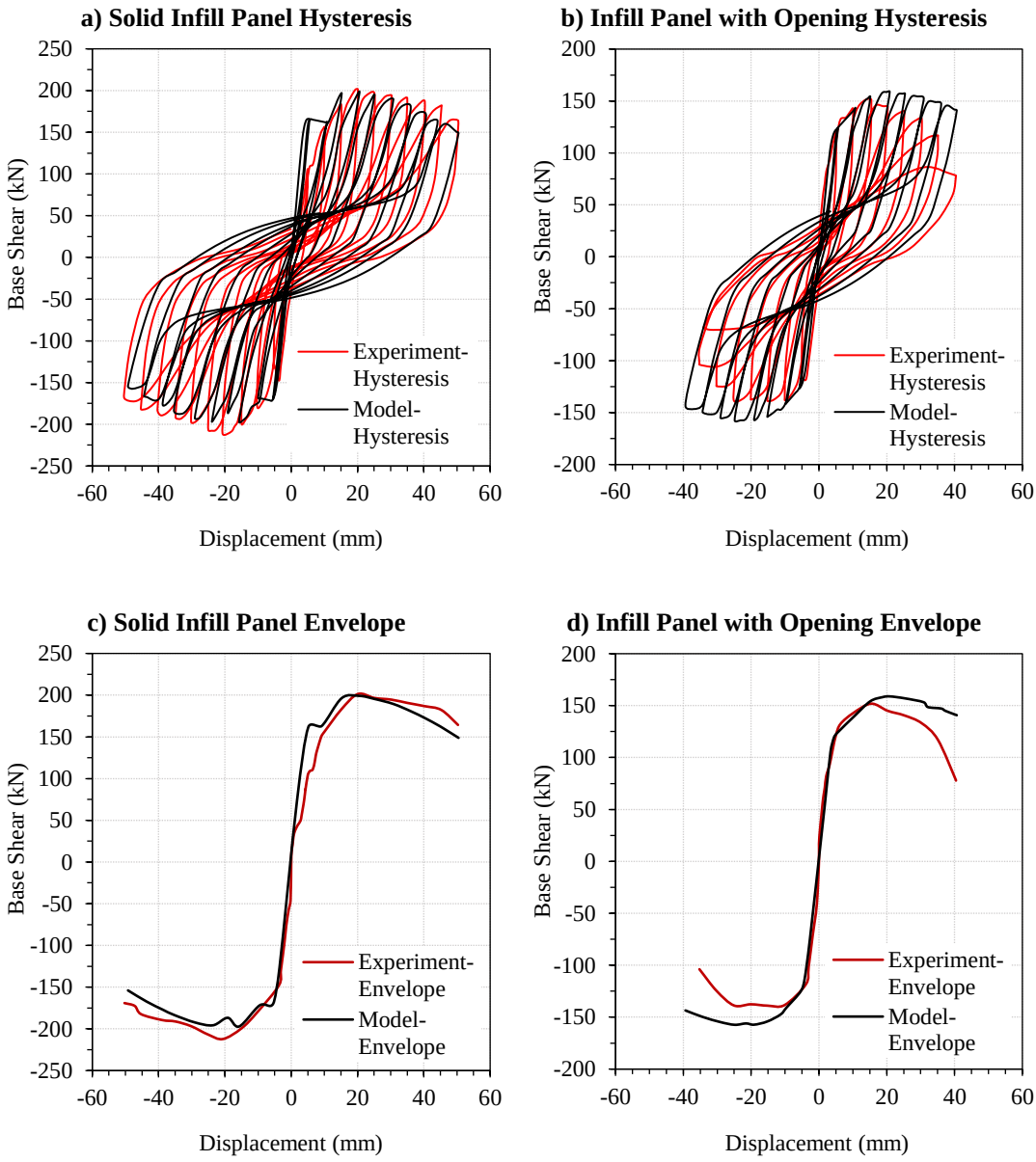

Figure 5.11 - Backbone and Hysteresis curves resulted from calibration of numerical infill model with experimental results of solid clay brick (SCB) (Tasnimi & Mohebkhah, 2011)

As a result, the model was set to be as realistic as possible by considering the location of masonry infills, lateral stiffness, strength of the elements and the effect of any opening (door and windows) on the panels. The expected failure mode of each masonry infill panel is illustrated in Figure 5.12 according to the experimental observations of Tasnimi & Mohebkhah (2011). The diagonal cracks indicate the direction of the equivalent strut.

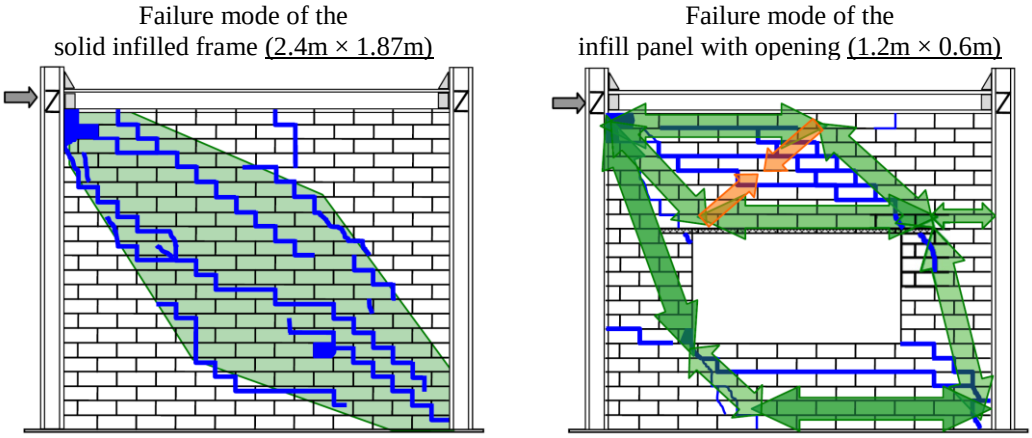

Figure 5.12 - Failure mode cases observed for each experimental sample
(Tasnimi & Mohebkhah, 2011)

The second infill type, consists of 200×300×300mm structural hollow clay block (HCB) units and type N masonry cement mortar. In-plane tests conducted by Flanagan & Bennett (1999), have been used for calibrating the infill model. Accordingly, the clay tiles were laid with their cores horizontal (side construction) using approximately 19 mm full bed joints, and only face shell mortar in the head joints. Each infill was bonded to the column and beam by snugly packing mortar between the steel and the tile. Mortar was not placed between the panel and the flanges of the enclosing columns. No reinforcement was used in the masonry. Prism tests on the specimen indicates a prism compressive strength of 5.6 MPa and elastic modulus of 5.3 GPa (Bennett et al., 1997). Similar to the first infill, the calibration is conducted on a single-storey, single-bay moment–resistant steel frame (Column: W250×45, Beam: W310×52), simulated and loaded after the experimental setup. In this case, experimental observations were limited to only solid panels, hence the infill with window opening is simulated following the observations of Tasnimi & Mohebkhah (2011), in which there is a drop in strength and stiffness of the SCB infill. The calibrated and original hysteresis of HCB and the observed damage at different displacements are presented in Figure 5.13. Figure 5.14, compares the experimental and simulated backbones, as well as the assumed backbone for infill panel with window opening. The obtained hysteresis and backbone for the infill model of HCB has a good agreement with the experimental observation. A minor discrepancy exists after the ultimate point at which the model cannot fully capture the strength drop.

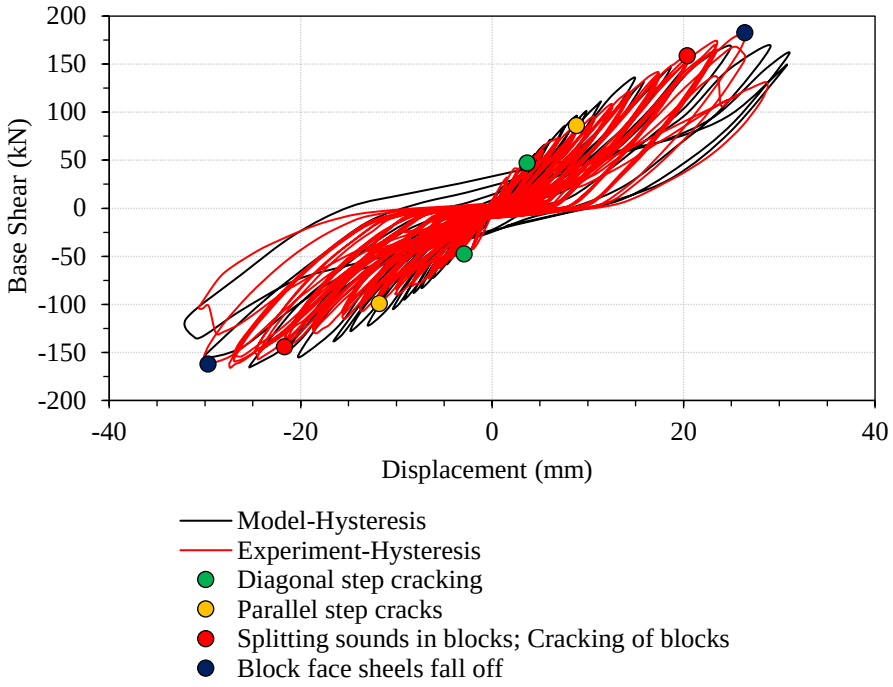

Figure 5.13 - Hysteresis curve resulted from calibration of numerical infill model with experimental results of hollow clay block (HCB) (R. Flanagan & Bennett, 1999)

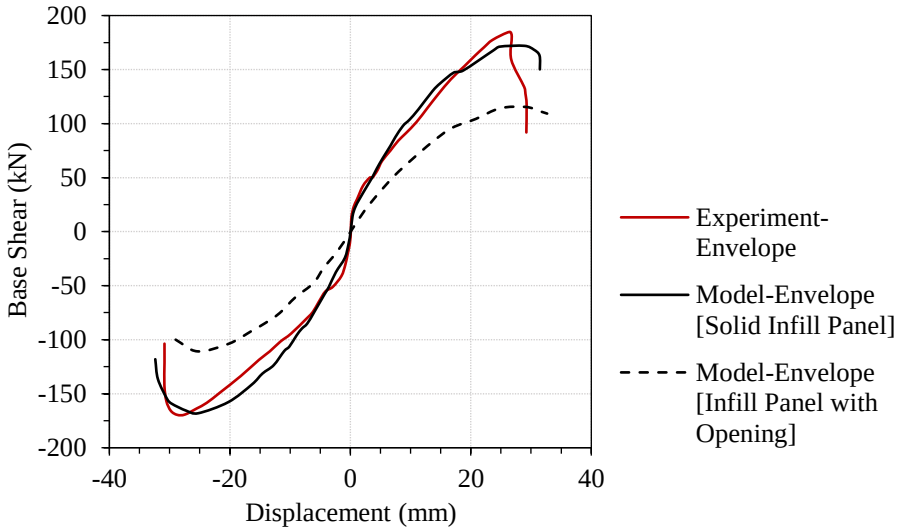

Figure 5.14 - Backbone curve resulted from calibration of numerical infill model with experimental results of hollow clay block (HCB) (R. Flanagan & Bennett, 1999)

Table 5.4, presents the parameters applied to characterise the equivalent strut model and its positioning within the frame for both SCB and HCB. The defining parameters of the masonry hysteresis model are presented in Table 5.5. The typical empirical values suggested in various studies are given in Table 5.6. Seventeen parameters need to be defined in order to fully characterise the response curve, from which nine are empirical parameters, related to the cyclic loading. A sensitivity studies carried out by Smyrou et al. (2011) have shown that only three of these empirical parameters (α_{ch}, γ_{un} and e_{x1}) play a significant role in the quantification of the

energy dissipation capacity of the infill panel. The extend of the defining parameters, allows the model to represent a wide range of fragile masonry materials.

Table 5.4 - General parameters for the infilled frame

Properties	**Definition**	**Solid Clay Brick (SCB)**		**Hollow Clay Block (HCB)**	
		Solid Infill Panel	**Infill with Opening**	**Solid Infill Panel**	**Infill with Opening**
Infill panel thickness (t_i)	Width of the panel brick alone or including plaster	0.110 m		0.195 m	
Out-of-plane failure drift	Defined as a percentage of storey height	5.0%		5.0%	
Strut Area 1 ($A1$)	Product of panel thickness (t_i) and equivalent width of strut (b_w)	0.022 m^2	0.011 m^2	0.021 m^2	0.010 m^2
Strut Area 2 ($A2$)	Accounts for the area reduction due to cracking of infill	45% of strut Area1	40% of strut Area1	42% of strut Area1	37% of strut Area1
Equivalent contact length (h_Z)	Accounting for the contact length between frame and infill panel (Stafford-Smith 1966) $0.5\pi\lambda^{-1}$	17% of vert. panel side		20% of vert. panel side	
Horizontal offsets (X_{oi})	Representing the reduction due to the depth of column	7.4% of horiz. panel side		5.0% of horiz. panel side	
Vertical offsets (Y_{oi})	Representing the reduction due to the depth of beam	5.8% of vert. panel side		5.0% of vert. panel side	
Proportion of stiffness assigned to shear (γ_s)	Proportion of the panel stiffness (computed by program) that should be assigned to the shear spring (typical: 0.2 to 0.6)	10%	20%	7%	12%
Specific weight (γ)	Volumetric weight of the panel	13 (kN/m^3)		10 (kN/m^3)	

Table 5.5 - Equivalent diagonal compressive masonry strut curve parameters

Curve Properties	**Solid Clay Brick (SCB)**		**Hollow Clay Block (HCB)**		**Typical Values**[1]
	Solid Infill Panel	**Infill with Opening**	**Solid Infill Panel**	**Infill with Opening**	
Initial young modulus (E_m)	5194 MPa	5194 MPa	5300 MPa	5300 MPa	$400f_{m\theta}$ - $1000f_{m\theta}$ (kPa)[2]
Compressive strength (f'_m)	7.4 MPa	8.5 MPa	5.6 MPa	5.6 MPa	-
Tensile strength (f_t)	0.12 MPa	0.12 MPa	0.10 MPa	0.10 MPa	-
Strain at maximum stress (ε_m)	0.0015	0.0015	0.0020	0.0015	0.001 - 0.005 (m/m)
Ultimate strain (ε_u)	0.024	0.024	0.015	0.015	-
Closing strain (ε_{cl})	0.004	0.004	0.004	0.004	0 - 0.005 (m/m)
Strut area reduction strain (ε_1)	0.001	0.001	0.001	0.001	0.0003 - 0.0010 (m/m)
Residual strut area strain (ε_2)	0.0027	0.0027	0.004	0.0032	0.0006 - 0.016 (m/m)

[1] According to Crisafulli (1997)

[2] Empirical relationships proposed by Smyrou (2006), Crisafulli (1997), Paulay & Priestley (1992), Hendry (1990), San Bartolome (1990), Sinha & Pedreschi (1983), Sahlin (1971)

Table 5.6 - Equivalent diagonal compressive masonry strut curve empirical parameters

Curve Properties	Solid Clay Brick (SCB)		Hollow Clay Block (HCB)		Typical Values
	Solid Infill Panel	Infill with Opening	Solid Infill Panel	Infill with Opening	
Starting unload. stiffness factor (γ_{un})	1.5	1.5	1.5	1.5	1.5 - 2.5 (-)
Strain reloading factor (α_{re})	0.2	0.2	0.2	0.2	0.2 - 0.4 (-)
Strain inflection factor (α_{ch})	0.7	0.7	0.7	0.7	0.1 - 0.7 (-)
Complete unloading strain factor (β_a)	1.5	1.5	1.5	1.5	1.5 - 2.0 (-)
Stress inflection factor (β_{ch})	0.9	0.9	0.9	0.9	0.5 - 0.9 (-)
Zero stress stiffness factor (γ_{plu})	1.0	1.0	1.0	1.0	-
Reloading stiffness factor (γ_{pr})	1.5	1.5	1.5	1.5	-
Plastic unloading stiffness factor (e_{x1})	3.0	3.0	3.0	3.0	-
Repeated cycle strain factor (e_{x2})	1.4	1.4	1.4	1.4	-

For the bilinear hysteresis shear curve, the parameters presented in Table 5.7 have been employed for both cases of solid and panel with opening.

Table 5.7 – Masonry shear curve parameters

Curve Properties	Solid Clay Brick (SCB)		Solid Clay Brick (SCB)		Typical Values
	Solid Infill Panel	Infill with Opening	Solid Infill Panel	Infill with Opening	
Shear bond strength (τ_0)	0.48 MPa	0.48 MPa	1.50 MPa	1.50 MPa	300 – 600 (kPa)[1] 100 - 1500 (kPa)[2] 100 - 700 (kPa)[3]
Friction coefficient (μ)	0.74	0.74	1.2	1.2	0.1 - 1.2 (-)
Maximum shear strength (τ_{MAX})	0.60 MPa	0.60 MPa	0.30 MPa	0.30 MPa	-
Reduction shear factor (α_S)	1.5	1.5	1.5	1.5	1.4 - 1.65 (-)

Empirical values proposed by [1] Hendry (1990), [2] Paulay & Priestley (1992), [3] Shrive (1991)

Beside the main defining parameters of strength and stiffness (i.e. f'_m and E_m), as expected the stress-strain relationship of the masonry material is heavily influenced by the ultimate and closing strain and the strain values allocated for the strut area's reduction and residual. These values should be extracted from experimental tests on masonry specimens. Moreover, according to the sensitivity study, factors such as the strut area at different strains ($A1$ and $A2$), the equivalent contact length (h_z) have a considerable impact on the response of the infilled panel. A summary of the sensitivity analysis, conducted on the solid clay brick is provided in Appendix-A for the most influential parameters.

5.6.3. Beam-Column Connections

A moment resisting frame (MRF) comprises of several structural components, which serve as lateral-force resisting elements and contribute to the flexural rigidity of the entire structure. Although columns and beams have a significant effect on the lateral load carrying behaviour of stated structures, the modelling of beam–column connections may be of equal importance once the structure goes beyond the elastic regime.

The actual effect of beam-column joint arrangement on the global performance of the structure is commonly ignored in design and analysis stages by treating most arrangements as fully rigid. Evidence of previous structural damage observed after the 1994 Northridge earthquake in California (M_w 6.7), the 1995 Hanshin-Awaji (Kobe) earthquake in Japan (M_w 6.9) and 2003 Bam earthquake in Iran (M_w 6.6), indicates the deficiency of joints as one of the most dominant causes of structural failure (FEMA-350 2000; Yamazaki & Murao 2000; Manafpour 2003). The primary distortion of steel beam-column connections is their rotational deformation, caused by the in-plane bending moment (Figure 5.15). This connection deformation has a destabilising impact on the frame by decreasing the stiffness of members. Furthermore, any increase in frame's drift will intensify the P-Δ effect. Thus, the non-linear behaviour of beam-to-column connections is of high importance and their influence on the global response of the index building should be included in the numerical analysis.

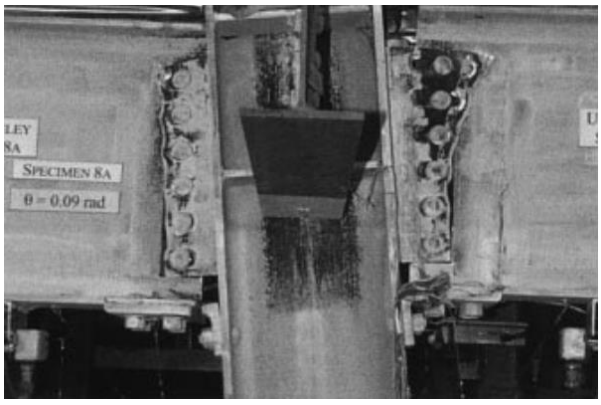

Figure 5.15 - Example of a partially restrained composite connection with seat angle;
Failure mode: crushing of concrete slab, fracture of shear tab and seat angle
(Liu & Astaneh-Asl et al. 2000)

The following sections, looks through the beam-column joint type of the index building. Initially the connection type is introduced and later a numerical approach is discussed for simulating the joint's behaviour in the nonlinear models.

5.*6.3.1. Partially Restrained Composite Connections*

Partially restrained composite connections (PR-CC) are partial strength connections which can withstand the moment induced by imposed, wind and seismic excitation in low-to-moderate height frames (Roberto T. Leon, 1998). Partial strength means that the nominal

strength of the connection is smaller than the beam's none-composite capacity. According to BS EN 1994-1-1 (clause 1.4.2), the word "composite" is used to indicate that the connection engages the reinforcing steel in the concrete slab to form the top portion of the moment resisting mechanism under the applied loadings. Hence, the role of the concrete slab is fundamental for the seismic performance of the connection and is mainly influenced by the type, amount and distribution of reinforcement embedded in the concrete flange and the shear connectors as shown in Figure 5.16.

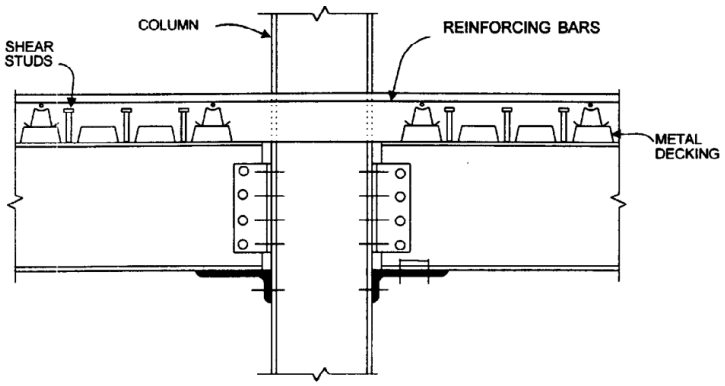

Figure 5.16 – Typical partially-restrained composite connection (PR-CC) (Roberto T. Leon, 1998)

The most important differences between a fully rigid and a partially rigid steel frame are that both nonlinear behaviour and the partial strength characteristics of the PR-CC should be incorporated in the analysis and design. In this case, the connection flexibility impacts the serviceability limit state, hence the required stiffness for drift control may govern the design. While at ultimate, PR-CC may lead to weak connection-strong column mechanism and second order effect must be considered. Although, due to the higher flexibility of partially restrained frames under lateral load compared to fully rigid frames, P-Δ effects are generally not more significant (FEMA P-751, 2012; Hajjar & Leon, 1998).

Stiffness, strength and rotation capacity of a composite connection depend on the load-deformation relationships of the joint components, including the steel connection, the reinforced concrete slab and the contact plates. The bottom portion is commonly supported by seat angles or double web angles to resist the shear. As further strength and stiffness is provided by the floor slab, additional shear studs and slab reinforcement are required in the negative moment regions adjacent to the columns, while the need for a top angle or top plate is eliminated.

In mathematical terms, a connection is classified partially restrained based on the ratio of the secant stiffness at service loads (K_{ser}) to the stiffness of the framing girder (Figure 5.17) (ANSI/AISC 360-10, 2010). In case $K_{ser} = {E\ I_g}/{L_g} \geq 20$, then the connection is considered

as fully restrained. If $K_{ser} = {E\ I_g}/{L_g} \leq 2$, it is acceptable to consider the connection to be simple. The connections having the stiffness between these two limits can be categorised as partially restrained. L_g and $E\ I_g$ are the length and bending rigidity of the girder respectively.

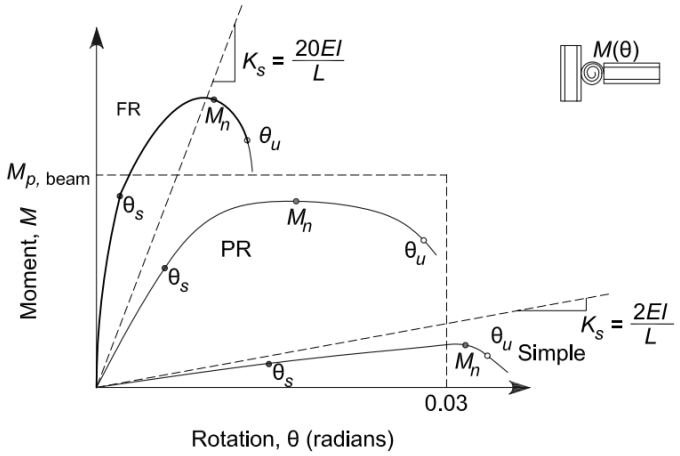

Figure 5.17 - Strength, stiffness and ductility characteristics of the moment-rotation response of a fully restrained (FR), partially restrained (PR) and simple connection (ANSI/AISC 360-10, 2010)

Many advantages of PR-CC would be lost in fully restrained connection, mainly due to larger design moments at columns, loss of ductility and hence increased susceptibility to local and lateral buckling (Figure 5.18). However, a larger number of frames are required to resist lateral load in comparison to a structure with fully restrained connections.

Generally, PR-CC connections tend to improve the performance of relatively weak steel connections. Due to their good hysteretic performance with minimal loss of stiffness, the connection is recommended for low-rise buildings in areas with moderate seismic risk (Hajjar & Leon, 1998). Utilising this type of connection instead of fully rigid ones can reduce the beam member size, leading to a more cost-effective design, especially in unbraced frames. Additionally, semi-rigid connections, introduce extra redundancy in the structure and an optimal distribution of bending moments in structural components.

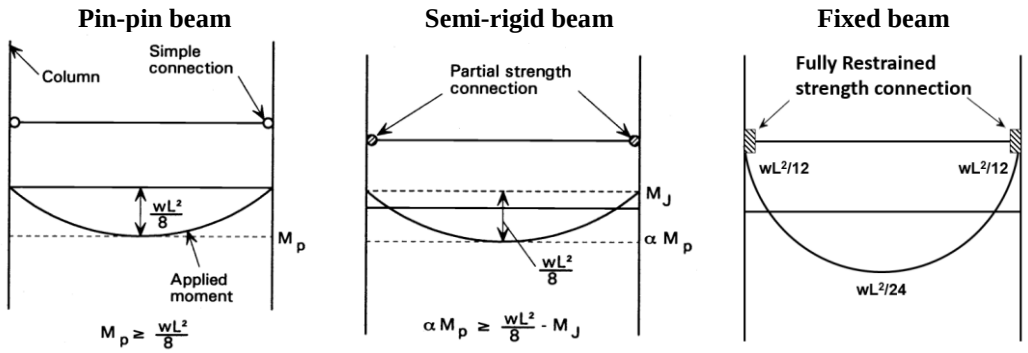

Figure 5.18 – Moment distributing of a simple frame subjected to a uniform distributed force (P) with three beam-column connection arrangement

The behaviour of PR-CC connections has received more attention after failure of composite connections (mainly welded) in 1994 Northridge (M_w 6.7) and 1995 Hanshin-Awaji (Kobe) earthquakes. A considerable number of empirical studies have been conducted on this type of connection to define appropriate hysteretic behaviour under monotonic and cyclic loading. Moment-rotation (M-θ) characteristics of semi-rigid connection with metal decking slabs were first investigated by Johnson and Hope-Gill (1972). Later, Ren et al (1995) and Anderson et al (2000) used different springs to represent the different components of the composite connections in order to calculate the joint stiffness, which is the basis of the component method and has been widely implemented in studies such as Tschemmemegg (1988), Madas (1993) and Rassati et al (2004).

In general, four types of partially restrained composite connections are implemented in steel framed structures as shown in Figure 5.19 (Roberto T Leon, 1998; Rassati et al., 2004).

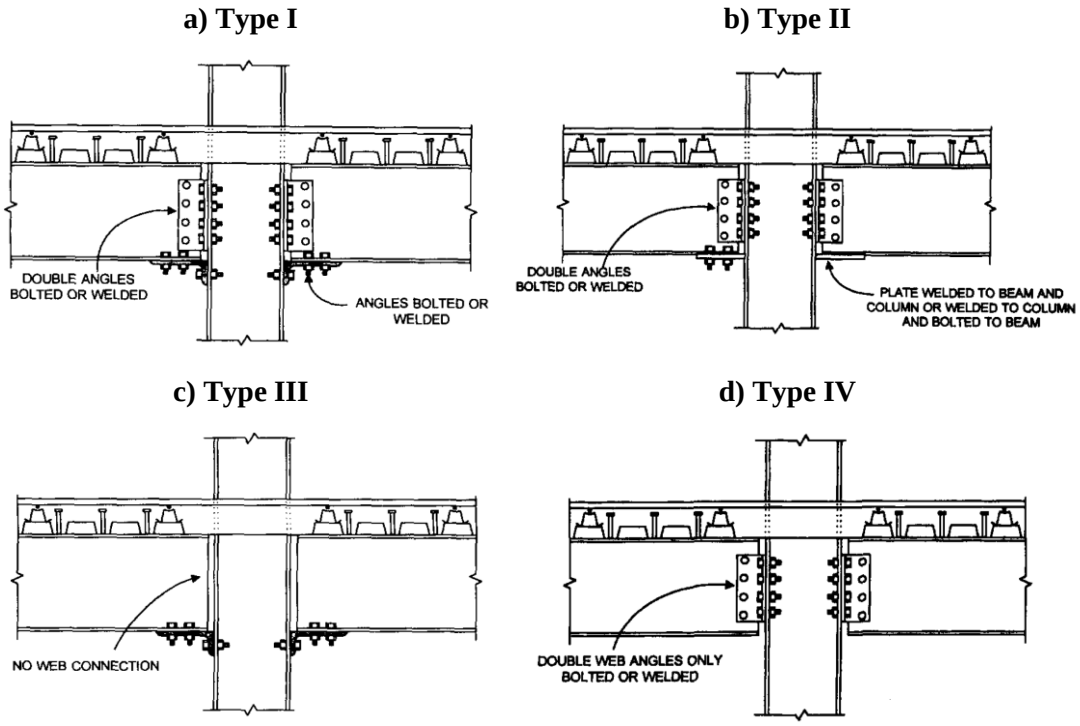

Figure 5.19 - Different arrangements of partially restrained composite connections (Rassati et al. 2004)

Type I: This type consists of a seat angle, a double angle shear connection to the web, and continuous slab reinforcement across column lines (Figure 5.19a). The seat angle provides the compression component in bearing, while under negative bending, the slab reinforcement provides the tension component of the couple. Due to high strength of the reinforcing steel and the larger moment arm between the tensile and compressive forces, this connection has a significantly higher moment capacity than a typical top and seat angle connection. Furthermore, PR-CC has a higher stiffness as the slab's reinforcement yields in almost pure

tension and at higher stress in comparison to a top steel angle. Additional stiffness can be gained by using fully tensioned high strength bolts which enhance the contribution of the web angles. The shear capacity of the bolt attaching the seat angle to the bottom beam flange is the controlling parameter in case of negative bending. However, under positive bending (load reversal) the bottom angle will pull out at relatively low loads, resulting in an unsymmetrical and degrading moment-rotation hysteresis behaviour. Thus, the thickness of the bottom angle should be sufficiently designed to provide a more symmetric hysteresis behaviour.

Type II: This connection consists of a bottom plate welded to the column, double web angles to resist shear and reinforced slab (Figure 5.19b). The bottom plate can either be welded to the beam with a full penetrative groove weld or bolted. The connection results in a very stiff system as the welded bottom plate carries both tension and compression forces directly. Under cyclic loading, a large initial stiffness and symmetric behaviour is observed. However, following the poor performance of welded connections in 1994 Northridge earthquake, this type of connection is not recommended for seismic regions.

Type III: This connection type has identical characteristics to type I, with the exception of not having the double web angles (Figure 5.19c). Due to the absence of web angles, there is no additional strength and restraint once the seat angle yields due to positive moment or the slab reinforcement yields due to negative moment. Thus, the seat angle must be designed in a way to transfer all axial forces, bending moments and shear forces.

Type IV: This connection only consists of bolted double web angles and the slab with continues reinforcement (Figure 5.19d). Although in general the angles are relatively weak, their moment capacity can be improved significantly by increasing their thickness and lowering their position toward the bottom flange of the beam.

Among the discussed arrangements of PR-CC, type I has been extensively tested experimentally and numerically under large cyclic loading (Leon, 1990; Liu & Astaneh-Asl, 2000; Tong et al., 2005).

5.6.3.2. Beam-Column Connections of the Index Building

In the case of the selected index building, the beam-column connections are categorised as partially restrained composite connection, comprising of a lightly reinforced concrete slab with metal deck covering the top flange of the beam. The beam is then connected to the column through a bolted plate, which at one end is welded to the flange of the column. Additionally, the beam is rested on a cleat angle, welded to the flange of the column and bolted the bottom flange of the beam. Figure 5.20, illustrates the actual beam-column connections of the building

under study. This arrangement is similar to Type I of partially restrained composite coinnections, discussed in section 5.6.3.1.

Figure 5.20 - Beam-column connection of the index building

Following the capacity design philosophy, the hinging region are required to be carefully detailed to dissipate energy and that all other elements in the structure remain essentially elastic as the maximum plastic capacity of the hinging regions is reached. Hence, the detailing of PR-CCs is required to provide stable, ductile yielding mechanism such as tension yielding of the angle legs rather than a sudden, brittle failure such as the bolt shearing.

Under gravity loads (negative moment) the slab reinforcement provides the tension part of the couple, while the angle in bearing acts as the compression member. Hence, the behaviour is governed by gradual yielding of the reinforcing bars and not by some brittle or semi-ductile failure mode (e.g. shear of bolts or local buckling of the bottom beam flange). This detailing adds significant moment capacity to the connection in comparison to a typical top and seat angle cleats, due to increase in steel strength and lever arm.

In case of seismic loading that induce moment reversals (positive moments) at the connections should be governed by gradual yielding of the bottom connection elements. Under these conditions the slab can transfer very large forces to the column by bearing if the slab contains reinforcement around the column in the two principal directions. This results in cracks in the slab and the yielding of the slab reinforcement will localise around the major cracks near the column. The bottom angle may pull out at relatively low loads resulting in unsymmetrical hysteresis behaviour. In this case, brittle failure modes to avoid include crushing of the concrete and buckling of the slab reinforcement. The composite connections will provide substantial strength reserve capacity, reliable force redistribution mechanisms (i.e., structural integrity), and ductility to frames. The detailing of the index building's connection indicates that the stated feature has been considered in the design.

Figure 5.21 shows a typical moment-rotation curve for PR-CC connections under cyclic loading, indicating a good energy dissipation capacity and some minor pinching loops as the rotations exceed 10 milli-radians. The envelope of the hysteresis indicates that the behaviour can be replicated through asymmetric elastic-plastic curve with isotropic hardening rule.

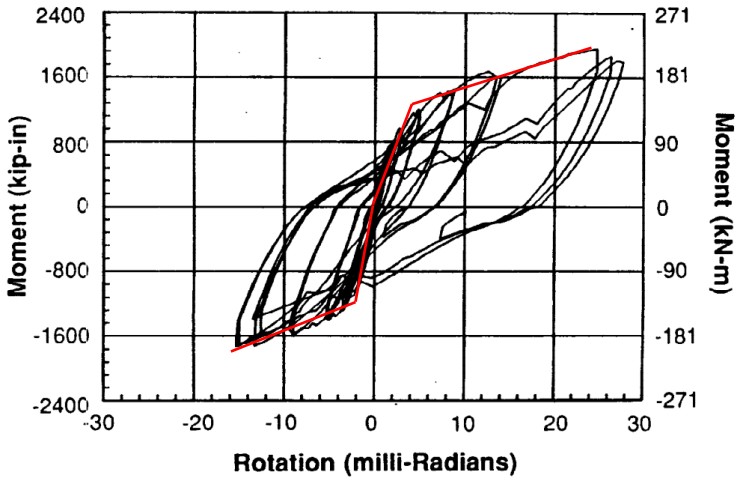

Figure 5.21 – Typical cycle moment-rotation hysteresis curves for PR-CC (Leon, 1996)

Majority of analysis software simulate the beam-column connections as fully rigid and are not fully capable of replicating the actual behaviour of semi-rigid connections and the flooring system, despite the number of studies dedicated to numerical simulation of the composite joints (Nogueiro et al., 2005; Vasdravellis et al., 2009; Vatansever & Yardimci, 2010). Therefore, a detailed and accurate M-θ curve of the PR-CC is a prerequisite for simulating the behaviour. The curve can be defined based on experimental studies on full-scale specimens or from catalogue of M-θ curves available in the literature considered (Braconi et al., 2008, 2007; Kumar & Smitha, 2013; Lee & Lu, 1989; Leon, 1987; Liu & Astaneh-Asl, 2000; Park et al., 2010; Rassati et al., 2004; Vasdravellis et al., 2009). Furthermore, detailed finite element models of the connection, in which all pertinent failure modes and the non-linear material properties of the connection components are incorporated, can indicate the behaviour.

An alternative is to utilise simplified models, in which behavioural aspects are lumped into simple spring (links) configurations and other modes of failure are eliminated by establishing proper ranges for the pertinent variables. Three-dimensional link elements with uncoupled axial, shear and moment actions, are commonly used to model pinned or flexible beam-column connections. The link element connects two coincident structural nodes and require the definition of an independent force-displacement (or moment-rotation) response curve for each of its local six degrees-of-freedom systems (i.e. F1, F2, F3, M1, M2, M3), including those for which the response of the two nodes is identical (Figure 5.22). The latter can be modelled by adopting a linear response curves with very large stiffness values, to guarantee no relative displacement occurs between the two nodes in that particular degree-of-freedom. The

numerical moment-rotation curve is idealised using an asymmetric elastic-plastic curve with isotropic hardening rule, which can represent the initial stiffness and the post-yield hardening in positive and negative regions up to the ultimate point, as indicated in Figure 5.21. For the selected index building, a total of 96 link elements have been defined at the connection joints in SeimoStruct (Figure 5.23).

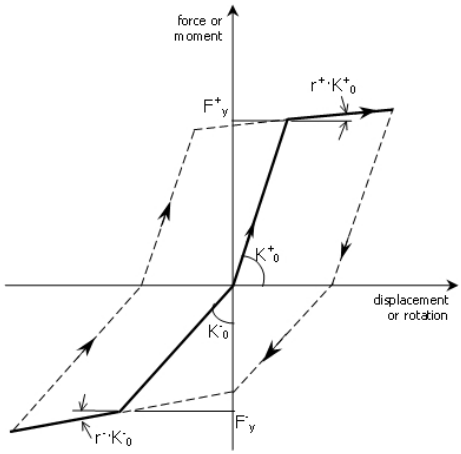

Figure 5.22 - Asymmetric elastic-plastic curve with isotropic hardening rule for simulating joint behaviour

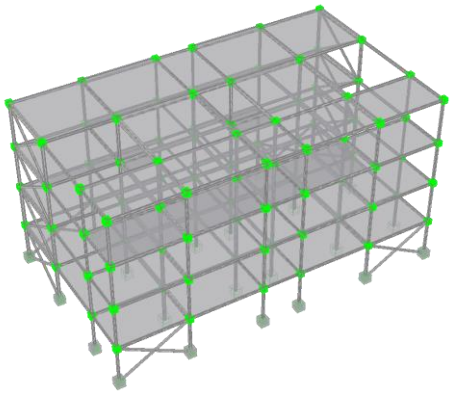

Figure 5.23 – Link elements implemented in the numerical model at every beam-column joint

The properties of the monotonic moment-rotation relationship for the idealised curve of PR-CC (i.e. positive and negative yield forces, initial stiffness and post-yield hardening ratio) can be predicted through experimental and parametric studies of ASCE Design Guidelines for Partially Restrained Composite Connections (1998), Leon & Bazzurro (2007) and FEMA P-751 (2012). The following are the formulation employed to define the numerical curve of the PR-CC designed for the selected index building.

For positive bending (slab in compression, bottom angle in tension)

$$M^{+} = C_1\left(1 - e^{-C_2\theta}\right) + (C_3 + C_4)\theta \tag{5.3}$$

where

$$C_1 = 0.240[(0.48A_{wL}) + A_{sL}](d + Y3)F_{yL}, \text{ N.m} \tag{5.4}$$

$$C_2 = 0.021(d + \frac{Y3}{2}) \tag{5.5}$$

$$C_3 = 0.010(A_{wL} + A_{sL})(d + Y3)F_{yL}, \text{ N.m} \tag{5.6}$$

$$C_4 = 0.065A_{wL}(d + Y3)F_{yL}, \text{ N.m} \tag{5.7}$$

Since the connection behaviour is not symmetrical with respect to either strength or stiffness, a second expression is needed for the connection under negative bending (slab in tension, bottom angle in compression):

$$M^{-} = C_1\left(1 - e^{-C_2\theta}\right) + C_3\theta \tag{5.8}$$

where

$$C_1 = 0.180[\left(4A_{rd}F_{yrd}\right) + \left(0.857A_{sL}F_{yL}\right)](d + Y3), \text{ N.m} \tag{5.9}$$

$$C_2 = 0.775 \tag{5.10}$$

$$C_3 = 0.007(A_{sL} + A_{wL})(d + Y3)F_{yL}, \text{ N.m} \tag{5.11}$$

θ = relative rotation (mrad)

A_{rd} = area of longitudinal slab reinforcement (m^2)

A_{sL} = gross area of seat angle leg ($\leq 1.5A_{rd}$) (m^2)

(For use in these equations, A_{sL} is limited to a maximum of $1.5A_{rd}$)

A_{wL} = gross area of double web angles for shear calculations (m^2)

(For use in these equations, A_{wL} is limited to a maximum of $2.0A_{sL}$)

d = depth of steel beam (m)

$Y3$ = distance from top of steel shape to centre of longitudinal slab reinforcement (m)

F_{yL} = yield stress of seat and web angle (N/m^2)

F_{yrd} = yield stress of slab reinforcement (N/m^2)

A_{sL} is limited to a maximum of $1.5A_{rd}$ to prevent estimating unrealistically stiff moment-rotation properties. Figure 5.24, presents the detailing of the considered partially-rigid composite connection with metal deck. Figure 5.25, is an example of the derived PR-CC moment-rotation curve through experimental and numerical approaches. The idealised curve for defining the link element behaviour is also illustrated.

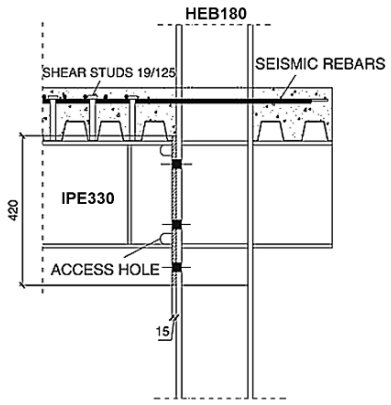

Figure 5.24 – Detailed sample partially-rigid composite connection with metal deck

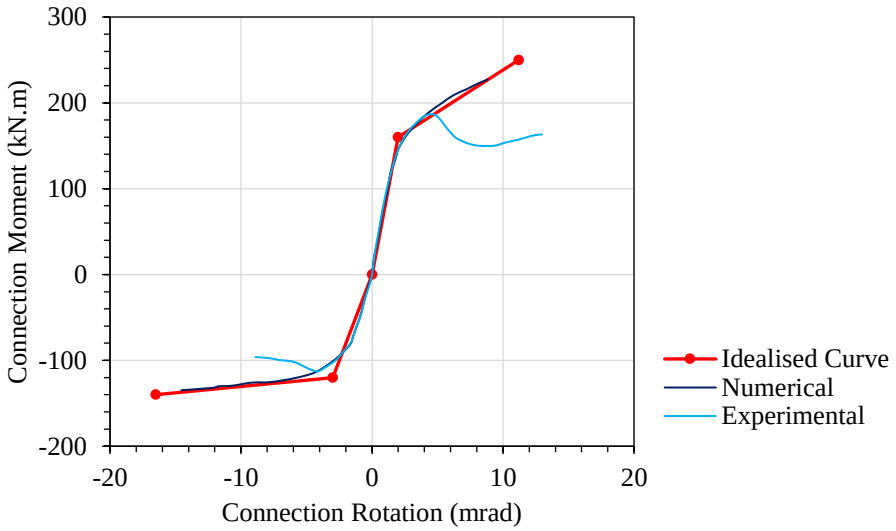

Figure 5.25 - Idealised curve applied for simulation of partially-rigid composite connection links

Due to the variation of steel beams sections, six different moment-rotation curves were generated to cover all beam-column joint arrangements of the index building. It should be noted that the floors are simulated as individual rigid diaphragms by constraining certain degree-of-freedom of slave nodes to a master node. The master node typically corresponding to the barycentre of the diaphragm. Great care should be taken while defining the master node, as constraining all the nodes of a given floor level to a rigid diaphragm may lead to an artificial stiffening and/or strengthening of the beams (SeismoSoft, 2014).

5.7. Defining Building Models

Eight hypothetic models have been defined by altering the arrangement of the infill panels, bracings and joint connections of the selected index building. Each of the proposed arrangements of the index building will be analysed through static and dynamic analysis methods, to evaluate the impact of the considered structural components on the global response of the structures. Hence, the most influential components can be identified and

implemented for simulating the rest of the defined index buildings. An overview of the considered models is presented in Table 5.8 along with the corresponding HAZUS (2003) and GEM (2015) building type as realistic notation of the index building. As stated in Chapter 3 and 4, the obtained seismic performance and fragility of the considered models and index buildings are compared to the ones suggested in HAZUS (2003), as it is extensively applied in design and assessment of the structures of the region under study.

Table 5.8 – Description and category of models under study

Model Ref.	**Description**	**HAZUS Building Typology***	**GEM Building Typology+**
M1 - BR+NB	Bare Steel Frame (rigid beam-column connections, all bracings removed, no infill panel considered)	S1H Mid-Rise	S/LFM+DUC/HEX:4/PLFR
M2 - BR	Bare Steel Frame (rigid beam-column connections, dual system, no infill panel considered)	S1H+S2H Mid-Rise	S/LH+DUC/HEX:4/PLFR
M3 - BS	Bare Steel Frame (semi-rigid beam-column connections, dual system, no infill panel considered)	S1H+S2H Mid-Rise	S/LH+DUC/HEX:4/PLFR
M4 - BS+NB	Bare Steel Frame (semi-rigid beam-column connections, all bracings removed, no infill panel considered)	S1H Mid-Rise	S/LFM+DUC/HEX:4/PLFR
M5 - IR+NB	Infill Steel Frame (rigid beam-column connections, all bracings removed, window & solid panels)	S5H Mid-Rise	S/LFM+LFINF+DUC/HEX:4/PLFR
M6 - IR+SP	Infill Steel Frame (rigid beam-column connections, dual system, only solid panels)	S5H Mid-Rise	S/LH+LFINF+DUC/HEX:4/PLFR
M7 - IR	Infill Steel Frame (rigid beam-column connections, dual system, window & solid panels)	S5H Mid-Rise	S/LH+LFINF+DUC/HEX:4/PLFR
M8 - IS	Infill Steel Frame (semi-rigid beam-column connections, dual system, window & solid panels)	S5H Mid-Rise	S/LH+LFINF+DUC/HEX:4/PLFR

* S1: steel moment frame; S2: steel brace frame; S5: steel frame with unreinforced masonry infill walls
H: high-code. Mid-Rise: 4-7 storeys.
High-Code, Moderate-Code, Low-Code and Pre-Code buildings are based on modern code (e.g., 1976 Uniform Building Code, 1985 NEHRP Provisions, or later editions of these model codes)
+ Material: S-Steel. Lateral load-resisting system: LFM-Moment frame; LFINF-Infilled frame; LH-Hybrid system
System ductility: DUC-Ductile; DNO-Non-ductile. Height: HEX. Shape of building plan: PLFR-Rectangular, solid

5.8. Eigenvalue Analysis

An Eigenvalue Analysis was conducted to evaluate the fundamental frequencies of vibration and mode shapes of the proposed models. The results will indicate the dominant structural response under dynamic loading. Referring, the fundamental period of vibration of each model is given in Table 5.9. By comparing the initial period of bare steel frames and the ones with the masonry infill, it is clear how the fundamental period reduces significantly because of infill presence. The general arrangement of the selected models is shown in Figure 5.26.

Table 5.9 – Modal properties of different hypothetic models

Model Ref.	Mode	Period (s)	Frequency (Hertz)	U_x (tonne)	U_x (%)	U_y (tonne)	U_y (%)	R_z (tonne)	R_z (%)	Mass (tonne)
M1 - BR+NB	T_{1y}	2.03	0.49	0.00	0.00%	554.08	79.27%	0.00	0.00%	700.62
	T_{1z}	1.69	0.59	15.13	2.16%	0.00	0.00%	38622.63	75.06%	
	T_{1x}	1.56	0.64	514.45	73.60%	0.00	0.00%	1164.30	2.26%	
M2 - BR	T_{1x}	1.33	0.75	387.19	62.97%	0.00	0.00%	0.30	0.00%	703.16
	T_{1y}	0.57	1.75	0.00	0.00%	473.68	77.03%	0.00	0.00%	
	T_{1z}	0.43	2.32	0.00	0.00%	0.00	0.00%	29857.04	69.84%	
M3 - BS	T_{1x}	1.79	0.56	431.97	61.63%	0.00	0.00%	0.91	0.00%	702.58
	T_{1y}	0.60	1.67	0.00	0.00%	543.19	77.49%	0.00	0.00%	
	T_{1z}	0.55	1.83	0.00	0.00%	0.00	0.00%	36499.40	70.47%	
M4 - BS+NB	T_{1x}	2.15	0.47	530.97	76.02%	0.00	0.00%	8.04	0.02%	700.05
	T_{1y}	2.03	0.49	0.00	0.00%	553.80	79.29%	0.00	0.00%	
	T_{1z}	1.81	0.55	0.12	0.02%	0.00	0.00%	39673.93	77.19%	
M5 - IR+NB	T_{1y}	0.56	1.78	0.06	0.01%	604.49	83.47%	70.25	0.13%	734.18
	T_{1x}	0.48	2.10	632.23	87.30%	0.04	0.01%	175.60	0.32%	
	T_{1z}	0.38	2.66	2.73	0.38%	1.34	0.18%	44084.43	81.05%	
M6 - IR+SP	T_{1y}	0.43	2.33	0.00	0.00%	581.21	79.97%	0.00	0.00%	760.48
	T_{1x}	0.34	2.96	592.73	81.56%	0.00	0.00%	29.90	0.05%	
	T_{1z}	0.27	3.77	0.47	0.06%	0.00	0.00%	42470.56	77.52%	
M7 - IR	T_{1y}	0.44	2.28	0.9	0.00%	574.5	0.79%	28.2	0.00%	760.48
	T_{1x}	0.41	2.43	584.1	0.76%	0.9	0.00%	44.8	0.00%	
	T_{1z}	0.29	3.45	0.71	0.09%	0.58	0.081%	40765.29	74.40%	
M8 - IS	T_{1y}	0.44	2.28	1.74	0.24%	573.28	78.94%	27.47	0.05%	760.48
	T_{1x}	0.42	2.39	554.15	76.31%	1.80	0.25%	45.22	0.08%	
	T_{1z}	0.29	3.44	0.74	0.10%	0.59	0.08%	40711.70	74.39%	

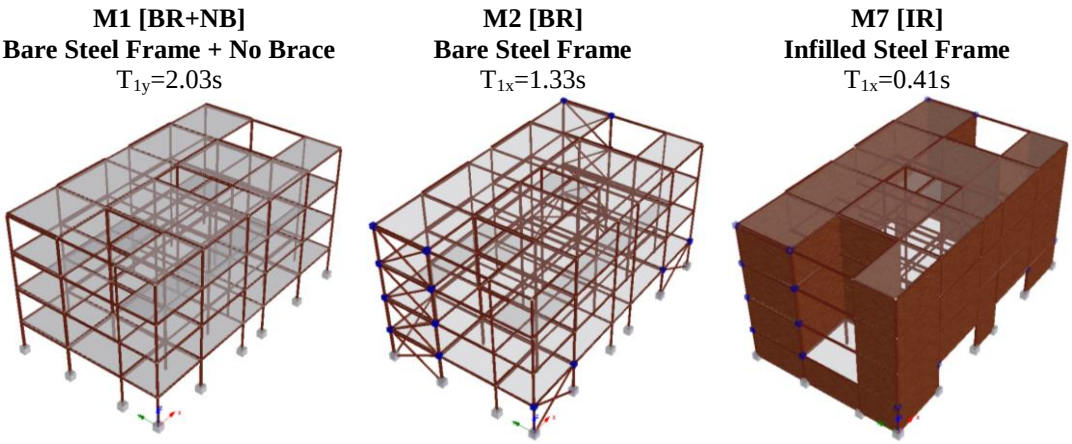

Figure 5.26 – General view of the index buildings' arrangement

Due to the box like behaviour of this type of steel frames and the fact that more than 90% of the mass is activated by the first three significant modes for each considered direction (X and Y), the influence of higher modes can be neglected. Hence, the structural behaviour is predominantly influenced by the first mode and nonlinear static procedures are considered a reliable means of obtaining the structural response (Fardis, 2009).

It is clear that the presence of masonry infill panels, stiffens the structure and increases its frequency. This increase is evident while comparing the frequency of M2 [BR] (f_{1x}=0.75Hz; f_{1y}=1.75Hz) and M7 [IR] (f_{1x}=2.43Hz; f_{1y}=2.28Hz), for which the only difference is in contribution of infills to the structural stiffness. Similarly, bracings have a significant influence and their presence will increase the frequency of the structure by introducing further stiffness. This impact is evident in comparing the bare framed structures, M1 [BR+NB] (f_{1x}=0.59Hz; f_{1y}=0.49Hz) and M2 [BR] (f_{1x}=0.75Hz; f_{1y}=1.75Hz). Regarding the effect of rigid and semi-rigid connection types, in case of bare frames a change in stiffness is observed, while for the infilled structures the resultant discrepancy can be overlooked. It is also important to note that the presence of infill panels stiffens the structure for rotation around its z-axis, while reducing the torsional modes.

5.9. Seismic Response Analysis

The correlation between simulating the structural characteristics and its seismic response can be evaluated by means of nonlinear static and dynamic analysis. Adopting an analysis procedure relies on several parameters such as the importance of the structure, its expected performance level (e.g. level of nonlinearity), the complexity of the structural characteristics, the amount of data available for developing a structural model, availability of computational expertise etc. This can be simplified as whether the response needs to be considered as linear

or nonlinear and the format in which the seismic actions are going to be applied on the model (e.g. equivalent lateral load or ground motion time history).

Guidelines such as ATC-40 (1996), BS EN 1998-1 (2004) and FEMA-440/ATC-55 (2005) recommend four analytical procedures for assessing the seismic response of buildings. With an ascending order of complexity, these methods are the Linear Static Procedure (LSP), Linear Dynamic Procedure (LDP), Nonlinear Static Procedure (NSP) and the Nonlinear Dynamic Procedure (NDP). It should be noted that the accuracy of each of the methods depends heavily on the detailing of structural modelling, thorough simulation of material behaviour and the characteristics of the applied ground motions.

Due to the existing limitations and less accurate predictions of the linear methods, the application of nonlinear approaches has raised considerably in the past decade. This is mainly due to the recent advancements in numerical modelling and substantial increase in computational powers. Hence, in case of seismically excited structure, majority of guidelines including FEMA-356 (2000) suggest the use of nonlinear analysis procedures. A comprehensive review of various analytical methods for seismic analysis can be found in (D'Ayala et al., 2015).

This section discusses the steps involved in analysing the selected index building through nonlinear static and dynamic methods under seismic excitation.

5.9.1. Nonlinear Static Analysis

In nonlinear static analysis, also known as static pushover (SPO), the structural model is subjected to a predetermined monotonically increasing lateral force, simulating the relative inertia forces generated at each mass concentration. Increasing the intensity of the loading, the sequence of structural yielding, cracking, formation of plastic-hinges is recorded as a function of the applied push. As the push continues and the structure enters its inelastic stage, the system will experience a loss of stiffness and a change in its vibration period. This method is mainly based on the assumption that the reaction of a structure is predominantly controlled by its fundamental mode of vibration and shape, while the shape remains constant and independent of time throughout its elastic and inelastic response.

Compared to the more accurate nonlinear response history analysis, pushover analysis can offer relative simplicity and reduced computational effort. The pushover analysis can expose the hidden structural weaknesses such as the storey mechanisms, strength and stiffness irregularities along with extensive deformation demands, which cannot be identified in an elastic analysis (Helmut Krawinkler, 1998). However, the method is not able to account for the effects of strong ground motion duration and cumulative energy dissipation, although this

is more applicable to tall structures where higher-mode effects can dominate the behaviour (Tjhin et al., 2006). Furthermore, the traditional pushover method lacks in identifying the progressive changes in the modal properties of the structure that occur due to yielding and cracking in post-elastic response domain, while ignoring the redistribution of inertia forces. This issue is addressed in adaptive pushover.

In this study, the pushover analysis was conducted for the stated building models using SeismoStruct (v.7.0.6) (SeismoSoft, 2014). Two load combinations are applied, 1.2DL + 0.5LL (200 kgf/m^2) and 0.9DL, where DL and LL are the dead and live load respectively (BHRC, 2007). The lateral load was applied as an incremental uniform load distribution and an inverted triangular distribution, performed independently for both longitudinal and transversal direction of the building in order to identify the weaker direction. Both FEMA 356 (2000) and BS EN 1998 (2004) recommend an envelope of a minimum of two load patterns, since a number of studies have highlighted the influence of load pattern on capturing the dynamic phenomenon through static analysis (Moghaddam et al., 2005; Mwafy & Elnashai, 2001). Response control was utilised for the loading phase and terminated the analysis once the control node, located at mass centre of the roof, reaches a drift of 0.3 metre, according to FEMA 356 (2000). This loading strategy is able to identify any irregular response features (e.g. soft storey), capture the softening post-peak branch of the response and obtain an even distribution of points on the force-displacement curve. The resultant static pushover curves for both bare and infilled frames in both longitudinal (x-direction) and transversal direction (y-direction) are shown in Figure 5.27 to Figure 5.30.

HAZUS (2003) proposes yield and ultimate capacity parameters for various structural types. For comparison, the pushover curves obtained through these points are also shown for high-, moderate- and low-code of mid-rise bare steel moment frame [S1] and mid-rise bare steel braced frame [S2]. It should be noted that HAZUS does not propose any defining parameter for structures categorised as steel frame with unreinforced masonry infill walls [S5] of any height or design level except low-code. This is because the local codes (e.g., 1976 Uniform Building Code, 1985 NEHRP Provisions, or later editions of these model codes) do not permit their construction. However, as the implemented macro model of infill resembles the effect of bracing, the pushover curve of the infilled frame can be compared to the high-code [S2].

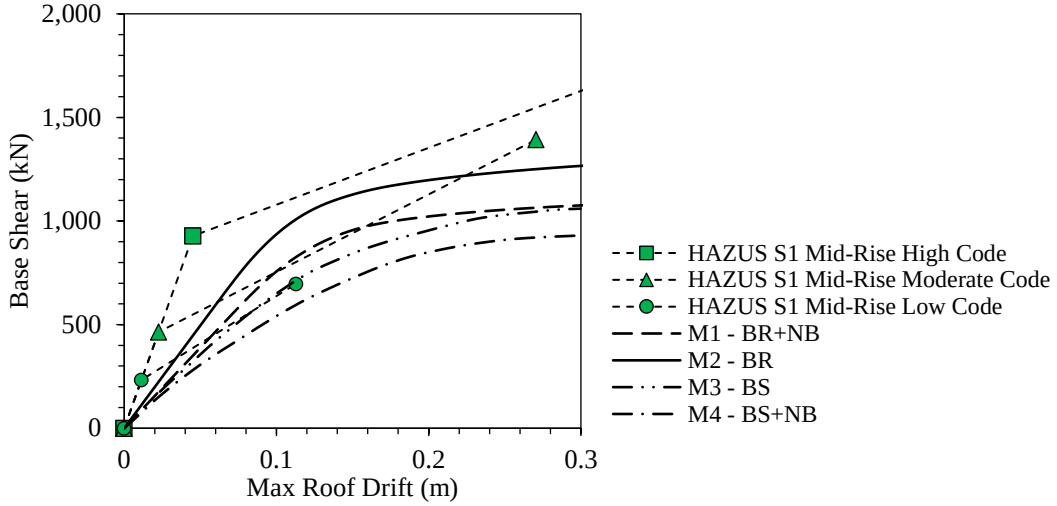

Figure 5.27 - Nonliner static pushover curve for bare steel frames pushed in longitudinal direction (x-direction)

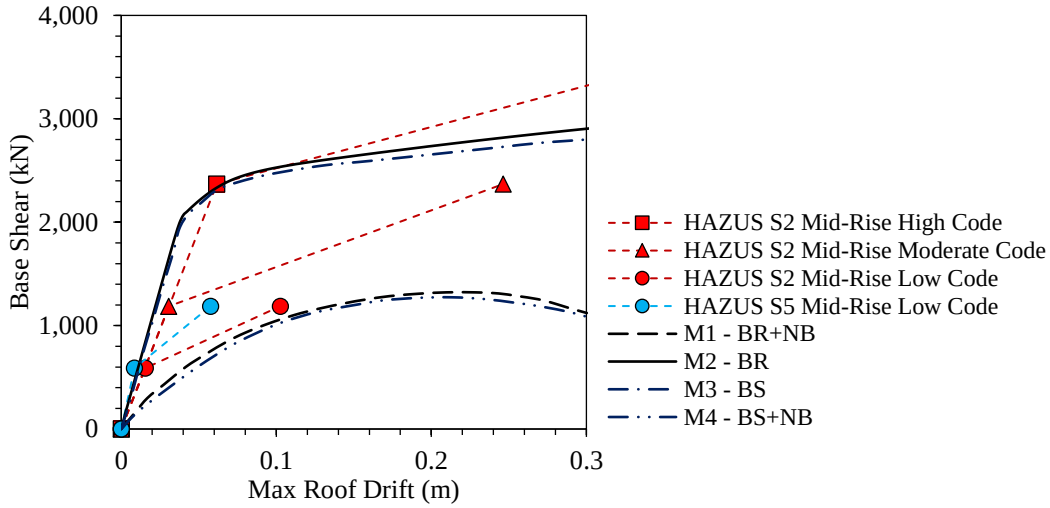

Figure 5.28 - Nonliner static pushover curve for bare steel frames pushed in transversal direction (y-direction)

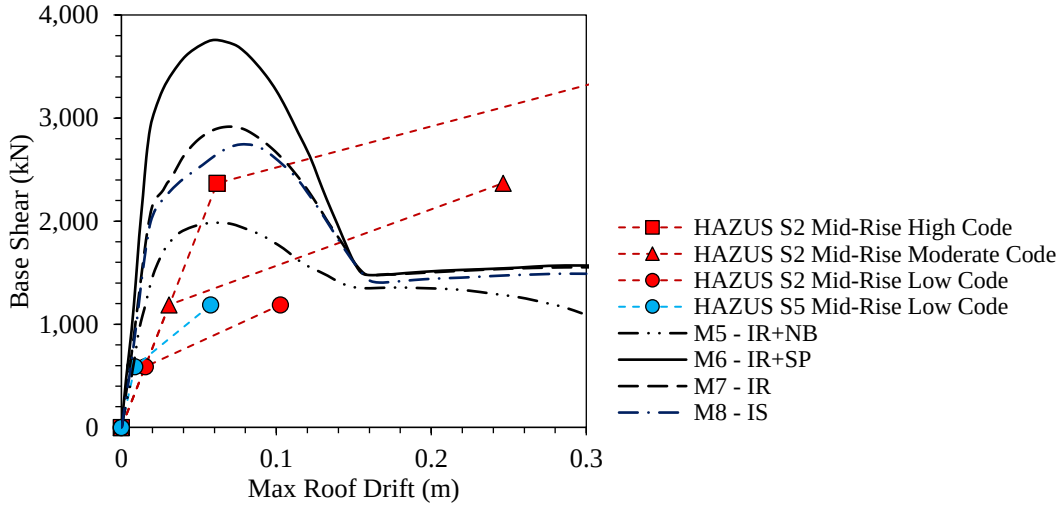

Figure 5.29 - Nonliner static pushover curve for infilled steel frames pushed in longitudinal direction (x-direction)

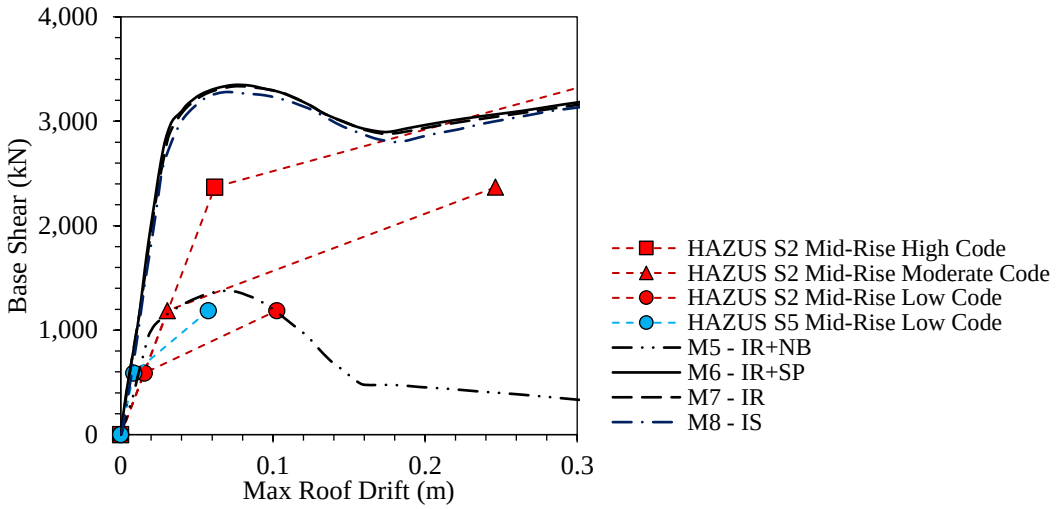

Figure 5.30 - Nonliner static pushover curve for infilled steel frames pushed in transversal direction (y-direction)

Comparing the performance of the structures with and without the infill panels, it is evident that even in a static pushover analysis, in which the cyclic behaviour is not considered, a substantial difference can be observed in terms of initial stiffness, peak capacity and ductility. In this case, the infill panels stiffen and strengthen the building significantly at relatively early drift stages while resulting in lower ductility than the bare frames. After passing the maximum capacity, a rapid strength drop can be observed due to failure of the panels. This sudden decrease is problematic and ignoring this effect in the assessment stage would also lead to unrealistic results in defining the damage states and hence estimating the performance thresholds, fragility functions and consequently the seismic losses. The substantial increase in the overall structural stiffness in infill frames, raises the natural frequency, causing the building to attract more lateral force depending on the applied seismic demand.

The contribution of bracings to the strength and initial stiffness of the structure is clear through Figure 5.27 and Figure 5.28, in which by removing the bracings in both case of bare and infilled (M1, M4 and M5), the structure loses its strength significantly. Also, the initial stiffness of the bare frame drops substantially, while in case of the infilled frames, the contribution of the panels assists in achieving identical stiffness. Once more, considering only the transversal direction (y-direction), all other models (M2, M3, M6, M7 and M8) have matching responses, whether the infills or the joints have changed. This makes sense as the primary lateral resisting system in y-direction is the bracings, hence the infills or joints have minor or no impact on the global response.

On the contrary, looking at Figure 5.29 and Figure 5.30, where the steel cross braces and MRF are the dominant lateral resisting systems, any alteration in the infill type (e.g. strength and stiffness) or beam-column connection (e.g. rigid and semi-rigid), will have a notable impact

on the building's global behaviour. For instance, considering all infills as solid panels, increases the strength of the structure without altering its initial stiffness.

Regarding the semi-rigid connection, their impact is more apparent when compared to the bare frame pushed in its longitudinal direction (x-direction), in which moment resisting frame is the dominant lateral resisting system. Accordingly, the presence of infill panels and bracings reduces the influence of semi-rigid connections.

Considering the pushover curves obtained from the HAZUS (2003) capacity curves, as they only include values for the yield and ultimate points of the capacity curve, none of the curves signify the softening part. Hence, a direct comparison between the obtained pushovers and HAZUS is not practical. However, a relatively similar initial stiffness is observed when the infill curve is compared to the [S5] low-code structure. In case of the bare steel frame pushed in x-direction, although HAZUS overestimates the initial stiffness, the capacity of [S1] high-code matched the one of M2 in the inelastic region. Similarly, for bare frame pushed in the y-direction, as the structural lateral resistance is mainly dependent on the bracing system, a good match is observed between M2 and [S2].

Figure 5.31, compares the deformed shapes of M2 and M7, pushed in their longitudinal direction (x-direction). It is evident that their failure mechanisms are different. In case of the bare steel frame, M2 (blue frame), formation of plastic hinges in the beams and columns, have led to the failure of the structure, which is considered as a safe and desired scenario. In the case of the infilled frame, M7 (red frame), the presence of bracings at the ground floor has shifted the failure to the first floor, at which the failure of the columns indicates a soft storey failure. Additionally, the infills have over-strengthen the upper storeys (3rd and 4th) of the structure, as it is evident from the minor deformation of the columns.

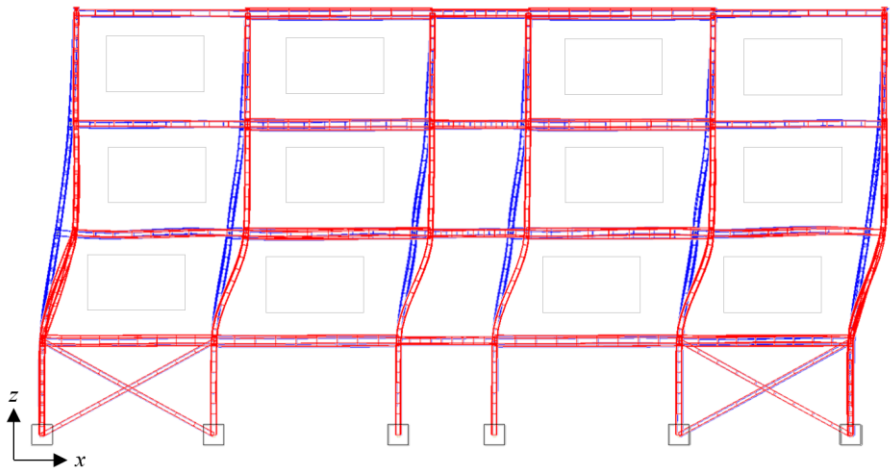

Figure 5.31 - Deformed shape for Model 2 (Blue Frame) and Model 7 (Red Frame).
(pushed up to 300mm displacement of top node)
(The window openings inside the infills are indicated with grey rectangles.)

5.9.2. Nonlinear Dynamic Analysis

The nonlinear time history analysis (NLTHA) offers further information regarding the cyclic response, the stiffness and strength degradation and also the amount of energy absorbed due to the hysteretic behaviour. An advantage of this analysis is that it accounts for the duration of the ground motion, which directly correlates with the magnitude of the ground shaking.

In this section only two of the proposed cases (M2 and M7) are analysed using the nonlinear dynamic method. M2 is a bare steel frame with rigid connections, this is a typical arrangement, which the majority of engineers consider the building to behave as during the design stage. M7 is a masonry infilled steel frame with rigid connections, which can be an acceptable resemblance of the actual building. Due to the similarity observed in the response of the infilled structures with rigid and semi-rigid connections, this section does not investigate their dynamic behaviour. Hence, the focus is to distinguish the seismic response of bare and infilled steel frame under a particular earthquake record. Following a scenario-based assessment, the 1990 Manjil-Rudbar earthquake (M_w 7.4) was selected from the database of the Iranian seismic records. The event caused a widespread damage to the northwest of Iran with an extreme shaking intensity (MMI X). The National Geophysical Data Centre (NGDC) estimated $8 billion of monetary damage and 35,000 to 50,000 casualties, which is the highest ever recorded in the region. The distance of the effected region (36.73°N 49.41°E) to Tehran is about 200km. Therefore, the event is of high importance and can be a good representative of a potential seismic activity.

Out of the seven regional stations which have documented the event, the time history recorded at the closest station, Abbar (RSN-1633 - R_{rup}=12.55 km), with the highest recorded peak ground acceleration (PGA) is applied to the longitudinal direction (x-direction) of the selected buildings (Figure 5.32).

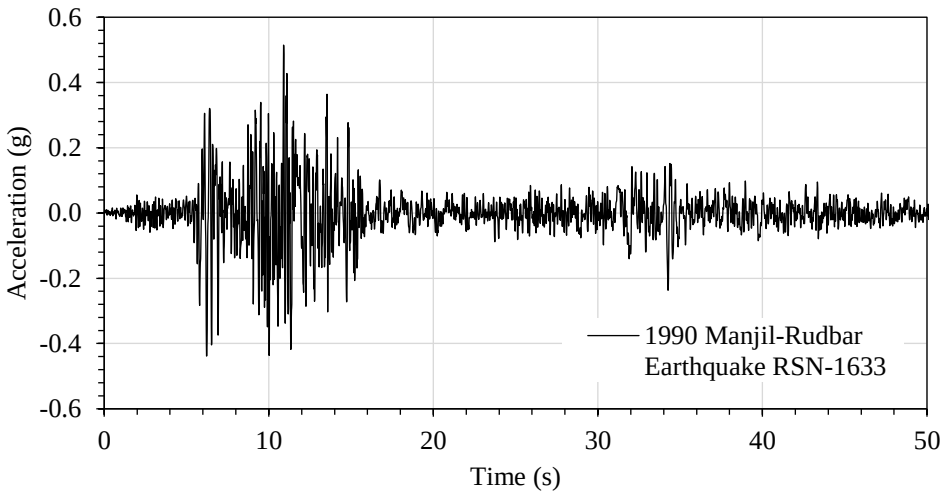

Figure 5.32 – Munjil-Rudbar earthquake time history record. PGA: 0.51g

Figure 5.33, illustrates the spectrum of the event recorded at seven different stations, along with the elastic design spectrum of the ISIRI-2800 assigned to Tehran region (design base acceleration: 0.35g, soil type II, 360 m/s < $V_{S,30}$ < 800 m/s). The fundamental period (T_1) of the two structures is also indicated on the graph.

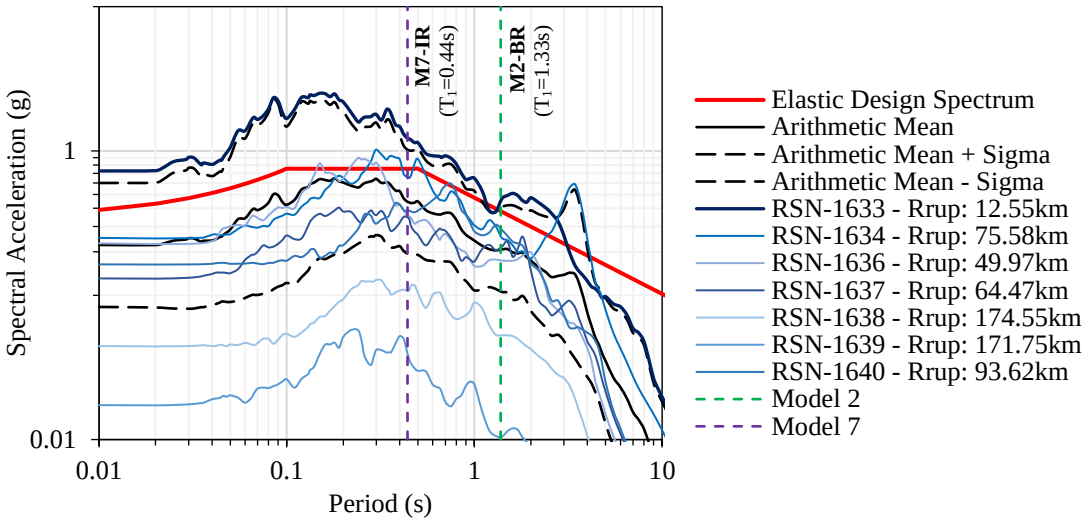

Figure 5.33 - Manjil-Rudbar earthquake spectra and ISIRI-2800 elastic design spectrum

A single component of the earthquake time history is applied at each base node in the x-direction. The response of each node is recorded in terms of displacement, velocity and acceleration. Diagrams presented in Figure 5.34 to Figure 5.36, indicate the extent of discrepancy obtained in the response of the two buildings, each representing the bare and infilled steel frames. For instance, the maximum displacement recorded for the bare frame is 0.27m, while for the infilled case is 0.20m. For sure, the observed variation influences the fragility analysis and consequently the vulnerability of the structure.

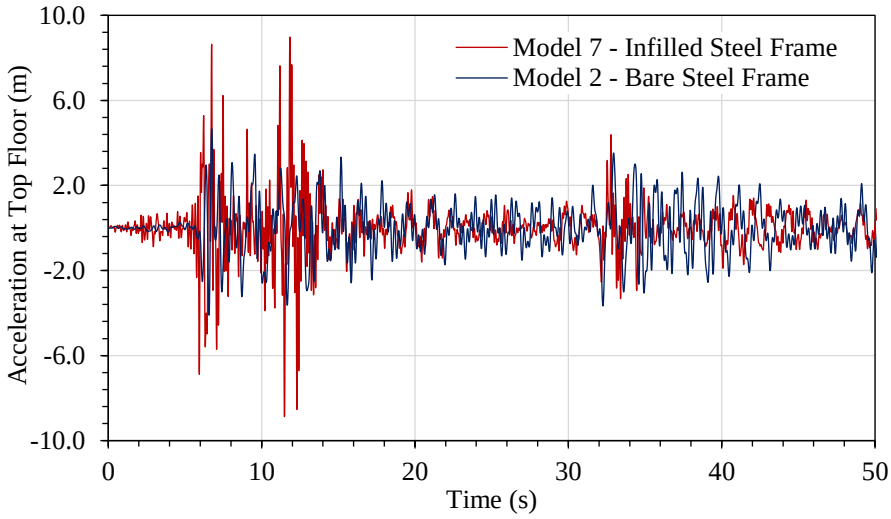

Figure 5.34 – Acceleration time history recorded at top floor node.
Maximum Acceleration; M2: 4.67 m/s^2, M7: 8.98 m/s^2

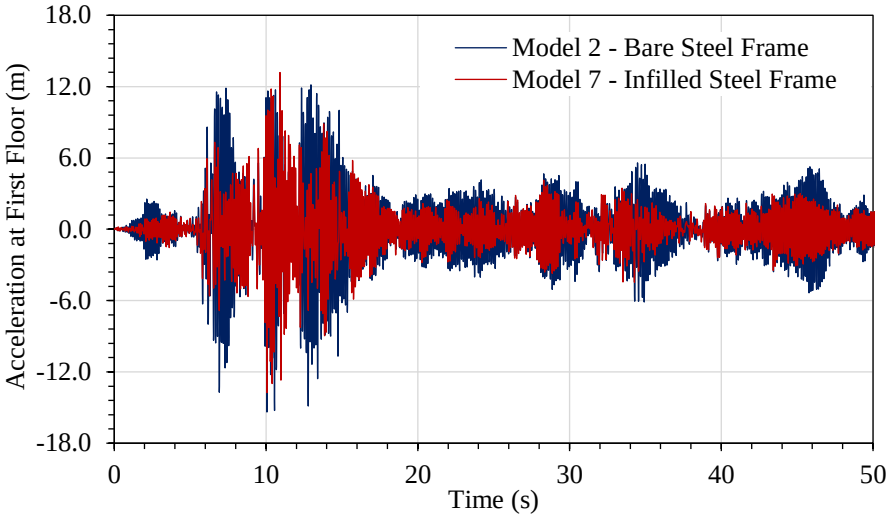

Figure 5.35 - Acceleration time history recorded at first floor node.
Maximum Acceleration; M2: 15.38 m/s^2, M7: 13.74 m/s^2

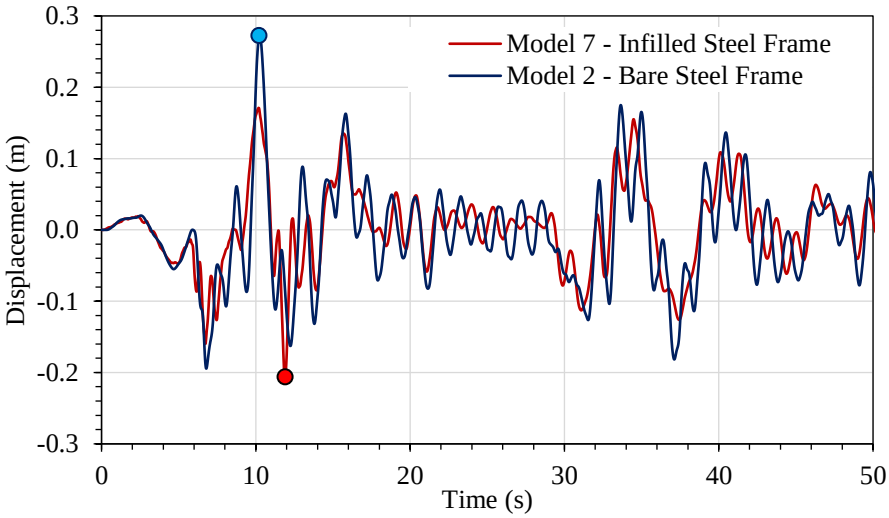

Figure 5.36 - Displacement time history recorded at top floor node.
Maximum Displacement; M2: 0.27m, M7: 0.20m

The inter-storey drift ratio (ISDR) at each floor of bare steel frame and the infilled steel frame are presented in Figure 5.37 and Figure 5.38, respectively. In case of M2, the higher ISDRs are observed at the 3rd floor, while the 2nd floor observes the highest ISDR values in the infilled steel frame. This clearly indicates influence infill has on the seismic performance and altering the failure mechanism and location.

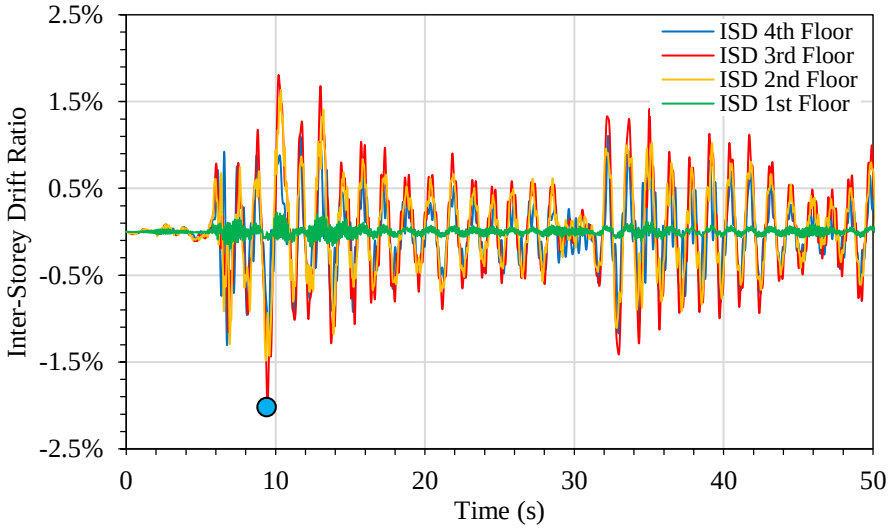

Figure 5.37 – Inter-Storey Drift Ratio for M2: Bare Steel Frame
MIDR at 3rd Floor (-2.00%)

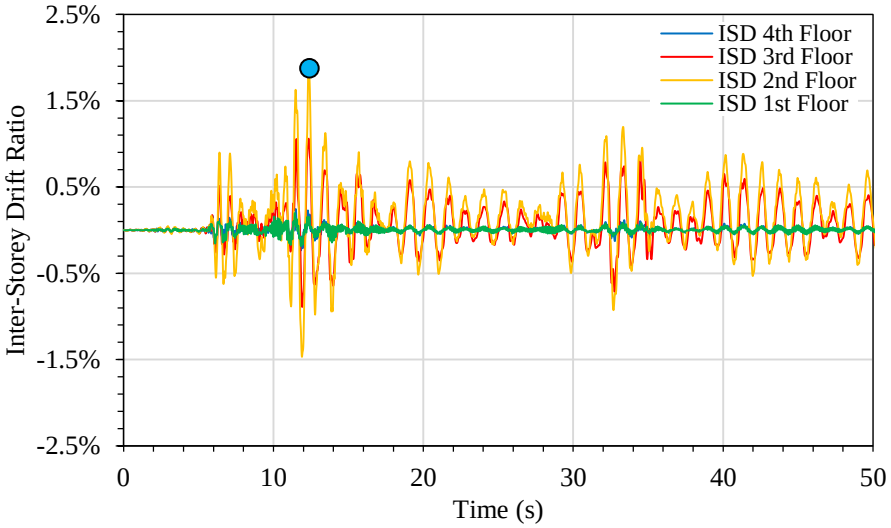

Figure 5.38 - Inter-Storey Drift Ratio for M7: Infilled Steel Frame
MIDR at 2nd Floor (+1.88%)

5.10. Conclusions

The existing disparity associated with building construction, from type of material to structural arrangement, which results in structures with completely diverse seismic characteristics, highlights the importance of an index building capable of representing a wide cohort of existing buildings. To this end, an index building is selected based on a real case design near Tehran, a highly seismic mega-city. The building is an acceptable representative of the residential mid-rise steel frame structures and the common construction practice of the region. Various aspects of the structure have been included in the simulation, such as the contribution of masonry infill panels and beam-column semi-rigid composite connections. Calibrating the mentioned elements with the experimental studies conducted on similar material and systems, gave the opportunity to have models close to the actual construction. Accordingly, to

understand the influence of each structural component, eight hypothetic models have been defined by altering the arrangement of the infill panels, steel bracings and beam-column connections of the selected steel frame. The composite semi-rigid beam-column had a substantial impact on the capacity of the bare steel frame. Moreover, the infilled frame was influence as well. Therefore, all beam-column connections of the index buildings with infill will be modelled as semi-rigid connection, according to the formulation proposed in ASCE (1998). To keep consistency with the original design assumptions, the bare frames will be modelled with rigid connection.

The results obtained from the modal analysis indicate a substantial increase in the initial stiffness due to presence of infill panels and the bracings. Consequently, the fundamental vibration frequency of the infilled framed structures was considerably higher in comparison to the bare framed ones. Furthermore, the seismic response of stated models was evaluated through nonlinear static (pushover) and dynamic (time history) analysis. It was concluded that the presence of infill panels increased the initial stiffness and peak capacity of the steel framed structure, however, a sudden reduction of strength is observed after passing the maximum capacity. Furthermore, the ductility of the infilled structure was much lower than the one of bare frames, which is mainly due to the increase of stiffness from infill panels. Moreover, analysing the bare and infilled framed structures through a scenario earthquake has shown a diverse dynamic behaviour. This clearly indicates that ignoring the impact of infill panels will result in imprecise estimation of response, which can lead to inaccurate seismic fragility and loss assessment.

Chapter 6 will discuss the application of simplified and advanced methods for evaluating the seismic performance and deriving the fragility functions of the discussed models. Identifying the most practical method with an acceptable level of accuracy, the performance and fragilities of the stated model, as well as the selected index buildings will be assessed.

Chapter 6 Seismic Performance & Fragility Assessment

6.1. Introduction

The precision of seismic response analysis procedures is directly related to the detailing of the structural model, characteristics of the applied ground motions and simulation of the material behaviour (Figure 6.1). The analysis method is selected mainly based on the importance of the structure and the seismic condition of the site. Furthermore, the availability of input data, required computational expertise and ultimately the scale (i.e. single structure vs. a portfolio) and objectives of the study have an impact on this procedure. A comprehensive guidance on the best use of various analytical methods for seismic analysis and vulnerability assessment is presented in D'Ayala et al. (2015).

Equivalent static method is the simplest practical procedure that was adopted by earliest seismic codes and is still in use. Although simple and practical, this procedure has many limitations when considering irregularity and nonlinearity in material and geometry. A broad range of structures can be assessed through response spectrum and static pushover procedures, however nonlinear time-history and dynamic pushover methods are expected to produce more realistic prediction of structural response considering a given seismic excitation. In theory, nonlinear time-history analysis has the capability to incorporate almost any type of material and geometrical behaviour. However, the use of time-history based analysis procedures is hindered by complexity and high computational effort (Kelly & Chambers, 2000; Mwafy & Elnashai, 2001).

This section investigates the level of accuracy and applicability of two simplified analysis methods for seismic performance assessment of infilled steel frames. The obtained response, in terms of seismic performance and fragility functions, will be compared to the ones obtained through more advanced dynamic approaches, which are expected to offer closer results to reality. Through this comparison, it can be concluded whether the simplified methods are capable of predicting the structural response within an acceptable range of accuracy or the more time consuming and resource intensive advanced methods are necessary.

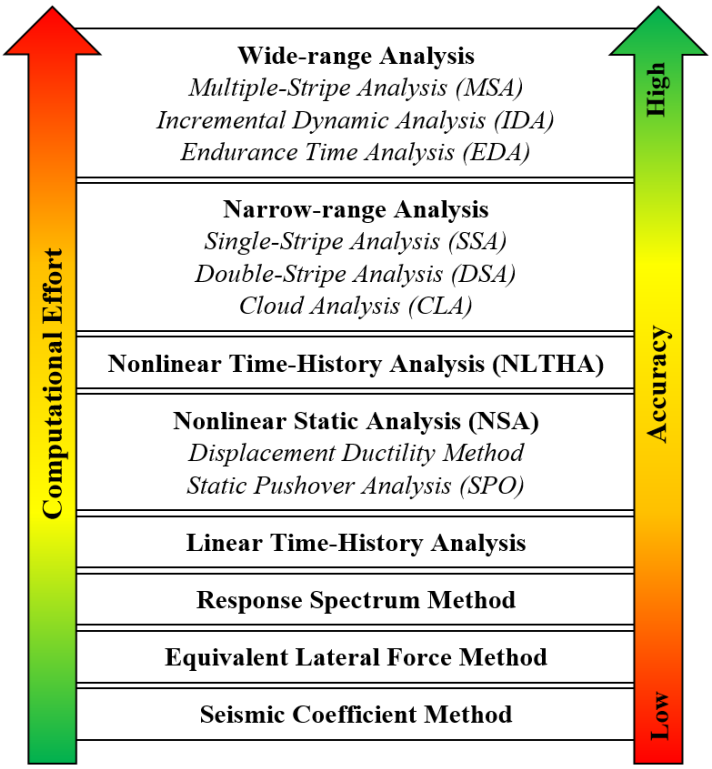

Figure 6.1 – Comparison of seismic analysis methods in terms of accuracy and corresponding computational effort

An extended version of the N2 method (Dolsek & Fajfar, 2005) and the FRACAS (Fragility through Capacity Spectrum Assessment, Rossetto et al., (2016)) have been chosen as the simplified approaches. The stated methods are commonly employed for performance assessment of different structural systems. Both methods follow the capacity spectrum approach through an iterative procedure, while the capacity of the structure is obtained through nonlinear static pushover analysis. The analysis is conducted on two of the index buildings discussed in Chapter 5 (M2-BR (Bare Steel Frame) and M7-IR (Infilled Steel Frame)). The evaluated seismic performance has been compared to the results of nonlinear dynamic methods, such as the cloud analysis (CLA) (Jalayer, 2003; Baker, 2006) and multiple-stripe analysis (MSA) (Jalayer & Cornell, 2009). The main focus is on the quantification of the resultant engineering demand parameters (EDPs) as maximum inter-storey drift ratio (MIDR) and the resulting fragility functions, which form the main input of probabilistic seismic risk and loss assessment. Furthermore, the sensitivity of fragility functions to different fitting techniques are investigated, while comparing the median and standard deviation derived through each method. The similarities and variations observed in the fragility functions are discussed to identify whether acceptable results can be achieved by relying on the outcome of the simplified methods.

Corresponding to the conclusive results, the most appropriate seismic analysis and fragility assessment methods are chosen to evaluate the seismic response and derive the fragility functions of the index buildings introduced in Chapter 4.

6.2. Simplified Analysis Methods

The popularity of nonlinear methods led to a breakthrough of simplified inelastic procedures for structural seismic assessment. These analytical approaches rely on the possibility of estimating the response of a building by using more practical analysis techniques and numerical tools rather than complex and computationally expensive nonlinear dynamic analysis. In other words, the main aim of simplified methods is to estimate demand within an acceptable accuracy range and with minimum analysis effort.

In the majority of simplified methods, the seismic behaviour of the structure is assessed through nonlinear static procedure, commonly known as the Static Pushover (SPO). As stated in Chapter 5, SPO is based on the assumption that the reaction of a structure is predominantly controlled by its fundamental period of vibration and mode shape (Helmut Krawinkler, 1998). The structural response of the multi degree of freedom system (MDoF), in terms of base shear and top (i.e. roof) drift, is employed by N2 and FRACAS to evaluate the structural capacity of a representative single degree of freedom (SDoF) system, in terms of spectral acceleration and spectral displacement. This is conducted on the basis of transforming the response of the MDoF system to acceleration-displacement response spectrum (ADRS) space (Figure 6.2), using the modal participation factors and the effective modal weight ratios, determined from the fundamental mode of the structure, through following equations:

$$S_a = \frac{V_b}{m^*} \tag{6.1}$$

$$m^* = \frac{\left(\sum_{j=1}^{N} m_j \phi_j\right)^2}{\sum_{j=1}^{N} m_j {\phi_j}^2} \tag{6.2}$$

$$S_d = \frac{u_n}{\Gamma} \tag{6.3}$$

$$\Gamma = \frac{\sum_{j=1}^{N} m_j \phi_j}{\sum_{j=1}^{N} m_j {\phi_j}^2} \tag{6.4}$$

where V_b is the base shear force, m^* is the effective modal mass for the fundamental mode of vibration (equivalent SDoF mass), N is the total number of floors, j is the jth floor element of the fundamental mode shape (ϕ_1), m_j is the lumped mass at the jth floor level, u_n is the top floor displacement and Γ is the transformation factor. The resultant SDoF curve is then

idealised by a bilinear or a multilinear elasto-plastic curve, which best fit the shape of the equivalent capacity curve.

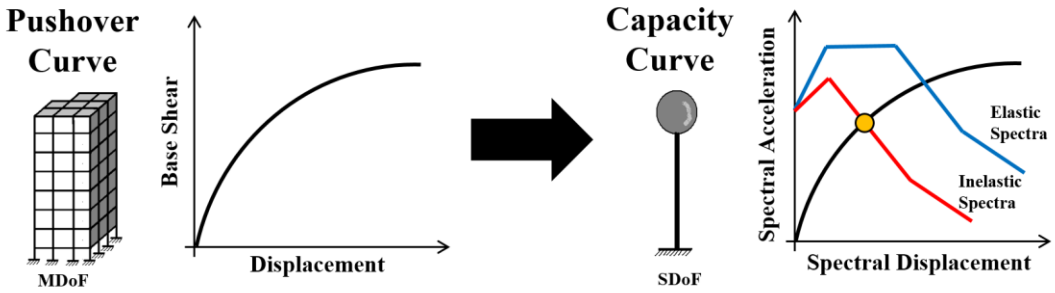

Figure 6.2 – Transformation of MDoF to SDoF in ADRS space

6.2.1. N2 Method

In the N2 method, following the assumption that hysteretic energy dissipates in ductile structures, the inelastic spectrum for constant ductility can be determined using a reduction factor (R) (Fajfar, 2000). Moreover, an equal displacement rule applies for the medium- and long-period range, which assumes that the displacement of the inelastic system is equal to the displacement of the corresponding elastic system with the same period. Hence, the inelastic response spectrum is derived in terms of the ductility factor (μ) and ductility reduction factors (R_μ), expressed as a function of the structural period (T^*) and the characteristic period of the ground motion (T_C). The characteristic period is defined as the transition period from the constant acceleration domain to the constant velocity domain of the elastic spectrum and depends on the frequency content of the ground motion. The inelastic displacement corresponding to the performance target from the equivalent SDoF system S_d^* is then derived directly using the following formula:

$$S_d^* = \frac{\mu}{R} S_{de}(T^*) \tag{6.5}$$

where S_{de} is the elastic displacement demand, T^* is the elastic period of the idealised equivalent SDoF system while defined as:

$$T^* = 2\pi \sqrt{\frac{m^* D_y}{F_y}} \tag{6.6}$$

where D_y and F_y represent the yield point's displacement and force respectively.

In the ADRS space, the performance point represents the intersection between the inelastic demand spectrum and the idealised capacity curve or the extension of its horizontal yield plateau. It should be noted that for short-period structures, as the inelastic displacements are

larger than the elastic ones, the reduction factor (R) will be smaller than the ductility (μ). Once the inelastic displacement is determined, the ground motion intensity is characterized by the spectral pseudo-acceleration corresponding to the first-mode elastic vibration period and 5% damping ratio ($S_a(T_1,5\%)$), obtained from the elastic spectrum. Spectral acceleration is an ideal predictor for the response of elastic SDoF systems. With respect to the PGA, the elastic response spectrum has the advantage to be primarily influenced by the energy contained within a number of cycles of ground motion and to be little influenced by a few spikes of very high acceleration (Newmark and Hall, 1982). In case of real structures, spectral acceleration is a relatively good predictor for MDoFs, as long as the response is dominated by its fundamental mode of vibration (Shome et al., 1998).

The entire process of evaluating the performance points and corresponding IM-EDPs is performed through an automated program. Due to limited number of iterations required to identify the performance point, only few seconds are spent on each given earthquake spectrum. For the selected 150 earthquake records, a complete N2 analysis was conducted in about 15 minutes using a desktop machine with a quad-core CPU (clockspeed @3.40GHz).

6.2.2. FRACAS

In contrary to N2 method, FRACAS does not rely on reduction factors or any indices to evaluate the inelastic spectrum from the elastic one. Instead, FRACAS discretises the idealised curve into pre-defined number of analysis points (AP). Each analysis point represents a SDoF defined by its unique elastic stiffness, period, ductility and hysteresis properties according to the idealised curve. The inelastic spectrum is determined by computation of spectral acceleration and spectral displacement, through conducting a simplified dynamic analysis on each of the discrete periods in the inelastic range. The obtained response for each AP corresponds to a point on the inelastic response spectrum. A Newton-Raphson iterative scheme is used to solve the dynamic non-linear equilibrium equation for the evaluation of the SDoF response. The number of considered analysis points play a critical role in estimating both elastic and inelastic response and consequently the positioning of the performance points. For this study, the idealised curve is divided into 20 parts up to its yielding point, while the post-yield is divided into 25 segments to achieve acceptable precision. Similar to N2 method, the intersection between the inelastic demand spectrum and the idealised capacity curve corresponds to the inelastic displacement of the SDoF system. The ground motion intensity is then characterized by the spectral acceleration at the fundamental period, obtained from the elastic spectrum. Different steps of FRACAS are shown in Figure 6.3.

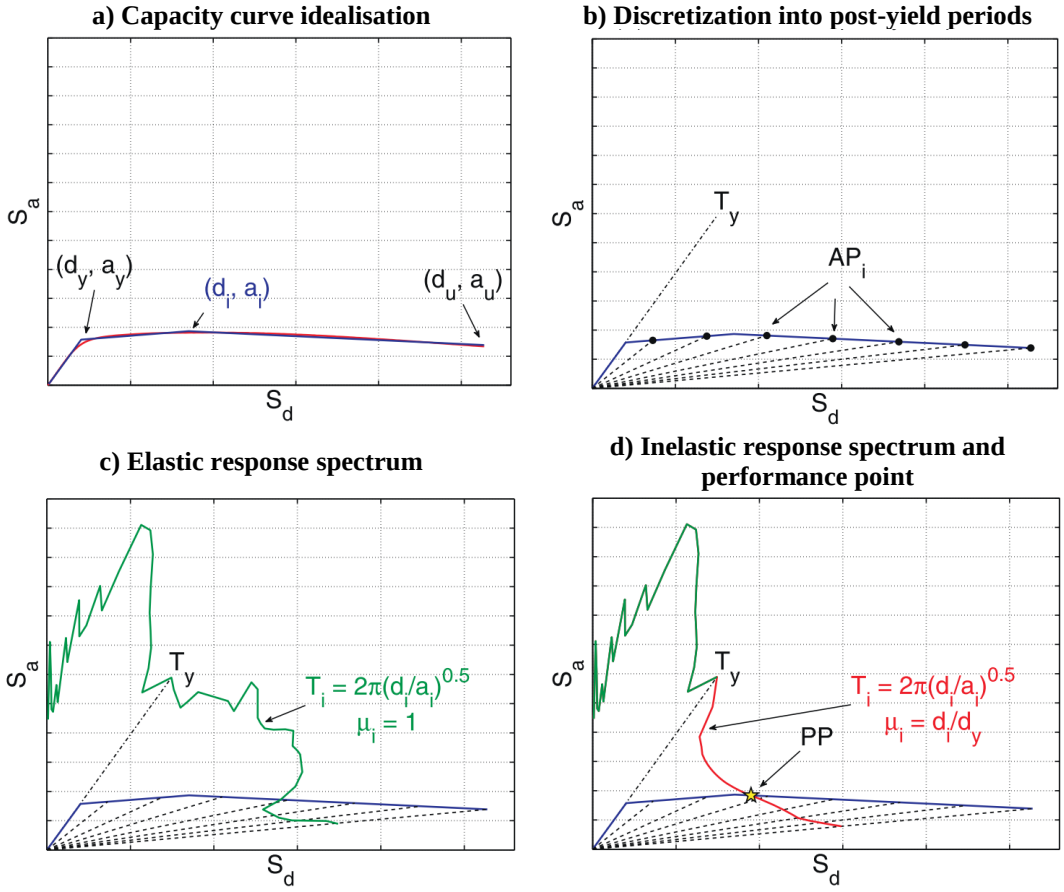

Figure 6.3 - Main steps of FRACAS for the derivation of the performance point (PP) using the trilinear idealization model.

(a) shows the fitting of the idealised trilinear curve to the structure capacity curve;
(b) shows the identification of Analysis Points (AP) covering the periods between yield and final point in the inelastic range;
(c) compares the elastic demand spectrum with the capacity curve at the point of intersection of the demand curve with the line representing the yield period of the structure;
(d) shows the determination of the Performance Point (PP)

In terms of running time and computational effort, as FRACAS evaluates the elastic and inelastic spectra through conducting dynamic analysis at the designated analysis points (AP), hence the running time and accuracy is directly influenced by the pre-defined number of pre-yield and post-yield APs, as well as the duration and time steps of the ground motions. Hence, in comparison to N2 method, FRACAS requires more computation effort and time to determine the performance points. For analysing the 150 ground motions under the stated conditions, in both case of M2-BR and M7-IR, FRACAS took about 2 hours 25 minutes to complete, which can be considered as a substantial time for a simplified method. The analysis was performed using a desktop machine with a quad-core CPU (clockspeed @3.40GHz).

It should be noted that the process of ground motion record selection is discussed in detail in the next section (6.2.3).

6.2.3. Performance Derivation

The fundamental period of the SDoF and consequently the resultant performance points are highly sensitive to the idealised curve. Therefore, the idealisation should be conducted with special care in order to properly replicate the initial period of the structure as well as the softening, peak, hardening and residual strength segments of the curve. According to De Luca et al. (2013), the elastic segment should match the initial stiffness of the exact capacity curve at 10% of the maximum base shear. This fitting rule is proposed in contrary to the 60% fit according to FEMA-356 (2000) or the area balancing criteria (i.e. equal energy) of BS EN 1998 (2004). The following hardening section should be fitted by minimising the area discrepancy up to the target point and the plastic segment should be set by matching the maximum strength value, regardless of balancing the areas or energies. Accordingly, the proposed near-optimal piecewise linear fit can offer nearly-unbiased low-error approximation of the dynamic response of nontrivial systems.

Due to the characteristics of the pushover response obtained for the infilled frames (M7-IR), in this study, the extended version of N2 is applied, in which the idealised curve can account for the substantial strength degradation of infill failure and the residual strength of the system (Dolsek & Fajfar, 2005). Hence, the proposed idealisation is capable of replicate the hardening and softening of the inelastic branch as well as the residual. On the contrary, the tri-linear (TL) model defined in FRACAS is only able to capture the softening of the inelastic backbone curve but not the residual strength. This impacts the estimated ductility at each of the designated analysis points and consequently the evaluated inelastic demand and the performance point. In case of the bare steel frame, an elastic perfectly plastic (EPP) model is utilised for the idealisation. An acceptable correlation is observed when comparing the structural properties of the SDoF system of each method with the ones of the eigenvalue analysis (Table 6.1).

Table 6.1 – Properties of SDoF system obtained from N2 and FRACAS methods

	Fundamental Period of Vibration T_1 (s)			**Total MDoF Mass m (tonne)**	**Equivalent SDoF Mass m^* (tonne)**	
	Eigenvalue Analysis	N2	FRACAS	Gravity Analysis	N2	FRACAS
M2-BR	1.328	1.330	1.331	692.0	370.3	370.0
M7-IR	0.439	0.444	0.440	722.0	437.1	436.0

Figure 6.4 illustrates the performance point obtained for the bare steel frame at the elastic region. Figure 6.5 and Figure 6.6 present the performance point obtained for the infilled models through both simplified methods in both elastic and inelastic region. The influence of different idealisation models on the resultant demand and performance point is evident in these figures.

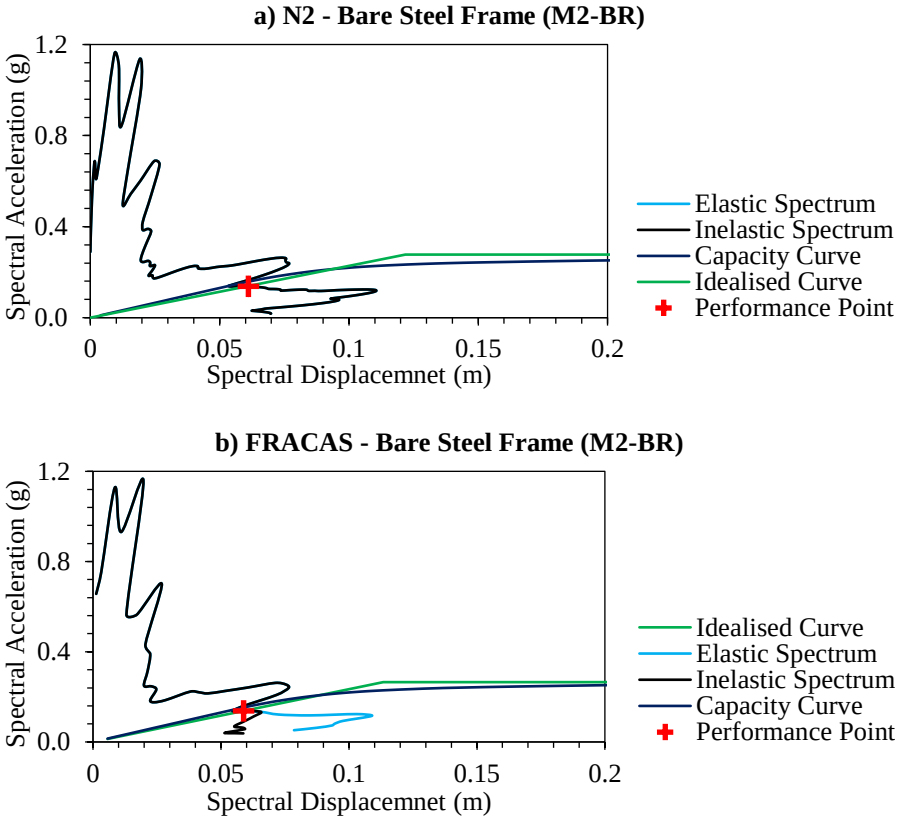

Figure 6.4 - Performance point, elastic and inelastic spectrum obtained through N2 and FRACAS for the bare steel frame (M2-BR) [EQ ID 46x - Mid Niigata Prefecture (M_w 6.3)]

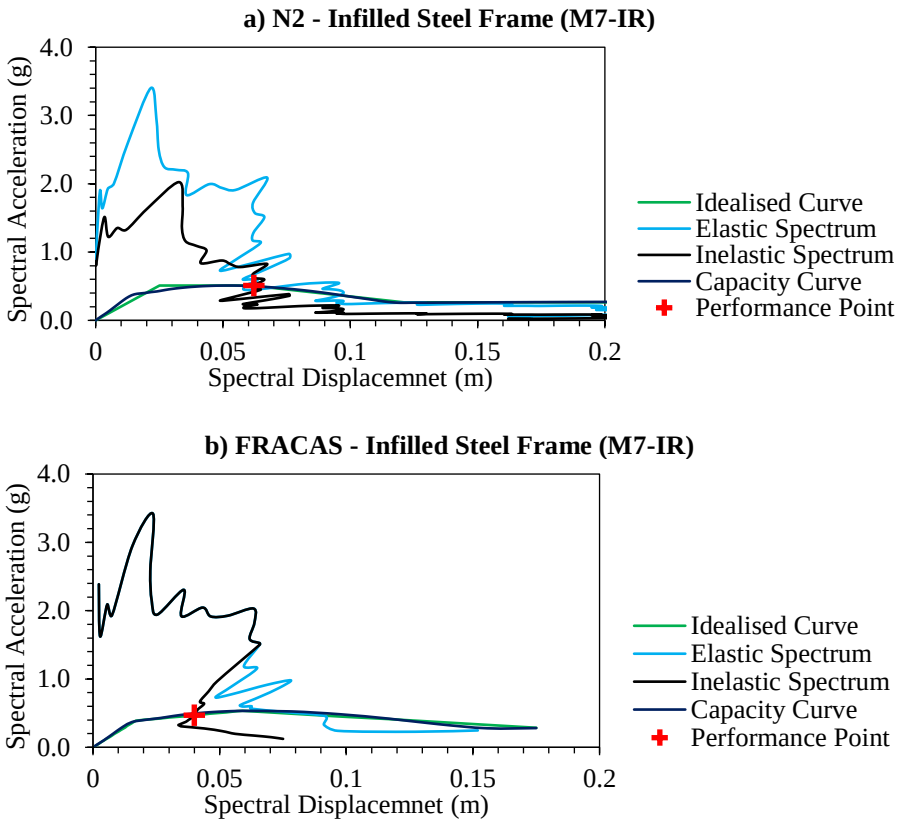

Figure 6.5 - Performance point, elastic and inelastic spectrum obtained through N2 and FRACAS for the infilled steel frame (M7-IR) [EQ ID 136x – Off Noto Peninsula (M_w 6.7)]

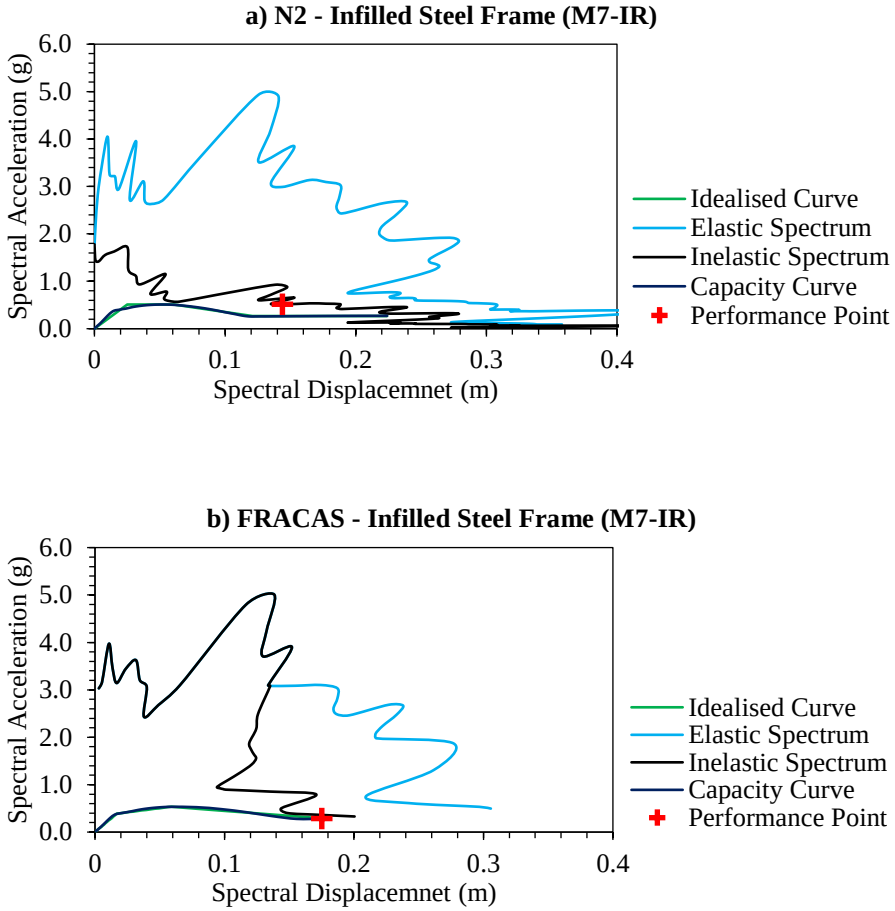

Figure 6.6 - Performance point, elastic and inelastic spectrum obtained through N2 and FRACAS for the infilled steel frame (M7-IR) [EQ ID 462x – Northridge (M_w 6.7)]

Both simplified methods allow the use of natural earthquake records, generating unsmoothed spectra as opposed to the conventional capacity spectrum method (Freeman et al., 1975), which utilises standardised design spectra. Therefore, the resultant performance points will account for the natural variability of the seismic demand. However, the outcomes are highly sensitive to the chosen ground motion records. Hence, it is essential that the selected suite of records accurately reflect the seismic hazard of the site under study (Luco & Bazzuro, 2007). To have a consistent input, for both N2 and FRACAS method, the 3rd version of SIMBAD ground motion database (Selected Input Motions for displacement-Based Assessment and Design) (Smerzini et al., 2014) has been employed. It includes a total of 467 tri-axial accelerogrammes, representing 130 worldwide seismic events. The suite includes worldwide shallow crustal earthquakes with moment magnitudes (M_w) ranging from 5.0 to 7.3 and epicentral distances (R_{epi}) approximately less than 35 km. The distribution of moment magnitude and epicentral distance of each event is illustrated in Figure 6.7. Further detail on characteristics of the comprising ground motions are provided in Appendix-B.

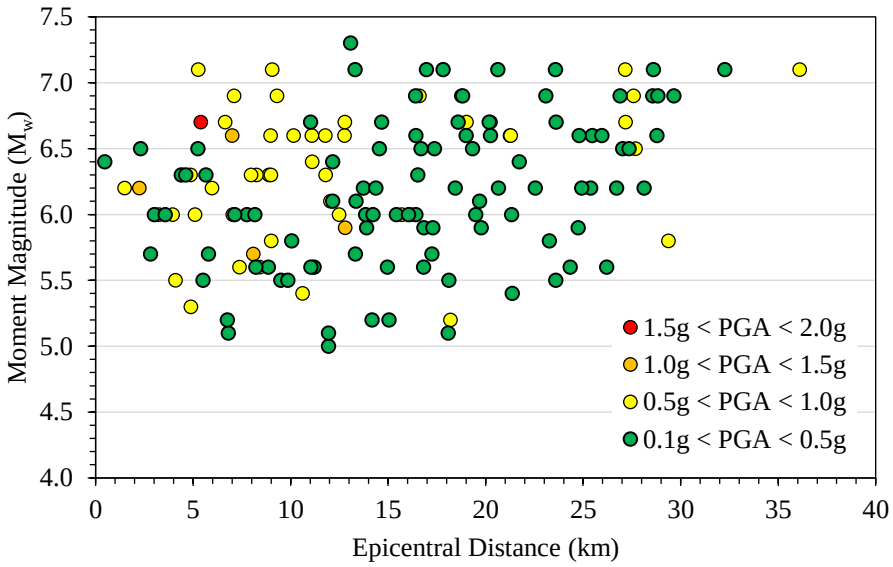

Figure 6.7 – Moment magnitude and epicentral distance of SIMBAD events

From each ground motion, only the component with the highest peak ground acceleration (PGA) has been chosen, leading to 150 ground motions, including main shocks and aftershocks. This extensive range ensures to provide records that cover a vast range of spectral acceleration values. The larger the dispersion of S_a values considered, the smaller the standard error in the estimation of the regression slope in the logarithmic scale will be (Jalayer et al., 2017).

The selected suite of records can trigger a vast range of structural responses without any scaling. The resultant response spectra of all 150 records are illustrated in Figure 6.8, along with their median and code based elastic response of the region under [2-3-2, ISIR-2800] (BHRC, 2007). The fundament periods of the models ($T_{1,M2}$=1.33s and $T_{1,M7}$=0.44s) are indicated on the elastic spectra. A reasonable match exists between the SIMBAD median and the code-based elastic spectrum. However, as the periods increases, the median drops to lower spectral accelerations in comparison to the code-base spectrum. For instance, at period of 2s, the code indicates an acceleration of 0.29g, while the median shows a value of 0.1g. Therefore, it is possible that majority of the ground motions exert low to moderate shaking to the buildings with periods higher than 1.5s. Although, the initial periods of the selected index building ranged from 0.21s to 3.6s, however, there are only 5 of 33 buildings, which their T_1 is close or passes 1.5 seconds. The stated buildings include 6 and 8 storey bare frames, which are not considered as typical buildings and are mainly introduced for comparison reasons. It is important to note that the records selected for cloud analysis does not need to be compatible with the uniform hazard spectrum of the location under study, as this will limit the record-to-record variation.

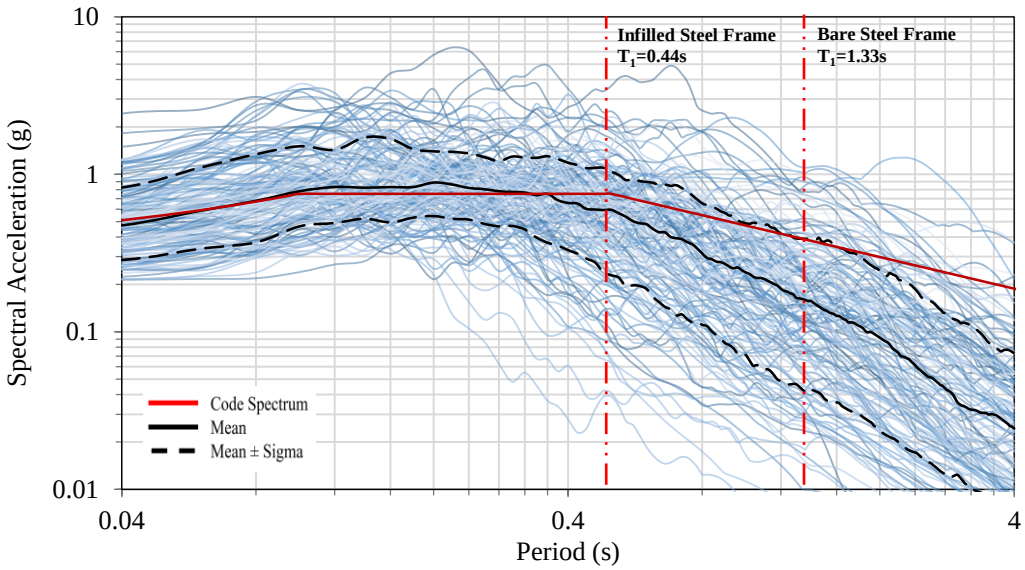

Figure 6.8 - Response spectra of 150 individual components of SIMBAD and the code based elastic response spectrum (ISIRI-2800)

As a result, a total of 150 performance points in terms of $S_a(T_1)$ - S_d* have been determined for the SDoF system through each of the simplified methods. Furthermore, the corresponding maximum inter-storey drift ratio (MIDR) of each performance point is obtained will be employed to derive fragility function as discussed in section 6.6. The MIDR is obtained by conversing the corresponding $S_a(T_1)$ and $S_d(T_1)$ of the SDoF back to the MDoF system and identifying the actual MIDR in all structural levels.

The obtained MIDR values, corresponding to the elastic and inelastic range of the structural response, are presented and compared in Figure 6.9. Results indicate a reasonably close estimate of MIDR for bare steel frame with an average error of 5.36%, where for 66% of the applied IMs, N2 resulted in higher MIDR (highest error 26.56%). In case of the infilled frame, the variation of results is much evident, where in general N2 predicts higher MIDR in 75% of the events with an average error of 29.11%, particularly in the inelastic region (highest error 66.91%). Around 32 records result in drift values denoting extensive damage and collapse for the bare frame (MIDR>2.5%), regardless of the applied method. In case of the infilled frame, 24 records result in high damage (MIDR>2.0%) using the N2 method, but only 15 records indicate identical damages through FRACAS. In general, the N2 method has estimated a higher EDP for the same applied earthquake, resulting in a more conservative estimation. This observed discrepancy can be explained by considering the curve idealisation, particularly for the inelastic segment and also the approach each method follows to evaluate the inelastic spectrum as stated in section 6.2.1 and 6.2.2. Hence, as the resultant shape and energy of the inelastic spectra vary, consequently the EDPs obtained through each method will differ. This inconsistency is more apparent in the EDP results, while the resultant IM values are very similar, as the fundamental periods are fairly identical.

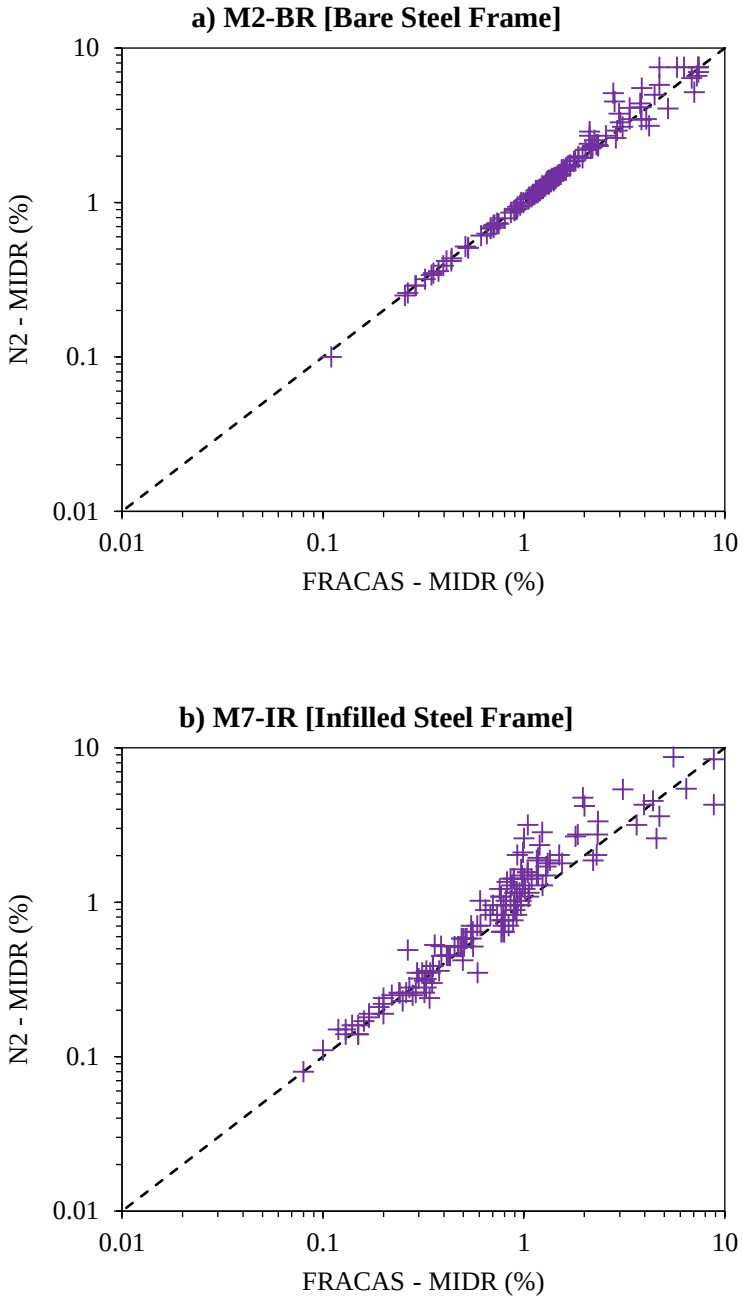

Figure 6.9 - Comparison of MIDRs obatined through N2 and FRACAS

6.3. Nonlinear Dynamic Methods – Cloud Analysis

The nonlinear demand estimation methods can be categorised into two general classes, narrow-range and wide-range methods (Jalayer & Cornell, 2009). This classification depends solely on the extent of the intensity measures employed to assess the demand. The single-stripe analysis (SSA), double-stripe analysis (DSA) and the cloud analysis (CLA) are among the narrow-range, in which a relatively limited number of scaled or unscaled records are considered.

The CLA is a relatively quick and efficient nonlinear dynamic procedure for seismic performance and fragility assessment. The IM-EDP points are obtained by conducting distinct nonlinear time history analyses (NLTHA) of the structure, using a set of original unscaled ground motions characterised by different spectral acceleration contents (Baker & Cornel, 2006). Analysing the structure through NLTHA, for a reasonable number of records, results in a characteristic cloud of points in an IM-EDP space, which typically form a rough ellipse when plotted. This is in contrast to the single-stripe method, which gives distinct stripes of response values corresponding to a pre-set IM value. A disparity between CLA and stripe methods (i.e. SSA and DSA) is in the regression model each adopts to obtain the conditional mean (μ) and standard deviation (β) for various structural response values given the IM. The CLA assumes a simple linear correlation between the logarithms of median EDP and the selected IM.

A limitation of the CLA method is its strong dependency on the suite of ground motions. The quantity and the distribution of the intensity measures in the sample of records have a great influence on the fragility parameters (the standard deviation and the median). In this study, the same suite of unscaled 150 records of SIMBAD, introduced in section 6.2.3, is used to conduct CLA. The response of the models was recorded as MIDR, by applying the ground motions in the weaker direction (x-direction) of the structures.

The analysis was conducted using the SeismoStruct (v.7.0.6) engine (SeismoSoft, 2014), on a desktop machine, with a quad-core CPU (clockspeed @3.40GHz). Up to eight earthquake records were analysed concurrently through parallel computing. In terms of computational intensity and time consumption, the run time is correlated with the duration and the number of time steps of the applied ground motion, as well as the complexity of the model. In case of M2-BR, the total run time was 18 hours (average runtime per record: 55min), while for M7-BR the complete analysis lasted for 22 hours (average runtime per record: 1hr 15min). As shown in Figure 6.10, the resultant MIDR of 150 records are treated as a bench mark for comparing alongside the values obtained through the simplified methods (i.e. N2 and FRACAS).

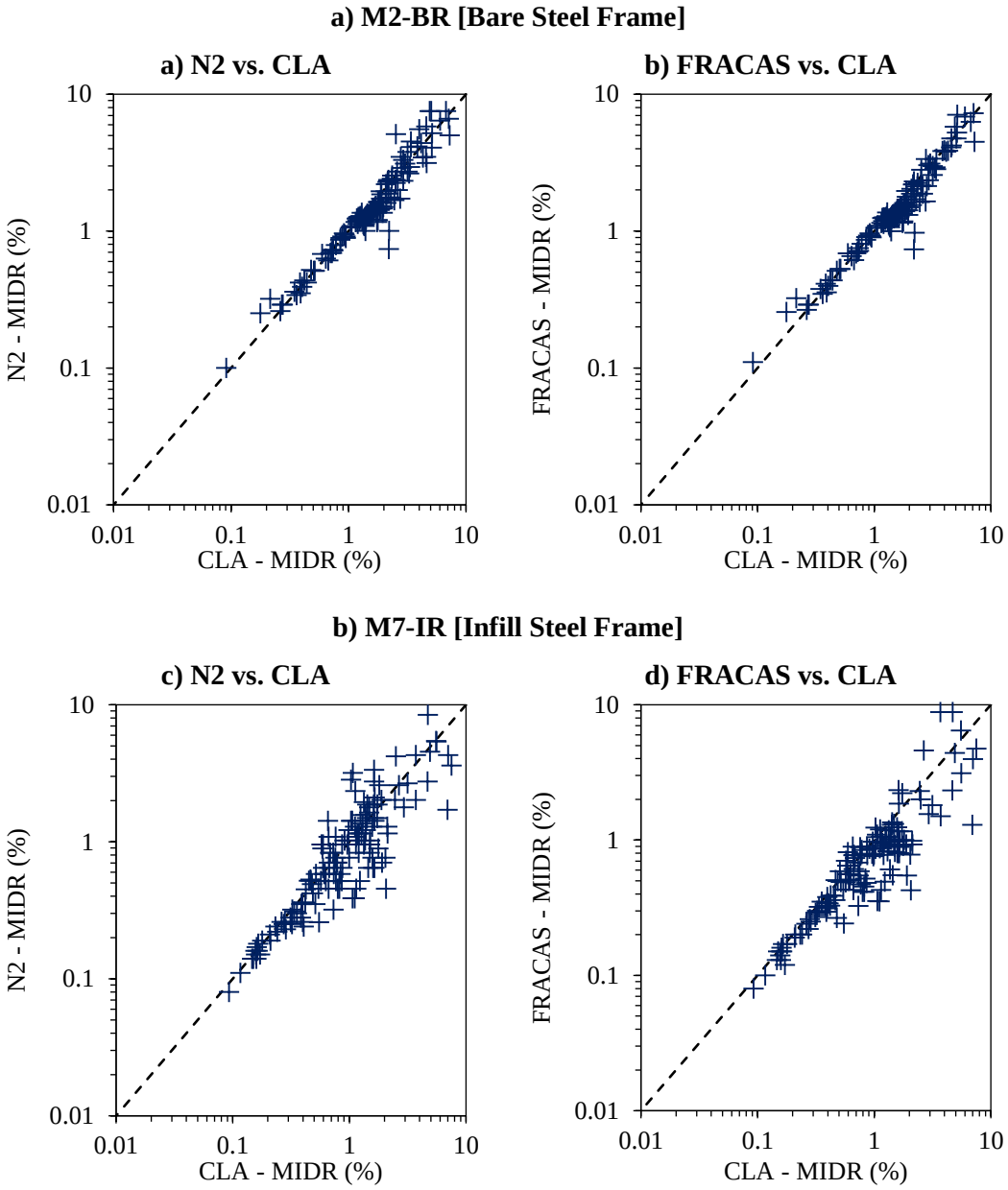

Figure 6.10 - Comparison of simplified methods with cloud analysis (CLA) in terms of MIDR for bare steel frame (a) and infilled steel frame (b)

In comparing the MIDR of the simplified methods against the ones obtained through the CLA, a good agreement is obtained in case of the bare steel frame, particularly in the elastic part (Figure 6.10a and Figure 6.10b). A diversion is observed for the inelastic EDPs. In general, both cases have underestimated the CLA results in more than 65% of instances (average error FRACAS: 15.56%, N2: 15.39%). This underestimation can be explained by considering the effect of higher modes in elastic and inelastic range of the response and also the cyclic deterioration of strength and stiffness due to the hysteresis models. The matching response of simplified methods in case of the bare steel frame was expected, as results of the two procedures had good agreement, especially in the elastic region (Figure 6.10a).

On the contrary, in the case of the infilled frame, despite a good agreement in the EDPs corresponding to the elastic behaviour of the structure, as the structure goes toward inelasticity a significant discrepancy is obtained. For majority of the cases, both simplified methods underestimated the CLA results. For N2 method, this underestimation has happened for more than 65% of the applied ground motions, with an average error of 26.98% (highest error 85.64%) (Figure 6.10c). In case of FRACAS, more than 82% of instances have resulted in an underestimation, with an average error of 29% (highest error 88.64%) (Figure 6.10d). Reasons for this underestimation is the incompetence of the simplified methods in capturing the actual behaviour of the infilled frame in terms of its capacity, hence miscalculating the inelastic demand, as well as the limitation of static pushover analysis in capturing the higher mode effects.

In general, the resultant underestimation of EDPs can deceive the fragility analysis to predict a more resistant structure.

6.4. Nonlinear Dynamic Methods – Multiple-Stripe Analysis

As stated previously, the outcome of the CLA analysis is highly sensitive to the selected suite of ground motions. Hence, the chosen records should provide sufficient intensity to comprise the entire range of building's seismic response, from minor drift to complete failure. The SIMBAD records, statistically provides an acceptable domain of intensity for estimating IM-EDPs and consequently the fragility functions. However, due to limitations in the catalogue of ground motion records at a given site or for a given source, it is often desirable to modify and scale a record to include a broader range of IM levels or utilise simulated ground motions (Galasso et al., 2013). Therefore, to curtail the margin of error, an additional analysis method is required, which can provide a broader range of IM-EDPs and consequently result in more precise fragility functions.

The wide-range methods, such as the incremental dynamic analysis (IDA) (Vamvatsikos & Cornell, 2002) and the multiple-stripe analysis (MSA) (Jalayer & Cornell, 2009), can output displacement-based demand over a wide range of numerically generated spectral accelerations and limit state probabilities. Both methods estimate the structural response by capturing the record-to-record variability based on increasing linear scaling of ground motions in amplitudes. In comparison to the narrow-range methods discussed in the previous section, both MSA and IDA require an extensive computational power and analysis effort. However, it should be noted that ground motion scaling may result in error as well.

In the case of IDA, typically a reduced number of records are scaled to multiple IM levels and the maximum EDP is computed at each scale level, through nonlinear dynamic analysis. The

IDA can be described as a "dynamic pushover", in which the applied dynamic loading, represented by a given accelerogramme with specific PGA and frequency content, is increased until the structure reaches global dynamic instability. IDA was initially adopted by FEMA 350 (2000) and has been mostly implemented to determine the global collapse capacity (FEMA, 2009). According to Shome (1999), for mid-rise buildings, ten to twenty records are usually sufficient to provide adequate accuracy in the estimation of seismic demands, assuming a relatively efficient IM is used (e.g. $S_a(T_1,5\%)$).

The MSA consists of a series of NLTHA, taking as reference a set of ground motion records that are scaled to various levels of pre-set spectral acceleration at a specified period, for instance the structure's fundamental period of vibration. In contrast to IDA curves, which are constructed by scaling the record to arbitrary spectral acceleration values, the MSA method can be constructed by a collection of spectral acceleration stripes. The output of MSA includes scatters of displacement demand values along multiple stripes of constant spectral acceleration values. Both IDA and MSA allow reusing the same motion to mimic variable intensities, which allows utilising fewer records than the CLA. Depending on the number of ground motions and the range of spectral accelerations, to which each record is scaled to, a thorough picture of the structural response at various levels of seismic intensity can be obtained. This will allow the structure to show its full range of response from elasticity to yielding and finally global collapse, while providing statistical information on demand over a wide range of IM values. A feature of MSA is that different record sets can be used for different levels of analysis, for instance reflecting higher magnitude at higher levels (Elefante et al., 2010). In case the same suite of records is utilised for all considered IM levels, as done in this study, the MSA outcome is a recompilation of the IDA results. Furthermore, the structure's general response trend (median) can be estimated along with the dispersion of the maximum inter-storey drift demand conditioned on the gradually increasing ground motion levels. Extensive discussion on MSA and IDA can be found in Jalayer (2003).

The far-field ground motion set, suggested in ATC-63 (FEMA P-695, 2009) has been utilised to conduct the MSA. This was mainly due to the lack of sufficient medium- to high-intensity earthquake record data for Iran. The suite consists of 22 record pairs, each with two horizontal components for a total of 44 ground motions. The records have a moment magnitude (M_w) range of 6.5 to 7.6 with an average magnitude of M_w 7.0 and all were recorded at sites located at a distance greater than or equal to 10 km from the fault rupture. According to the soil classification of NEHRP (FEMA-450, 2004), 16 sites are classified as stiff soil site (type D) and the remaining are classified as very dense soil (type C). The spectral shapes of the stated ground motions were not a criterion in the selection process as the proposed earthquake suite of FEMA P-695 can be applied to any structure independent of site hazard or structural type.

Therefore, the selection of the applied records was not reliant on the natural period, any building-specific property of the structure or the hazard disaggregation, or other site-dependent or hazard-dependent properties. Furthermore, as indicated in Figure 6.11, the median of P-695 has a good agreement with the median of the code-based elastic response spectrum (ISIRI-2800) utilised in design of the index buildings. However, it should be noted that having a good match with the code response spectrum does not necessarily imply spectral shape compatibility at all intensity levels at the first mode spectral acceleration ($S_a(T_1)$). This is evident, particularly in case of structures with lower frequency of vibration. Further detail on characteristics of the comprising ground motions are provided in Appendix-B.

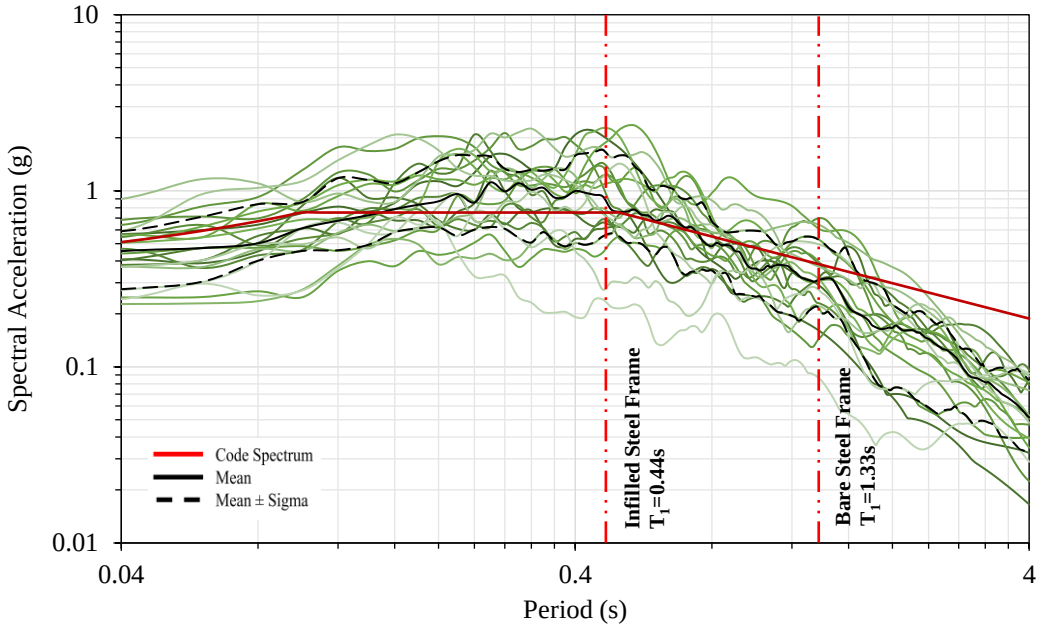

Figure 6.11 - Response spectra of 22 individual components of the normalised far-field records of FEMA P695 and the code based elastic response spectrum (ISIRI-2800)

Similar to the SIMBAD suite, in order to reduce the computational effort, only the component with the highest peak ground acceleration has been employed. Each of the resultant 22 ground motions were scaled to a number of distinct spectral acceleration values with respect to the structures' fundamental period. A total of twenty-five dynamic analyses were conducted on each record with intensity measures ranging from 0.1g to 2.5g, in increments of 0.1g, indicating a large record-to-record variability. Although an intensity of 2.5g might appear too high, the latest probabilistic seismic hazard assessment at the index building's location indicates intensities of similar values for the 5% and 2% probability of exceedance in 50-year life time of the structures, particularly for infilled frames with low period of vibration. The scaling was defined in a way to cover the entire range of the structural seismic response, from elasticity to collapse, while avoiding unrealistic levels of intensity. Figure 6.12, illustrates the P-695 record spectra before (grey) and after (coloured) scaling and matching the fundamental period of the infilled structure to the highest applied acceleration (i.e. 2.5g).

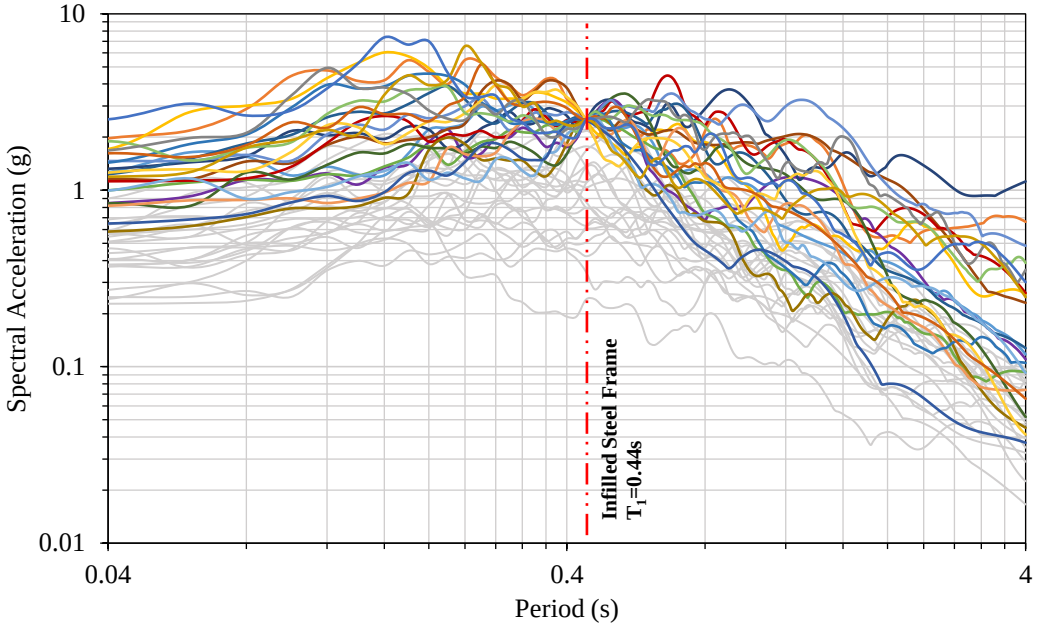

Figure 6.12 - Comparing original spectra of P-695 records (grey) to scaled records to 2.5g (coloured) at the fundamental period of the infilled steel frame

All nonlinear dynamic analyses are conducted utilising the SeismoStruct (v.7.0.6) engine (SeismoSoft, 2014). As stated, the analysis run time is directly correlated to the duration and number of steps of the applied ground motion. Hence, assuming that the computational cost for each run is the same, the more the ground motion is scaled, the longer for MSA to complete. However, as the increments between intensities decreases (i.e. increase in number of scaled records), the precision of the analysis increases. In this case, considering the range of applied accelerations (0.1g to 2.5g) and their increments (0.1g), a total of 550 runs should be conducted for each model with thousands of degrees-of-freedom. To overcome this computational intensive and time-consuming task, all analyses were conducted using a 16-vCPU virtual cloud server of Amazon Web Services (AWS). Operating parallel runs, 16 ground motions can be analysed at the same time through high speed processors (clockspeed @3.40GHz). In this case, the total run time, for M2-IR model was about 27 hours (average runtime per record: 45min), while for M7-BR the analysis lasted for about 34 hours (average runtime per record: 1hr). The analysis included all of the 22 scaled records, applied only to the weaker direction (x-direction) of the buildings, to be consistent with simplified methods and CLA. In case CLA is conducted using the same virtual server, the total runtime will be around 10 hours. However, considering the extensive number of IM-EDPs obtained through MSA in comparison to CLA, the extended runtime of MSA is justified by its precision.

The MSA results, presented in Figure 6.13, indicate the $S_a(T_1,5\%)$ of the scaled ground motions and their corresponding MIDR values. The results can be summarised into the 16th, 50th (i.e. the median), and 84th fractile curves by estimating the respective percentile values given the range of the $S_a(T_1)$ values.

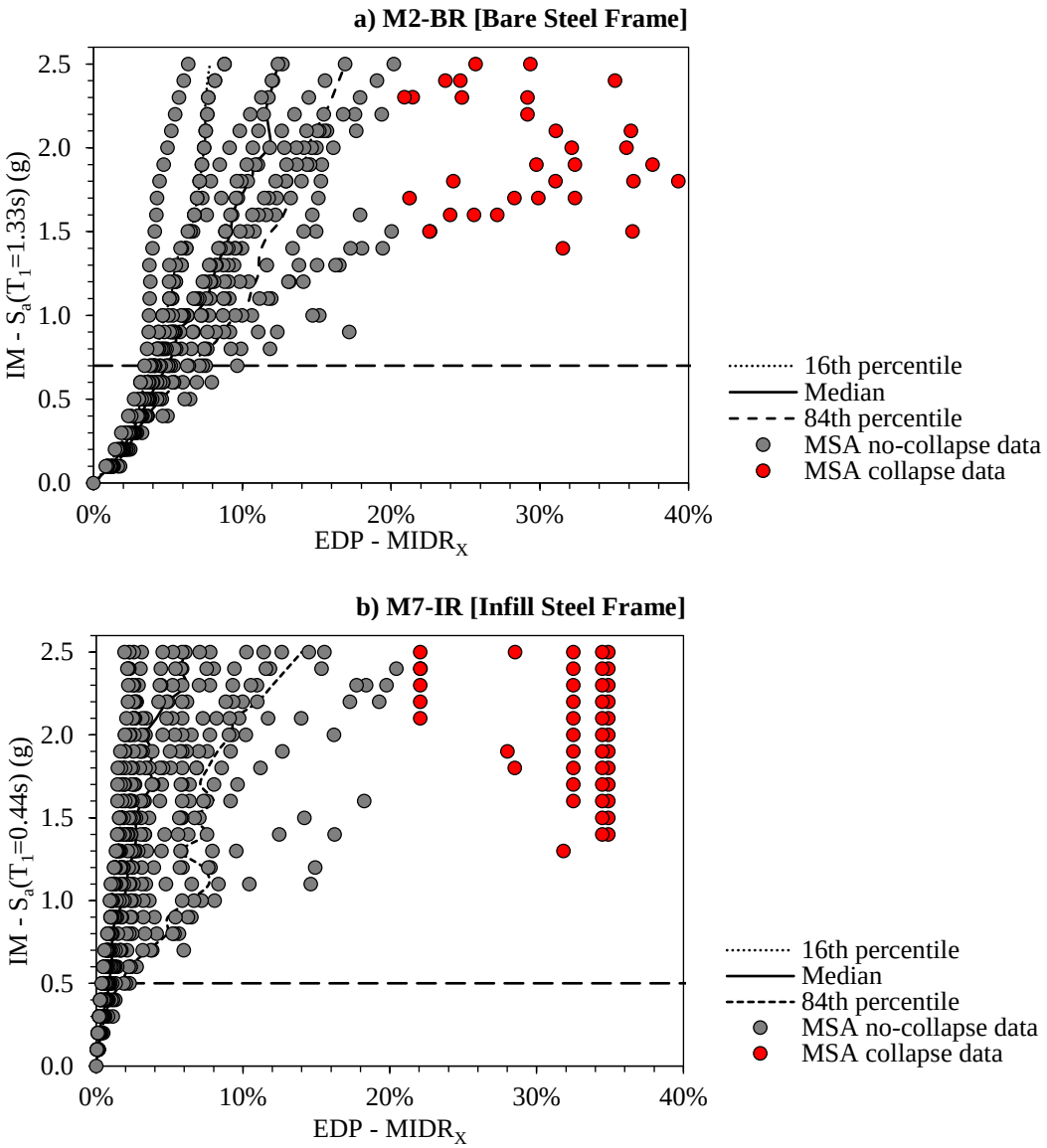

Figure 6.13 – IM-EDP results (response points) obtained through MSA for M2: bare steel frame (a) and M7: infilled steel frame (b); the red dots represent the collapsed cases in which the model did not converge or significantly large drift was obtained for a minor increase of intensity

As expected, for certain values of $S_a(T_1)$ applied, the bare steel frame undergoes a larger deformation compared to the stiffer infilled steel frame. Large dispersions are associated to intensities higher than 0.7g for the bare and 0.5g in case of the infilled frame, at which the structure has entered its inelastic phase. It should be noted that in cases, due to the nature of the record, the numerical model does not converge or results in unrealistically large deformation and inter storey drift, before reaching the highest given IM value (i.e. 2.5g). This is considered as collapse and so the model would not fulfil the entire acceleration range. This condition is more evident for the bare model, in which after an acceleration of 1.4g, for most of the applied earthquakes, the structure reaches the collapse stage and therefore only a limited number of points are plotted. These points are indicated with red circles on Figure 6.13. In case of M2, 33 runs and for M7 48 runs resulted in collapse.

6.5. Defining Damage Limit States

A critical stage of fragility function derivation includes characterising appropriate damage states and allocating rational global and local damage thresholds for the structure under study. In order to define appropriate damage states, the recommendations of a number of guidelines and codes such as FEMA 356 (2000), BS EN 1998-3 (2005), HAZUS (2003), and ASCE/SEI 41-13 (2013) have been reviewed.

For the infilled frame, as the initial lateral resistance is mainly provided by the masonry infill walls, and damage thresholds for these are not defined in the previous references, the experimental observations of Tasnimi & Mohebkhah (2011) and Flanagan & Bennett (1999) have been used. In this case the initial lateral resistance is provided by the infill walls. Upon cracking of the infill walls, the steel frame will provide further lateral resistance, while the infills act as diagonal compression struts for the surrounding frame. Collapse occurs when the infill walls disintegrate, resulting in compression failure of the masonry struts and subsequently the steel frame loses its stability. In terms of numerical modelling, collapse is when excessive global displacement-based demands are obtained, or when the software is not able to converge.

Accordingly, four levels corresponding to slight, moderate, extensive and complete structural damage (collapse), have been defined for the overall performance of the building characterised as follows:

Slight (DS1): hairline cracks (diagonal or horizontal) appear on some of the infill walls, some bricks near the beam-column interaction start to break and crush. A number of critical steel members reach their yielding point.

Moderate (DS2): large cracks (diagonal or horizontal) on most infill walls, a number of bricks dislodged and fall, partial and full collapse of few walls, some walls may bulge out-of-plane, failure at some steel connections, as some critical members may fail, and the structure might undergo a permanent lateral deformation.

Extensive (DS3): total failure of many infill walls and loss of stability of steel frame, bracings and moment connections start to fail, some infill walls may bulge out-of-plane, consequently the structure loses its lateral resistance. Some steel frame connections may have failed. Structure may exhibit permanent lateral deformation or partial collapse due to the failure of some critical members.

Complete (DS4): all infill panels disintegrate resulting in compression failure of the masonry struts and the steel frame has lost its stability completely, resulting in an imminent or immediate structural collapse.

There is indeed a gap in the literature regarding the mapping between EDP and the resulting damage states, which can only be filled through extensive experimentation and analysis (Moehle & Deierlein, 2004). Therefore, most common approaches rely on the definition of a certain EDP threshold that will imply the occurrence of a damage state. For this study, consistent with the choice of EDP used to indicate the structural response, specific values of MIDR are set as quantifiable global indicators for each stated damage state. MIDR is a suitable choice for moment-resisting frames (MRF), since it relates the global response of the structure to joint rotations, in which most of the inelastic behaviour of the MRF is concentrated. The shear capacity could also be a reliable indicator of the damage progress, especially in presence of the infill panels, however as the index building consists of steel frame and masonry panels, the selected EDP should be a representative of both structural components. Therefore, the flexural and shear capacity along with the behaviour of each structural element have been investigated through the static pushover analysis and their influence was considered in the allocation of the damage thresholds.

The damage threshold values employed for the fragility curves derivation are presented in Table 6.2. The table also contains the threshold values suggested by HAZUS (3003) in terms of inter-story drift for mid-rise moment resisting frame (MRF) [S1] and mid-rise steel braced frame [S2] with different design and built qualities. Figure 6.14, illustrates the resultant curves of non-linear static pushover analysis of the M2-BR and M7-IR and the positioning of the allocated damage thresholds in terms of MIDR.

Table 6.2 - Assigned damage thresholds in terms of maximum inter-storey drift ratio (MIDR).

Building Types according to HAZUS:
[S1M] Mid-Rise Bare Steel Moment Frame, [S2M] Mid-Rise Bare Steel Braced Frame

Damage Limit State	**M2-BR**	**M7-IR**	**HAZUS Inter-Story Drift at Threshold of Damage State**						
			S1M High Code	**S1M Mod. Code**	**S1M Low Code**	**S2M High Code**	**S2M Mod. Code**	**S2M Low Code**	**S5M Low Code**
Slight	0.99%	0.32%	0.40%	0.40%	0.40%	0.33%	0.33%	0.33%	0.20%
Moderate	1.87%	1.02%	0.80%	0.69%	0.64%	0.67%	0.58%	0.53%	0.40%
Extensive	2.57%	2.26%	2.00%	1.50%	1.35%	2.00%	1.56%	1.33%	1.00%
Complete	3.84%	4.03%	5.33%	4.00%	3.33%	5.33%	4.00%	3.33%	2.33%

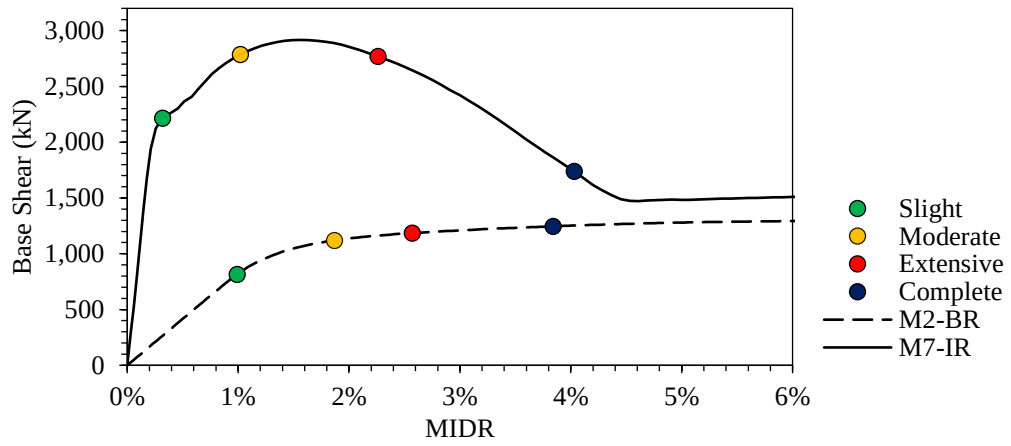

Figure 6.14 - Indication of damage thresholds at global structural level

Implementing fixed damage thresholds assists the process of deriving the analytical seismic fragility functions. However, having pre-set damage thresholds ignores the uncertainty in the evaluation of damage thresholds, which will not be reflected in the dispersion of the derived fragility functions. Further discussion on uncertainty involved with selection of damage thresholds and how other studies, such as HAZUS (2003) account for are provided in section 7.2.3 of Chapter 7.

The performance and response points obtained from each of the simplified and nonlinear dynamic analysis methods are presented in Figure 6.15, along with the allocated damage thresholds. It should be noted that regardless of the type of structural analysis and method applied for identifying the performance points, the same damage thresholds have been considered for all IM-EDP values to derive the fragility functions. It is clear that all four methods have a considerable concentration of points in the slight and moderate damage regions and therefore, similar fragility functions are expected for these damage states. However, for higher intensities and damage thresholds (i.e. Extensive and Complete), the IM-EDPs of MSA have a higher concentration of points in comparison to the simplified and CLA methods. This is due to the relatively smaller number of SIMBAD records capable of generating the necessary excitation to push the structure's response beyond extensive and collapse damage thresholds. Although, the range of applied SIMBAD ground motion intensities seem adequate for bare frame, in the case of infilled frame with higher capacity and stiffness, stronger earthquakes are required to induce a considerable damage. The MSA method is able to resolve this issue by scaling the records. Therefore, the fragility functions obtained through MSA results can be more reliable than the CLA method, as the generated fragility functions are based on many more simulation cases, although some possible bias from the record scaling process has been pointed out by previous studies (Luco and Bazzuro, 2007).

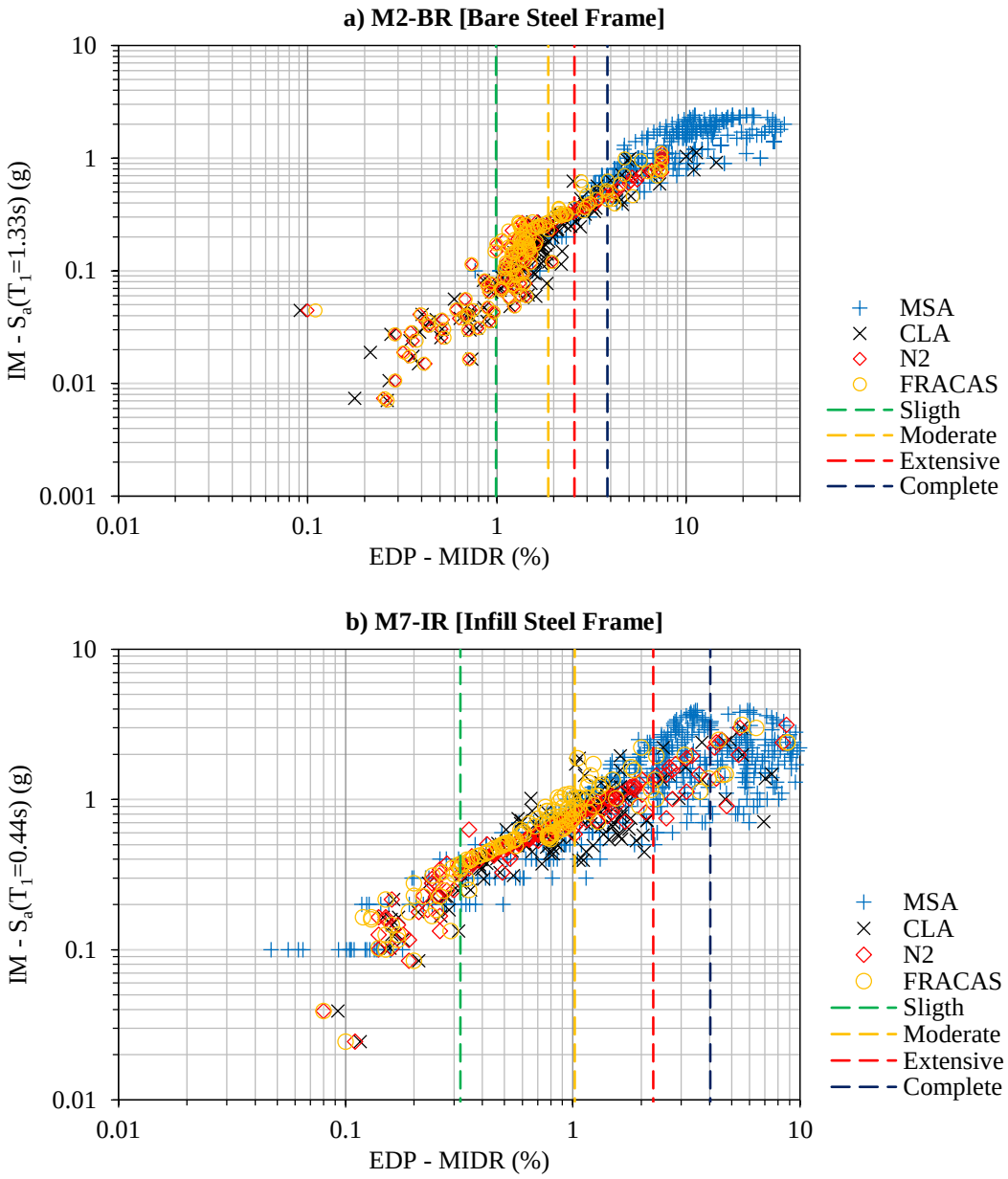

Figure 6.15 - Comparison of IM-EDP obtained from simplified and nonlinear dynamic analysis methods in terms of spectral acceleration.

The EDPs and their corresponding IMs in terms of the peak ground acceleration, obtained with the simplified methods and the CLA, are shown in Figure 6.16. The correlation of the performance expressed in terms of MIDR to the PGA is clearly much poorer than to the $S_a(T_1)$ for both structural types. Furthermore, in case of PGA, not only the information on the duration of the earthquake is lost, but also the information on the frequency content. Several studies (e.g. Shome et al. (1998)) have shown that spectral acceleration at the structure's fundamental period is more efficient and sufficient than the non-structure-specific IMs, such as PGA. Therefore, for this study all fragility functions are derived only in terms of spectral acceleration at the fundamental period of the structure under study.

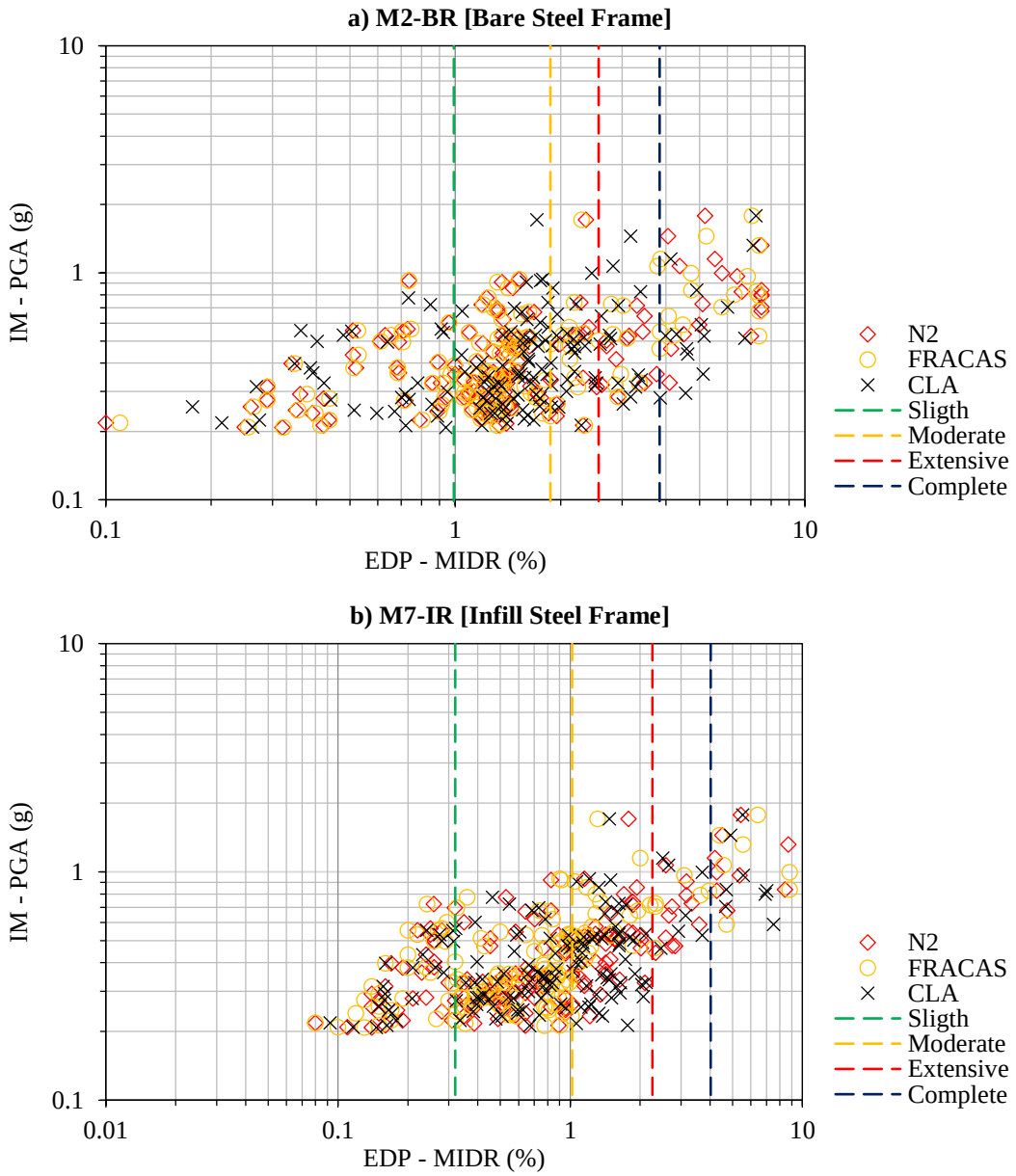

Figure 6.16 - Comparison of IM-EDP obtained from simplified and nonlinear dynamic analysis methods in terms of peak ground acceleration.

6.6. Fragility Function Derivation

Fragility functions are one of the fundamental tools in the process of seismic loss and performance assessment. In simple terms, fragility functions describe the probability of attaining or exceeding different damage limit states, such as collapse, given a level of ground shaking (Mackie & Stojadinović, 2005). The fragility functions are customarily described by a lognormal cumulative distribution function (CDF) as follows:

$$P_f(DS \geq ds_i \mid IM) = \Phi\left(\frac{\ln IM - \mu}{\beta}\right) \tag{6.7}$$

where $P_f(ds \geq DS_i \mid IM)$ is the probability of being at or exceeding a specific damage state (DS_i), given a ground motion (IM), $\Phi()$ is the standard lognormal (Gaussian) cumulative distribution function (CDF) and μ is the median of the fragility function (i.e. the IM level with 50% probability of or exceedance). β is the standard deviation of the natural logarithm of IM for damage state ds_i, which can incorporate the aspects of uncertainty and randomness for both capacity and demand. Thus, the fragility curves are defined by two parameters, the median and the standard deviation which indicates the dispersion. A number of approaches are developed for estimating the fragility parameters based on the implemented seismic performance assessment method and the level of simulation that accounts for the effect of uncertainty. The analytical fragility functions of the studied index buildings are derived by implementing appropriate statistical curve fitting methods to the IM-EDPs obtained through each of the simplified and advanced methods.

A thorough discussion of different statistical sampling and regression procedures commonly used for developing fragility functions can be found in Lallemant et al. (2015) and Baker (2015). As suggested, three appropriate fitting techniques are the Maximum Likelihood (ML) (Shinozuka et al., 2000), Generalised Linear Regression method (GLM) with a probit link function (Basöz & Kiremidjian, 1998) and Least Square method (LS) (Baker, 2007).

In case of the least square regression (Baker, 2007), for a chosen probabilistic damage threshold, the IMs are selected in a way that roughly half of the points are below that damage threshold and the rest above it, resulting in an interval for the lognormally distributed IM values. By performing piece-wise regression over each IM interval, the fragility parameters (i.e. median and dispersion) can be computed using the following relations:

$$\ln(EDP) = \ln(b) + a\ln(IM) \tag{6.8}$$

$$\begin{cases} \mu_{ds_i} = \exp\left(\ln\left(\frac{ds_i}{a}\right)\Big/_{b}\right) \\ \beta_{ds_i} = \dfrac{STDEV(lnIM_i)}{a} \end{cases} \tag{6.9}$$

where a and b are the coefficients of the logarithmic linear regression. A drawback of this method is the way it calculates the standard deviation (β) of the error. The dispersion is calculated over the entire IM range, resulting in similar values for all fragility curves of various damage levels. This issue can be resolved by performing a piece-wise regression over different IM intervals, hence allowing the power law and the dispersion to vary at different IM levels (Cărăuşu & Vulpe, 1996). Generally, in comparison to other regression approaches, the LS method requires far fewer IM-EDP values to result in an accurate fragility curve (Gehl et al., 2015).

Both GLM and Maximum likelihood consider EDPs as binary variables (i.e. Bernoulli trials, 1 if damage, 0 if not), commonly used for regression analysis of dichotomous data such as collapsed or non-collapse structures. GLMs are a variation of ordinary linear regression, in which the predictor variables are linearly related to the response via a link function (g), as follows:

$$g(\mu) = P_f(ds \geq DS_i \mid IM) = g^{-1}(a + b.\ln(IM)) \tag{6.10}$$

where μ is the expected response given predictor variables, a and b are the unknowns of the statistical model. $g()$ is the link function, used to represent the optimization problem in a linear space, which can be obtained through any of the following:

$$g(\mu) = \Phi^{-1}(\mu) \tag{6.11}$$

$$g(\mu) = log\left(\frac{\mu}{1-\mu}\right) \tag{6.12}$$

$$g(\mu) = log[log(1-\mu)] \tag{6.13}$$

where Φ is the standard normal cumulative distribution function. The functional parameters of the link function are then estimated depending on the distribution of the binary variables with respect to IM. For instance, in case of the probit link function the conditional mean response (μ), representing the fragility curve becomes:

$$\mu = \Phi\left(\frac{\ln(IM) - \alpha}{\beta}\right) \tag{6.14}$$

where in all cases the fragility parameters, α and β are obtained as follows:

$$\begin{cases} \alpha = \exp(-\dfrac{a}{b}) \\ \beta = \dfrac{1}{b} \end{cases} \tag{6.15}$$

b is the slope and a is the intercept for the fragility curve corresponding to the damage state (ds_i).

All three of the discussed fitting techniques have been applied to the 550 IM-EDPs of MSA to derive fragility curves for different damage states (Figure 6.17). Comparing the derived fragility functions indicates that due to the large number of IM-EDPs obtained, all three fitting methods result in closely matching curves for both structures. Moreover, the results are enclosed by the 95% and 5% confidence bounds (CB) derived using a bootstrap analysis (Efron & Tibshirani, 1994) of the data points. Such analysis is aimed at determining the significance of the obtained curves by measuring the statistical error related to the estimated quantities, generated by considering the specified confidence bounds.

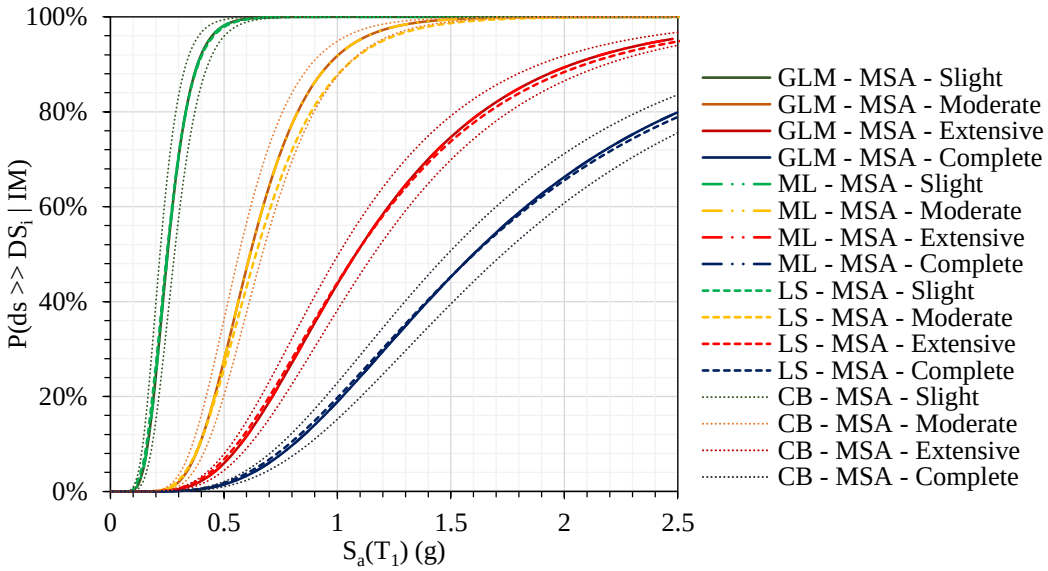

Figure 6.17 – Comparing different fragility fitting functions on MSA results for infilled steel frame

It should be noted that, depending on the number and dispersion of the IM-EDPs, the choice of a statistical model fitting technique can have an influence on the obtained fragility functions. For instance, Figure 6.18 illustrates the divergence of fragility curves derived for the cloud of IM-EDPs using the GLM and a least square regression.

The median and dispersion for each damage state fragility function is given in Table 6.3. GLM is the equivalent of an iterative weighted linear regression, which can be used to obtain the maximum likelihood estimates of parameters with exponential distribution. According to Rossetto et al. (2014), the GLM method is theoretically more valid than the least square method, in which the assumptions may be violated by the data used for the fragility assessment. While, least square is the most common approach, GLM uses the complete data without any aggregation and/or unnecessary dismissal and associates a distribution which is a better suit to the nature of the response variables.

In cases where limited number of data point are available, particularly in higher damage states, GLM performs better. Hence, the generalised linear regression with a probit link function is applied, in which the EDP values are transformed into binary variables and a link function is employed to represent the optimisation problem in the linear space.

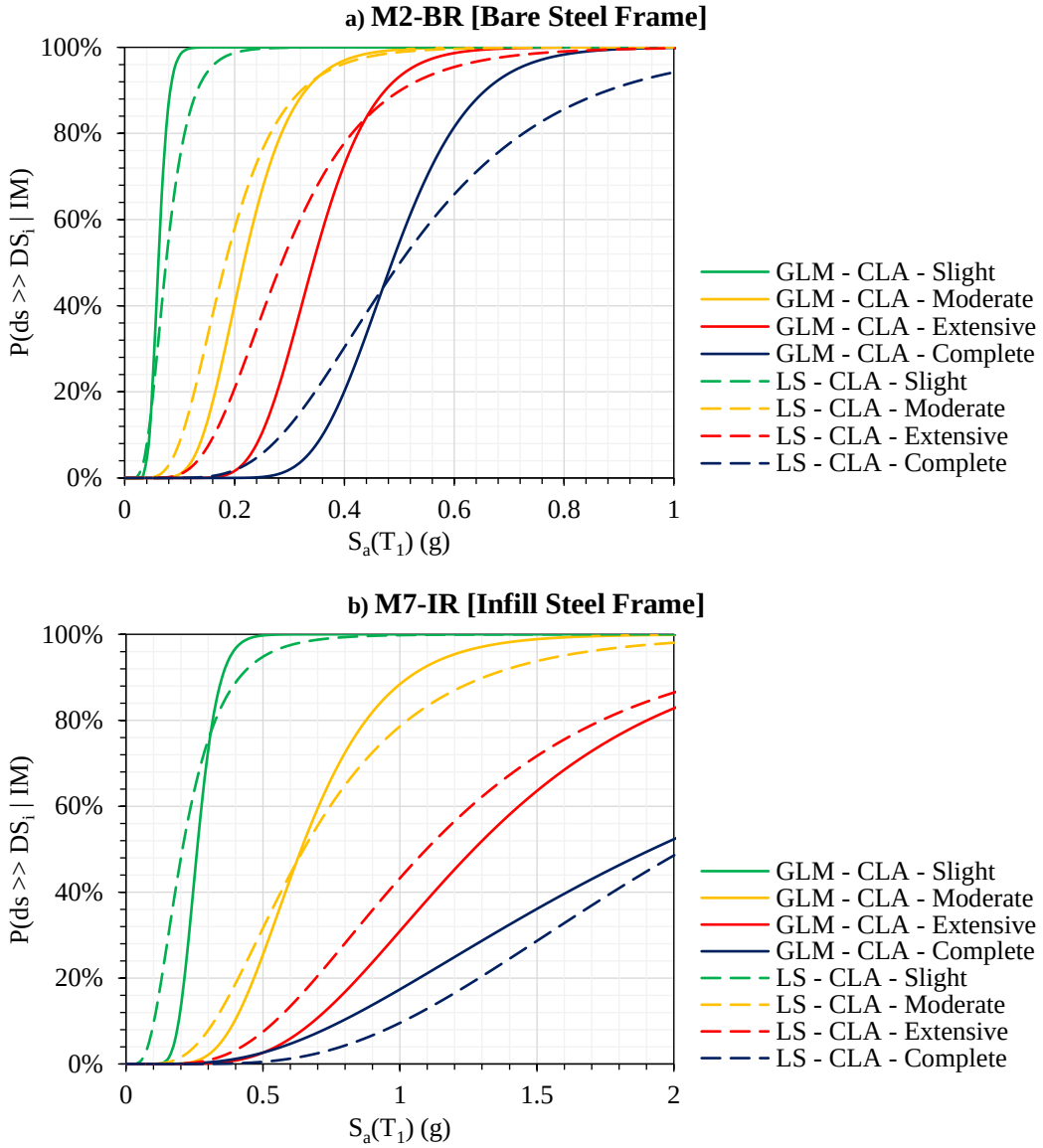

Figure 6.18 – Comparing different fragility fitting functions on cloud results for bare and infilled steel frame

Table 6.3 - Median (μ [g]) and Dispersion (β) values of fragility curves obtained through Generalised Linear Model (GLM) and Least Square (LS) for cloud analysis of bare and infilled steel frame

	Bare Steel Frame				Infilled Steel Frame			
Damage State	**GLM**		**LS**		**GLM**		**LS**	
	μ	β	μ	β	μ	β	μ	β
Slight	0.06	0.237	0.08	0.440	0.26	0.234	0.21	0.545
Moderate	0.22	0.326	0.18	0.440	0.64	0.373	0.65	0.545
Extensive	0.34	0.252	0.29	0.440	1.27	0.480	1.10	0.545
Complete	0.49	0.234	0.50	0.440	1.94	0.695	2.04	0.545

For this study, in order to derive the fragility functions for the IM-EDPs generated by the simplified methods and the nonlinear dynamic analysis, the GLM fitting approach is selected. The fragility curves of the mid-rise bare and infilled steel frame, obtained through each of the four analysis methods are presented in Figure 6.19 and Figure 6.20 respectively. The median and dispersion values of each fragility function is given in Table 6.4 and Table 6.5.

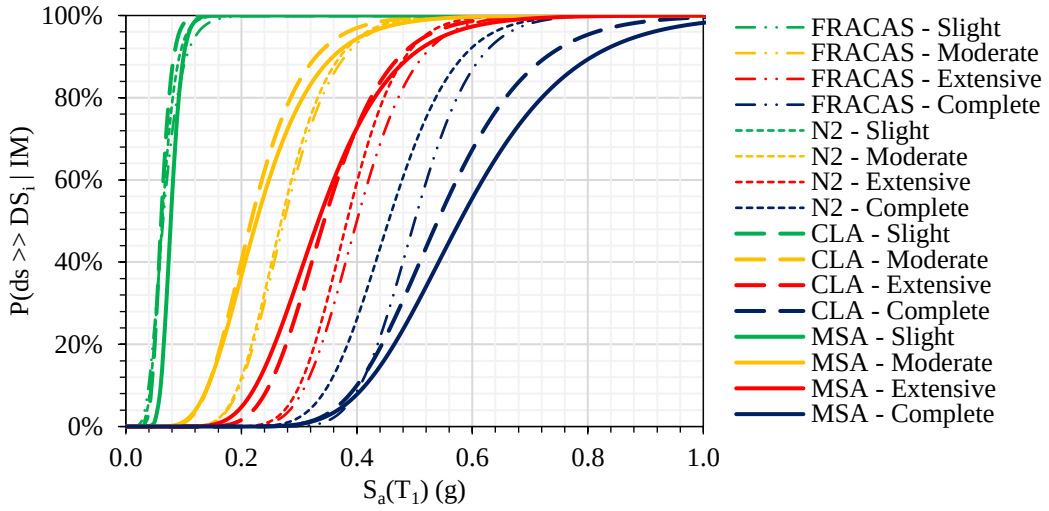

Figure 6.19 - Comparison of fragility curves obtained for bare steel frame from simplified and nonlinear dynamic methods

Table 6.4 - Median (μ [g]) and Dispersion (β) values of fragility curves obtained through Generalised Linear Model (GLM) technique for simplified and nonlinear dynamic analysis methods for bare steel frame

Damage State	**N2**		**FRACAS**		**CLA**		**MSA**	
	μ	β	μ	β	μ	β	μ	β
Slight	0.06	0.301	0.06	0.381	0.06	0.239	0.08	0.196
Moderate	0.27	0.251	0.27	0.254	0.22	0.326	0.23	0.360
Extensive	0.39	0.052	0.40	0.173	0.34	0.252	0.33	0.305
Complete	0.50	0.163	0.50	0.247	0.54	0.234	0.58	0.260

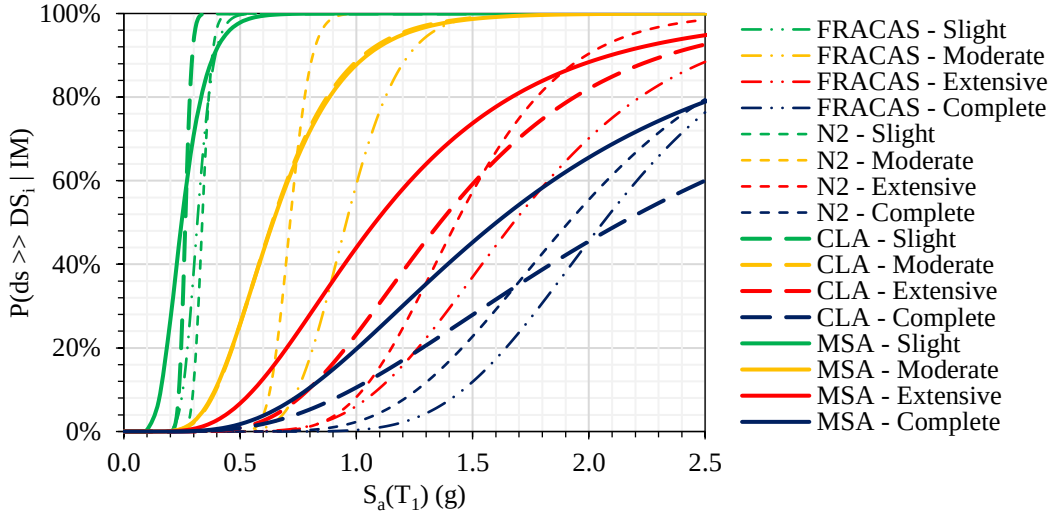

Figure 6.20 - Comparison of fragility curves obtained for infilled steel frame from simplified and nonlinear dynamic methods

Table 6.5 – Median (μ [g]) and Dispersion (β) values of fragility curves obtained through Generalised Linear Model (GLM) technique for simplified and nonlinear dynamic analysis methods for infilled steel frame

Damage State	**N2**		**FRACAS**		**CLA**		**MSA**	
	μ	β	μ	β	μ	β	μ	β
Slight	0.34	0.095	0.32	0.171	0.26	0.084	0.25	0.347
Moderate	0.71	0.100	0.96	0.193	0.64	0.373	0.64	0.382
Extensive	1.30	0.257	1.68	0.334	1.48	0.421	1.08	0.515
Complete	1.91	0.325	2.06	0.269	2.14	0.609	1.60	0.554

Figure 6.21 shows the difference obtained in the median of the fragility curves, derived through different analysis methods, when compared to the ones of the MSA for all damage states. Similarly, the dispersions are compared in Figure 6.22.

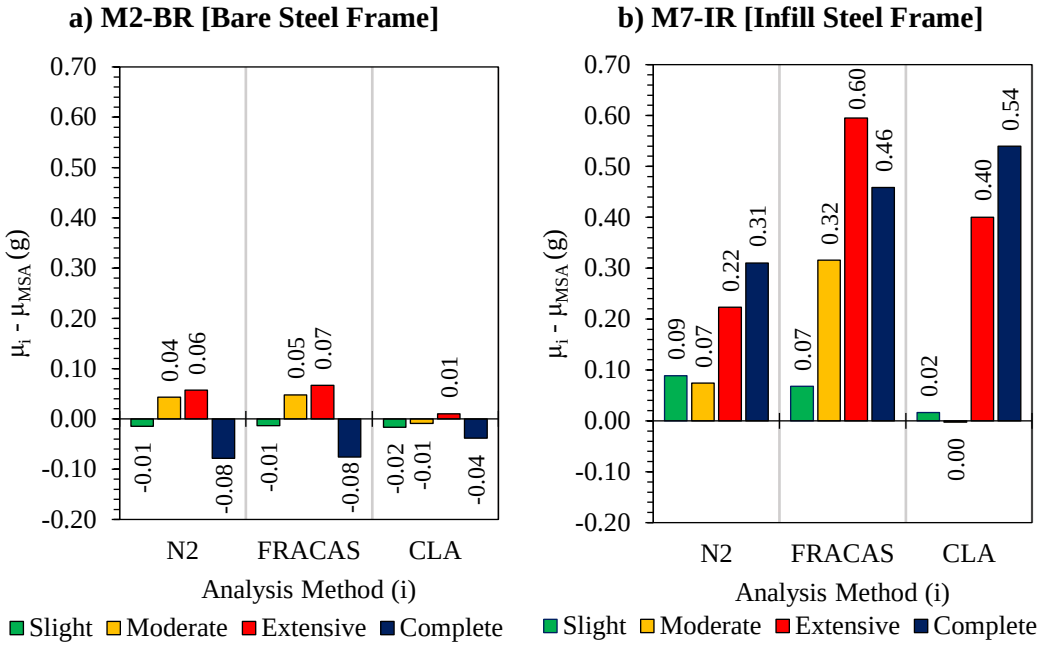

Figure 6.21 – Difference obtained in Median (μ [g]) of fragility function derived from MSA and other analysis methods (positive value indicates a higher value than the one of MSA)

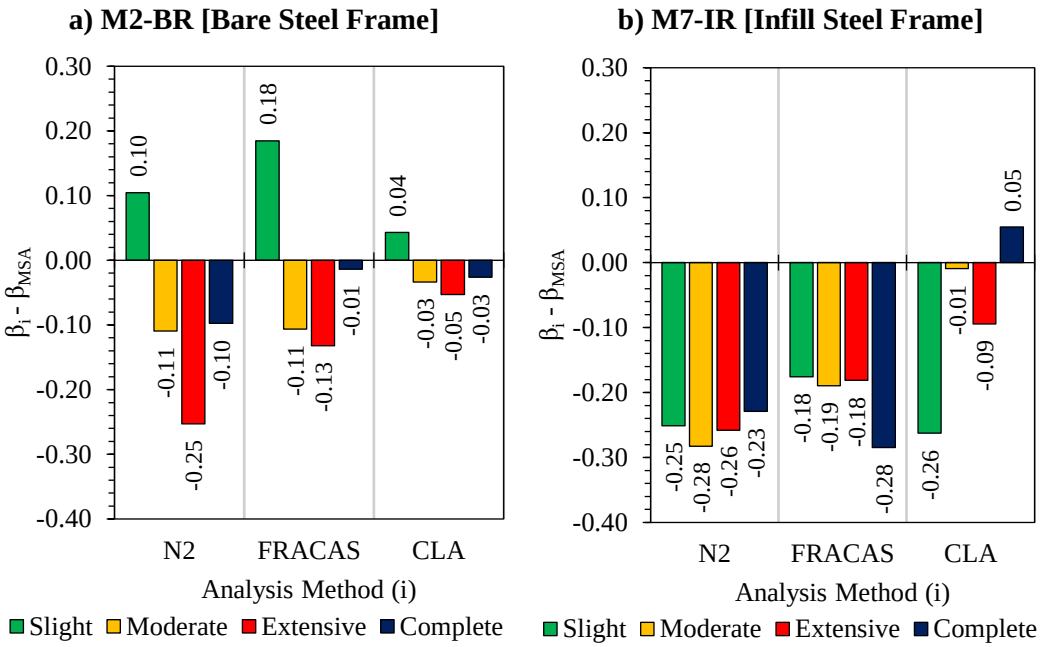

Figure 6.22 – Difference obtained in Dispersion (β) of fragility function derived from MSA and other analysis methods (i) (positive value indicates a higher value than the one of MSA)

In case of the bare frame, as expected, the fragility functions of the slight damage state, which mainly corresponds to the lower intensities and the elastic response, give relatively similar probability of damage and have close median and dispersion values. According to Figure 6.9a,

the performance points of both simplified methods matched quite well, therefore the obtained fragility curves are generally very close with similar median values. However, in comparison to the fragility curves of the MSA, the simplified methods underestimate the moderate (error in median FRACAS: 21%, N2: 19%) and extensive (error in median FRACAS: 20%, N2: 17%) damage states as they have underestimated the EDPs.

For all the damage states of the bare structure, MSA and CLA have comparable median and dispersion, except for higher IM values (i.e. Complete) for which MSA resulted in considerably higher number of EDP-IMs. Hence an overestimation of collapse damage is observed in the fragility curves of N2, FRACAS and CLA when compared to the MSA. This behaviour is clearly evidence from the obtained medians (Figure 6.21a). The observed diversity, particularly at higher intensities, can be explained by the quantity of response points each method determined.

In case of the infilled steel frame, both simplified methods have underestimated the damage as it is clear from Figure 6.20 and Figure 6.21a. The difference in median of MSA and simplified methods has reached up to 0.31g and 0.6g for the N2 and FRACAS respectably in higher damage states. The CLA has resulted in matching fragility curves for slight and moderate damage states, with negligible difference in median. However, as the intensity rises, the median and dispersion of CLA passes the MSA, resulting in an underestimation in expected damage at intensities higher than 0.4g (considering T_1=0.44s). This is due to the higher capacity of the infilled framed structure compared to the bare frame and the fact that the suite of 150 unscaled earthquake records are not strong enough to generate sufficient amount of IM-EDPs in the intervals of extensive and complete damage states. This resulted in errors of 40% and 54% in estimating the median of CLA for extensive and complete damage states, respectively.

Although the simplified methods resulted in matching curves to the ones of CLA and MSA at lower intensities (i.e. slight damage), however as the structure goes under more inelastic deformation, the simplified methods start to underestimate the damage. The true impact of this damage underestimation becomes evident when estimating the seismic vulnerability and loss. For this study, to reach an acceptable accuracy in vulnerability assessment and account for the record-to-record variability, the fragility functions of the defined index buildings, corresponding to different damage states, will be generated based on the IM-EDPs obtained from MSA, utilising the ground motions of ATC-63 (FEMA P-695, 2009). Furthermore, a fitting technique proposed by Baker (2015) will be used to estimate the fragility parameters (μ and β). The method has a straightforward approach in evaluating the fragility functions for stripes of EDPs obtained for given IM values, which suites well with the MSA results. The

method is based on minimising the sum of squared errors (SSE) between the observed fractions of the damage state and probabilities of damage predicted by the fragility function. Mathematically, this can be expressed as follow:

$$\{\mu, \beta\} = argmin \sum_{j=1}^{m} \left(\frac{z_j}{n_j} - \Phi\left(\frac{\ln(x_j/\mu)}{\beta} \right) \right)^2 \quad (6.16)$$

where Φ() is the standard normal cumulative distribution function, μ is the median of the fragility function, β is the standard deviation of $lnIM$, m corresponds to the number of IM level considered, z is the number of cases reaching or exceeding the damage state out of n number of ground motions with $IM = x_j$.

So far, for the discussed analysis only a single component of the earthquake, with the highest PGA was applied to the weaker direction of the structure. Next section will discuss whether this approach is reliable to conduct the MSA or alternative methods should be applied to derive the IM-EDPs of the selected index buildings.

6.7. Bi-directionality of Earthquake

In typical buildings, the resistant elements are oriented according to the two principle axes of the structure to resist load due to gravity and seismic excitation. In common practice, the seismic response is evaluated based on the analysis outcome of the structure excited by uni-directional earthquakes. However, as the earthquake strikes, the two horizontal orthogonal components of the ground motion act simultaneously on the building, while the excitation angle is unknown. The norm of seismic resistant design and assessment recommends carrying out two analyses according to the principal axes of the building, considering the structure like a three-dimensional system. The earthquake actions are then applied as single components along at least two perpendicular directions, arbitrarily defined by the designer. The structural response is then estimated by analysing each component one at a time for the considered axis of the building and combining the outcomes together through various methods. A commonly used combination procedure to determine the response is the Square Root of Summation Squares (SRSS)(Eq. 6.17).

$$R_{SRSS} = \sqrt{(R^{0^\circ})^2 + (R^{90^\circ})^2} \quad (6.17)$$

where R^{0° and R^{90° each represent a response obtained along one of the perpendicular directions of the analysis. Reyes-Salazar et al. (2008) concluded that the SRSS rules could underestimate the combined response and the energy dissipation mechanism should be considered as accurately as possible. To overcome this underestimation the following formula

(Eq. 6.18) was proposed to estimate the response of structure when both horizontal components are applied in separate instincts.

$$R_{20\%} = 1.2 \cdot max\{R^{0^\circ}; R^{90^\circ}\} \tag{6.18}$$

In general, the seismic assessment of the structures is commonly conducted based on a worst-case scenario. In this case, the highest possible demand is obtained by selecting the side with the lowest stiffness, while the static or dynamic analysis is only conducted in that direction by applying a single horizontal earthquake component with the largest PGA (uni-directional earthquake). This is because in most cases the buildings are either analysed as a two-dimensional structure or as an equivalent simplified single degree of freedom system. Furthermore, analysing the structure for both earthquake components, either concurrently or one at a time, will significantly increase the analysis time, which is not desirable.

In order to initiate the seismic analysis of the index buildings, the number of considered earthquake components, and their applied directions should be decided. The reason for this is the extensive computation time and power required to analyse the building under both horizontal components simultaneously. To determine the impact of earthquake components and whether applying a single component to the weaker direction is sufficient, the discussed index buildings (M7-IR and M2-BR) are analysed under both horizontal components of the 1990 Manjil-Rudbar earthquake (M_w 7.4) recorded at Abbar station (RSN1633-L and RSN1633-T). The acceleration and displacement response spectrum of each horizontal component are shown in Figure 6.23. The fundamental periods of the infilled and bare frames are indicated on the graphs.

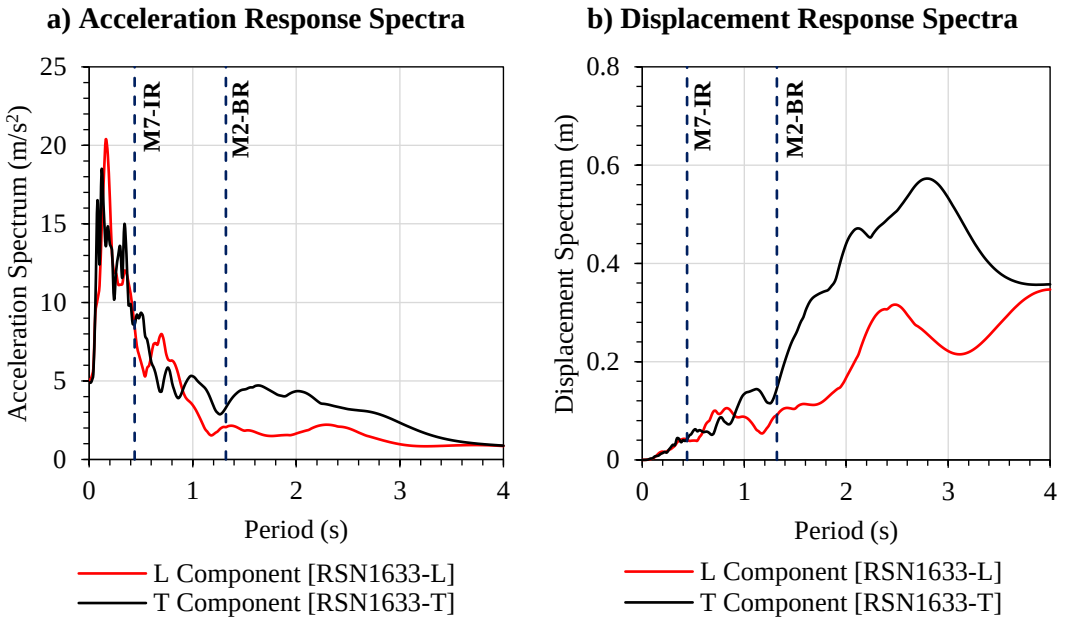

Figure 6.23 – Acceleration (a) and Displacement (b) response spectra for horizontal components of the 1990 Manjil-Rudbar earthquake record

Initially, each of the record components (i.e. L- and T-components) are applied individually at the principle axes, transverse (Y-dir) and longitudinal (X-dir) of the infilled steel frame and the nonlinear time history displacement of the structure is measured and the maximum displacement determined (Figure 6.24).

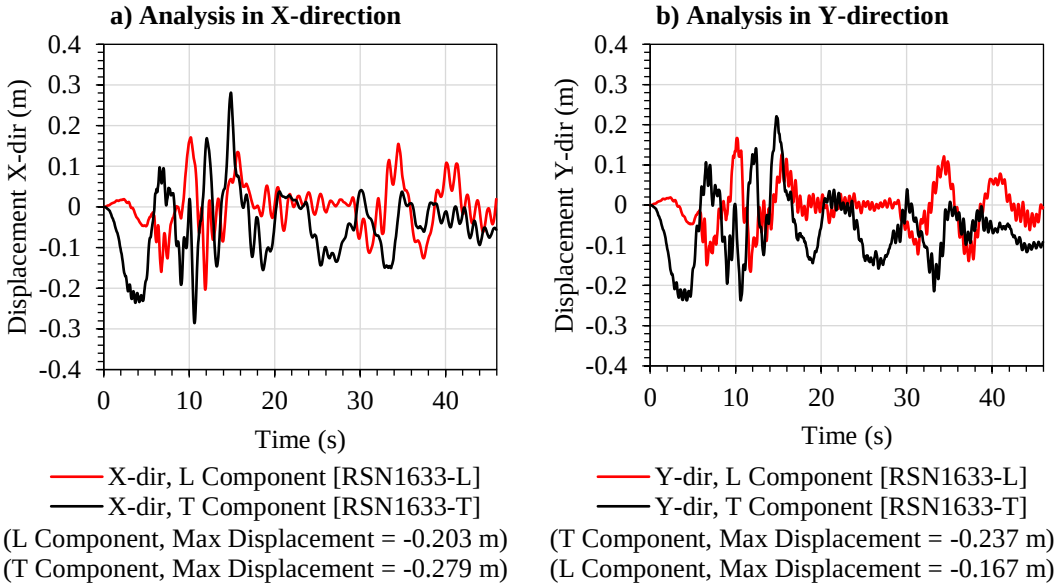

Figure 6.24 – Displacement response obtained for the principle axes of M7-IR, as each earthquake component of the 1990 Manjil-Rudbar earthquake is applied separately to each axis

The graphs illustrated in Figure 6.25, indicate the top node (i.e. roof) displacement response of the infill structure when both horizontal components of the earthquake are applied concurrently. Each of the components are applied once at the longitudinal direction (X-dir) and once at the transverse direction (Y-dir) of the structure. The maximum displacement recorded for each direction of the structure are shown. As expected, the displacements are sensitive to the direction each record component is applied.

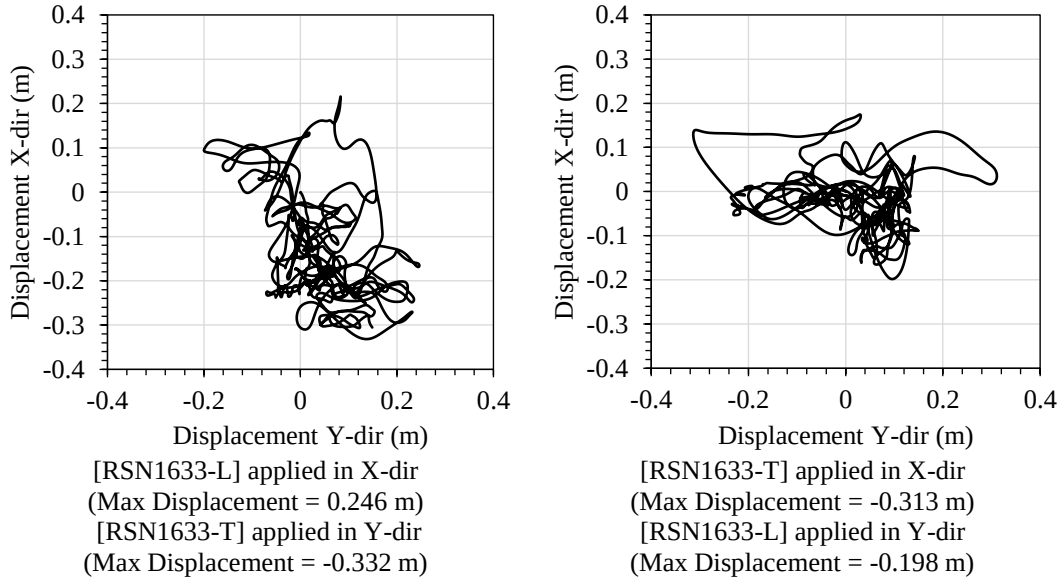

Figure 6.25 – Top node displacement as both horizontal components of the 1990 Manjil-Rudbar earthquake are applied concurrently to principle axes of M7-IR

Figure 6.26, compares the displacement obtained by combining the outcome obtained through analysing each of the components separately (Combining Uni-directional Analysis) as shown in Figure 6.24, with the resulted response from concurrent application of the horizontal components (Bi-directional Analysis), as presented in Figure 6.25. A considerable variation is observed in the trend of the response and also maximum values.

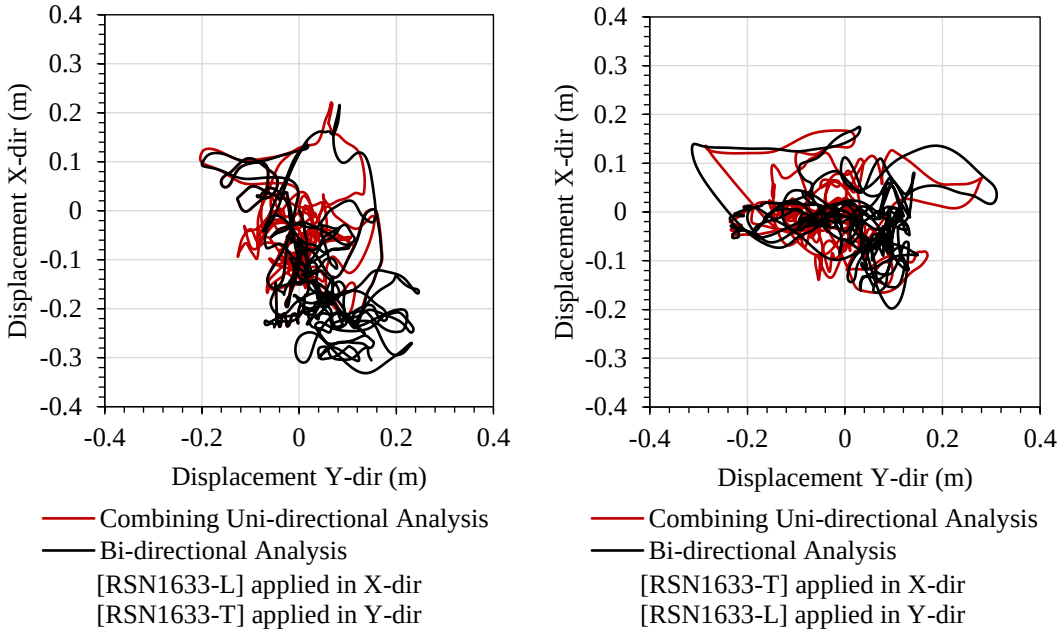

Figure 6.26 - Comparison of response obtained through separate analysis of each components (uni-directional) and the concurrent application of both horizontal components (bi-directional) on M7-IR

Conducting the same investigation on the bare steel frame (M2-BR), each horizontal component is applied individually to each principle axes of the building (Figure 6.27).

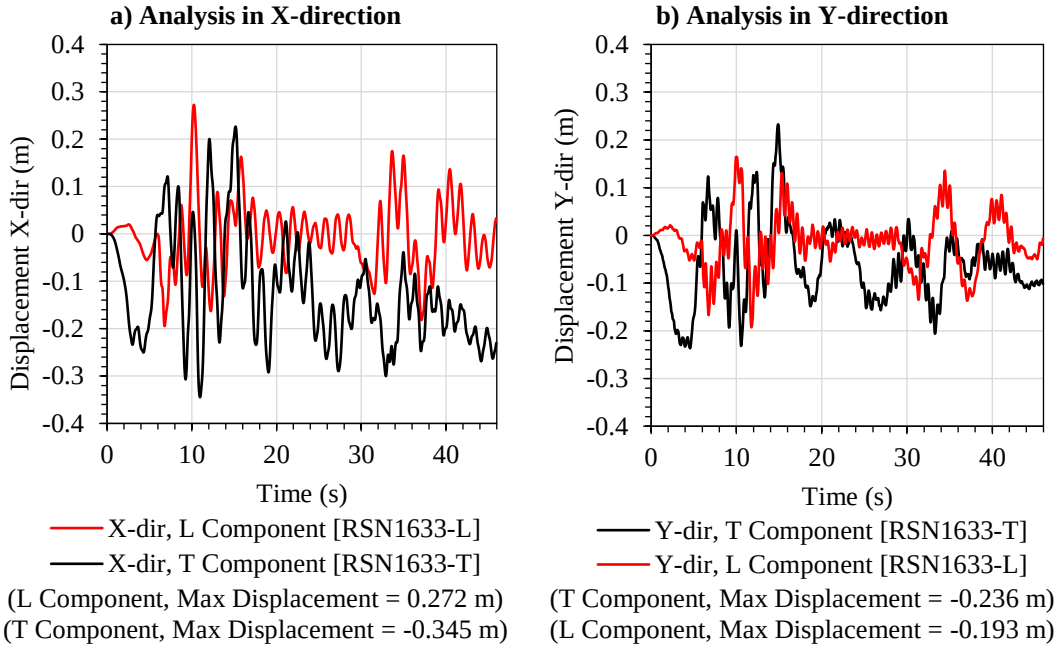

Figure 6.27 - Displacement response obtained for the principle axes of M2-BR, as each earthquake component of the 1990 Manjil-Rudbar earthquake is applied separately to each axis

In case both horizontal components of the earthquake are applied concurrently, the response of the bare frame will be as shown in Figure 6.28.

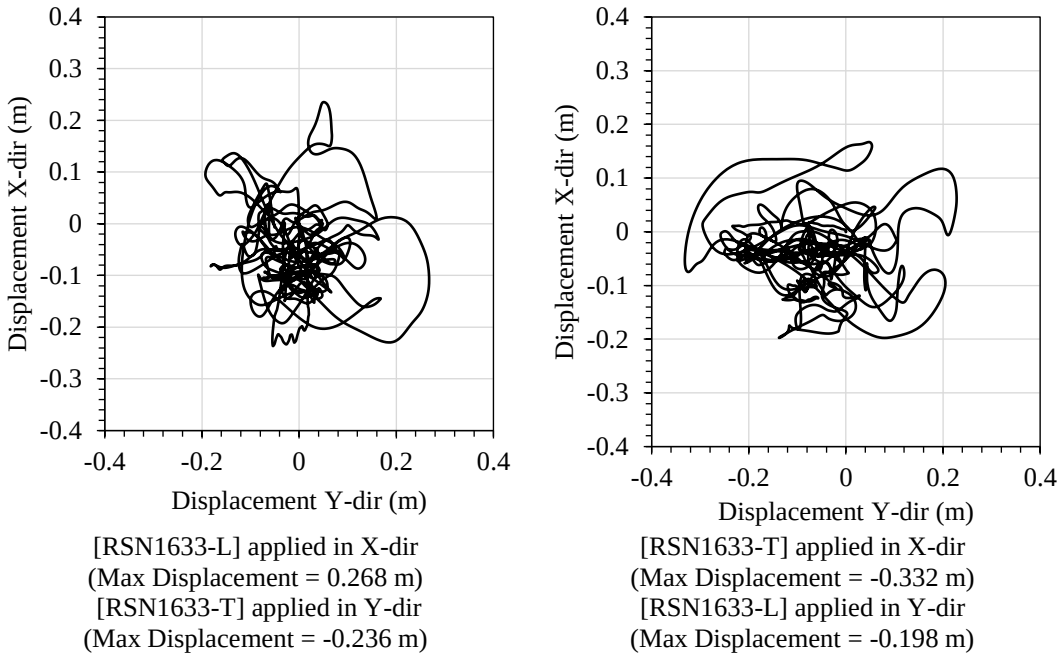

Figure 6.28 - Top node displacement as both horizontal components of the 1990 Manjil-Rudbar earthquake are applied concurrently to principle axes of M2-BR

Comparing the response obtained through bi-direction analysis (Figure 6.28) and combination of the individual response of each component (uni-directional) as shown in Figure 6.27, a better agreement is observed in case of the bare frame when compared to the infilled frame (Figure 6.26), as presented in Figure 6.29.

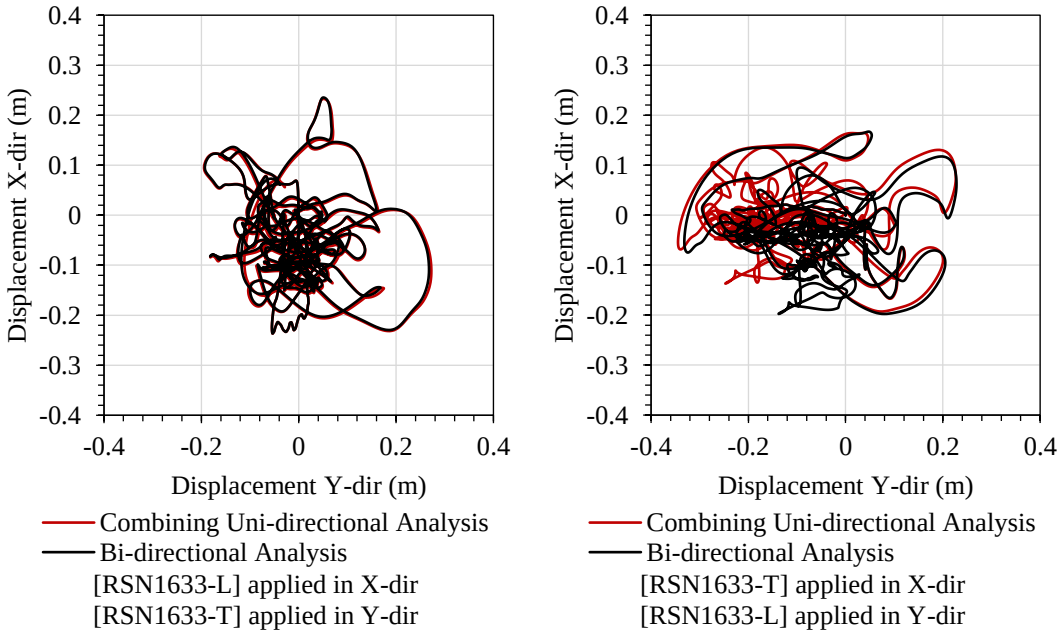

Figure 6.29 - Comparison of response obtained through separate analysis of each components (uni-directional) and the concurrent application of both horizontal components (bi-directional) on M2-BR

Following the recommendations of the codes and available studies, maximum response obtained through the stated formula, R_{SRSS} and $R_{20\%}$ are compared to R_{x+y}, which represents the maximum resultant response of the structure when the two horizontal components of the earthquake are applied concurrently at the principle axes.

Table 6.6 – Response obtained through bi-directional analysis and different combination methods (positive error indicates overestimation)

Component applied to the principle axis	R_{x+y} **(m)**	R_{SRSS} **(m)**	**Error**	$R_{20\%}$ **(m)**	**Error**
M7-IR (Infilled Steel Frame)					
L → X-dir ; T → Y-dir	0.332	0.264	-20%	0.285	-14%
T → X-dir ; L → Y-dir	0.332	0.316	-5%	0.343	3%
M2-BR (Bare Steel Frame)					
L → X-dir ; T → Y-dir	0.268	0.308	15%	0.327	22%
T → X-dir ; L → Y-dir	0.332	0.350	5%	0.413	24%

In general, the recommended combination methods overestimated the response of the bare frame, while underestimating the response obtained for the infilled frame. In case of the bare frame, the outcomes can be considered as conservative. On the contrary, the underestimation of infill response will have a negative effect on the obtained IM-EDPs and consequently the fragility and vulnerability functions. Similar conclusions are drawn by studies like Fernandez-Davila et al. (2000) and Reyes-Salazar et al. (2008). Hence, to address the stated shortcoming of combination methods, the seismic performance of the defined index buildings is evaluated as both components of the earthquake are applied concurrently. In this case, the component with the highest PGA is applied to the weaker direction of the structure assuming a worst-case scenario. The maximum response will be recorded and utilised to obtain the EDPs.

It should be noted that the effect of vertical component is neglected as its influence is very minor compared to the other components. Moreover, earthquake has an arbitrary excitation angle and may affect the structure from any direction. In this case, the main direction of the earthquake motion is not necessarily identical to the principle axes of the structure, hence the response changes with variation of the ground motion angle (Lagaros, 2010; Rigato & Medina, 2007). The directionality of the earthquake and how it impacts the structural response is out of the scope of this research project.

6.8. Index Building Fragility Functions

Investigating different stages and aspects of the seismic fragility derivation, the most applicable methods and approaches have been identified in this chapter. The stated methods are applied to the index buildings, defined in Chapter 4. Multiple-stripe analysis is employed to obtain the IM-EDPs of each index building. For each ground motion, both horizontal components are applied to the structure concurrently, following a worst-case scenario, for which the component with the highest PGA is applied to the direction of the structure with less stiffness. Each record is scaled from 0.05g to 2.5g with an increment of 0.05g, resulting in a total of 1000 IM-EDPs. It should be noted that, subject to the structure, the analysis might have terminated at lower intensities due to failure of the structure, indicated by obtaining large deformation for any small increment of the intensity or issues related to the numerical convergence. In case of bare steel frames, formation of plastic hinges in the beams and columns, have led to the failure of the structure, which is considered as a safe and desired scenario. However, in case of the infilled frames, the dominant failure is due to soft storey, triggered by failure of infill panels at one of the storeys. This failure is identified by achieving a relatively excessive inter-storey drift at one of the floors.

The nonlinear dynamic analysis is conducted using the SeismoStruct (v.7.0.6) engine on 16-vCPU (clockspeed @3.40GHz) virtual cloud servers of Amazon Web Services (AWS), capable of parallel computing. The fragility function parameters are evaluated through least square fitting technique proposed by Baker (2015). The run time varied substantially from approximately 8 hours for the 2 storey bare frames to around 160 hours for the 8 storey infilled frame models.

To present the results, each of the introduced index buildings are categorised into groups based on their number of storeys and bays. The fundamental period (T_1) of each index building, values utilised as thresholds for different damage states in terms of inter-storey drift ratio and the obtained fragility parameters (μ and β) are presented in the following tables (Table 6.7 to Table 6.21). The allocated damage thresholds are shown on the nonlinear static pushover curve (Base Shear vs. MIDR) of each building (Figures Figure 6.30, Figure 6.33,Figure 6.36, Figure 6.39 and Figure 6.42). For each group, the IM-EDPs obtained through CLA and MSA, in terms of $S_a(T_1)$ and MIDR are presented for the buildings with the highest and lowest capacity along with their damage thresholds for better validation (Figure 6.31, Figure 6.34, Figure 6.37, Figure 6.40 and Figure 6.43). Furthermore, the seismic fragility curves of the stated buildings are presented in terms of spectral acceleration corresponding to the structure's fundamental period of vibration (Figure 6.32, Figure 6.35, Figure 6.38, Figure 6.41 and Figure 6.44). All derived fragility curves are presented in Appendix-C.

Due to the variation observed in the fundamental period of the index buildings, a direct comparison between the obtained IM-EDPs and fragility functions is not possible. However, the seismic performance and expected damage of the buildings can be assessed through estimation of expected losses under various earthquake scenarios. Moreover, by integrating the seismic hazard of the location and the obtained fragility functions, the mean annual frequency of exceeding the damage states can be derived and compared. A thorough discussion on the results of this operation and expected losses is presented in Chapter 7 of this study. The fragility functions generated through the discussed methodology in this chapter are utilised for the vulnerability assessment and life cycle cost analysis of the selected case studies.

6.8.1. Seismic performance and fragility function components for 2 Storey - 4 Bay (X-dir) & 3 Bay (Y-dir)

Table 6.7 – Building category and fundamental period for 2 Storey - 4 Bay (X-dir) & 3 Bay (Y-dir)

	HAZUS Category	GEM Category	T_1 (s)
2Storey-L-SGF-Bare	S1L Low-Rise	S/LFM+DNO/HEX:2	0.80
2Storey-L-SGF-Infill HCB	S5L Low-Rise	S/LFINF+DNO/HEX:2	0.32
2Storey-L-SGF-Infill SCB	S5L Low-Rise	S/LFINF+DNO/HEX:2	0.32
2Storey-L-MRF-Bare	S1H Low-Rise	S/LFM+DUC/HEX:2	0.78
2Storey-L-MRF-Infill HCB	S5H Low-Rise	S/LFINF+DUC/HEX:2	0.30
2Storey-L-MRF-Infill SCB	S5H Low-Rise	S/LFINF+DUC/HEX:2	0.30

Table 6.8 – Damage threshold values for different damage limit states for 2 Storey - 4 Bay (X-dir) & 3 Bay (Y-dir)

	DS1 - Slight	DS2 - Moderate	DS3 - Extensive	DS4 - Complete
2Storey-L-SGF-Bare	0.69%	1.47%	2.70%	4.30%
2Storey-L-SGF-Infill HCB	0.50%	0.98%	2.04%	2.77%
2Storey-L-SGF-Infill SCB	0.20%	0.79%	2.69%	4.32%
2Storey-L-MRF-Bare	0.78%	1.79%	3.06%	4.14%
2Storey-L-MRF-Infill HCB	0.35%	0.92%	2.08%	3.01%
2Storey-L-MRF-Infill SCB	0.21%	1.10%	2.94%	4.20%

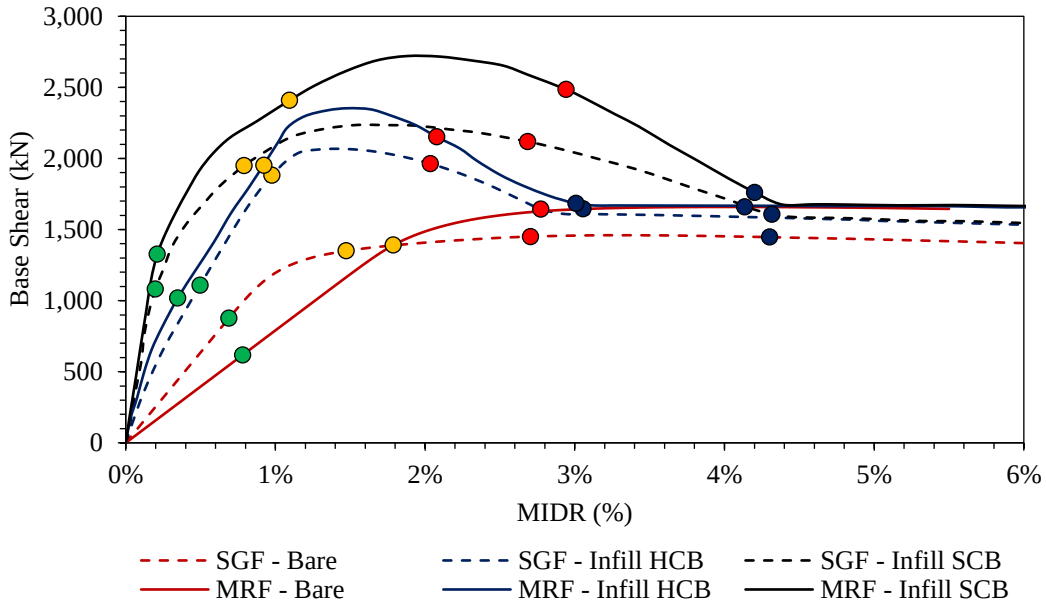

Figure 6.30 – Nonlinear static pushover curves and allocated damage thresholds for 2 Storey - 4 Bay (X-dir) & 3 Bay (Y-dir)

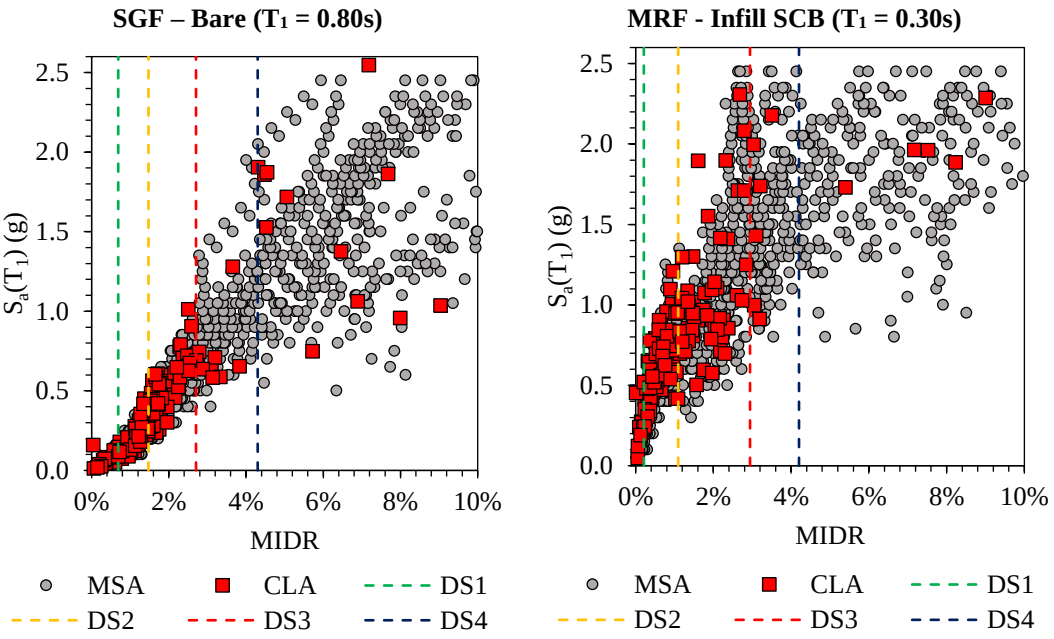

Figure 6.31 – Performance response (IM-EDP) obtained from MSA and CLA for 2 Storey - 4 Bay (X-dir) & 3 Bay (Y-dir)

Table 6.9 – Fragility function parameters, Median (μ [g]) and Dispersion (β) values for 2 Storey - 4 Bay (X-dir) & 3 Bay (Y-dir)

	DS1 – Slight		**DS2 - Moderate**		**DS3 - Extensive**		**DS4 - Complete**		**Avg.**
	μ	β	μ	β	μ	β	μ	β	β_{Avg}
2Storey-L-SGF-Bare	0.09	0.120	0.29	0.239	0.68	0.208	1.02	0.236	0.201
2Storey-L-SGF-Infill HCB	0.22	0.502	0.33	0.461	0.62	0.379	0.86	0.488	0.457
2Storey-L-SGF-Infill SCB	0.14	0.363	0.44	0.411	1.41	0.475	1.99	0.424	0.418
2Storey-L-MRF-Bare	0.07	0.008	0.12	0.457	0.45	0.245	0.72	0.275	0.246
2Storey-L-MRF-Infill HCB	0.17	0.419	0.48	0.344	1.07	0.447	1.59	0.480	0.422
2Storey-L-MRF-Infill SCB	0.19	0.377	0.65	0.335	1.22	0.405	1.69	0.406	0.381

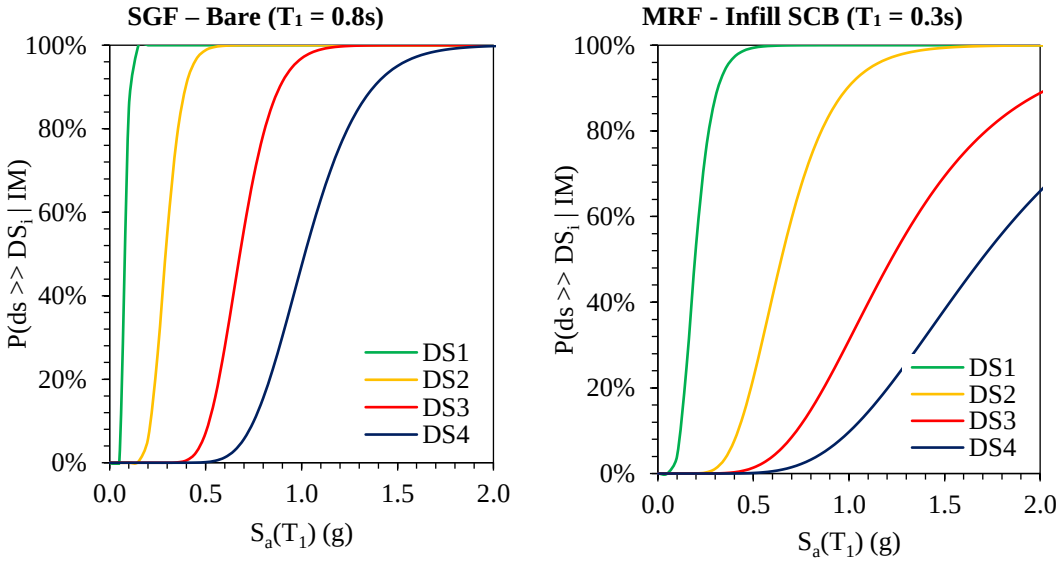

Figure 6.32 – Fragility curves obtained for the allocated 2 Storey - 4 Bay (X-dir) & 3 Bay (Y-dir)

6.8.2. Seismic performance and fragility function components for 2 Storey - 2 Bay (X-dir) & 1 Bay (Y-dir)

Table 6.10 – Building category and fundamental period for 2 Storey - 2 Bay (X-dir) & 1 Bay (Y-dir)

	HAZUS Category	GEM Category	T_1 (s)
2Storey-S-SGF-Bare	S1L Low-Rise	S/LFM+DNO/HEX:2	0.68
2Storey-S-SGF-Infill HCB	S5L Low-Rise	S/LFINF+DNO/HEX:2	0.25
2Storey-S-SGF-Infill SCB	S5L Low-Rise	S/LFINF+DNO/HEX:2	0.27
2Storey-S-MRF-Bare	S1H Low-Rise	S/LFM+DUC/HEX:2	0.40
2Storey-S-MRF-Infill HCB	S5H Low-Rise	S/LFINF+DUC/HEX:2	0.21
2Storey-S-MRF-Infill SCB	S5H Low-Rise	S/LFINF+DUC/HEX:2	0.24

Table 6.11 – Damage threshold values for different damage limit states for 2 Storey - 2 Bay (X-dir) & 1 Bay (Y-dir)

	DS1 - Slight	DS2 - Moderate	DS3 - Extensive	DS4 - Complete
2Storey-S-SGF-Bare	0.54%	1.16%	2.02%	3.16%
2Storey-S-SGF-Infill HCB	0.34%	0.88%	1.84%	2.84%
2Storey-S-SGF-Infill SCB	0.25%	0.85%	2.22%	4.28%
2Storey-S-MRF-Bare	0.65%	1.32%	2.41%	3.77%
2Storey-S-MRF-Infill HCB	0.39%	1.03%	1.97%	2.93%
2Storey-S-MRF-Infill SCB	0.33%	0.96%	2.73%	4.53%

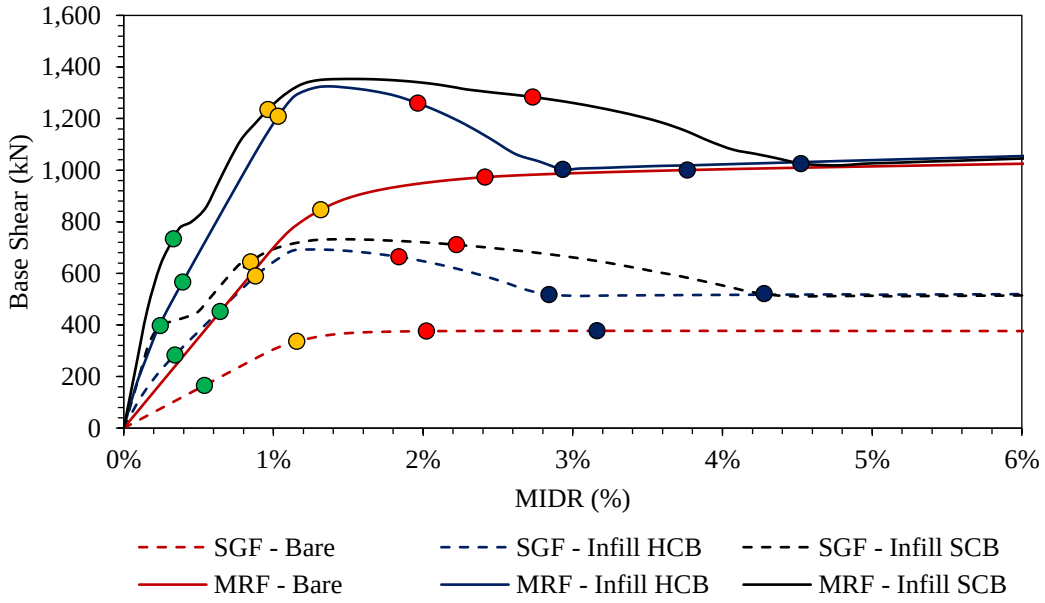

Figure 6.33 - Nonlinear static pushover curves and allocated damage thresholds for 2 Storey - 2 Bay (X-dir) & 1 Bay (Y-dir)

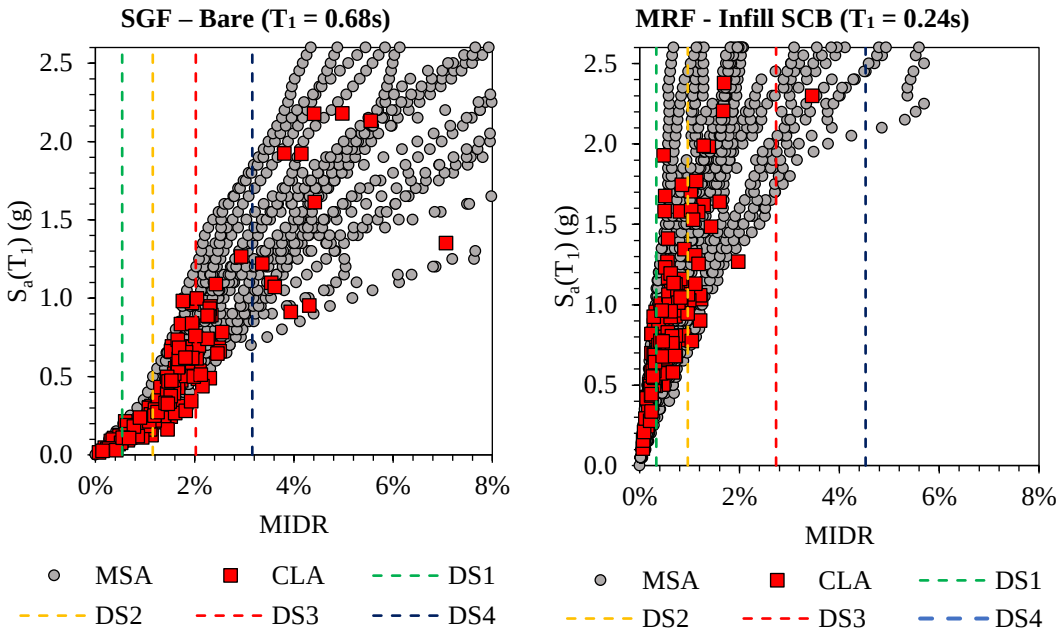

Figure 6.34 – Performance response (IM-EDP) obtained from MSA and CLA for 2 Storey - 2 Bay (X-dir) & 1 Bay (Y-dir)

Table 6.12 – Fragility function parameters, Median (μ [g]) and Dispersion (β) values for 2 Storey - 2 Bay (X-dir) & 1 Bay (Y-dir)

	DS1 - Slight		DS2 - Moderate		DS3 - Extensive		DS4 - Complete		Avg.
	μ	β	μ	β	μ	β	μ	β	β_{Avg}
2Storey-S-SGF-Bare	0.09	0.278	0.24	0.269	0.71	0.253	1.16	0.282	0.271
2Storey-S-SGF-Infill HCB	0.33	0.369	0.60	0.482	1.27	0.478	1.86	0.540	0.467
2Storey-S-SGF-Infill SCB	0.35	0.335	0.68	0.379	1.46	0.488	2.63	0.663	0.466
2Storey-S-MRF-Bare	0.26	0.370	0.71	0.225	1.94	0.230	2.97	0.252	0.269
2Storey-S-MRF-Infill HCB	0.57	0.333	1.13	0.396	2.38	0.344	2.77	0.251	0.331
2Storey-S-MRF-Infill SCB	0.51	0.376	1.31	0.370	2.71	0.290	3.18	0.204	0.310

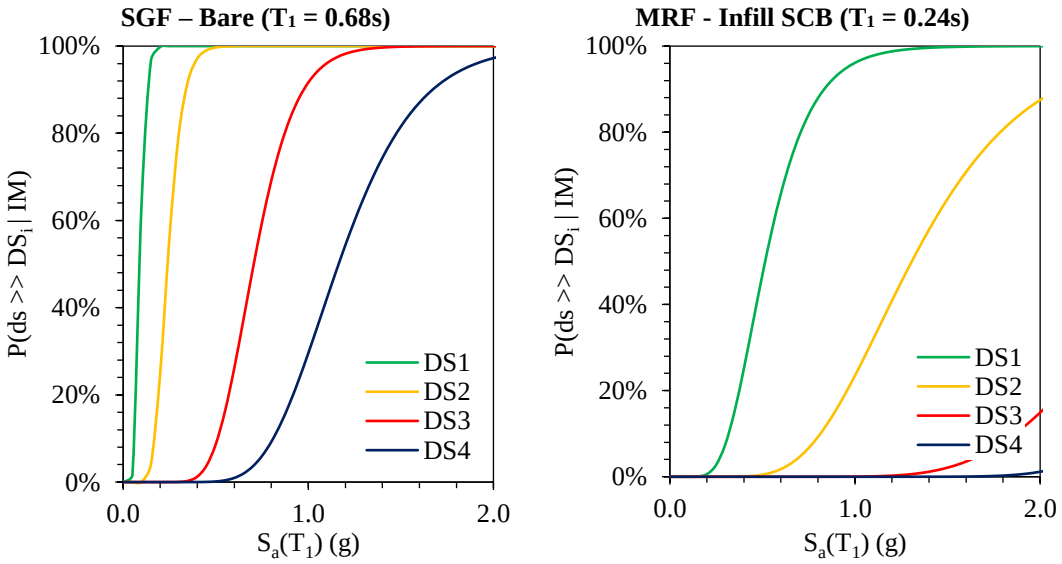

Figure 6.35 - Fragility curves obtained for the allocated 2 Storey - 2 Bay (X-dir) & 1 Bay (Y-dir)

6.8.3. Seismic performance and fragility function components for 4 Storey - 4 Bay (X-dir) & 3 Bay (Y-dir)

Table 6.13 – Building category and fundamental period for 4 Storey - 4 Bay (X-dir) & 3 Bay (Y-dir)

	HAZUS Category	GEM Category	T_1 (s)
4Storey-SGF-Bare	S1L Mid-Rise	S/LFM+DNO/HEX:4	1.84
4Storey-SGF-Infill HCB	S5L Mid-Rise	S/LFINF+DNO/HEX:4	0.74
4Storey-SGF-Infill SCB	S5L Mid-Rise	S/LFINF+DNO/HEX:4	0.72
4Storey-MRF-Bare	S1H Mid -Rise	S/LFM+DUC/HEX:4	1.46
4Storey-MRF-Infill HCB	S5H Mid -Rise	S/LFINF+DUC/HEX:4	0.70
4Storey-MRF-Infill SCB	S5H Mid -Rise	S/LFINF+DUC/HEX:4	0.68

Table 6.14 – Damage threshold values for different damage limit states for 4 Storey - 4 Bay (X-dir) & 3 Bay (Y-dir)

	DS1 - Slight	DS2 - Moderate	DS3 - Extensive	DS4 - Complete
4Storey-SGF-Bare	0.91%	1.38%	2.27%	3.22%
4Storey-SGF-Infill HCB	0.38%	0.85%	2.07%	2.92%
4Storey-SGF-Infill SCB	0.24%	0.65%	2.56%	4.29%
4Storey-MRF-Bare	0.86%	1.39%	2.31%	3.40%
4Storey-MRF-Infill HCB	0.42%	0.95%	2.21%	3.24%
4Storey-MRF-Infill SCB	0.21%	0.94%	2.65%	4.59%

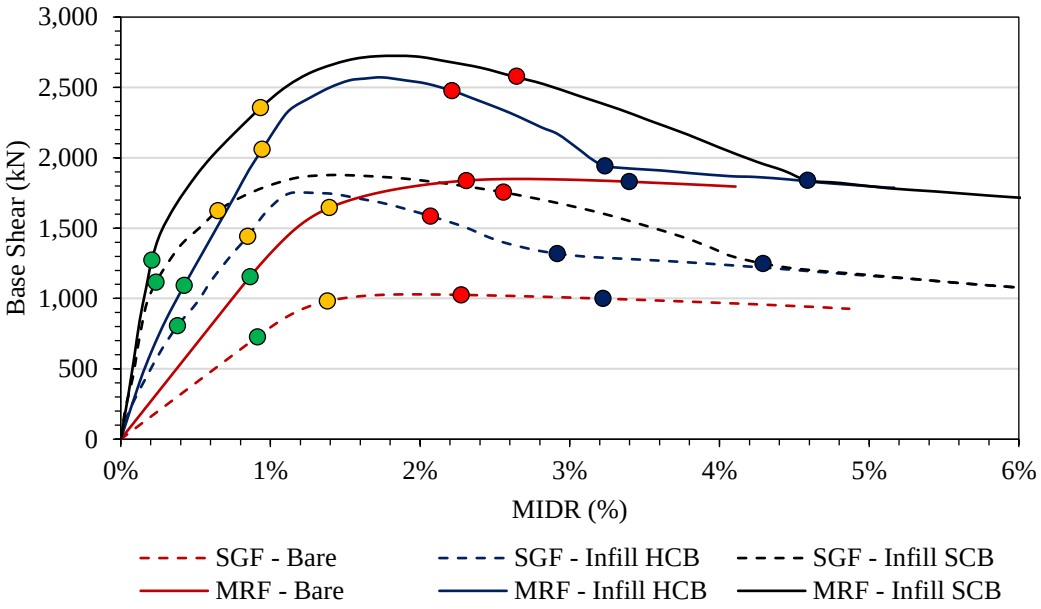

Figure 6.36 - Nonlinear static pushover curves and allocated damage thresholds for 4 Storey - 4 Bay (X-dir) & 3 Bay (Y-dir)

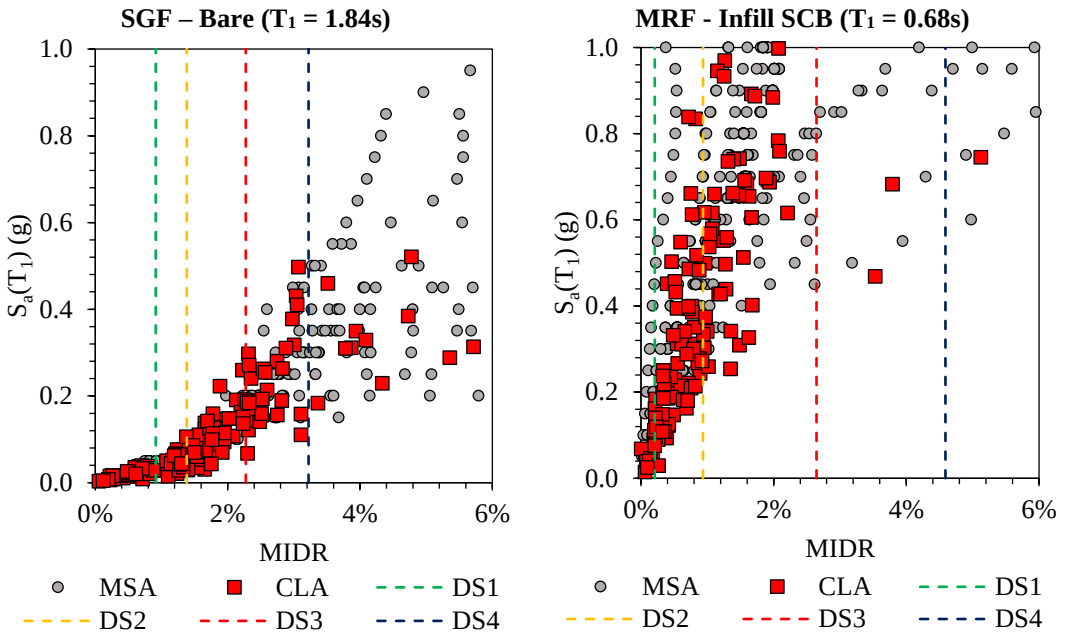

Figure 6.37 – Performance response (IM-EDP) obtained from MSA and CLA for 4 Storey - 4 Bay (X-dir) & 3 Bay (Y-dir)

Table 6.15 – Fragility function parameters, Median (μ [g]) and Dispersion (β) values for 4 Storey - 4 Bay (X-dir) & 3 Bay (Y-dir)

	DS1 - Slight		**DS2 - Moderate**		**DS3 - Extensive**		**DS4 - Complete**		**Avg.**
	μ	β	μ	β	μ	β	μ	β	β_{Avg}
4Storey-SGF-Bare	0.09	0.098	0.14	0.068	0.20	0.151	0.33	0.350	0.167
4Storey-SGF-Infill HCB	0.13	0.446	0.24	0.478	0.53	0.449	0.76	0.565	0.485
4Storey-SGF-Infill SCB	0.12	0.309	0.25	0.329	0.75	0.501	1.14	0.535	0.418
4Storey-MRF-Bare	0.11	0.175	0.17	0.167	0.25	0.257	0.45	0.279	0.220
4Storey-MRF-Infill HCB	0.17	0.357	0.31	0.337	0.64	0.351	0.79	0.389	0.358
4Storey-MRF-Infill SCB	0.16	0.288	0.51	0.177	1.23	0.258	1.75	0.189	0.228

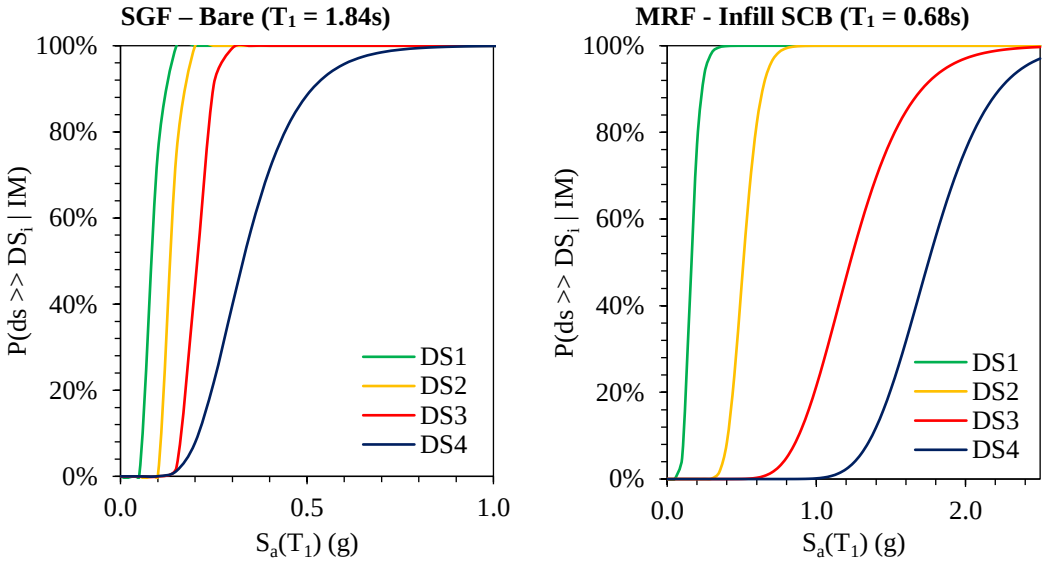

Figure 6.38 - Fragility curves obtained for the allocated 4 Storey - 4 Bay (X-dir) & 3 Bay (Y-dir)

6.8.4. Seismic performance and fragility function components for 6 Storey - 4 Bay (X-dir) & 3 Bay (Y-dir)

Table 6.16 – Building category and fundamental period for 6 Storey - 4 Bay (X-dir) & 3 Bay (Y-dir)

	HAZUS Category	GEM Category	T_1 (s)
6Storey-SGF-Bare	S1L Mid-Rise	S/LFM+DNO/HEX:6	2.70
6Storey-SGF-Infill HCB	S5L Mid-Rise	S/LFINF+DNO/HEX:6	1.00
6Storey-SGF-Infill SCB	S5L Mid-Rise	S/LFINF+DNO/HEX:6	1.02
6Storey-MRF-Bare	S1H Mid-Rise	S/LFM+DUC/HEX:6	1.96
6Storey-MRF-Infill HCB	S5H Mid-Rise	S/LFINF+DUC/HEX:6	0.96
6Storey-MRF-Infill SCB	S5H Mid-Rise	S/LFINF+DUC/HEX:6	0.98

Table 6.17 – Damage threshold values for different damage limit states for 6 Storey - 4 Bay (X-dir) & 3 Bay (Y-dir)

	DS1 - Slight	DS2 - Moderate	DS3 - Extensive	DS4 - Complete
6Storey-SGF-Bare	0.89%	1.51%	2.73%	3.85%
6Storey-SGF-Infill HCB	0.48%	0.93%	2.13%	3.01%
6Storey-SGF-Infill SCB	0.21%	1.04%	2.58%	4.15%
6Storey-MRF-Bare	0.84%	1.73%	2.86%	4.15%
6Storey-MRF-Infill HCB	0.48%	0.89%	2.04%	2.97%
6Storey-MRF-Infill SCB	0.21%	0.84%	2.64%	4.46%

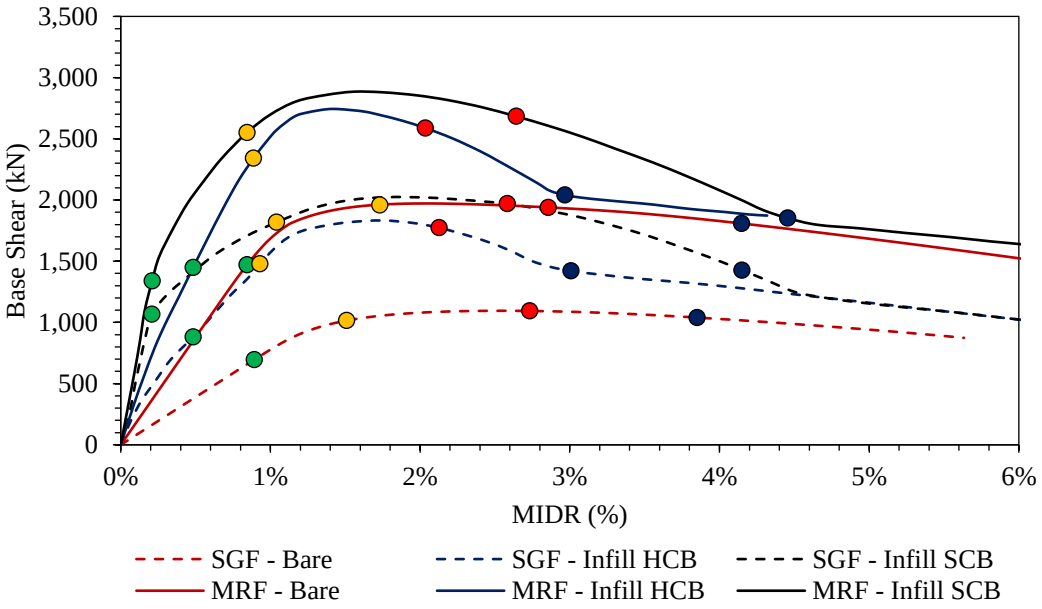

Figure 6.39 - Nonlinear static pushover curves and allocated damage thresholds for 6 Storey - 4 Bay (X-dir) & 3 Bay (Y-dir)

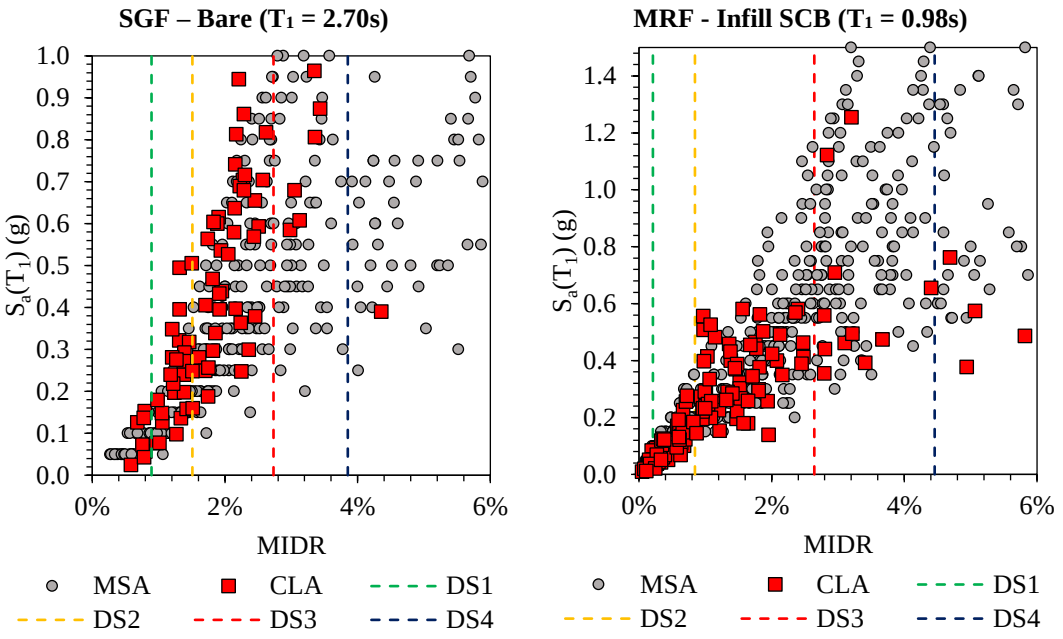

Figure 6.40 – Performance response (IM-EDP) obtained from MSA and CLA for 6 Storey - 4 Bay (X-dir) & 3 Bay (Y-dir)

Table 6.18 – Fragility function parameters, Median (μ [g]) and Dispersion (β) values for 6 Storey - 4 Bay (X-dir) & 3 Bay (Y-dir)

	DS1 - Slight		DS2 - Moderate		DS3 - Extensive		DS4 - Complete		Avg.
	μ	β	μ	β	μ	β	μ	β	β_{Avg}
6Storey-SGF-Bare	0.09	0.370	0.19	0.235	0.44	0.472	0.58	0.491	0.392
6Storey-SGF-Infill HCB	0.11	0.279	0.19	0.383	0.36	0.418	0.47	0.465	0.386
6Storey-SGF-Infill SCB	0.12	0.285	0.20	0.339	0.48	0.427	0.65	0.479	0.382
6Storey-MRF-Bare	0.09	0.391	0.24	0.344	0.52	0.237	0.74	0.325	0.324
6Storey-MRF-Infill HCB	0.10	0.363	0.17	0.361	0.40	0.267	0.55	0.344	0.334
6Storey-MRF-Infill SCB	0.07	0.258	0.20	0.318	0.56	0.338	0.80	0.429	0.336

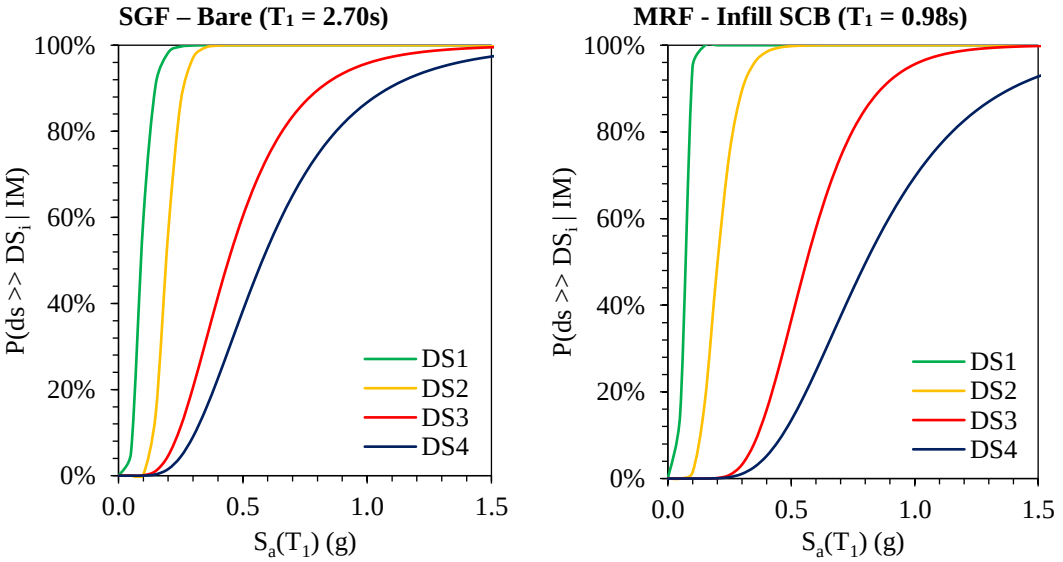

Figure 6.41 – Fragility curves obtained for the allocated 6 Storey - 4 Bay (X-dir) & 3 Bay (Y-dir)

6.8.5. Seismic performance and fragility function components for 8 Storey - 4 Bay (X-dir) & 3 Bay (Y-dir)

Table 6.19 – Building category and fundamental period for 8 Storey - 4 Bay (X-dir) & 3 Bay (Y-dir)

	HAZUS Category	GEM Category	T_1 (s)
8Storey-SGF-Bare	S1L High-Rise	S/LFM+DNO/HEX:8	3.60
8Storey-SGF-Infill HCB	S5L High-Rise	S/LFINF+DNO/HEX:8	1.34
8Storey-SGF-Infill SCB	S5L High-Rise	S/LFINF+DNO/HEX:8	1.36
8Storey-MRF-Bare	S1H High-Rise	S/LFM+DUC/HEX:8	3.50
8Storey-MRF-Infill HCB	S5H High-Rise	S/LFINF+DUC/HEX:8	1.38
8Storey-MRF-Infill SCB	S5H High-Rise	S/LFINF+DUC/HEX:8	1.40

Table 6.20 – Damage threshold values for different damage limit states for 8 Storey - 4 Bay (X-dir) & 3 Bay (Y-dir)

	DS1 - Slight	DS2 - Moderate	DS3 - Extensive	DS4 - Complete
8Storey-SGF-Bare	0.58%	1.21%	2.37%	3.54%
8Storey-SGF-Infill HCB	0.35%	0.84%	2.06%	3.33%
8Storey-SGF-Infill SCB	0.20%	0.91%	2.59%	4.05%
8Storey-MRF-Bare	0.66%	1.21%	2.45%	3.70%
8Storey-MRF-Infill HCB	0.42%	0.83%	2.14%	3.33%
8Storey-MRF-Infill SCB	0.21%	1.00%	2.48%	4.65%

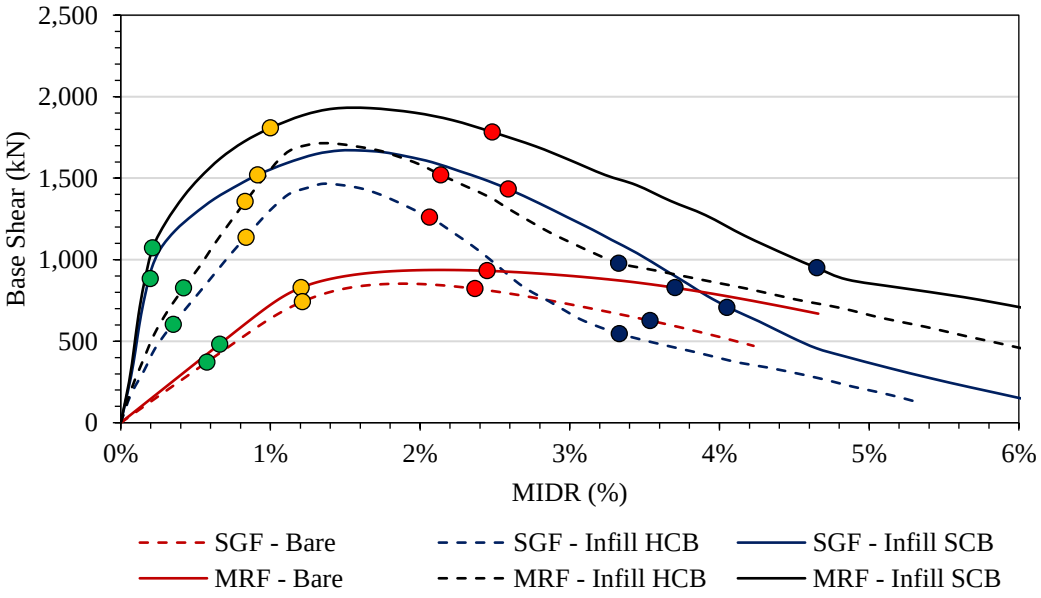

Figure 6.42 - Nonlinear static pushover curves and allocated damage thresholds for 8 Storey - 4 Bay (X-dir) & 3 Bay (Y-dir)

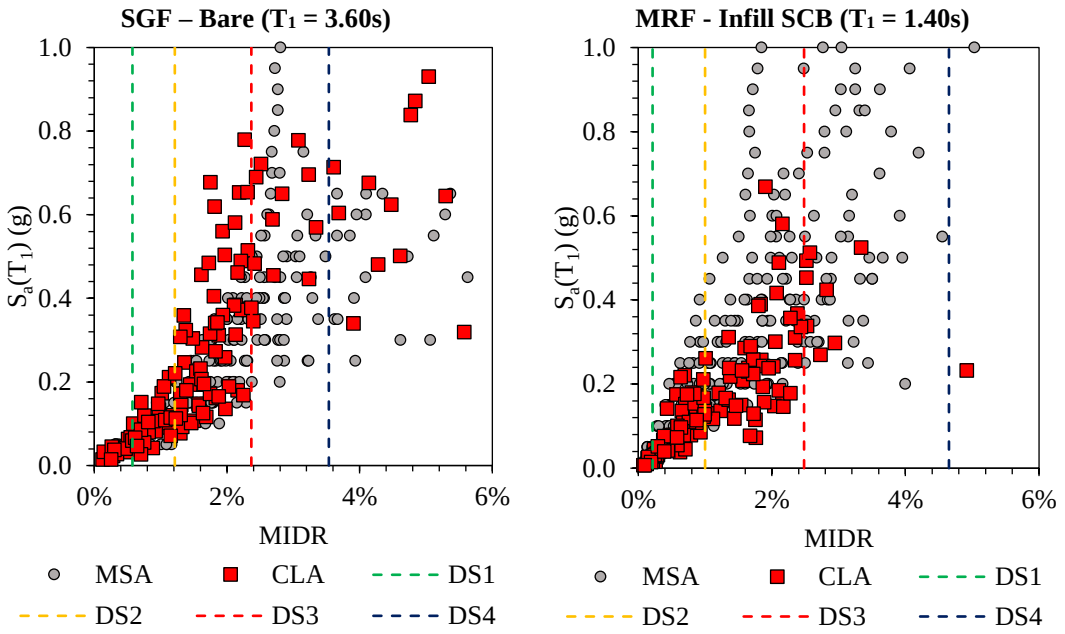

Figure 6.43 – Performance response (IM-EDP) obtained from MSA and CLA for 8 Storey - 4 Bay (X-dir) & 3 Bay (Y-dir)

Table 6.21 – Fragility function parameters, Median (μ [g]) and Dispersion (β) values for 8 Storey - 4 Bay (X-dir) & 3 Bay (Y-dir)

	DS1 - Slight		**DS2 - Moderate**		**DS3 - Extensive**		**DS4 - Complete**		**Avg.**
	μ	β	μ	β	μ	β	μ	β	β_{Avg}
8Storey-SGF-Bare	0.09	0.113	0.16	0.271	0.29	0.368	0.40	0.425	0.294
8Storey-SGF-Infill HCB	0.06	0.432	0.15	0.422	0.31	0.452	0.41	0.452	0.439
8Storey-SGF-Infill SCB	0.09	0.102	0.18	0.336	0.40	0.442	0.48	0.468	0.337
8Storey-MRF-Bare	0.11	0.303	0.17	0.334	0.31	0.506	0.40	0.504	0.412
8Storey-MRF-Infill HCB	0.09	0.268	0.20	0.337	0.34	0.496	0.45	0.528	0.408
8Storey-MRF-Infill SCB	0.09	0.349	0.17	0.436	0.38	0.477	0.50	0.517	0.445

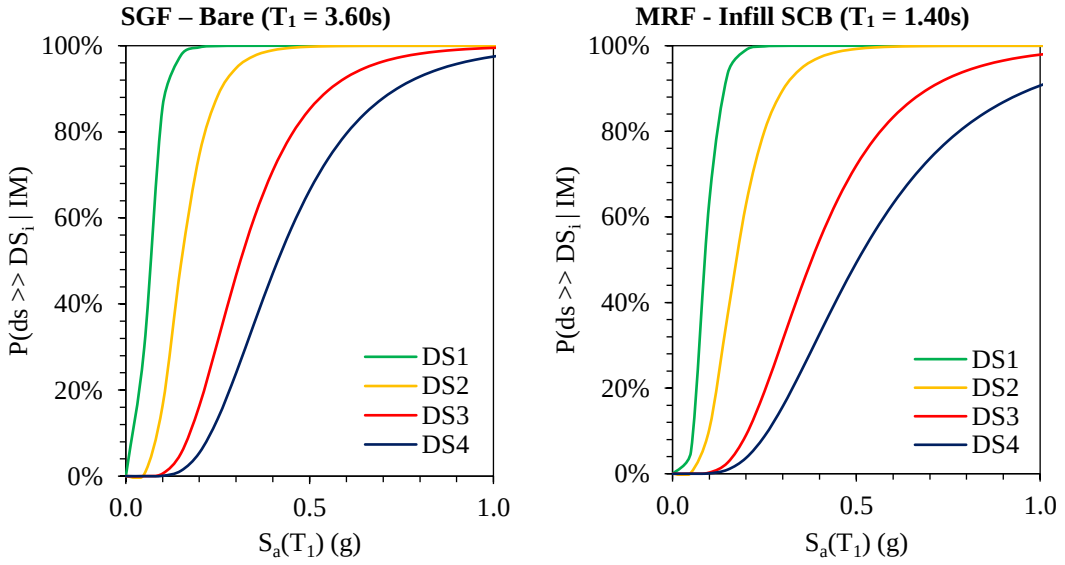

Figure 6.44 - Fragility curves obtained for the allocated 8 Storey - 4 Bay (X-dir) & 3 Bay (Y-dir)

6.9. Conclusions

This section investigated the applicability and accuracy of two simplified analysis methods, N2 and FRACAS, in contrast to more advanced but computationally intensive nonlinear dynamic approaches (CLA). A bare and an infilled steel frame, simulated after a real case as discussed in Chapter 4, are selected for this assessment. The analysis was conducted using a suite of 150 single component earthquake records, selected from the database of world events of the SIMBAD ground motion database.

Both simplified methods, the N2 and FRACAS, adapt the capacity spectrum assessment method and are capable of utilising natural records to estimate the performance points of the structure under various earthquake intensities. The main difference between the stated methods lies primarily in the approach each one follows to determine the inelastic spectrum utilising the idealised capacity curve. As long as the idealised curves of both simplified methods result in identical initial stiffness and fundamental period, the performance points of the elastic region are in good agreement. However, as the structure undergoes nonlinear deformation, the N2 method resulted in higher EDPs. This diversion was particularly greater in case of the infilled frame, for which a higher EDP in 75% of the applied IMs was achieved, with an average error of 30%.

Comparing the obtained EDPs with the ones of CLA, similarly an excellent agreement is observed in the linear region, for both bare and infilled frame. However, for the performance points of the inelastic region, an underestimation of EDP was obtained, particularly for the infilled frame. In 65% of the events, N2 has miscalculated the MIDRs of the infilled frame, while FRACAS has underestimated in 82% of the cases with an average error of 29%.

To observe the impact of this dispersion on the fragility function, the ones derived based on the obtained IM-EDPs of simplified and CLA are compared. As a bench mark, fragility function of both structures is obtained through MSA, utilising 22 scaled records of ATC-63. As expected, all fragility curves had identical trend at lower intensities (e.g. slight). However, for higher intensities, the simplified methods start to underestimate the damage. For instance, in case of the infilled steel frame, comparing the median (μ) of the fragility curves, derived after MSA to the ones of the N2, a variation of 0.22g and 0.31g is noted for the extensive and complete damage states, while FRACAS resulted in a difference of 0.60g and 0.46g for the same damage states. This damage underestimation will impact the seismic vulnerability and the expected losses, hence nonlinear dynamic methods are recommended for analysing the infilled steel frames.

Further discussion is provided on various fitting techniques for deriving the fragility functions. Accordingly, the fragility function parameters are evaluated through least square fitting technique proposed by Baker (2015). Four damage states are defined, while considering the composite behaviour of the infill-frame. For each damage state a corresponding threshold is allocated in terms of inter storey drift ratio. It is also concluded that both horizontal components of the earthquake should be applied concurrently to obtain precise MIDRs.

Investigating different stages and aspects of the seismic fragility derivation, the most applicable methods and approaches have been identified in this chapter. Accordingly, the fragility functions of the defined index buildings, as stated in Chapter 4 are obtained. Different components of the analysis are presented, such as the IM-EDPs obtained through CLA and MSA, damage thresholds and the pushover curves.

The spectral acceleration at the fundamental period of each index building is used as the intensity indicator. Therefore, a direct comparison between the obtained IM-EDPs and fragility functions is not possible. However, the seismic performance and expected damage of the buildings can be assessed through estimation of expected losses under various earthquake scenarios. Following the methodology discussed in this chapter, fragility functions for three infilled steel frames with different qualities of construction are generated and discussed in Chapter 7. The seismic vulnerability and life cycle cost of the stated buildings are estimated and compared to an identical bare steel frame.

Chapter 7 Structural Vulnerability & Life Cycle Cost Analysis

7.1. Introduction

The increasing population in earthquake prone cities, poor construction quality and lack of building code enforcement are the primary causes of the substantial structural damage and number of victims in recent earthquakes, particularly in the developing countries (Sawires et al., 2015). The seismic risk assessment of built-up areas and its resultant losses are directly associated with the level of earthquake hazard, building vulnerability and the rate of exposure. Among these three pillars, the structural vulnerability is of immense importance as the engineering research can intervene, improve and in cases control the seismic response of existing buildings. Therefore, it is possible to reduce the level of vulnerability and consequently the level of physical damage, life loss and economic loss (Vicente et al., 2008).

Assessing the seismic vulnerability of the building stock and estimating the resulting losses, is a critical element not only for predicting physical damage and economic impact of future seismic events, but also for establishing preparedness plans by the national authorities and decision makers to optimally allocate resources and reduce the consequences of earthquakes. Furthermore, the outcome of vulnerability assessment can be utilised in risk mitigation strategies through calibrating and advancing the seismic design codes of new buildings or implementing strengthening measures for existing ones. The additional cost in improving the seismic resistance can be quantitatively compared with the potential losses which can then be mitigated or avoided (Calvi & Pinho, 2006).

The seismic vulnerability and loss estimation are greatly influenced by the performance and failure mechanism of the structures. Detailed and realistic evaluation of structural performance under earthquake excitation plays a key role in the formulation of the earthquake vulnerability model (Calvi & Pinho, 2006). As demonstrated in Chapters 5 and 6 of this study, in case of masonry infilled steel frame structures, the final performance and failure mechanism differs to that expected during the design and analysis of a bare steel frame. This is mainly due to the resultant interaction and composite behaviour of the frame and the infill.

In this chapter, the vulnerability of masonry infilled steel framed structures is investigated by focusing on the mid-rise index building introduced in Chapter 5, based on a mass residential development in Iran. Modifying some properties and characteristics of the selected building, three models with different seismic performances are generated, each representing a quality of construction, characterised according to the local experts' opinion (D'Ayala et al., 2015). Utilising the latest probabilistic seismic hazard data of the location under study and the obtained analytical fragility functions, the seismic vulnerability at building level is determined through estimating the mean damage ratio under various levels of earthquake intensities. Furthermore, to have a broader view of the resulting vulnerability and economic losses, three distribution scenarios for construction quality are defined for a population of 400 building. Moreover, the impact of infill panels on loss estimation is quantified by comparing the obtained results to the losses evaluated for a bare frame of the same structure under intensities with different probabilities of occurrence. The seismic vulnerability assessment follows the stages discussed in GEM guidelines for conducting analytical vulnerability assessment on low- and mid-rise buildings (D'Ayala et al., 2015).

To conclude, a life cycle cost (LCC) analysis is conducted following the approach of Wen & Kang (2001), on the index buildings representing different qualities of construction. The analysis utilises the latest data obtained through probabilistic seismic hazard assessment of the location under study. Accordingly, the expected structural damage and the consequences associated with structural damage such as injuries and fatalities are evaluated. The analysis outcome indicates the importance of detailing in simulation, regional hazard and influence of structural and non-structural components on the expected costs during the life service of the building.

7.2. Structural Vulnerability

Vulnerability assessment is the central pillar of any seismic loss estimation method and tool. Existing vulnerability assessment methods vary depending on their input data and assumptions. The quantification of seismic hazard, the building damage assessment methods used, the classification of buildings by typologies, all affect the expenditure and precision of the outcomes (Bertogg et al., 2002). The first comprehensive methodology, containing models for estimating potential losses of buildings from earthquake hazard at an urban scale was established as part of a regional damage assessment tool known as HAZUS (1997). Its latest multi-hazard edition, HAZUS v2.0 (2012), includes fragility functions for buildings, utilities and transportation networks, capable of estimating the risk due to earthquake, as well as flood and hurricane. Despite a limited number of analytical approaches, the majority of the fragility functions were obtained following an expert judgment approach on structures commonly built

in the United States, according to the methodology and data presented in ATC-13 (ATC-13, 1985) and ATC-25 (FEMA-224, 1991).

Several earthquake loss estimation methodologies and tools have been developed for other regions around the world, for instance, RISK-UE (Milutinovic & Trendafiloski, 2003) project followed by (Ilki et al., 2007), as well as SELENA (Seismic Loss Estimation Using a Logic Tree Approach) (Molina et al., 2010; Molina & Lindholm, 2005) and DBELA (Displacement-Based Earthquake Loss Assessment) focusing mainly on European structural typologies (Silva et al., 2013) and EQRM (Geoscience Australia's Earthquake Risk Model) for Australia (Robinson et al., 2014), SRM-LIFE (Papaioannou, 2004) for Greece and the Global Earthquake Model (GEM) approach for all regions (Porter et al., 2012). As part of the RELUIS program, Cosenza and Monti (2009) investigated the vulnerability of existing reinforced concrete buildings in Italy, while Erdikt et al. (2003) evaluated the vulnerability of reinforced concrete and masonry structures of Istanbul. Among the latest developments is the SYNER-G project, which has gathered several fragility functions for the most important elements at risk including masonry and reinforced concrete structures (Pitilakis et al., 2014). A considerable number of research has focused on development of seismic vulnerability assessment techniques and seismic loss evaluation, looking at different structural and non-structural arrangements (Alam et al., 2012; Calvi & Pinho, 2006; Guéguen et al., 2007; Lang & Bachmann, 2004; Lantada et al., 2009; Roca et al., 2006; Sucuoğlu et al., 2007). However, none has investigated the vulnerability and expected economic loss in masonry infilled steel framed structures.

As discussed in Chapter 2, there are four approaches commonly used to establish structural vulnerability and fragility functions (Rossetto et al., 2014; Porter, 2017):

(a) Empirical approach, which follows the damage statistics from past earthquake observations and can result in the most realistic assessment. However, this method is highly specific to a particular seismo-tectonic, geotechnical and built environment. Inaccuracies may appear for particular building damage classification, as damage due to multiple earthquakes may be aggregated.

(b) Judgemental approach, in which the functions are developed based on the opinion of experts. It has the advantage of being easily modified to include numerous factors and various structural characteristics. The reliability of the functions relies solely on the experience of the consulted experts. Thus, the majority of focus is on local structural types, typical configurations, detailing and materials following the inherent knowledge of the experts (ATC-13, 1985). Although this method might be useful in regions lacking historic damage records and specific analytical studies, it is increasingly discounted in favour of analytical approaches.

(c) Analytical approach, which is based on damage distribution simulation, using numerical analytical tools. Depending on the considered detailing and uncertainty, this method can reduce bias and increase the reliability of the vulnerability estimate for different structures. However, the substantial computational effort involved and limitations in modelling capabilities is the main downfall of this method. The vulnerability outcome are highly sensitive to the adopted analysis method, idealisation, seismic hazard, and damage models, which results in significant discrepancies in the seismic risk assessments (Casotto et al., 2015; Silva et al., 2014).

(d) Hybrid approach, in which multiple data sources are utilised to result in an accurate determination of vulnerability. The derived vulnerability functions can compensate for the scarcity of observational data, subjectivity of judgmental data and the modelling deficiencies of analytical procedures. Although, modification of analytical or judgment based relationships with observational data and experimental results are not always straight forward (Kappos et al., 1995).

The type of preferred method relies on the objective of the assessment, as well as the availability of data, tools and implementation knowledge. Figure 7.1, demonstrates the outlined approaches in the order of increasing computational effort.

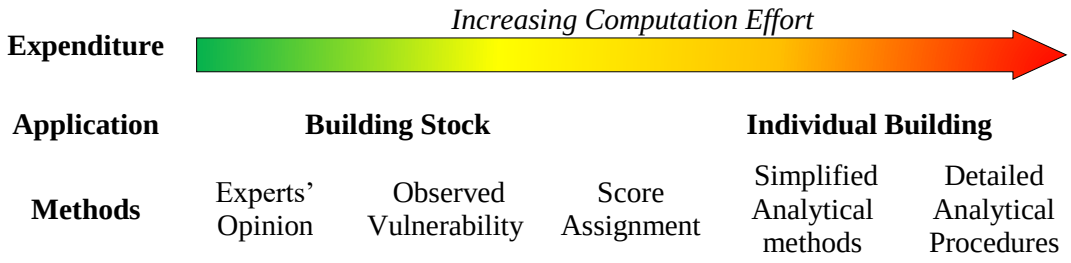

Figure 7.1 - Methods for the assessment of the vulnerability of buildings

In this study, the vulnerability assessment follows an analytical approach, since the seismic response and fragility functions of the structures were estimated through numerical methods. Referring back to PEER's probabilistic assessment framework (Figure 7.2), as previously discussed in Chapter 1, in this chapter the four main analysis steps (i.e. hazard analysis, structural analysis, damage analysis, and loss analysis) are brought together and applied to a case study in order to evaluate the expected seismic losses or Decision Variables (DV), in terms that are meaningful for decision makers. Generally speaking, the DVs can be estimated in terms of direct value losses, downtime (or restoration time), and casualties (Moehle & Deierlein, 2004). The focus of this study is the value losses, expressed in terms of mean damage ratio. Each of the assessment steps are discussed in the following sections.

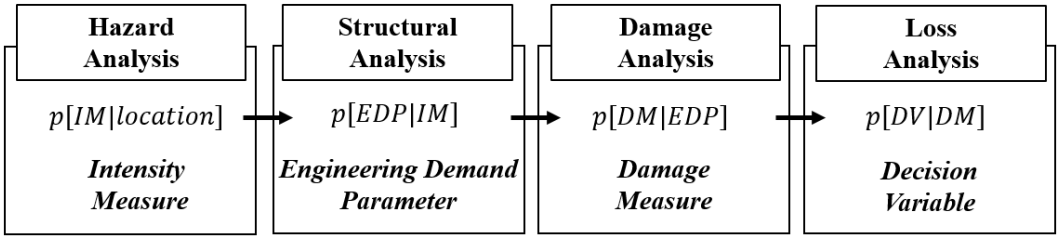

Figure 7.2 – Composing steps of the PEER's probabilistic assessment framework (Fajfar & Krawinkler, 2004)

7.2.1. Characteristics of the Studied Index Buildings

Following the case discussed in Chapter 5, the investigated mid-rise, four storey residential building has been selected for this seismic vulnerability assessment. The building represents the most common steel structure of a mass residential development. Due to the scale and regional distribution of constructed units, it is expected to have the same typology with varying quality of construction and hence performance. In order to account for the possible variation observed in the construction quality, three possible alternatives of the same structure have been modelled by slightly altering some of the models' characteristics, such as the quality or type of the infill material as well as the beam-column connections (e.g. rigid or semi-rigid composite). These are known as the secondary modifier, which do not necessarily change the building's class, however they may alter the performance within the building class (D'Ayala et al., 2015).

The proposed qualities are elicited according to the local experts' opinion on dominated construction practices in Iran, while the buildings are categorised according to their perceived quality and post damage ductility. The first model (HighQ), represents the highest quality of all, having a fully rigid beam-column connection and the strongest infill panels (i.e. solid clay bricks [SCB]). The second one (MidQ), has semi-rigid composite connection, which also takes into account the effect of the 0.15m tick concrete slab, while a weaker infill panel (i.e. hollow clay block [HCB]) has been employed. The third model (LowQ), has the same connection and infill as the MidQ, however it has been assumed that the bracing connections at the bottom floor were not sufficiently designed and implemented, therefore they do not contribute to the structural lateral resistance under seismic excitation.

To have a better understanding of the infills' influence on the vulnerability, the selected building is also analysed as a bare frame with rigid connections and bracings. This can represent a case in which the infills have no interaction with their surrounding frame, hence only their mass in considered as a distributed load on the beams. As discussed, this is the closest representation to how most designers and codes consider the buildings to behave during the design stage, by considering the infill panels as permanent loading on beams. Table 7.1, summarises the distinct characteristics for each of the mentioned models.

Table 7.1 - Masonry infill properties and lateral load resisting system of the selected buildings

Model Ref.	Infill Compressive Strength [MPa]		Infill Specific Weight (kN/m^3)	Infill Elastic Modulus (MPa)	Infill Thickness (mm)	Lateral load resisting system modifier
	Full	Window				
HighQ	7.4	8.0	10.0	5.1×10^3	0.11	Rigid connection + Bracing
MidQ	6.0	6.0	11.8	5.8×10^3	0.19	Semi-Rigid connection + Bracing
LowQ	6.0	6.0	11.8	5.8×10^3	0.19	Semi-Rigid connection/ No Bracing
Bare	-	-	-	-	-	Rigid connection + Bracing

An Eigenvalue Analysis was performed to estimate the buildings' elastic natural period of vibration (T_1) and mode shapes (Table 7.2). The results indicate that all three models, representing different qualities of construction, have similar modal behaviour. Since the masonry infill materials used in each of the cases, have different elastic modulus, specific weight and thickness, a variation is observed in the buildings' frequency of vibration and total mass. As expected, the structure with the lowest quality, has the lowest stiffness, as the bracings do not provide any stiffness to the structural system. It should be noted that despite their lack of contribution to the lateral resistance, the mass of bracings' material has been included. Similarly, in case of the bare frame, the mass of infill panels is included, assuming solid clay bricks. The small variation observed is due to the bottom infill panels, which the model was not able to consider.

Table 7.2 - Modal properties of the selected models

Model Ref.	Mode	Period (s)	Freq. (Hertz)	U_x (tonne)	U_x (%)	U_y (tonne)	U_y (%)	R_z (tonne)	R_z (%)	Mass (tonne)
HighQ	1	**0.41**	**2.43**	**584.1**	**0.76**	0.9	0.00	44.8	0.00	760.48
	2	0.44	2.28	0.9	0.00	574.5	0.79	28.2	0.00	
	3	0.29	3.45	0.7	0.00	0.5	0.00	40765.2	0.74	
MidQ	1	**0.43**	**2.32**	**572.0**	**0.76**	1.1	0.00	44.6	0.00	736.72
	2	0.46	2.19	1.0	0.00	607.3	0.79	45.8	0.00	
	3	0.31	3.26	0.6	0.00	0.9	0.00	46063.8	0.75	
LowQ	1	**0.50**	**2.01**	**656.4**	**0.87**	0.0	0.00	195.6	0.00	736.72
	2	0.59	1.70	0.0	0.00	631.1	0.84	111.5	0.00	
	3	0.40	2.51	2.9	0.00	2.0	0.00	49831.2	0.81	
Bare Frame	1	**1.33**	**0.75**	**387.2**	**0.63**	0.0	0.00	0.3	0.00	703.16
	2	0.57	1.75	0.0	0.00	473.6	0.77	0.0	0.00	
	3	0.43	2.32	0.0	0.00	0.0	0.00	29857.0	0.70	

The base shear coefficient versus roof drift ratio curves, obtained through nonlinear static pushover analysis of the 4 models in their longitudinal direction (x-direction), clearly indicate a reduction in capacity and initial stiffness moving from high to low quality (Figure 7.3). As expected, the beam-column rigid connections along with the high strength of the infill panels, composed of solid clay bricks, results in a higher peak lateral capacity and stiffness in the HighQ model. Comparing the response of the MidQ and the LowQ, although both have the same type of infill masonry, a slight reduction in the lateral capacity and stiffness is observed

in the LowQ model, as well as a lower ductility. This is mainly due to the contribution of concentric bracings in the structure's lateral resistance of MidQ, which does not influence the response of the LowQ model. The response of the bare steel frame is also included for comparison. Accordingly, all assumed models tend to have a similar response to the bare frame after the infill panels have failed and the resistance is solely fulfilled by the steel frame.

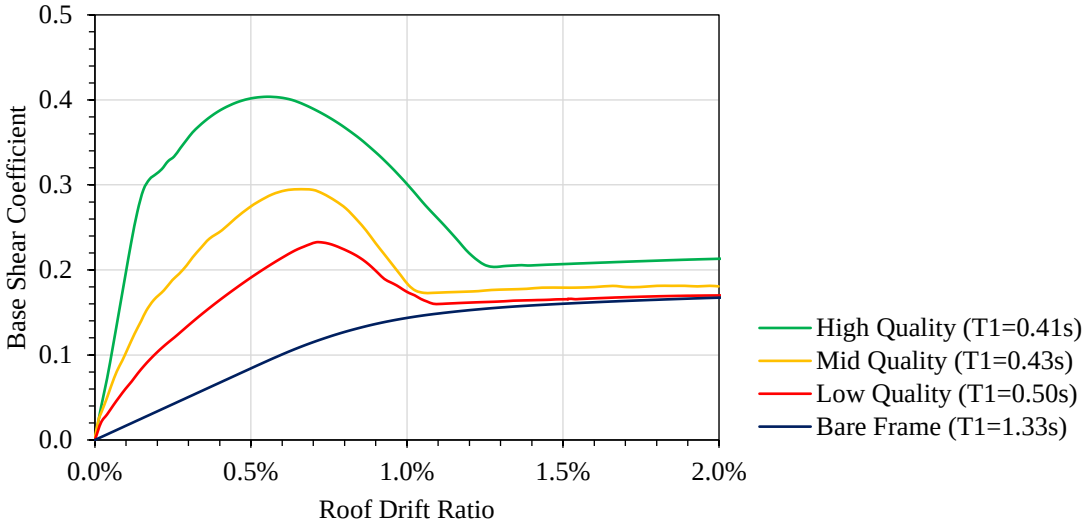

Figure 7.3 – Pushover curves of all considered models in the weak direction

7.2.2. Seismic Hazard of the Location

In order to assess the vulnerability of a structure against the earthquake shaking, one must determine the annual probability (or rate) of exceeding some level of earthquake ground shaking at the site of interest, for a range of intensity levels. Hence, to have an accurate estimation of the vulnerability, the geological characteristics and seismic activities of the region, in which the selected building models are located had to be identified and estimated.

Extreme natural events, such as earthquakes, which have potential to cause considerable structural and non-structural damage, are unpredictable and happen randomly in time. Due to the history dependency of earthquake hazards and also independency of sources contributing to the hazard, the arrival of earthquakes can be approximated by stochastic models. In probabilistic seismic hazard assessment (PSHA), the occurrence of seismic events or exceedance of an intensity measure (IM) threshold x at a site of interest, is described via a homogeneous Poisson process (HPP), in which the events are independent with stationary increments (i.e. memory less) (McGuire, 2004). To compute the rate of $IM > x$ (hazard rate), given the occurrence of an earthquake, the following formulation is applied:

$$\lambda(IM > x) = \lambda(M > m_{min}) \cdot \int_{m_{min}}^{m_{max}} \int_{r_{min}}^{r_{max}} P[IM > x \mid m, r] \cdot f_M(m) \cdot f_R(r)\, dr\, dm \quad (7.1)$$

where $\lambda(M > m_{min})$ is the rate of occurrence of earthquakes greater than m_{min} from the source, and $\lambda(IM > x)$ is the rate of $IM > x$. The term $P[IM > x \mid m, r]$ is estimated using a ground motion prediction equation (GMPE), representing the probability of exceeding the intensity threshold, given an earthquake of magnitude m and a separation distance of r. In addition, $f_M(m)$ and $f_R(r)$ are the joint probability density functions (PDF) of the earthquake magnitude and distance random variables. In case these two can be considered independent, f_M can be obtained from Gutenberg-Richter relationship and f_R depends on the source-site configuration.

To generalize the analysis and consider cases with more than one source, by recognizing that the rate of $IM > x$ when considering all sources is simply the sum of the rates of $IM > x$ from each individual source, Eq. 7.2 can be written as:

$$\lambda(IM > x) = \sum_{i=1}^{n_{source}} \lambda(M > m_{min}) \cdot \int_{m_{min}}^{m_{max}} \int_{r_{min}}^{r_{max}} P[IM > x \mid m, r] \cdot f_M(m) \cdot f_R(r)\, dr\, dm \qquad (7.2)$$

In this study, the seismic hazard level of the region under study will be extracted from the latest regional PSHA studies. For the sake of this application, the studied building population is considered part of a new city development (14,500 building units), situated close to the city of Tehran, locality known as Safa-Dasht (35.65°N 50.90°E). A comprehensive PSHA study was conducted on the greater Tehran region in 2008 by Gholipour et al. (2008). The stated data will be utilised as the main reference for evaluating the hazard of the site under study. The following seven ground motion prediction equations (GMPE) or "attenuation" models have been employed in this PSHA:

- Campbell & Bozorgnia (2008)
- Boore & Atkinson (2008)
- Chiou & Youngs (2008)
- Abrahamson & Silva (1997)
- Boore et al. (1997)
- Campbell & Bozorgnia (2002)
- Sadigh et al. (1997)

Accordingly, the seismic hazard analysis followed the soil type profiles proposed in NEHRP (FEMA P-1050, 2015) and ASCE 7-16 (2016). As the assigned soil profile for the index buildings is based on the local design code ISIRI-2800 (BHRC, 2007), a correlation between the two provisions should be established based on the average shear velocity range of each soil profile considered. Based on the initial design assumptions, according to ISIRI-2800, the buildings are located on a semi-compact soil condition (type II of ISIRI-2800, 375m/s < $V_{S,30}$

≤ 750m/s), whose average shear velocity at depth of 30 metre corresponds to soil class C (366m/s < $V_{s,30}$ ≤ 762m/s) of NEHRP and ASCE 7-16. A comparison of the ranges considered for the average soil shear wave velocity of the mentioned codes is presented in Table 7.3.

Table 7.3 - Soil profile categories of NEHRP and ISIRI-2800

	NEHRP (2015) / ASCE 7 (2016)		**ISIRI-2800 (2007)**	
Soil Profile	**Site Class**	**Average Soil Shear Wave Velocity (m/s)**	**Site Class**	**Average Soil Shear Wave Velocity (m/s)**
Hard rock	A	$V_{s,30} > 1524$	Type I	$V_{s,30} > 750$
Rock	B	$762 < V_{s,30} \leq 1524$		
Soft rock & very dense soil	**C**	**$366 < V_{s,30} \leq 762$**	**Type II**	**$375 < V_{s,30} \leq 750$**
Stiff soil profile	D	$183 < V_{s,30} \leq 366$	Type III	$175 < V_{s,30} \leq 375$
Soft soil profile	E	$V_{s,30} \leq 183$	Type IV	$V_{s,30} \leq 175$

For each of the tabulated soil profiles of NEHRP, the expected peak ground acceleration as well as the spectral acceleration (S_a) at seven spectra periods (i.e. 0.2s, 0.4s, 0.75s, 1.0s, 1.5s, 3.0s, 4.0s) are evaluated following the PSHA results, as presented in Figure 7.5. The expected intensities are estimated for various earthquake return periods of 75yr, 475yr (ISIRI-2800 Design-Basis Earthquake - DBE), 975yr and 2475yr (ISIRI-2800 Maximum Considered Earthquake - MCE), corresponding to 50%, 10%, 5% and 2% probability of exceedance in 50-year life time of the building, respectively.

Considering only the site class of the buildings under study (i.e. Soft Rock [site class C; Type II]), the peak ground acceleration and the spectral acceleration corresponding to different spectra periods for various return periods at the coordinate of the selected buildings are presented in Table 7.4. Furthermore, the seismic hazard maps corresponding to MCE and DBE, in terms of PGA and S_a(T=0.2s) are shown in Figure 7.4. It should be noted that the seismic hazard maps associated with S_a(T=0.2s) are the only available ones with the closest period to the structures under study. Comparing the figures, it is evident that a substantial variation exists in the expected ground shaking acceleration associated to different periods of vibration and return periods. It is crucial to recognise this variation in the seismic vulnerability analysis. Using these values, response spectra of the location under study can be generated for different return periods and compared to the design response spectra of the code ISIRI-2800 (2007) corresponding to a return period of 475 years in 50-year life span of the building, as illustrated in Figure 7.5. Accordingly, except some minor underestimation of spectral acceleration at periods of 0.3s to 0.4s, the code design spectrum is on the safe side by overestimating the acceleration values at various periods of vibrations.

Table 7.4 - Ground motion acceleration (g) for different period values of Soft Rock (site class C; Type II ISIRI-2800), (Gholipour et al., 2008)

Spectra period, T (s)	**50% probability in 50 years (75yr Return Period)**	**10% probability in 50 years (475yr Return Period)**	**5% probability in 50 years (975yr Return Period)**	**2% probability in 50 years (2475yr Return Period)**	**Code Design Spectrum ISIRI-2800 (2007)**
0.00	0.194	0.394	0.496	0.635	0.350
0.20	0.468	0.933	1.187	1.577	0.875
0.40	0.342	0.726	0.937	1.230	0.875
0.75	0.217	0.519	0.684	0.960	0.668
1.00	0.167	0.398	0.526	0.752	0.551
1.50	0.109	0.254	0.341	0.480	0.421
3.00	0.042	0.109	0.144	0.202	0.265
4.00	0.028	0.073	0.100	0.137	0.219

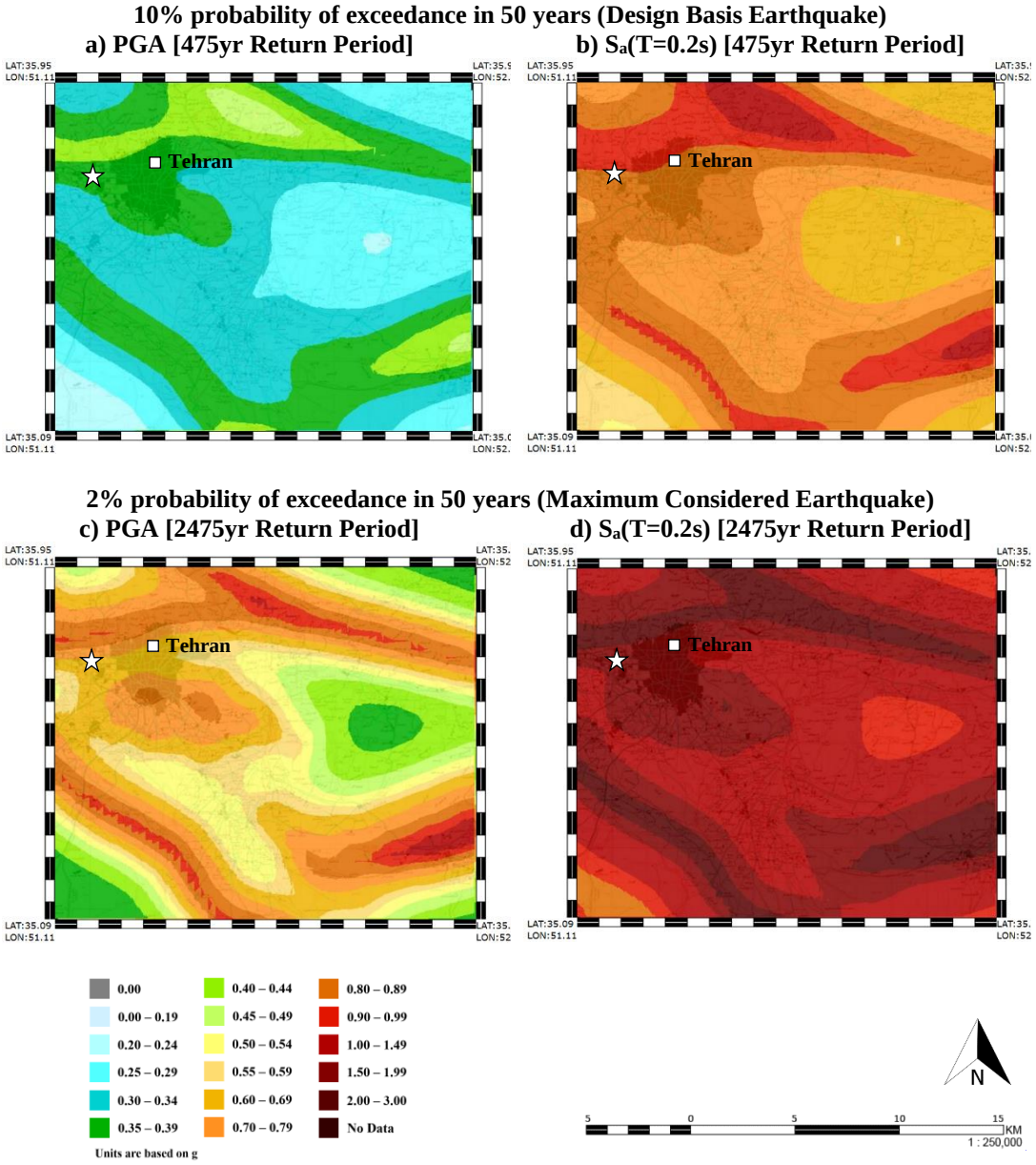

Figure 7.4 - Seismic hazard map of Safa-Dasht PGA and S_a(T=0.2s), indicated with a white star extracted from PSHA of the greater Tehran region (Gholipour et al., 2008)

Highlighting the fundamental period of the selected models on the response spectra illustrated in Figure 7.5, it is evident that the attracted spectral acceleration decreases as the considered construction quality drops. The seismic hazard curves obtained for each of the selected buildings are presented in Figure 7.6. The hazard curve indicates the annual probability of exceedance for the given intensities according to the initial period of the buildings. The results are used to estimate the economic losses and to conduct the life cycle cost analysis. As stated earlier, due to the variation in structural frequency of the selected buildings and sensitivity of the ground shaking, the characteristics of the seismic hazards should be allocated accordingly. Although, this impact can be minor for structures with close fundamental period, it has been included throughout different stages of the analysis.

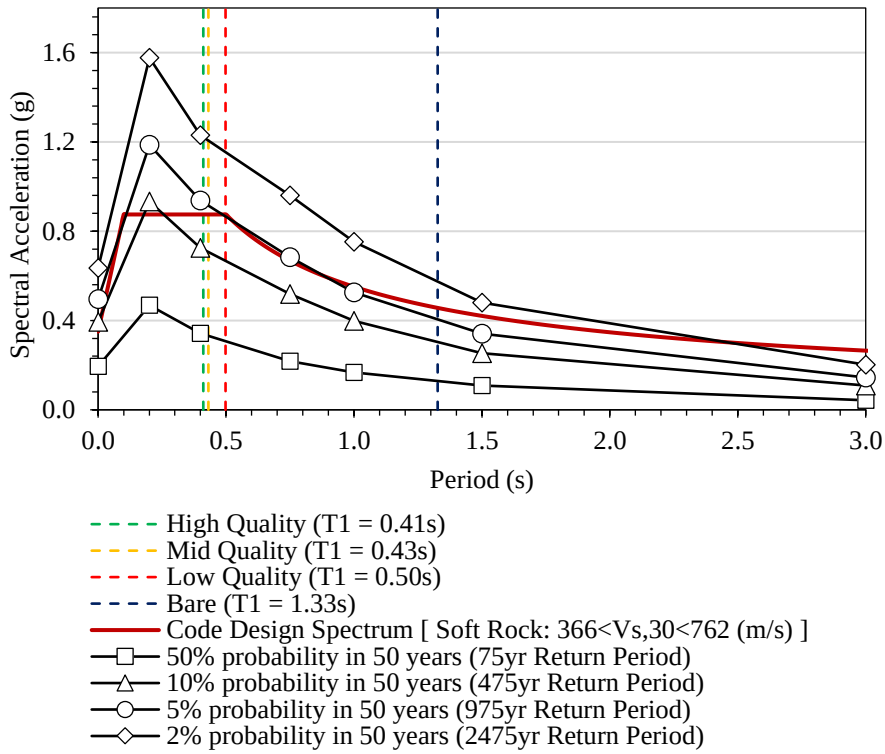

Figure 7.5 – Response spectrum of Soft Rock (site class C; Type II) for different return periods according to the seismic hazard assessment of Tehran and ISIRI 2800 (2007) elastic response spectrum. The fundamental period of the buildings is included.

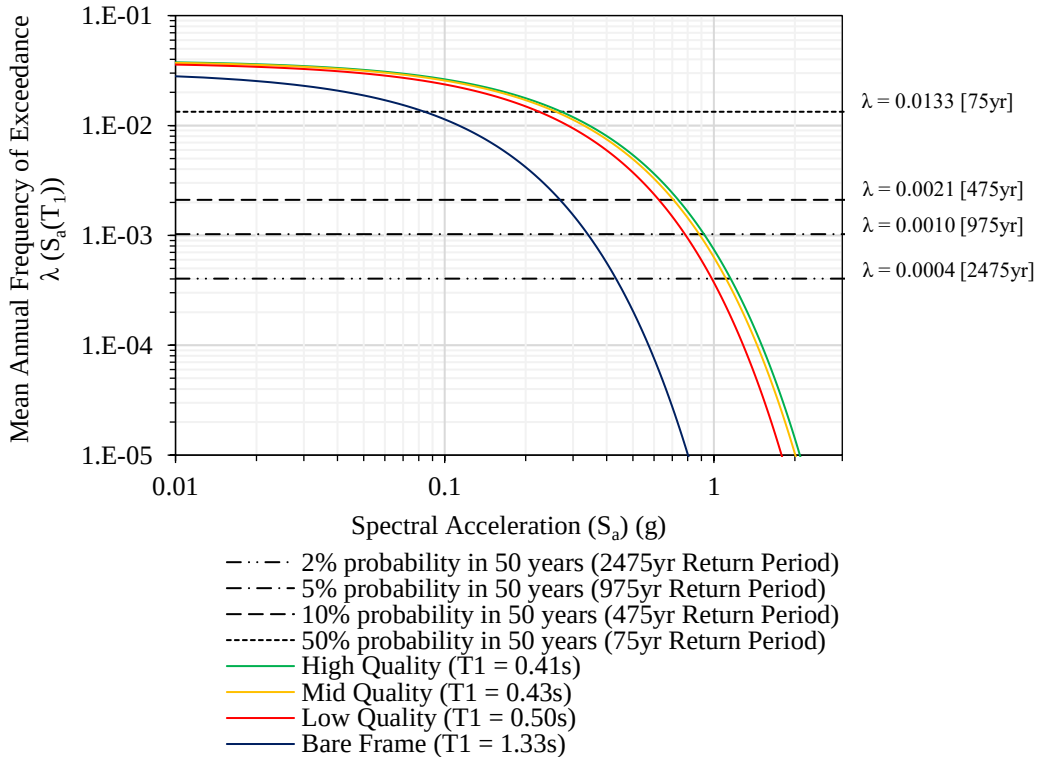

Figure 7.6 – Seismic hazard curve of Safa-Dasht for different fundamental periods (T_1) extracted from PSHA of the greater Tehran region (Gholipour et al., 2008). The annual frequencies corresponding to different return periods are also indicated.

7.2.3. Structural Analysis and Fragility Assessment

Having identified the expected seismic ground shaking acceleration for each of the selected models, based on the seismic hazard assessment of the location, the response of the structures should be evaluated. Moreover, to estimate the seismic vulnerability of each building, the fragility functions corresponding to different damage states need to be evaluated. This section discusses the estimated seismic performance and fragility functions obtained according to the methodology stated in Chapter 3.

As discussed thoroughly in Chapter 6, the performance the four models are estimated through multiple-stripe analysis (MSA). A suite of 22 record pairs are used, scaled to desired intensities at the fundamental periods of the structures. The horizontal component of each earthquake with the highest peak ground acceleration is applied to the weakest direction of the building, while the other direction was excited simultaneously by the other horizontal component. The effect of earthquake's vertical component is ignored in this study. Moreover, the effect of directionality has been neglected due to the excessive computational effort, assuming that the considered seismic loading condition will result in the highest response (i.e. EDP) in terms of inter-storey drift ratio and consequently damage.

The following sets of figures (Figures 7.7, 7.9, 7.11 and 7.13) present the seismic response, obtained through nonlinear analysis methods conducted on each of the selected buildings in terms of IM-EDPs. Similar to previous analysis, for measuring seismic intensity, the first mode spectral acceleration ($S_a(T_1)$) in the weaker direction is used as IM, while the response is evaluated as the maximum inter-storey drift ratio (MIDR).

To estimate the performance and subsequently the vulnerability of the selected building, the fragility functions are derived using the data obtained through MSA. The Least Square fitting technique proposed by Baker (2015) is applied to the performance points for the four damage states, as discussed in Chapter 6 (i.e. slight, moderate, extensive, complete). For each of the models, Tables 7.5, 7.7, 7.9 and 7.11 present the resultant median and lognormal standard deviation of each fragility curve, along with the damage threshold considered for the damage states in terms of inter-storey drift ratio (ISDR). The fragility curves of each model, from which the vulnerability estimation will be based on, are demonstrated in Figures 7.8, 7.10, 7.12 and 7.14. Moreover, utilising the fragility functions, the probability of reaching each of the damage states are estimated for the expected spectral accelerations corresponding to earthquakes of four common return periods (i.e. 75yr, 475yr, 975yr, 2475yr). The obtained values will be used in section 7.2.4 to determine and comparison the expected economic losses.

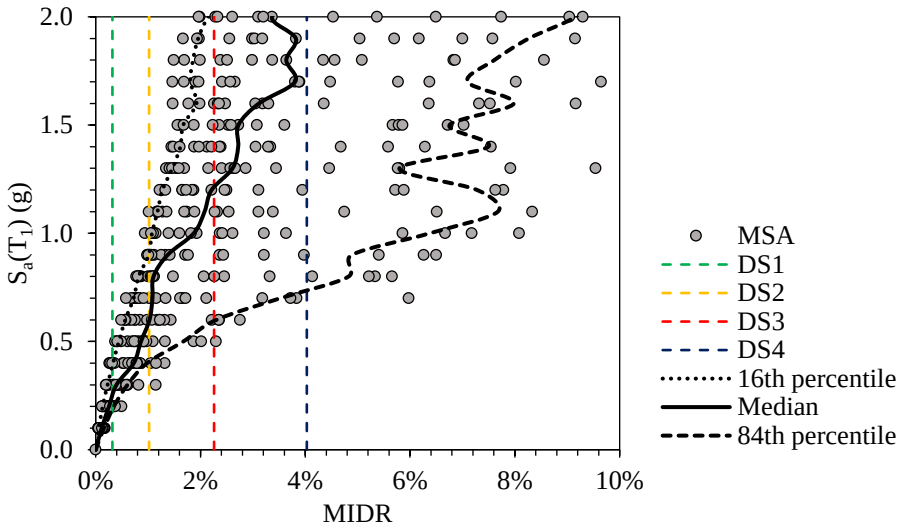

Figure 7.7 - Performance response (IM-EDP) obtained from MSA for High Quality building

Table 7.5 - Fragility function parameters, Median (μ [g]) and Dispersion (β) values and damage thresholds for High Quality building

	DS1 Slight	DS2 Moderate	DS3 Extensive	DS4 Complete
Median [g]	0.25	0.63	1.09	1.61
Dispersion	0.336	0.375	0.532	0.553
Damage Threshold (ISDR)	0.32%	1.02%	2.26%	4.03%

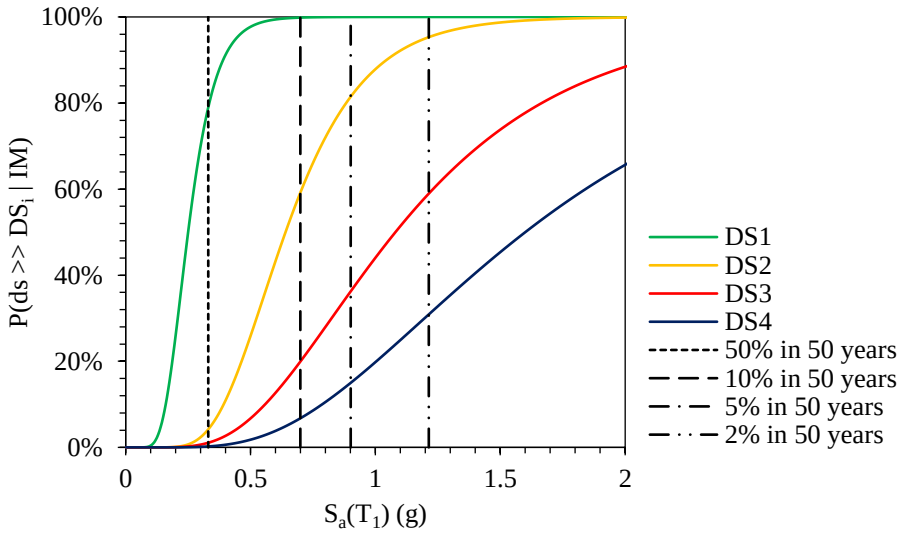

Figure 7.8 – Fragility curves for High Quality building

Table 7.6 – Probability of exceeding different damage states at the considered earthquake intensities for High Quality building

Ground Motion	$S_a(T_1)$ (g)	DS1 Slight	DS2 Moderate	DS3 Extensive	DS4 Complete
50% probability in 50 years (75yr Return Period)	**0.33**	50.31%	2.07%	0.46%	0.32%
10% probability in 50 years (475yr Return Period)	**0.70**	99.51%	43.26%	12.85%	6.96%
5% probability in 50 years (975yr Return Period)	**0.90**	99.97%	67.83%	26.21%	14.57%
2% probability in 50 years (2475yr Return Period)	**1.21**	100.00%	88.62%	47.89%	28.87%

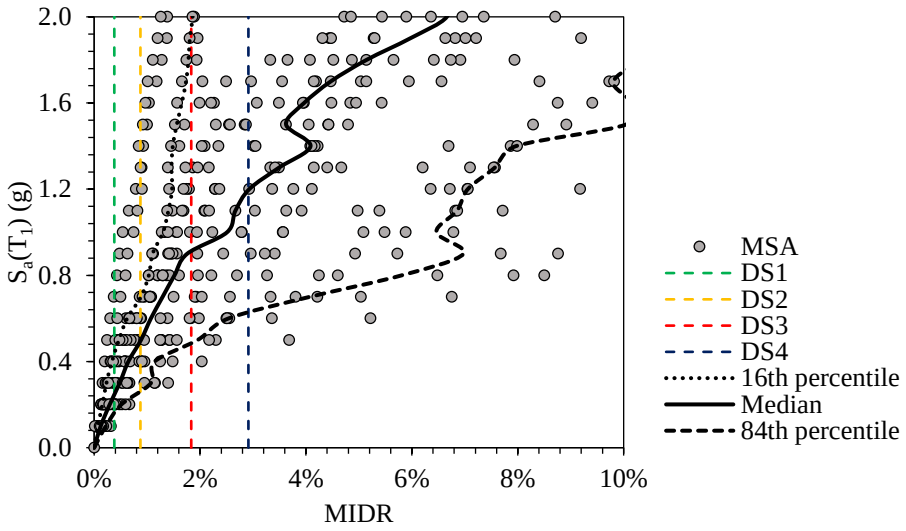

Figure 7.9 - Performance response (IM-EDP) obtained from MSA for Mid Quality building

Table 7.7 - Fragility function parameters, Median (μ [g]) and Dispersion (β) values and damage thresholds for Mid Quality building

	DS1 Slight	DS2 Moderate	DS3 Extensive	DS4 Complete
Median [g]	0.25	0.47	0.91	1.14
Dispersion	0.528	0.519	0.628	0.677
Damage Threshold (ISDR)	0.38%	0.87%	1.83%	2.91%

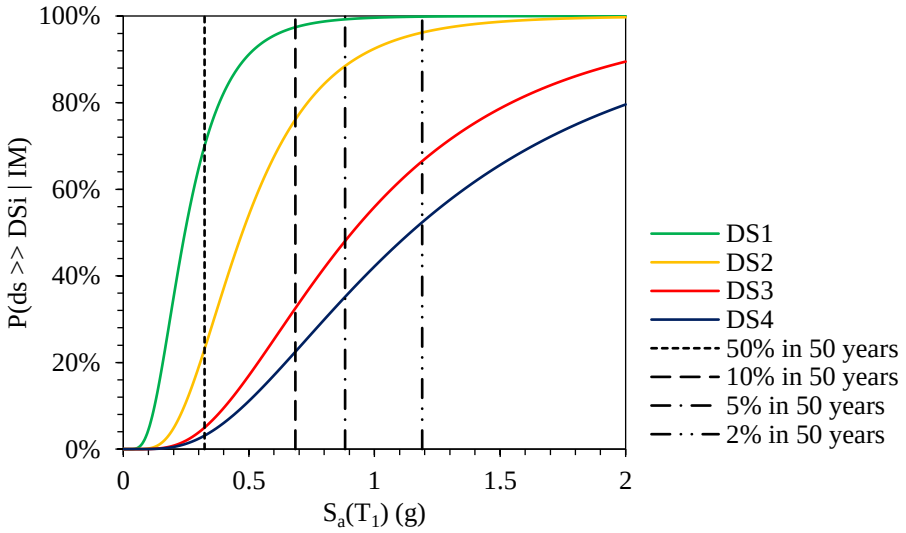

Figure 7.10 - Fragility curves for Mid Quality building

Table 7.8 - Probability of exceeding different damage states at the considered earthquake intensities for Mid Quality building

Ground Motion	$S_a(T_1)$ (g)	DS1 Slight	DS2 Moderate	DS3 Extensive	DS4 Complete
50% probability in 50 years (75yr Return Period)	**0.32**	70.02%	23.12%	4.98%	3.12%
10% probability in 50 years (475yr Return Period)	**0.69**	97.41%	76.10%	32.53%	22.48%
5% probability in 50 years (975yr Return Period)	**0.88**	99.23%	88.45%	48.04%	35.15%
2% probability in 50 years (2475yr Return Period)	**1.19**	99.86%	96.18%	66.48%	52.37%

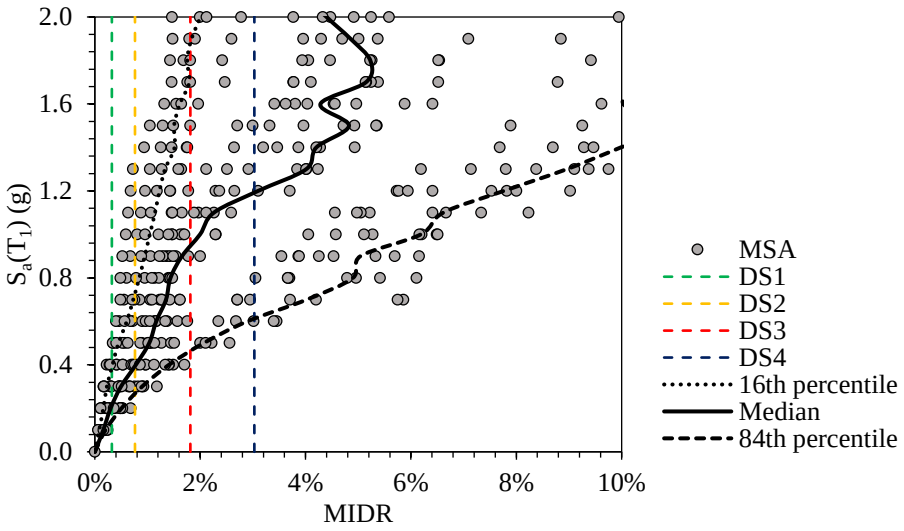

Figure 7.11 - Performance response (IM-EDP) obtained from MSA for Low Quality building

Table 7.9 - Fragility function parameters, Median (μ [g]) and Dispersion (β) values and damage thresholds for Low Quality building

	DS1 Slight	DS2 Moderate	DS3 Extensive	DS4 Complete
Median [g]	0.22	0.42	0.85	1.10
Dispersion	0.501	0.516	0.547	0.556
Damage Threshold (ISDR)	0.32%	0.76%	1.81%	3.03%

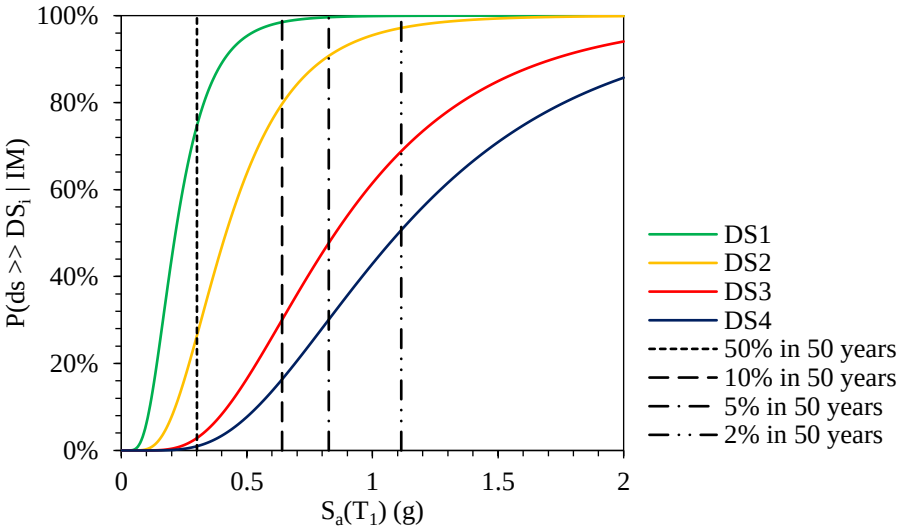

Figure 7.12 - Fragility curves for Low Quality building

Table 7.10 - Probability of exceeding different damage states at the considered earthquake intensities for Low Quality building

Ground Motion	$S_a(T_1)$ (g)	DS1 Slight	DS2 Moderate	DS3 Extensive	DS4 Complete
50% probability in 50 years (75yr Return Period)	**0.30**	74.68%	26.43%	2.86%	0.98%
10% probability in 50 years (475yr Return Period)	**0.64**	98.50%	79.69%	30.05%	16.36%
5% probability in 50 years (975yr Return Period)	**0.83**	99.63%	90.73%	47.72%	30.10%
2% probability in 50 years (2475yr Return Period)	**1.11**	99.95%	97.16%	68.81%	50.67%

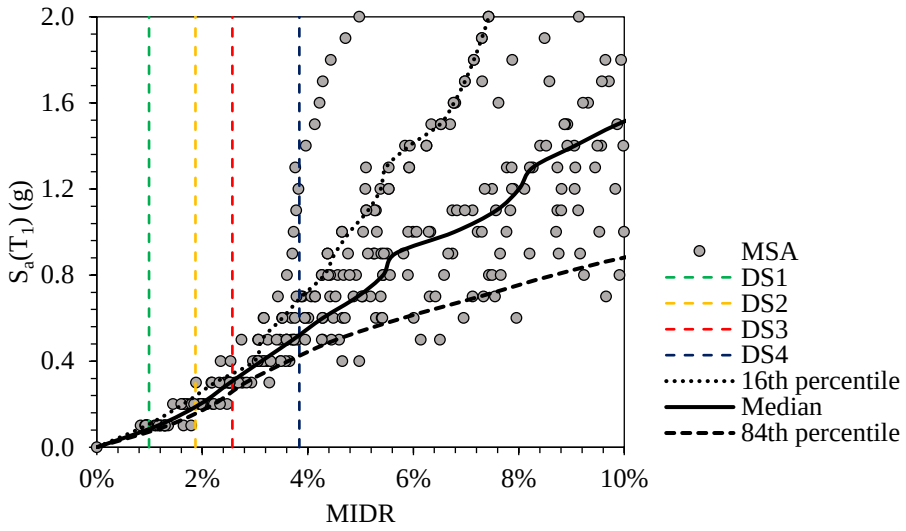

Figure 7.13 - Performance response (IM-EDP) obtained from MSA for Bare Frame building

Table 7.11 - Fragility function parameters, Median (μ [g]) and Dispersion (β) values and damage thresholds for Bare Frame building

	DS1 Slight	DS2 Moderate	DS3 Extensive	DS4 Complete
Median [g]	0.08	0.25	0.34	0.58
Dispersion	0.201	0.354	0.326	0.257
Damage Threshold (ISDR)	0.99%	1.87%	2.57%	3.84%

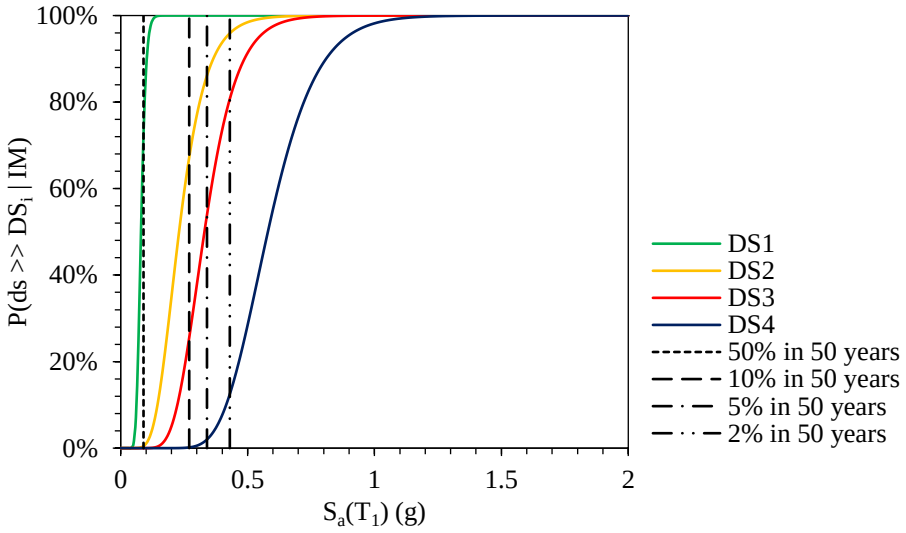

Figure 7.14 - Fragility curves for Bare Frame building

Table 7.12 - Probability of exceeding different damage states at the considered earthquake intensities for Bare Frame building

Ground Motion	$S_a(T_1)$ (g)	DS1 Slight	DS2 Moderate	DS3 Extensive	DS4 Complete
50% probability in 50 years (75yr Return Period)	**0.09**	99.96%	47.25%	0.03%	0.00%
10% probability in 50 years (475yr Return Period)	**0.21**	100.00%	99.79%	73.36%	4.54%
5% probability in 50 years (975yr Return Period)	**0.30**	100.00%	99.99%	97.62%	32.78%
2% probability in 50 years (2475yr Return Period)	**0.44**	100.00%	100.00%	99.98%	84.53%

As the response of the structures was measured according to spectral acceleration corresponding to the first mode of vibration ($S_a(T_1)$), a direct comparison of the derived fragility functions to each other or to ones proposed by other studies is not possible. Furthermore, the structural fragility functions derived as part of HAZUS project are originally in terms of spectral displacement corresponding to the initial period of the considered SDoF system ($S_d(T_1)$). Thus, again a direct comparison is not possible as the initial period of the modelled structures are completely different as stated in Table 7.13. Hence, to have a better understanding of the selected buildings, fragility functions in terms of peak ground acceleration (PGA) are derived and compared with the ones proposed in HAZUS (2003). It should be noted that the reason for this comparison is the extensive application of HAZUS provision in design and assessment of the structures of the region under study.

Utilising the 550 performance points obtained through MSA, the corresponding PGA values are obtained from the selected suite of 22 earthquake records for different scaling. The median and lognormal standard deviation of obtained performance points are calculated following the generalised linear method fitting technique.

Table 7.13 – Comparing fundamental period of HAZUS buildings with the selected buildings

Building Type	**Description**	**Period (s)**
HAZUS - S1M Pre-Code	Mid-Rise Steel Moment Frame – Pre-Code	1.07
HAZUS - S1M Low-Code	Mid-Rise Steel Moment Frame – Low-Code	1.07
HAZUS - S1M Moderate-Code	Mid-Rise Steel Moment Frame – Moderate-Code	1.08
HAZUS - S1M High-Code	Mid-Rise Steel Moment Frame – High-Code	1.08
HAZUS - S2M Pre-Code	Mid-Rise Steel Braced Frame – Pre-Code	0.87
HAZUS - S2M Low-Code	Mid-Rise Steel Braced Frame – Low-Code	0.87
HAZUS - S2M Moderate-Code	Mid-Rise Steel Braced Frame – Moderate-Code	0.86
HAZUS - S2M High-Code	Mid-Rise Steel Braced Frame – High-Code	0.86
HAZUS - S5M Pre-Code	Mid-Rise Steel Frame with UMIW – Pre-Code	0.65
HAZUS - S5M Low-Code	Mid-Rise Steel Frame with UMIW – Low-Code	0.65
HAZUS - S5M Moderate-Code	Mid-Rise Steel Frame with UMIW – Moderate-Code	-
HAZUS - S5M High-Code	Mid-Rise Steel Frame with UMIW – High-Code	-
High Quality	Mid-Rise Steel Frame Hybrid System with UMIW	0.41
Mid Quality	Mid-Rise Steel Frame Hybrid System with UMIW	0.43
Low Quality	Mid-Rise Steel Frame Hybrid System with UMIW	0.50
Bare Steel Frame	Mid-Rise Steel Frame Hybrid System	1.33

Figure 7.15, illustrates the fragility curves of the selected models in terms of PGA. The median and standard deviation of each fragility curve is presented in Table 7.14.

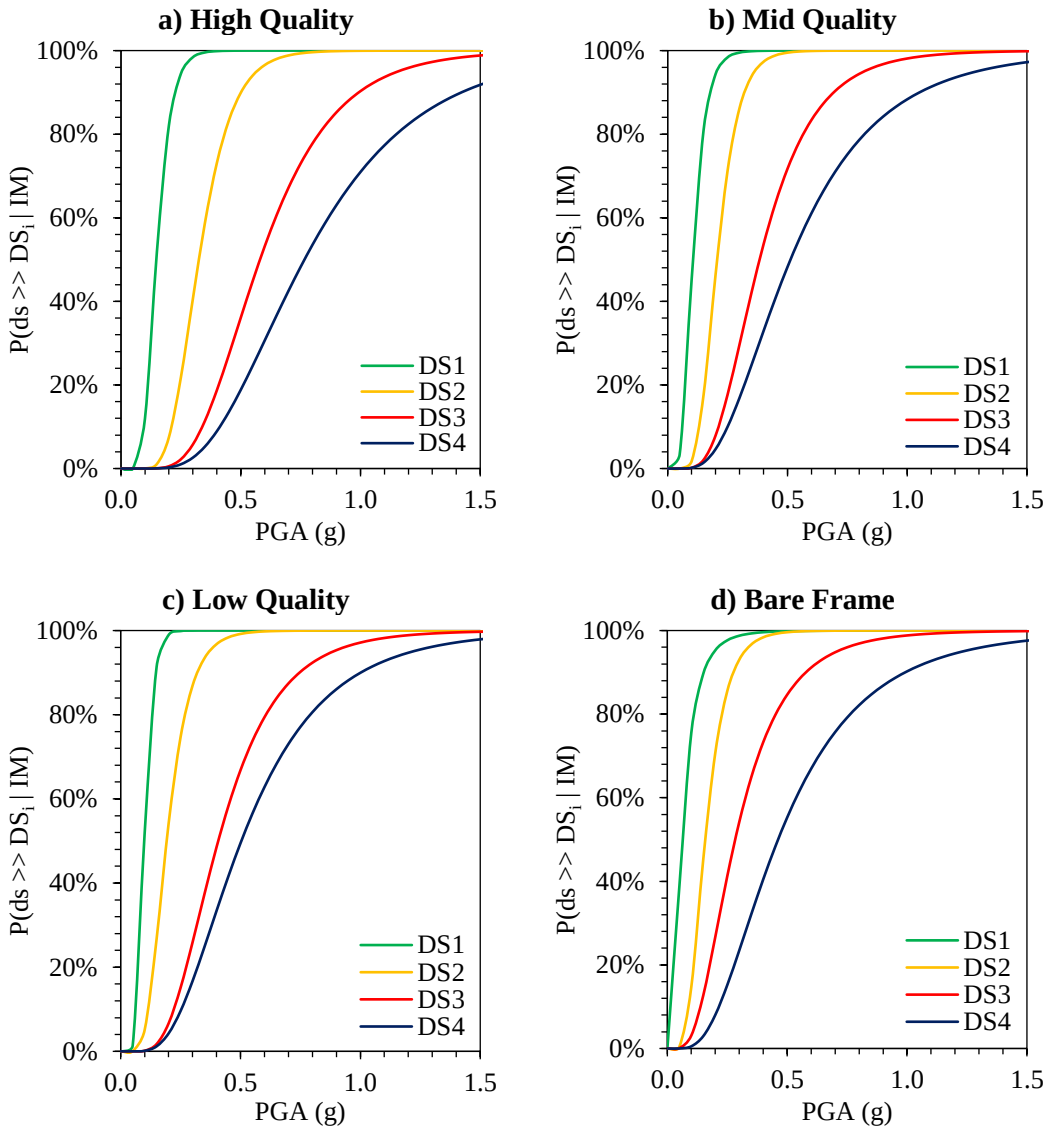

Figure 7.15 – Fragility curves derived for each of the selected buildings in terms of PGA

Table 7.14 – Median (g) and Dispersion value derived for fragility curves in terms of PGA

	DS1 - Slight		DS2 - Moderate		DS3 - Extensive		DS4 - Complete		Avg.
	μ	β	μ	β	μ	β	μ	β	β
HighQ	0.15	0.330	0.33	0.337	0.58	0.419	0.77	0.482	0.392
MidQ	0.11	0.406	0.21	0.343	0.38	0.462	0.51	0.560	0.443
LowQ	0.10	0.306	0.19	0.398	0.41	0.473	0.50	0.536	0.428
Bare Frame	0.06	0.708	0.16	0.435	0.28	0.557	0.46	0.597	0.574

The median values of derived fragility functions are compared to values suggested by HAZUS for mid-rise steel structures with different structural systems and designed codes as presented in Table 7.15 and Figure 7.16. The variation of median in case of HAZUS, increases as the damage states progress. Therefore, a larger difference is observed when comparing the medians in case of DS4, while the designated medians in both case of DS1 and DS2 have similar values. Furthermore, as expected the braced structures have higher medians than moment resisting frame and the infilled frames.

Comparing the median values of HighQ model with the ones of HAZUS, the values allocated for DS1 and DS2 are generally higher than all other values. While, in case of DS3, the median agrees with the one of S2M Moderate-Code and DS4 has values close to S1M Moderate-Code.

Table 7.15 – Median [g] values suggested in HAZUS and the ones obtained for the selected buildings

Damage State	S1M Pre-Code	S1M Low-Code	S1M Moderate-Code	S1M High-Code	S2M Pre-Code	S2M Low-Code	S2M Moderate-Code	S2M High-Code	S5M Pre-Code	S5M Low-Code	HighQ	MidQ	LowQ	Bare Frame
DS1	0.09	0.12	0.13	0.14	0.10	0.12	0.14	0.14	0.09	0.11	0.15	0.11	0.10	0.06
DS2	0.14	0.18	0.21	0.26	0.14	0.18	0.22	0.27	0.14	0.18	0.33	0.21	0.19	0.16
DS3	0.23	0.29	0.44	0.62	0.28	0.35	0.53	0.73	0.28	0.34	0.58	0.41	0.38	0.28
DS4	0.39	0.49	0.82	1.43	0.47	0.58	0.97	1.62	0.43	0.53	0.77	0.51	0.50	0.46

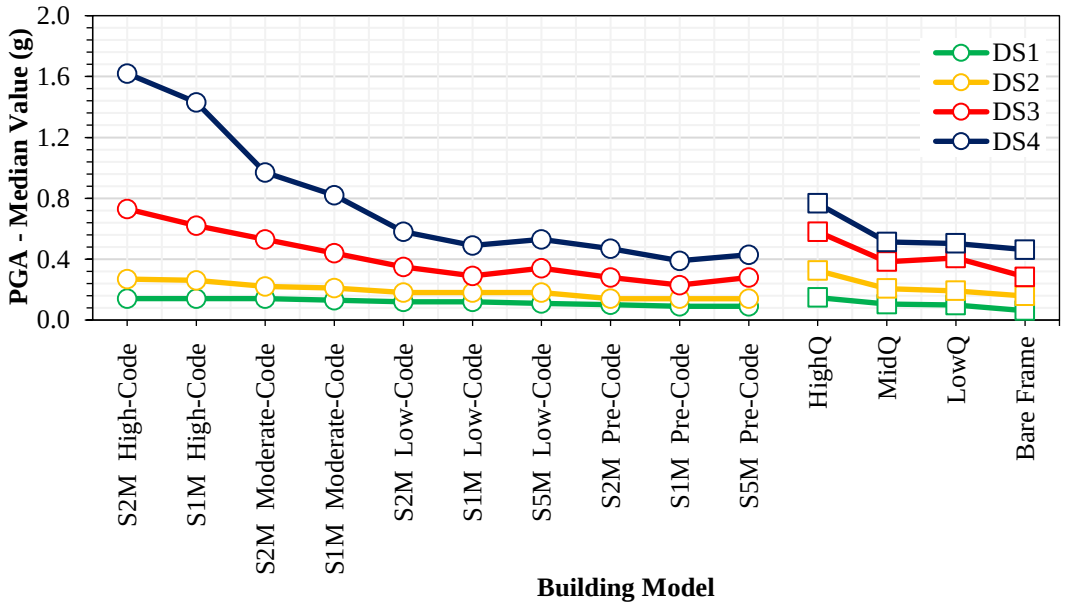

Figure 7.16 – Graphical comparison of Median [g] values suggested in HAZUS and the ones obtained for the selected buildings

The variation observed between the median values of HAZUS and the ones obtained for the considered models, can be explained by focusing on two crucial aspects. First, is the definition of damage states and their allocated thresholds, which clearly are not identical to the ones used for assessing the selected buildings (Table 7.16 and Figure 6.18). In case of HAZUS the dispersion values are mainly allocated following experts' opinion. The total variability associated to each structural damage state β_{Sds} is modelled by combination of three contributors to structural damage variability β_C, β_D and $\beta_{M(Sds)}$. The approach assumes that the variability of building response depends jointly on demand and capacity, thus a complex process of convolving probability distribution of demand spectrum and the capacity curve (structural model) has been implemented in developing the fragility function.

$$\beta_{Sds} = \sqrt{[CONV(\beta_C, \beta_D)]^2 + [\beta_{M(Sds)}]^2} \quad (7.3)$$

The lognormal standard deviation parameter ($\beta_{M(Sds)}$) is introduced to consider the resultant uncertainty in estimating the median value of the threshold of each damage state (ds). In this case, a dispersion of 0.4 is proposed by HAZUS [section 5.4.3.4] for all structural damage states regardless of the building type and damage level. A dispersion value (β_C) is also introduced to account the variability of the capacity (response) properties of the model building type. For buildings constructed according to code provisions this value is 0.25 and for pre-code buildings is 0.30. Furthermore, β_D is the lognormal standard deviation parameter that describes the variability of the demand (record-to-record variability). As discussed in Chapter 6, simplified methods do not necessarily capture the full nonlinearity of the structures, particularly in case of infilled steel frames.

Table 7.16 – HAZUS inter-storey drift at threshold of different damage states

Damage State	S1M Pre-Code	S1M Low-Code	S1M Moderate-Code	S1M High-Code	S2M Pre-Code	S2M Low-Code	S2M Moderate-Code	S2M High-Code	S5M Pre-Code	S5M Low-Code
DS1	0.32%	0.40%	0.40%	0.40%	0.27%	0.33%	0.33%	0.33%	0.16%	0.20%
DS2	0.51%	0.64%	0.69%	0.80%	0.43%	0.53%	0.58%	0.67%	0.32%	0.40%
DS3	1.08%	1.35%	1.57%	2.00%	1.07%	1.33%	1.56%	2.00%	0.80%	1.00%
DS4	2.67%	3.33%	4.00%	5.33%	2.67%	3.33%	4.00%	5.33%	1.87%	2.33%

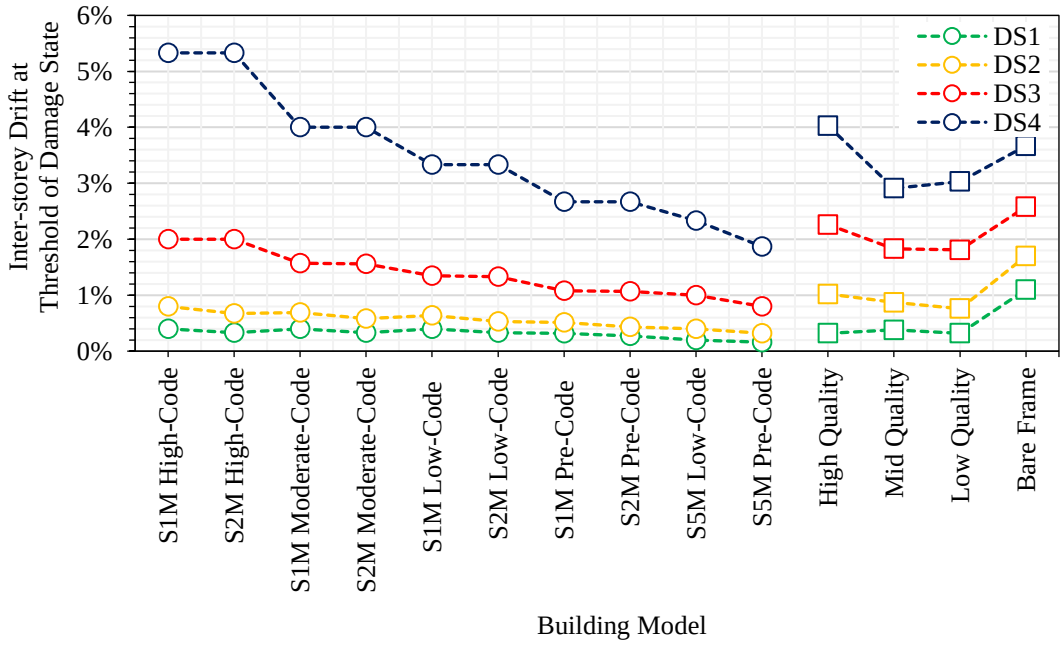

Figure 7.17 - Graphical comparison of inter-storey drift at threshold of damage states suggested by HAZUS and the ones utilised for analysing the performance of selected buildings

7.2.4. Economic Loss Assessment

The structural damage indicator has limited use from the perspective of the decision making, administrative, finance and insurance sector, since it does not quantify the monetary consequences of the damage (Sadegh Azar et al., 2004). In order to relate the derived structural fragilities and damage to economic losses and measure the cost of the damage, the predicted seismic damage is commonly quantified using Damage Ratio (DR), defined as follows (ASTM E-2026, 1999):

$$DR = \frac{Repair\ costs\ of\ a\ building}{Value\ of\ the\ undamaged\ building\ (Replacement\ value)} \tag{7.4}$$

The damage ratio has been referred to as Damage Factor or Cost Ratio in number of studies (e.g. ATC-13 (1985) and Whitman (1973). Damage ratios are generally determined through either expert judgement or empirical post-earthquake studies of loss data. In seismic loss estimation, a damage ratio is assigned to each of the considered damage states. Mean Damage Ratio (MDR) is the expected value of the DR at given earthquake intensities (Hill & Rossetto, 2008). Mean damage ratio can be evaluated for any given seismic intensity (*I*) by multiplying the probability of each damage state by its corresponding damage ratio. If the resultant MDR is multiplied by the actual construction cost of a building (i.e. replacement value), then the expected total damage can be expressed in terms of a currency for the unit building or per unit area (Eq. 7.5).

$$MDR_{ds,I} = \sum_{ds=1}^{i} P(ds_i|I) * DR_{ds_i} \tag{7.5}$$

A number of studies, such as Whiteman (1973), ATC-13 (FEMA, 1999), have proposed DR values corresponding to different structural damage states. The HAZUS earthquake loss estimation methodology (FEMA 1999) also provides a predefined set of cost ratios for buildings to be used with its damage scale where more accurate information is unavailable. A comparison of damage ratios suggested by different studies is presented in Table 7.17. The considerable variation observed suggest the specificity of cost ratios to location.

In this study, due to lack of experimental and post-earthquake observation data for Iran, to the author's knowledge, the upper bound damage ratio values suggested in Risk-EU project (Mouroux, 2004) and HAZUS (2003) are utilised to derive the economic losses of the selected buildings.

Table 7.17 - Damage ratios (ranges or central cost) used in different studies and locations (% replacement value)

Structural Damage State	Whitman (1973) [San Francisco]	ATC-13 [California]	HAZUS [California]	Blong (2003) [Australia]	Timchenko (2002) [Georgia]	Roca et al (2006) [Spain]	Di Pasquale et al (2005), [Italy]	Mouroux (2004), (RISK-UE) [Europe]
Slight	0.05-1.25	1-10	2	1-5	2	1	1	2-5
Moderate	1.25-20	10-30	10	5-20	10	20	10	10-20
Extensive	20-65	30-60	50	20-60	30	40	35	50
Complete	65-100	60-100	100	90-100	80-100	80-100	75-100	80-100

Having the damage ratios defined, the cost of each residential unit and cost per building is estimated according to the 2017 data obtained through Building & Housing Research Centre (BHRC) and Statistical Centre of Iran (SCI, 2016). It should be noted that the construction cost per metre square is based on the cost breakdown of 2015 and includes the entire structural material (steel, masonry units for internal and external walls, foundation concrete and reinforcement), non-structural components (e.g. doors, windows, facilities, flooring, wall finishing, stair, electrical and mechanical elements) and cost of skilled labour and machinery. A mean total construction cost of $150 per metre square (1 USD = 30,000 IRR) is estimated regardless of the building's quality of construction based on the original structural detailing and construction cost breakdown. Furthermore, the studied location includes 14,500 residential units out of which about 35% (4,800 units) include identical 4 storey steel framed structures with masonry panels, each accommodating 12 units. More info on the general arrangement of the structures and costs can be found in Table 7.18.

Table 7.18 – General info of structural arrangement and costs of the selected building

No. of Residential Units per Floor	4
No. of Floors per Building (excluding parking)	3
No. of Units per Building	12
Assumed No. of Buildings	400
Residential Unit Area	68.15 m^2
Parking & Storage Area	303.18 m^2
Hallways & Stairs Area	52.00 m^2
Total Building Area	1,172.98 m^2
Total Leasable Area	817.80 m^2
Construction Cost per m^2	$150.00
Total Construction Cost per Residential Unit	$10,222.50
Total Construction Cost per Building (Total Building Area)	$175,947.00
Total Construction Cost of 400 Buildings	$70,378,800.00

To estimate the economic losses, a vulnerability curve can be computed for each set of derived fragility functions. This is obtained by summing up, at each given intensity (i.e. $S_a(T_1)$), the expected damage percentage for each damage state, multiplied by their allocated damage ratio. This summation gives the damage ratio at the corresponding intensity. Plotting the obtained MDR values for increasing ground shaking measures, results in a curve which presents the vulnerability of the structure at any given seismic intensity (Figure 7.18-left). Similar to the case of fragility curves, as the initial periods of the selected structures are different, a direct comparison of obtained vulnerability curves is not possible. An option is to compare the expected repair costs under different earthquake scenarios. For instance, considering the intensities corresponding to the earthquakes with different probabilities of occurrence, such as the ones with return periods of 75, 475, 975 and 2475 years, the expected repair cost for a residential unit, a building (Figure 7.18-right) or the entire building distribution can be estimated.

As the probability of earthquake occurrence in the 50-year life time of the building decreases (i.e. return period increases), the estimated repair cost increases, because the expected earthquake intensity and corresponding damage increases. Therefore, an increase in cost is anticipated as the quality of the building drops. This is the case, when comparing the HighQ to the other qualities. However, subjected to the regional hazard characteristics, the MidQ building is experiencing more damage than the LowQ building, although it has shown a better performance. This highlights the influence of the regional seismic hazard on the estimated losses. In case of the bare frame, for earthquakes with high probability of occurrence (e.g. 50% and 10% in 50year), the building has the lowest or identical repair cost to HighQ building. This is mainly due to the relatively extended fundamental period (T_1=1.33s) of the bare frame, which attracted much less acceleration compared to the infilled frames. However, for earthquakes with low probability of occurrence (e.g. 2% in 50year), the structure suffers more damage in comparison to the other buildings, which results in the highest predicted repair cost. It is evident that considering the structures under study simply as bare steel frames, while ignoring the impact of masonry infills can lead to inaccurate estimation of losses.

a) High Quality

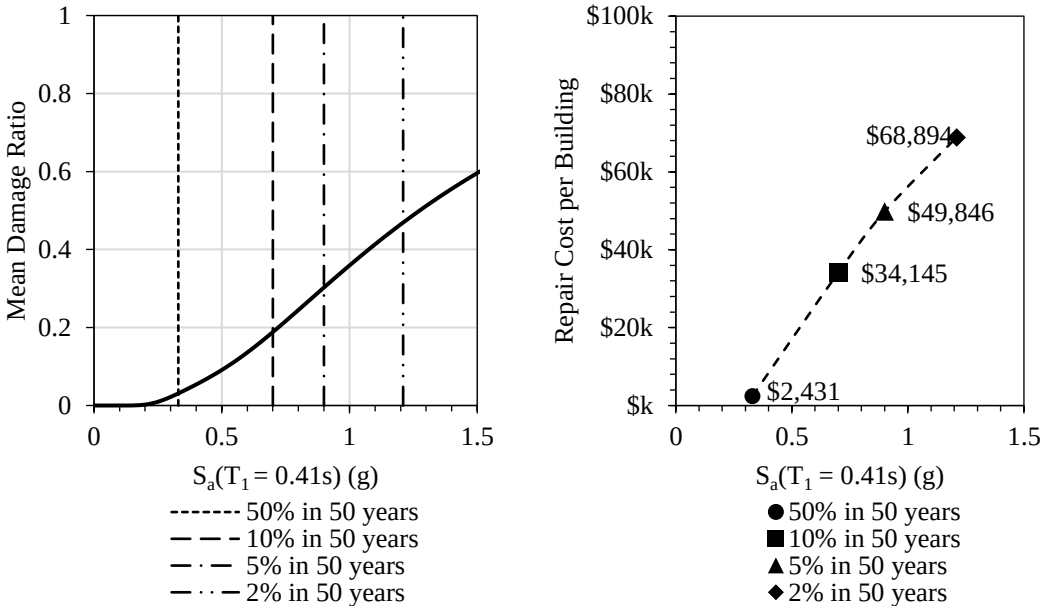

b) Mid Quality

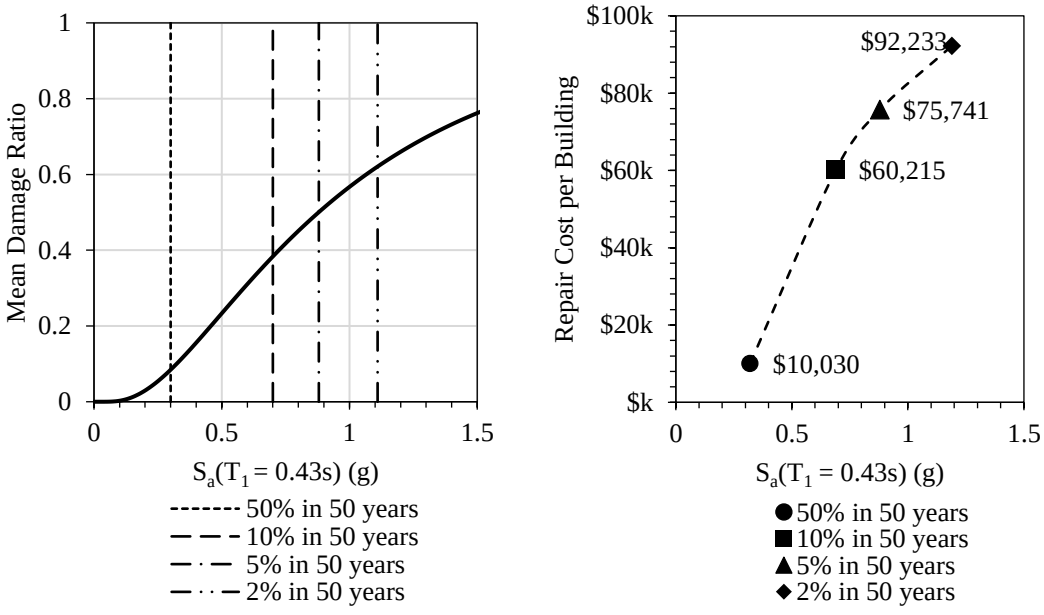

c) Low Quality

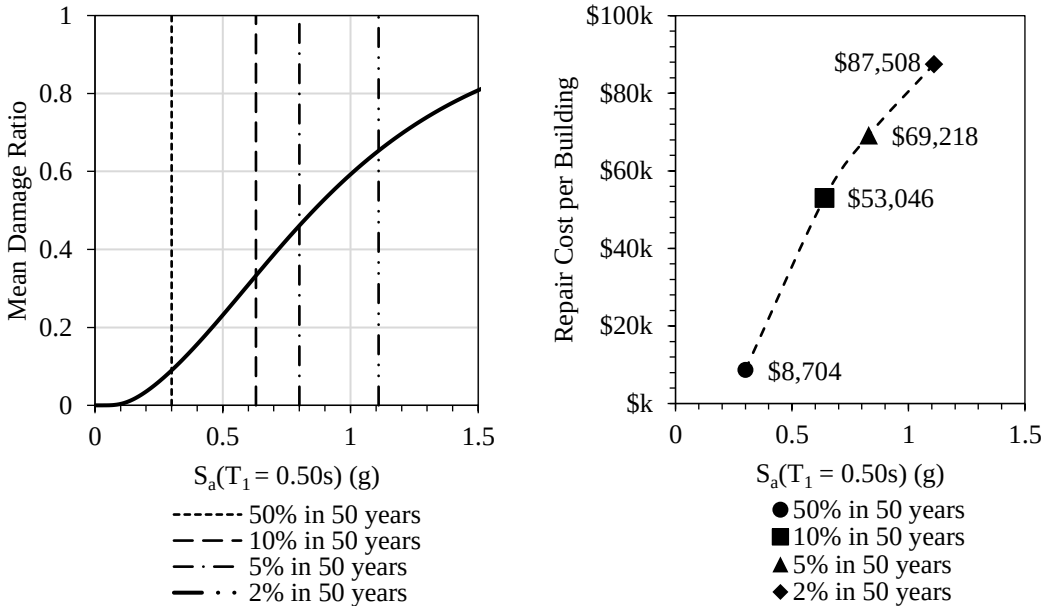

d) Bare Frame

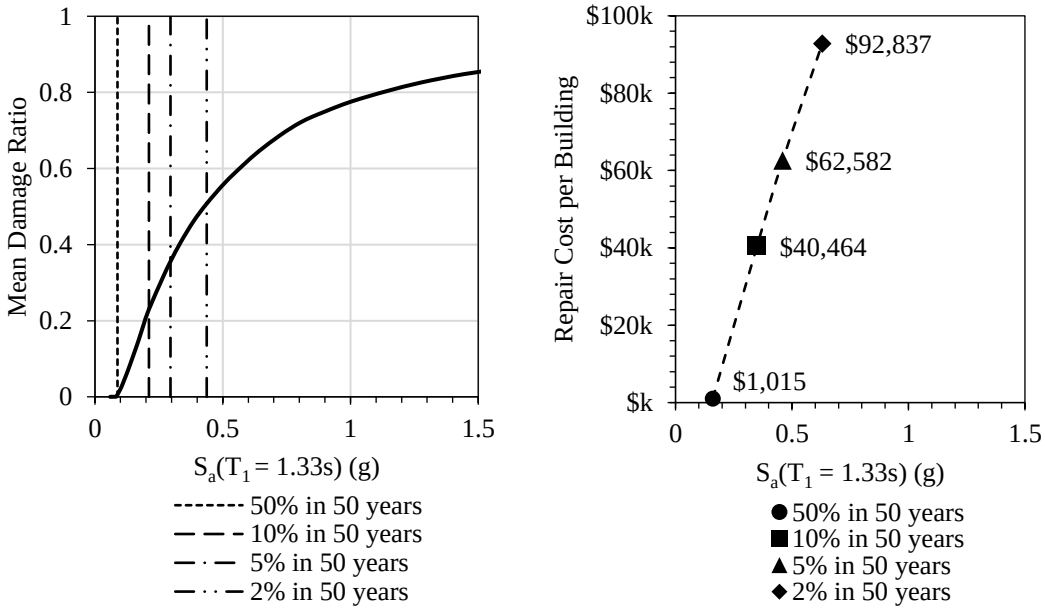

Figure 7.18 – right: vulnerability curves for buildings with different qualities of construction, left: the expected repair cost per building at intensities corresponding to earthquakes with four different probability of occurrence (i.e. return periods: 75yr, 475yr, 975yr, 2475yr)

Representing the seismicity in terms of annual probability of exceedance, gives the opportunity of comparing the analysed MDRs of the structures against the expected hazard level as shown in Figure 7.19. The resultant graph demonstrates that in case of mid quality buildings, higher MDR should be expected for earthquakes with annual probabilities exceeding up to $\lambda = 0.0004$ (i.e. return period of 2475 years, Maximum Considered Earthquake) (Figure 7.20). While, the estimated MDR for the bare frame is close to the high-quality structure up to earthquake with return periods of 475 years (i.e. 10% in 50-year life time of the building). Therefore, in case the buildings are assessed as bare frame, while majority are characterised as low- to mid-quality infilled frames, an under-estimation of repair cost should be expected under design-basis earthquake. On the other hand, as the earthquake return period increases (i.e. 5% and 2% in 50-year life time of the building), the MDR of bare frame starts rising toward the MDR of low- and mid- quality buildings. This observation, clearly indicates that the impact infill panels have on the capacity, stiffness, ductility should not be ignored, as the resultant fragility function will underestimate the expected damages, resulting in unrealistic seismic losses. Furthermore, the stiff panels will significantly alter the stiffness of the structure, as a result the building's frequency of vibration shifts as well as changing the structural demand.

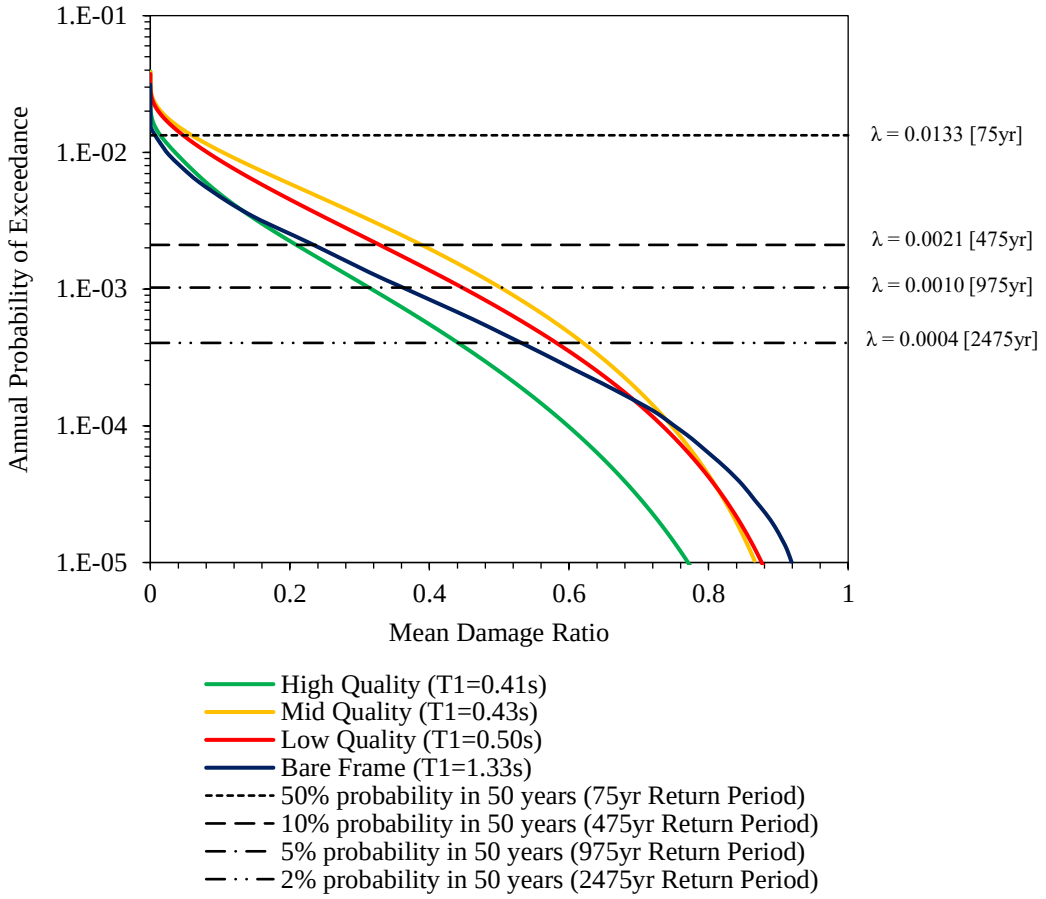

Figure 7.19 – Estimated mean damage ratio of selected buildings for earthquake with different annual probability of exceedance

Table 7.19 and Figure 7.20, present the total repair cost per metre square and the expected mean damage ratios, corresponding to the earthquakes with the considered return periods. The points discussed above are clearer when comparing the MDR of bare frame corresponding to 75yr and 2475yr to the infilled frame buildings.

Table 7.19 – Estimated total repair cost and mean damage ratio (MDR) for each of the selected buildings for earthquakes with four different return periods.

Return Period	**High Quality**		**Mid Quality**		**Low Quality**		**Bare Frame**	
	Total Repair Cost ($/m²)	*MDR*	*Total Repair Cost ($/m²)*	*MDR*	*Total Repair Cost ($/m²)*	*MDR*	*Total Repair Cost ($/m²)*	*MDR*
75yr	$2.10	1%	$8.98	6%	$7.49	5%	$0.87	1%
475yr	$31.60	21%	$58.56	39%	$49.92	33%	$34.50	23%
975yr	$47.11	31%	$75.06	50%	$66.99	45%	$53.35	36%
2475yr	$66.64	44%	$93.11	62%	$87.06	58%	$76.15	51%

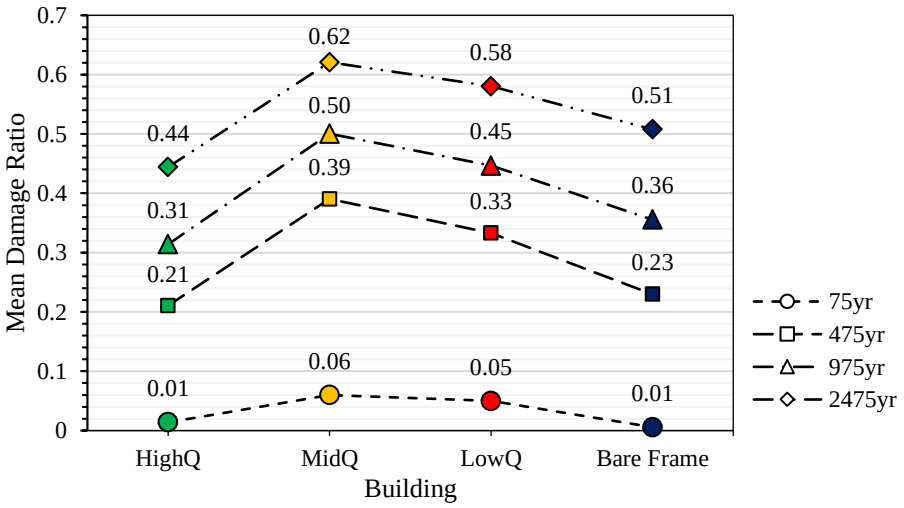

Figure 7.20 – Mean damage ratios obtained for each of the selected buildings for earthquakes with four different probabilities of occurrence (i.e. return periods: 75yr, 475yr, 975yr, 2475yr)

Looking at the estimated repair costs of the masonry infilled structures, as expected the building with the highest quality has the lowest repair cost and MDR. However, in case of low and mid quality buildings, although performance and resultant fragilities of the structures differ, as the mid quality building attracts higher intensities, the resultant damage estimation is slightly higher than the low-quality building.

So far, the calculated economic losses were presented per residential unit or per building, while considering different qualities of construction. To have a more precise loss evaluation and quantify the vulnerability of the location under study, the distribution of each building model has been accounted by considering three exposure distribution scenarios. The three

distributions are obtained, the first through solicitation of local experts' opinion, the second by assuming equal distribution and the third by assuming a large proportion of low quality buildings.

The distribution according to experts' opinion, is based on judgement of local engineers and inspectors, currently involved in identical projects under construction in the studied region. Around 25 engineers, including the ones directly responsible for the case under study have been questioned and an average of their opinion is implemented for this analysis. The characteristics of the considered buildings and their representative qualities have been explained during the interview and the experts were asked to give a distribution percentage for each of the cases, focusing mainly on the site under study. A similar distribution is proposed in the GEM guidelines, for which the index buildings are categorised into three groups based on their quality (Poor, Typical, Good). The typical quality has the highest proportion of the building population, while the poor and good have equal but lower fractions.

The third scenario with a larger proportion of low quality buildings, can be labelled as a conservative case, since it is expected to see higher losses in low-quality buildings. However, according to the above analysis, the mid-quality buildings, despite their relatively better performance, are ensuing higher monetary losses.

Figure 7.21, illustrates the distribution percentages considered for this analysis. The GEM guidelines, propose a similar approach

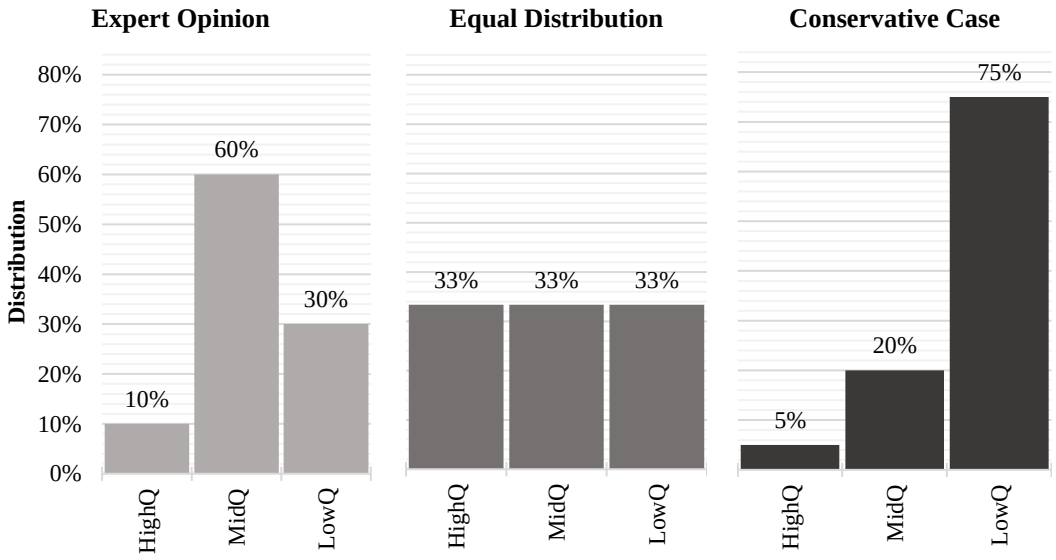

Figure 7.21 - Distribution percentages considered for structural loss estimation

As mentioned earlier, the total constructing cost for the buildings has been estimated at $150 per metre squared, regardless of the building's quality. A total of 400 building units, comprising 48'000 residential units, are located at the site. Therefore, the suggested distribution percentages will be applied to the 400 buildings (Table 7.20).

Table 7.20 – Distribution scenarios proposed for structural loss estimation of 400 buildings

Building Model	**Equal Distribution**		**Expert Opinion**		**Conservative**	
	Distribution (%)	No.	Distribution (%)	No.	Distribution (%)	No.
High Quality	33.3%	133	10.0%	40	5.0%	20
Mid Quality	33.3%	133	60.0%	240	20.0%	80
Low Quality	33.3%	133	30.0%	120	75.0%	300
Bare Frame	0.0%	0	0.0%	0	0.0%	0

To estimate the total structural losses, the specified four earthquake scenarios with decreasing probability of exceedance have been studied. The corresponding intensities were implemented to each of the three exposure distribution scenarios. The total structural losses, for the 400 buildings, are determined by summing up the losses evaluated for each of the building models according to their distribution. The highest total losses are expected to be derived for the conservative case, as it comprises a greater proportion of buildings with low quality (300 buildings). However, the final estimations indicate a slightly higher total loss for the expert opinion distribution ($45.21M). This is mainly due to the high repair cost of mid-quality buildings, which comprises the majority of building stock (60%) in this cohort. Moreover, Figure 7.22 and Figure 7.23 indicate that in both case of conservative and expert opinion distributions, the high-quality buildings did not play a dominant role in the total losses. On the other hand, as expected, the equal distribution scenario resulted in the lowest total losses ($43.05M), mainly due to a higher proportion of high quality buildings (33%) with lower repair cost (Figure 7.24).

The total losses of the bare steel frame are also calculated as a bench mark. The results show a substantial underestimation for all cases, regardless of the return period or the distribution. This underestimation can affect the resource allocation in pre- and post-earthquake planning.

The discussed outcomes, clearly indicate the crucial role of construction quality and its consequential structural performance, on the estimated vulnerability. Also, the impact of structural distribution and the local seismic hazard on the expected losses cannot be neglected.

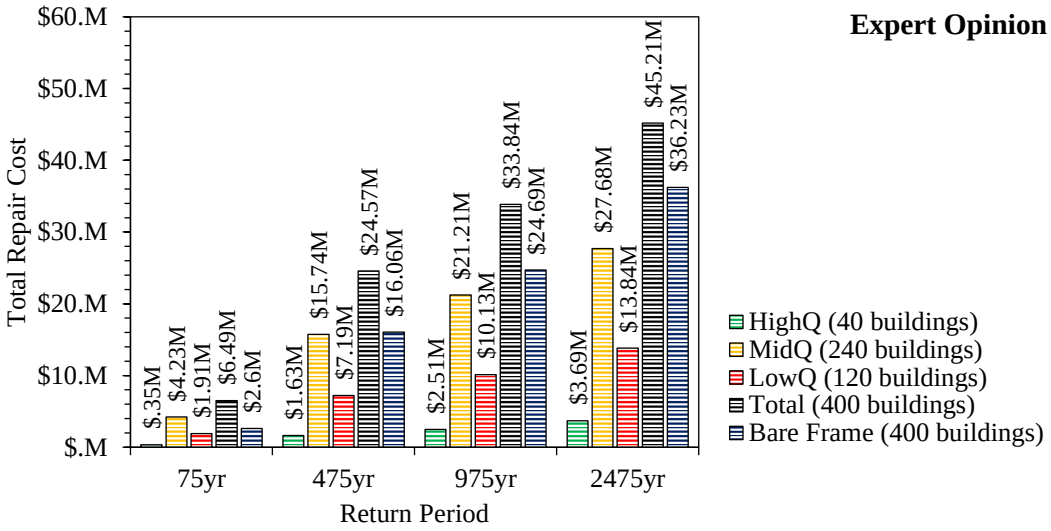

Figure 7.22 – Estimated total repair cost in case of expert's opinion distribution

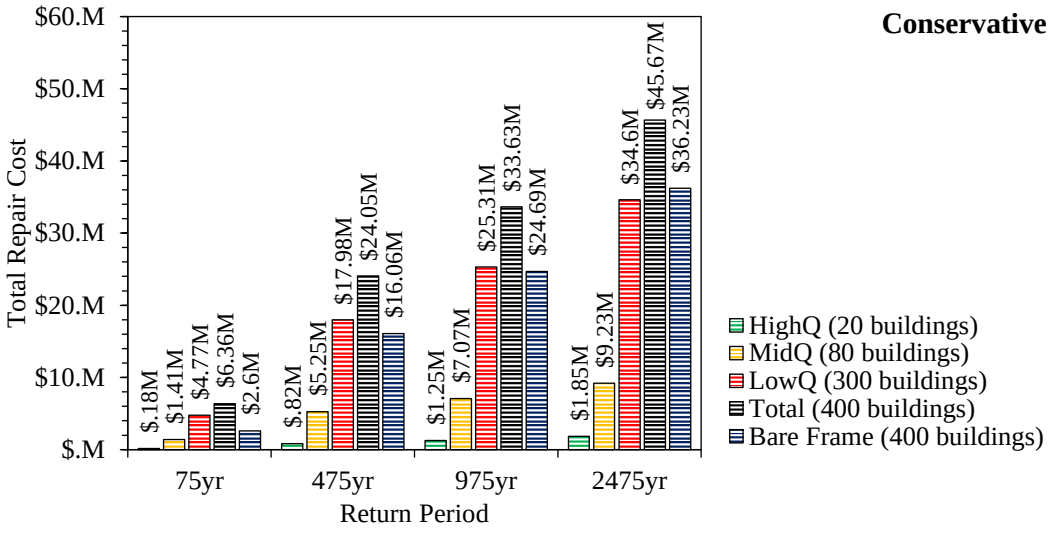

Figure 7.23 – Estimated total repair cost in case of conservative distribution

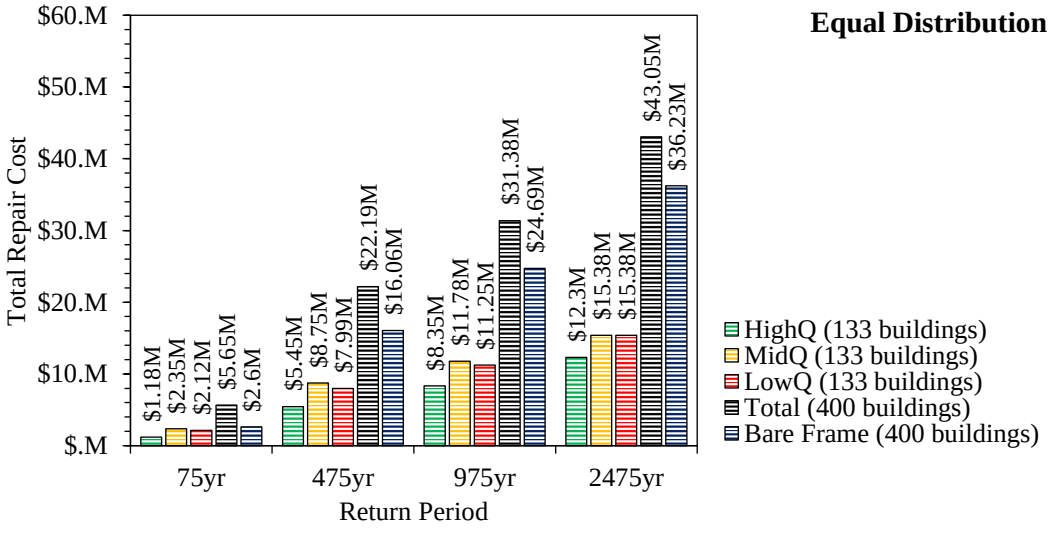

Figure 7.24 – Estimated total repair cost in case of equal distribution

7.3. Life Cycle Cost

Initial construction cost and the expected seismic damage cost throughout the lifetime of the structure are usually the two most important parameters for decision making (Mitropoulou et al., 2011). Providing a reliable estimation of structural responses at various seismic hazard levels is one of the major obstacles in accurately evaluating the seismic damage cost to the building stock.

The life-cycle cost (LCC) represents an estimate of the entire cost over the expected service life time of the building (e.g. 50 years). Generally, this includes the initial investment, maintenance and repair costs and commonly refers to the deterioration of the structural components' capacity over time due to phenomena such as corrosion or deterioration of the joints or the bearings (Frangopol et al., 2001). However, life-cycle cost may also refer to repair cost related to the damage caused by natural hazards, such as wind or earthquake. In this case, the lifecycle cost is related to the possible losses due to unsatisfactory performance of the structure under loading with random occurrence and intensity during its life (Biondini & Frangopol, 2016).

The life-cycle cost analysis (LCCA) principles are based on economic theories and have been used as decision-support tools in industrial and commercial projects. Life cycle cost analysis can be applied to investigate the optimum cost-effective structural design or the most cost-effective level of retrofitting or strengthening, particularly in regions prone to extreme events (Frangopol et al., 2001). In this case, an optimum seismic performance of a building can be defined as a reasonable balance between the initial investment cost of improving seismic performance and the prospective losses due to expected earthquakes (Lagaros et al., 2006). The LCCA process should also include both direct economic and human life losses within a given social context (Sanchez-Silva et al., 2011). Hence, LCCA can be regarded as an indicator of structural seismic performance, if the cost of structural and non-structural damage due to future earthquakes can be quantified with sufficient reliability. Furthermore, having a rational prediction of the structural deterioration and its consequential cost at each stage of building's operational life can assist in managing and allocation of financial resources, intended for repair, replacement or redesign and reconstruction activities. Many studies have determined the optimal seismic design by minimising the life cycle cost. For instance, Liu et al. (2004) suggested an optimization procedure to design steel moment-resisting frame buildings by minimizing the structure's LCC within a performance-based seismic design framework.

The total life cycle cost (C_{Total}) of a structural system, may refer either to the design-life period of a new structure or to the remaining life period of an existing retrofitted structure.

This cost can be expressed as a function of the expected operating time period (e.g. $t = 50\ years$) and the design variable vectors (s) as follows (Wen & Kang, 2001):

$$C_{Total}(t, s) = C_{IN}(s) + C_{LS}(t, s) \tag{7.6}$$

where C_{IN} is the initial cost of constructing a new structure or retrofitted existing facility. This cost represents the land price, material, operation and the labour cost for the construction of the building. As the land price and non-structural component costs are constant for all design alternatives, they can be eliminated from the total cost calculation. For steel-framed structures, the initial cost is usually considered to be proportional to the total weight of its components. The initial cost may also be influenced by other parameters such as the cost of connections, or other detailing that influences the performance. Other parameters that affect the initial cost include the cost of non-structural components, the cost of coating against fire or corrosion, the cost of heating or electrical instalments or any sort of aesthetic components. Since, the construction period is not considered in the model, C_{IN} is not time-dependent. As discussed in section 7.2.4 of this chapter, the estimation cost for the selected buildings is set to \$150 per unit area (m^2) over the 1172.98 m^2 total area of the building, with a gross leasable area of 817.80 m^2 as presented in Table 7.18.

The term C_{LS} is the ‘‘limit state cost’’, referring to the potential damage cost from earthquakes that may occur during the life of the structure. It accounts for the cost of damage repair, the cost of injury, recovery or human fatality. It can also include direct or indirect economic losses associated with loss of content, rental and income after the seismic event (Mitropoulou et al., 2011; Wen & Kang, 2001). The quantification of these losses in financial terms depends on several socio-economic parameters. It should be mentioned that in the calculation of C_{LS} a regularization factor is used that transforms the costs in to present values. The most difficult cost to quantify is the cost corresponding to the loss of human life. Several approaches exist for this estimation, ranging from purely insurance and economic reasoning to more sensitive that consider the loss of a human being irreplaceable (Bruneau et al., 2003; Warszawski et al., 1996). For this study, as the main focus is on the structural performance, the cost of injury and fatality are extracted from the insurance premiums tailored for the location under study. Other expenses such as maintenance costs, which are not necessarily a consequence of earthquake damage, but may arise during the life of the structure are also omitted.

Based on a Poisson process model of the earthquake occurrences and an assumption that damaged buildings are immediately retrofitted to their original intact conditions after every major damage due to seismic excitation, the following formula can be applied to estimate the limit state cost considering N limit states, as proposed by Wen and Kang (2001):

$$C_{LS}(t,s) = \frac{\nu_E}{\lambda}\left(1 - e^{-\lambda t}\right)\sum_{i=1}^{N} C_{LS}^{i} P_i \tag{7.7}$$

where ν_E is the annual occurrence rate of significant earthquakes (M_w > 6.0) modelled by Poisson process, which for the site under study is estimated as 0.0132 (Gholipour et al., 2008). λ is the constant annual momentary discount rate, which aims to convert the cost due to hazard that occurs in the future into present monetary value. Rational values for the discount rate range from 3% to 6% (FEMA-227, 1992; Lagaros et al., 2006). In this analysis λ is selected as 3%, an appropriate value for the location under study according to (Rackwitz, 2006). It should be noted that the final life cycle cost is extremely sensitive to the discount value. C_{LS}^{i} is the limit-state dependent cost for the i^{th} limit state, while P_i is the probability of the i^{th} limit state being reached, given the earthquake occurrence calculated as follows:

$$P_i = P_i(\Delta > \Delta_i) - P_{i+1}(\Delta > \Delta_{i+1}) \tag{7.8}$$

where Δ_i and Δ_{i+1} are the lower and the upper bounds of the ith limit state for the two adjacent damage states considered. Then the probability of any given limit state being reached $P_i(\Delta > \Delta_i)$, given the earthquake occurrence $\Delta\lambda_{IM}(x_i)$, can be calculated using the following equation. The probability of earthquake occurrence is determined using the site-specific hazard curves corresponding to the initial period (T_1) of each of the buildings under study.

$$P_i(\Delta > \Delta_i) = \sum_{all\ x_i} P(DS \geq ds_i \mid IM = x_i)\,.\,|\Delta\lambda_{IM}(x_i)| \tag{7.9}$$

The $P(DS > ds_i \mid IM = x_i)$ represents the probability of exceeding a specific limit state (ds_i) given the level of seismic intensity (x_i), which is obtained from the fragility function estimation. $\lambda_{IM}(x_i)$ is the annual frequency of exceeding a given intensity measure value x_i, hence $|\Delta\lambda_{IM}(x_i)| = |\lambda_{IM}(x_i) - \lambda_{IM}(x_{i+1})|$ is approximately the annual frequency of intensity measure being equal to $IM = x_i$. The derivation process for fragility functions and annual probability of exceeding a limit-state, for the buildings under study, has been discussed thoroughly in sections 7.2.2 and 7.2.3.

Depending on the analysis and availability of data, the limit-state dependent cost for the i^{th} limit-state (C_{LS}^{i}) can be expressed in different forms. In this study, the following format is implemented for the LCCA:

$$C_{LS}^{i} = C_{dam}^{i} + C_{con}^{i} + C_{ren}^{i} + C_{inc}^{i} + C_{rel}^{i} + C_{inj,m}^{i} + C_{inj,s}^{i} + C_{fat}^{i} \tag{7.10}$$

where C_{dam}^{i} is the repair cost of structural damage due to earthquake. C_{con}^{i} is the loss of contents cost due to structural damage that in this study is quantified by the maximum inter-

storey drift, while this can also be estimated as a function of floor acceleration. C_{ren}^{i} is the loss of rental cost, C_{inc}^{i} is the income loss cost, C_{rel}^{i} is the cost of relocation where applicable. $C_{inj,m}^{i}$ and $C_{inj,s}^{i}$ are the cost of minor and serious injuries respectively and C_{fat}^{i} is the cost of human fatality. These cost components are all related to the level of structural damage attained. An occupancy rate of four persons per each residential unit (68 m^2; 2 bedrooms) has been considered based on the social function classification data (FEMA-227, 1992). Loss of function time and down time are considered as the time required to recover the full functionality of the building. This is evaluated according to ATC-13 (1985) for earthquake engineering facility classification 16 and mid-rise moment resisting steel frames.

Rents and other incomes may be suspended during this period and relocation cost may also be incurred. In this study, the cost of relocation has not been included. The economic losses can be divided into two factors, rental and income (e.g. store). The studied building typologies' use is only residential, hence no disruption of the commercial activities should be expected. The rental cost loss is expected to be proportional to the duration of the complete or partial loss function. Furthermore, the values allocated for injuries and fatalities are based on typical injury and life insurance pay out provided in the region under study.

A summary and calculation formula used for each of the cost components are presented in Table 7.21. The estimation of cost components are according to Wen & Kang (2001) and Lagaros (2007), tailored to the location under study. A more detailed assessment might be necessary on further social and economic aspects to evaluate the expected cost.

Table 7.21 - Formulae for calculation of the cost components in USD ($)

Variable	Cost Category	Calculation Formula	Basic Cost
C_{dam}^{i}	*Damage/Repair*	Replacement Cost × Floor Area × Mean Damage Index	\$150/m^2
C_{con}^{i}	*Loss of Contents*	Unit Contents Cost × Floor Area × Mean Damage Index	\$50/m^2
C_{ren}^{i}	*Rental*	Rental Rate × Gross Leasable Area × Loss of Function	\$4.6/month/m^2
C_{inc}^{i}	*Income*	Rental Rate × Gross Leasable Area × Down Time	-
C_{rel}^{i}	*Relocation*	Relocation Cost × Gross Leasable Area × Loss of Time	-
C_{inj}^{i},m	*Minor Injury*	Minor Injury Cost Per Person × Expected Minor Injury Rate × Floor Area × Occupancy Rate*	\$5'000/person
C_{inj}^{i},s	*Serious Injury*	Serious Injury Cost Per Person × Expected Serious Injury Rate × Floor Area × Occupancy Rate*	\$50'000/person
C_{fat}^{i}	*Human Fatality*	Death Cost Per Person × Expected Death Rate × Floor Area × Occupancy Rate*	\$2'500'000/person

*Occupancy rate 4 persons/unit

The mean damage indices are selected according to the central values proposed in ATC-13 (1985) and restated in FEMA 227 (1992) and Risk-UE (2004).

Table 7.22 - Limit state parameters for cost evaluation according to ATC-13 (1985) and FEMA 227 (1992)

Limit State	MDR (%)	Expected minor injury rate	Expected serious injury rate	Expected death rate	Loss of function (%)	Down time (%)
No Damage	0	0	0	0	0	0
Slight	5	3.00E-03	4.00E-04	1.00E-04	9.5	9.5
Moderate	20	3.00E-02	4.00E-03	1.00E-03	34.8	34.8
Extensive	50	3.00E-01	4.00E-02	1.00E-02	65.4	65.4
Complete	100	4.00E-01	4.00E-01	2.00E-01	100	100

Table 7.23 - Detail of limit-state dependent cost

Limit State	Damage/ Repair	Loss of Contents	Rental	Minor Injury	Serious Injury	Human Fatality
No Damage	$0 k	$0 k	$0 k	$0 k	$0 k	$0 k
Slight	$880 k	$205 k	$36 k	$1 k	$1 k	$12 k
Moderate	$3,519 k	$821 k	$131 k	$7 k	$9 k	$117 k
Extensive	$8,797 k	$2,053 k	$246 k	$70 k	$94 k	$1,173 k
Complete	$17,595 k	$4,105 k	$376 k	$94 k	$938 k	$23,460 k

The service life of the structure is only considered up to 50 years, in agreement with the local design code (ISIRI 2800). The expected life cycle of the buildings with different construction quality levels are shown in Figure 7.25 and Figure 7.26. The presented life cycle cost values are normalised to the initial cost of construction C_{IN}.

As LCCA is extremely sensitive to cost of fatality and injury, the total life-cycle cost has been estimated for two cases, in which the limit-state dependent cost is calculated once with (Figure 7.25) and once without (Figure 7.26) considering the cost of injury and death.

Similar to the observations of section 7.2.4, the bare frame underestimates the costs in comparison to both low and mid quality buildings. Moreover, the mid-quality building shows a higher expected cost during its service life. This is directly related to the higher MDR and seismic vulnerability of mid quality building in comparison to the others, which is mainly due to the seismic hazard characteristics of the location under study. For instance, at the end of the 50-year, the life cost of mid-quality is about $226,000, while the low-quality building is about 213,000. This value is $197,000 and $199,000 for the high-quality and bare frame, respectively.

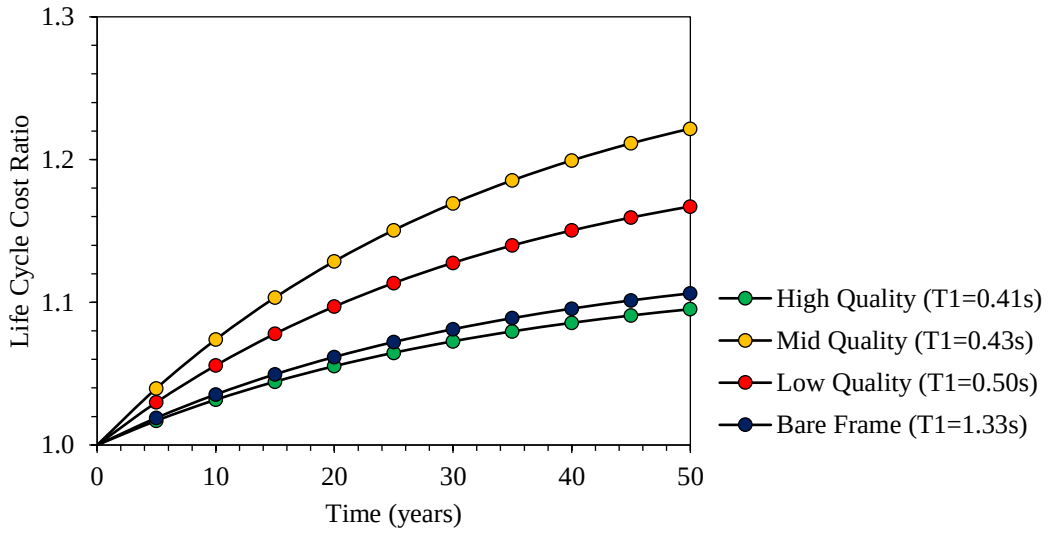

Figure 7.25 - Life cycle cost analysis in 50 years including injury and fatality for selected building typologies

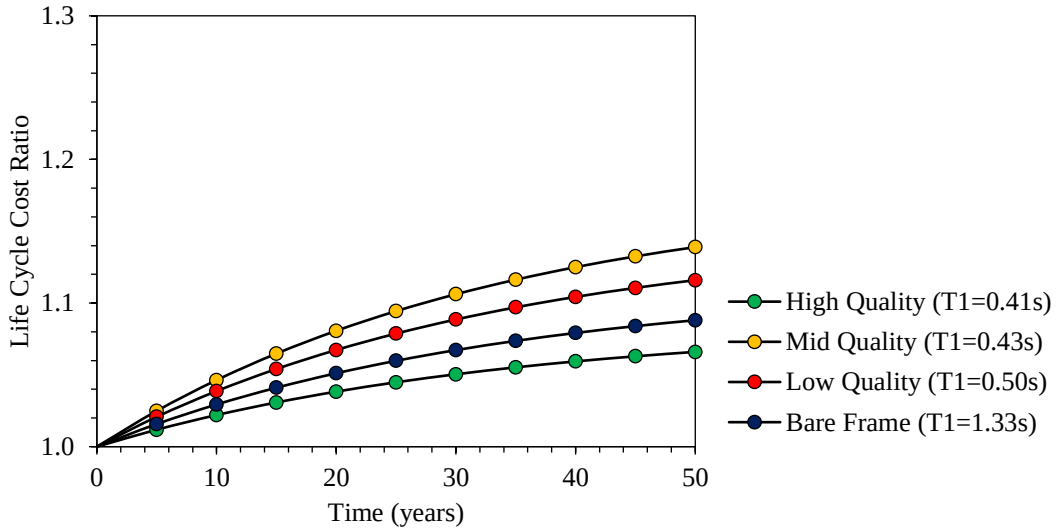

Figure 7.26 - Life cycle cost analysis in 50 years excluding injury and fatality for selected building typologies

Moreover, it is evident that the cost of injury and human fatality have a considerable impact on the final estimations. For example, in case of mid and low-quality buildings, the total life-cycle cost at the end of 50-years increases by 8.27% and 5.41% respectively. The sensitivity of the bare frame to the cost of fatality and injury is not as much as the structures with infill, with an increase of just 2% at the end of 50-year service life. This behaviour can be explained by considering the annual probability of exceeding damaging earthquake intensity for the bare frame at the site of study, which is much lower compared to the infilled frames. Hence, the formulation of LCC works in favour of the bare frame by resulting in lower probabilities of damage according to the derived fragility functions. This can be clearly observed by comparing the hazard maps of the location for spectral accelerations of 0.2s (close to infilled

frames) and 1.0s (close to the bare frame) for 10% probability of exceedance in 50-year life of buildings.

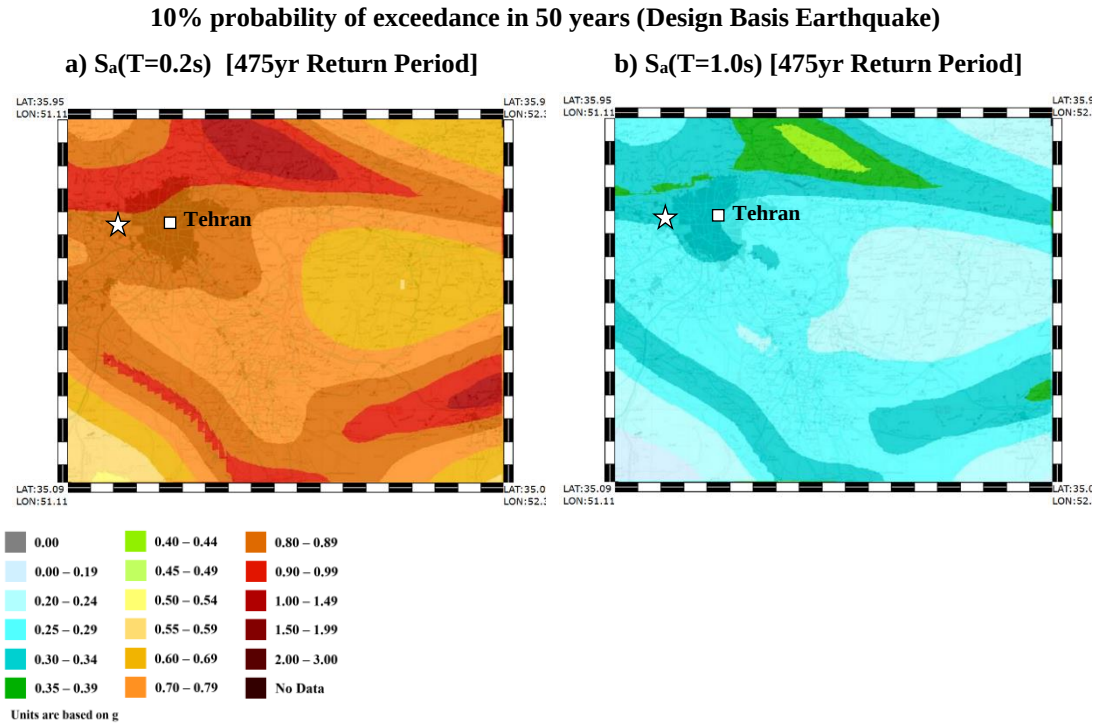

Figure 7.27 - Seismic hazard map of Safa-Dasht for Sa(T=0.2s and 1.0s), indicated with a white star extracted from PSHA of the greater Tehran region (Gholipour et al., 2008)

7.4. Conclusions

To evaluate the seismic losses, the comprising components of performance based seismic assessment framework, including the seismic hazard, structural vulnerability and exposure are investigated and linked. The process is presented on the same mid-rise residential building which was discussed thoroughly in Chapter 5. This is an acceptable representative of existing mid-rise masonry infilled steel frame buildings, as well as the ones being constructed in seismically active parts of the world, especially the Middle-East.

The latest probabilities seismic hazard assessment (PSHA) of the region under study is utilised to extract the most realistic expected seismic intensities and their probabilities. The site-specific hazard curves according to the fundamental period of the selected structures are obtained. A more detailed investigation is conducted at four earthquake intensities with decreasing probabilities of exceedance, including the design-basis earthquake (i.e. 475yr return period) and maximum considered earthquake (i.e. 2475yr return period).

The vulnerability of the selected structure has been evaluated in terms of mean damage ratio for various intensities of seismic excitation. Furthermore, three qualities of construction have

been assumed and simulated by altering three parameters; the beam-column connection types, masonry infill material and the contribution of bracings to the seismic resistance of the structural system. The fundamental frequencies of vibration in all three models are close enough to assume they still belong to the same typology and performance. The fragility functions of each model, at different damage states have been derived through conducting multiple-stripe analysis on a suite of scaled earthquake records, as discussed in detail in Chapters 5 and 6. Additionally, to investigate the influence of infill panels on the seismic losses, the obtained vulnerability and economic results are compared to the ones of a bare steel frame with the same structural arrangement and characteristics.

The simulated construction qualities had a considerable influence on the final monetary loss estimations. As anticipated, the structure with the highest quality of construction had the best performance among all cases, with the lowest expected repair cost and subsequently mean damage ratio at any given intensity. While, in contrary to expectations, the structure with the low-quality demonstrated a better performance than the mid-quality building, resulting in lower estimation of seismic losses. Having relatively close seismic responses and fragility functions, due to the lower fundamental period of the mid-quality structure, it attracted higher spectral accelerations than the low-quality building, which in return resulted in higher probability of damage and losses. This observation indicates the crucial role the seismic hazard characteristics of the region have on the estimated losses but also, very importantly how sensitive the vulnerability and seismic losses are to a small modification in the structural characteristics.

To gain a better understanding of the discussed phenomena, three exposure distribution scenarios for a population of 400 buildings are introduced. A percentage is allocated to each of the considered qualities of construction and the final expected losses for four different earthquakes with increasing intensities are studied. The result of each distribution is compared to a case in which all 400 buildings are assumed to behave as bare steel frames. In all cases, the bare steel frames under estimated the total losses under various distributions of infilled frames. The obtained results indicate the significant influence of detailing in modelling and realistic knowledge of exposure on the seismic loss estimation.

Furthermore, a life cycle cost analysis is conducted for each of the selected buildings throughout their 50-year service life. Having a rational forecast of structure's life cycle cost can assist in financial resource allocation and management of both pre- and post- disaster. Two cases have been considered in this analysis, one including the expected cost of injury and fatality, while the second neglected these costs. For both cases, a similar observation to the vulnerability and loss assessment is obtained, with the mid-quality building having the highest

cost among all cases and the high-quality building having the lowest, as expected. The life cycle cost of the bare steel frame was close to the high quality if the cost of injury and fatality was included. It should be noted that, although the bare frame has a weaker performance, however, due to its higher vibration period at its first mode (T_1=1.33s), the structure tends to attract much less acceleration than the infilled frames. This has a major influence on the estimated seismic performance and consequently the vulnerability and losses.

All in all, the observed sensitivity of the seismic loss evaluation and life cycle cost analysis indicates the necessity for accurate estimation of structural vulnerability and detailed regional seismic hazard assessment and exposure. Therefore, the analytical seismic fragility functions derived in this study can play a vital role in this assessment. The proposed functions include sufficient detailing in order to evaluate the probable damage and losses of infilled steel frame structures, with an acceptable level of precision.

Chapter 8 Conclusions & Future Research

8.1. Introduction

Monetary and human loss estimation, with an acceptable degree of precision, is a necessity for any disaster planning and management undertaking. In case of earthquake, vulnerability functions representing different structural typologies are employed to estimate the losses through measuring the probability and extent of structural and non-structural damage at various levels of ground shaking. However, as the seismic performance of structures are subjected to their arrangement and characteristics, distinct fragility and vulnerability functions are required for assessing buildings of different typologies. Lack of applicable seismic fragility and vulnerability functions has a negative effect on the precision of loss estimation and life cycle cost assessment.

Identifying the shortcoming of accessible and applicable seismic fragility and vulnerability functions for low- to mid-rise masonry infilled steel framed structures, this study focused on various aspects of numerical modelling and analytical assessment of these building types to generate such function, following a robust and reliable approach. A highly seismic region with a considerable presence of infilled steel frames was chosen as a case study for further vulnerability evaluation. Various modelling techniques and assessment methods were implemented to validate the most suitable approaches to evaluate the expected losses with an adequate level of accuracy under certain expected ground shakings and through the life span of the introduced index buildings.

This chapter presents a summary of the different tasks followed to address the aims and objectives of this research project and discusses the main findings and conclusions at each stage. Furthermore, a number of recommendations for further enhancement of this study are proposed.

8.2. Summary & Conclusions

Reviewing the available literature and post-earthquake damage observation on the seismic performance of masonry infilled steel framed structures, it is clear that these structures have

demonstrated a poor performance and far from expectations, under moderate to extreme seismic excitation. Further investigation suggests that the extent of damage can be correlated mainly to the response of masonry infill panel and the resultant composite system, which has a substantial impact on the global behaviour of the structure. However, generally in design and assessment stages of stated structures, the presence of infill panels is completely ignored and their influence is solely considered as permanent loading, distributed on their supporting beams.

Bearing in mind the extensive number of residential and commercial steel framed buildings, both existing and under construction, in countries with high seismicity, it is imperative to have a good understanding of their behaviour under various levels of seismic shaking. The seismic response of the structures can be evaluated through detailed numerical models, replicating various structural components including the infills, according to experimental observations. Utilising the measured seismic performance, fragility functions and subsequently vulnerability functions can be derived, both being vital components for seismic damage assessment, mitigation measures and disaster management. The accuracy of resultant vulnerability functions has a direct correlation to the precision of monetary and human loss estimation. Therefore, simplified methods that neglect the presence of highly influential structural features will result in over- or under-estimation of losses as well as the life cycle costs.

Hence, this study investigated the seismic performance, vulnerability and the expected losses of masonry infilled steel framed structures under various levels of seismic shaking. To demonstrate the importance of accurately modelling such features, the response outputs are compared to the ones of identical bare steel frames. The assessment is conducted through a methodology based on the performance-based seismic assessment (PBSA), following the concepts introduced by the Pacific Earthquake Engineering Research (PEER) Centre (Porter, 2003). To this end a number of stages are completed to address the defined objectives of the project.

The steel structures constructed in Iran have been chosen as the case study for this research. The high seismicity of the location as well as the extensive and emerging occurrence of steel framed structures in the construction industry for both residential and commercial purposes, made the selected location a unique case. Evidence of damaged steel framed structures in past earthquake events in different locations of the country, such as 2003 Bam (M_w 6.6) and 2017 Iran–Iraq (M_w 7.3) earthquake, have also highlighted the necessity of a comprehensive assessment. Different components of the outcomes can be utilised for strengthening interventions, improving the design codes, updating the seismic risk assessment and assist in disaster management and planning of the country.

Investigating the prevailing characteristics of existing and newly designed low- to mid-rise steel structures through detailed drawings, 33 index buildings have been defined. The buildings were generated by altering properties such as the structural system (moment resisting frame or simple gravity frame) and infill material (solid clay bricks or hollow clay blocks), as well as modifying the structural configuration (e.g. number of storeys, frames, bays) following the most common features identified. Finalising the structural arrangements and characteristics, each building was designed following the local practice and design codes through commercial software ETABS (v.2015). The code-based design approach neglects the impact of infills on strength, stiffness and ductility of the structure and the infills' contribution is solely considered as permanent loading on the beams. Additionally, a number of simulations were based on a real case mid-rise residential building, which is part of a government led campaign of large estate developments in the country and therefore represents a considerable number of steel framed buildings with identical specifications occurring in different seismically prone regions of the country. Hence, the defined index buildings represent well the stock of low- to mid-rise steel frame structures with distinctive seismic performance, either existing or currently being built in Iran, as well as other countries in the Middle-East.

The index buildings have been modelled using fibre-based finite element method in three dimensions, simulating the behaviour of different structural components such as the infill panels and composite semi-rigid beam-column connections. The software SeismoStruct (v.7.0.6) has been employed for modelling and nonlinear static and dynamic analysis of the buildings. The software is capable of evaluating large displacement behaviour of space frames, while taking into account both geometric nonlinearity and material inelasticity spread along the member's length and across the section's depth, allowing for accurate estimation of damage accumulation.

To replicate the infill panels' response under dynamic loading, a nonlinear macro model proposed by Crisafulli & Carr (2007) is implemented. The model comprises of six strut elements, accounting for the compressive and shear forces separately and can well simulate the most common failure modes identified for infilled steel frames (Shing & Mehrabi, 2002), including compressive failure, flexural cracking, toe crushing and shear failure of the infill panel. The infill material hysteresis has been calibrated with experimental studies conducted on solid clay brick (Tasnimi & Mohebkhah, 2011) and hollow clay blocks (R. Flanagan & Bennett, 1999), in both forms of solid panels and panels with window opening for higher precision. During the calibration process, the parameters defining the cyclic behaviour of the masonry material are studied in detail and for the most influentials, a sensitivity analysis has also been carried out. Accordingly, parameters such as the thickness of the panel, width and area of the struts before and after reaching the cracking strain and the equivalent contact length

between panel and frame are shown to have a high impact on the cyclic behaviour of the infill panel-frame system, and hence on the global structural response.

Furthermore, according to the collected data, composite semi-rigid beam-column connections are identified as the most common connection type. Therefore, instead of the more commonly assumed fully rigid connection, typically used in frame analysis, link elements have been implemented at every beam-column joint to more accurately replicate the response. The moment-rotation response of the links is defined based on an asymmetric elastic-plastic curve with isotropic hardening, calibrated according to experimental and parametric studies of ASCE (1998) and Leon & Bazzurro (2007). The simulation's output showed a clear difference in response between the rigid and semi-rigid connections, therefore the beam-column connections of the infilled steel frames were simulated accordingly.

The influence of different structural elements, such as the infill panels, bracings and joint connections have been studied through nonlinear static and dynamic analysis by altering the components' arrangement of the real case building. The results indicated a significant enhancement in initial stiffness and capacity of the structural system, due to the introduction of the infills and bracings. However, as the seismic shaking increases to a point at which the majority of the infill panels fail, a sudden and substantial drop in strength and stiffness is observed. The resulting damage modes of the frames' main components, in turn leads to a reduced reserve of ductility in comparison to the corresponding bare frame. This increase in stiffness, also causes the frequency of the structure to rise, attracting higher seismic excitation. The failure mechanism of the buildings has altered as well. In the bare steel frames, formation of plastic hinges in the beams and columns, have led to the failure of the structure, which is considered as a safe and desired scenario. However, in case of the infilled frames, the dominant failure is due to soft storey, triggered by failure of infill panels at one of the storeys. Comparing the seismic response of infilled and bare steel frames, under both static and dynamic loading, indicates that the vulnerability assessment of an infilled steel frame structures should not be conducted according to the response of an identical bare steel frames.

To evaluate the IM-EDPs and derive the seismic fragility functions, the performance of the building, both as infilled and as bare frame, has been computed by implementing four analysis methods with increasing levels of complexity and computational effort. The intention is to understand whether the infilled steel frames can be analysed through less computationally expensive capacity spectrum methods (N2 and FRACAS) or more advanced but time consuming and resource intensive nonlinear dynamic methods, such as cloud analysis (CLA) and multiple-stripe analysis (MSA), are required to reach an acceptable precision.

As demand, a suite of 150 single component earthquake records, selected from the database of world events of the SIMBAD ground motion database (Smerzini & Paolucci, 2013), are adopted and applied to the weaker direction of the index buildings. In case of bare frame, both methods resulted in close EDPs in terms of MIDR, where on general N2 has predicted higher values in 66% of the cases with an average error of 5%. On the contrary, the difference obtained for the infilled frames was considerably greater, as N2 estimated a higher EDP in 75% of the applied IMs, with an average error of 30%, mainly in the inelastic region. Comparing the obtained EDPs with the ones of CLA, despite the excellent agreement in the linear behaviour, in general an underestimation is observed in both structures, particularly for the infilled frame. In 65% of the events, N2 has miscalculated the MIDRs of the infilled frame (average error 27%, highest error 86%), while FRACAS has underestimated in 82% of the cases (average error 29%, highest error 89%). This issue is mainly due to the approach each method follows to estimate the inelastic spectrum utilising the idealised capacity curve.

To further investigate the precision of the simplified methods, the obtained IM-EDPs are employed to derive fragility functions for various damage states and compared to the ones of CLA. Additionally, the fragility functions obtained through MSA, utilising 22 scaled records of ATC-63 (FEMA P-695, 2009), are employed as bench marks. In general, although the simplified methods resulted in matching fragility curve to the ones of the CLA and MSA at lower intensities (i.e. slight damage), as the structure undergoes more inelastic deformation, the simplified methods start to underestimate the damage. In case of the infilled steel frame, comparing the median (μ) of the fragility curves, derived after MSA to the ones of the N2, a variation of 0.22g and 0.31g is noted for the extensive and complete damage states, while FRACAS has resulted in a difference of 0.60g and 0.46g for the same damage states. Furthermore, considering the dispersions obtained through the MSA, on average an error of 25% and 20% is obtained for the N2 and FRACAS, respectively. The resultant damage underestimation will clearly impact the seismic vulnerability and loss assessment, hence nonlinear dynamic methods are recommended for analysing infilled steel frames.

A critical limitation of the advanced methods is the extended duration of the analysis and the extensive computational power required. To overcome this issue, high-performance virtual cloud servers are employed, capable of parallel computing. Therefore, to have an accurate prediction of the seismic performance, while accounting for the record-to-record variability, the fragility functions of the index buildings are generated based on a widespread of about 1000 IM-EDPs obtained through the MSA.

A critical stage in deriving fragility functions is defining the damage states and indicating the thresholds accordingly. In lack of applicable damage states, for each of the 33 index buildings,

four damage states with corresponding thresholds were expressed in terms of inter-storey drift ratio while considering the composite behaviour of the infilled frame. The damage thresholds were based on the global behaviour of the structure as well as the experimental and numerical response of individual components. For instance, any shear failure of infill panels was monitored and correlated to the corresponding threshold. For better validation, the proposed thresholds are assessed on static pushover curves as well as the IM-EDP graph of both CLA and MSA. Comparing the defined thresholds to the ones suggested in guidelines such as HAZUS (2003), it is apparent that the limits are heavily case sensitive and simply categorising the buildings solely based on the height and their lateral resistance system is not sufficient and may lead to unreliable fragility functions.

Various fitting techniques are applied to the generated IM-EDPs to drive fragility functions for different damage states. As anticipated, exercising different fitting techniques including GLM (Basöz & Kiremidjian, 1998), least square (Baker, 2015) and maximum likelihood (Shinozuka et al., 2000), fragility functions with varied parameters were derived. For instance, for the infilled frame, a considerable disagreement was observed when applying GLM ($\mu_{Extensive}$= 1.27g, $\beta_{Extensive}$= 0.48) and least square ($\mu_{Extensive}$= 1.10g, $\beta_{Extensive}$= 0.54) techniques to the IM-EDPs of CLA, particularly for higher damage states (e.g. extensive and complete damage states), for which the number of IM-EDPs is modest and their dispersion is high. However, as the number of utilised IM-EDPs increases the observed diversion decreases. Utilising the mentioned fitting techniques on a large and well-distributed number of IM-EDPs obtained through MSA, the resultant fragility functions will have comparable properties with negligible variance. For this study, the fragility function parameters are evaluated through least square fitting technique proposed by Baker (2015). The method has a straightforward approach in evaluating the fragility functions for stripes of EDPs obtained for given IM values, which suites well with the MSA results.

Additionally, as the buildings were simulated in three-dimensional environment, in order to increase the accuracy of the seismic response, an investigation was conducted on how the earthquake components should be applied to the structure. Comparing the dynamic response of the structure when both components are applied concurrently to the case in which only a single component is applied to the weakest direction, a clear inconsistency is observed. Moreover, applying each ground motion component separately and later combining the results, as suggested in a number of codes (e.g. ASCE 41 (2013)), also showed inconsistency. For instance, an underestimation was observed when combining the responses of each direction through SRSS method with an estimated error of 20%. The observed discrepancy is particularly large in case of infill structures. Hence, to evaluate the performance of the defined index buildings, both components of the earthquake are applied concurrently, while the

component with the highest PGA being applied to the weakest direction of the structure, assuming a worst-case scenario. The impact of vertical component as well the directionality of the earthquake is neglected in this study.

The generated fragility functions are presented in terms of spectral acceleration at the fundamental period of the structure. Peak ground acceleration was shunned due to the poor correlation of performance and intensity attained during the analysis. The proposed index buildings comprise of a wide scale of initial periods, ranging from short periods mainly for stiffer infilled structures to long periods representing the taller bare steel frames with more flexibility. Hence, a direct comparison between the fragility functions obtained for identical bare and infilled steel frame is not viable. However, the expected monetary loss under intensities with certain return periods can highlight the obtained diversity between the bare and the infilled steel structures, as well as the impact of the structural quality.

To evaluate the seismic losses, the comprising components of performance based seismic assessment framework, including the seismic hazard, structural vulnerability and exposure need to be assessed and linked. To this end, the latest probabilistic seismic hazard assessment (PSHA) of the region under study is utilised to extract the most realistic expected seismic intensities and their probabilities, particularly, for four earthquake intensities with decreasing probabilities of exceedance, including the design-basis earthquake (DBE) (i.e. 475yr return period) and maximum considered earthquake (MCE) (i.e. 2475yr return period).

Focusing on the index building established after a real case infilled steel frame, three qualities of construction have been assumed and simulated. High-, mid- and low-quality buildings are defined by considering various combination in the structural components. This is achieved by altering three structural parameters; the beam-column connection types (rigid-, semi-rigid), masonry infill material (SCB, HCB) and the contribution of bracings to the seismic resistance of the structural system. Although a distinction is detected in their fundamental frequencies of vibration (f_{HighQ}=2.43Hz, f_{MidQ}=2.32Hz, f_{LowQ}=2.01Hz), in general all of the three buildings were still categorised under the same typology and expected performance. The distinctive seismic performance obtained, in terms of strength, stiffness and ductility, confirmed the importance of considering the probabilistic distribution of structural parameters and the sensitivity of response to the quality of material and construction.

The vulnerability functions of the stated buildings have been evaluated in terms of mean damage ratio (MDR), at various intensities of seismic excitation. As anticipated, the structure with the highest quality of construction had the best performance among all cases, with the lowest expected repair cost and subsequently MDR at any given intensity. For instance, in case of earthquakes with 10% probability of exceedance in 50-years (DBE), the MDR of high-

quality building was estimated at 21%. However, in contrary to expectations, the structure representing the lowest quality showed a better performance ($MDR_{LowQ@DBE}$=33%) than the one labelled as mid-quality building ($MDR_{MidQ@DBE}$=39%), resulting in lower estimation of seismic losses. In this case, having relatively close seismic responses and fragility functions, due to the lower fundamental period of the mid-quality structure ($T_{1,MidQ}$=0.43s), it attracted higher spectral accelerations than the low-quality building ($T_{1,LowQ}$=0.50s), which in return resulted in higher probability of damage and losses. This observation indicates the crucial role the seismic hazard characteristics of the region has on the estimated losses but also, very importantly how sensitive the vulnerability and seismic losses are to a small modification in the structural characteristics. For instance, the total repair cost (TRC) per unit area estimated for the high-quality building, under the DBE intensity ($31.60/m^2) was equal to 54% and 63% of the repair cost evaluated for the mid- ($58.56/m^2) and low-quality ($49.92/m^2) buildings, respectively. The same phenomena were observed in greater extent when comparing the MDR of the infilled and bare steel frames. For instance, under the DBE intensity, the MDR of a mid-rise bare frame ($T_{1,Bare\ Frame}$=1.33s, $S_a(T_1)$=0.27g) will underestimate the one of a typical mid-quality infilled frame ($T_{1,Infilled\ Frame}$=0.43s, $S_a(T_1)$=0.69g) by 16%.

Furthermore, three distribution scenarios were introduced (equal, expert opinion, conservative), each comprising a percentage of each of the stated structures to produce a population of 400 buildings. The estimated losses for each distribution under various earthquake intensities are compared to a case in which all 400 buildings are assumed to behave as a bare steel frame. In all considered cases, the bare steel frames under estimated the losses. For instance, for an earthquake with 10% probability of exceedance in 50-years, the TRC of 400 bare steel frames, underestimated the TRC of the distributed scenarios by about 27%. The obtained results indicate the significant influence of detailing in modelling and realistic knowledge of exposure on the seismic loss estimation. Hence, utilising a fragility function specifically developed for a bare steel frame for the case of an infilled steel frame can be hazardous and should be avoided in case of any seismic design and risk assessment.

In addition to seismic loss estimation under explicit ground shakings, the expected damage during the 50-year service life of the infilled steel frame is investigated. Having a rational forecast of structure's life cycle cost can assist in financial resource allocation and repair forecasting. The predicted life cycle cost considered two cases: accounting for the repair cost, loss of content, loss of rental cost as well as including or excluding serious and minor injury costs, and human fatality. In both cases, a similar observation to the vulnerability and loss assessment is obtained, with the mid-quality building having the highest cost among all cases, while the high-quality and the bare steel frame having the lowest life cycle cost. Similar to the

vulnerability cases, the reason why bare frame showed a better performance than the mid- and low-quality infilled frames, is due to its higher fundamental period of vibration ($T_{1,Bare\ Frame}$=1.33s), thus the structure tends to attract much less acceleration than the infilled frames (T_1≈0.40s).

All in all, although the presence of infill panels improves the capacity of the steel structure, however the resultant raise in stiffness will drop the fundamental period of vibration, which may force the building to attract higher intensities. Therefore, assessing the building as a bare steel frame will result in a miscalculation of the seismic response and consequently an underestimation in the seismic vulnerability and loss estimation, as part of the performance-based seismic assessment. The generated fragility functions can enrich the inadequate collection of existing functions devoted to bare and infilled steel frame building, while addressing the stated issues. The fragility functions are of great importance for insurance valuation, as well as pre- and post-disaster management. Moreover, the implementation of the proposed methodology and the observations can improve the Global Earthquake Model (GEM) guideline on analytical vulnerability assessment, as this structural typology is not considered explicitly (D'Ayala et al., 2015b).

8.3. Recommendations for Future Work

- For the region under study, 33 index buildings were defined following the most common structural features, covering a good proportion of existing and newly designed buildings. However, majority of index buildings did not include any irregularity in plan and height. Furthermore, the distribution of infill walls in both case of solid and with window opening have been mainly symmetric. Certainly, structures with diverse irregularities and component arrangement exist, which will result in different seismic performance and failure mechanism. Hence, depending on the importance of the building, the impact of these irregularities and various configurations should be considered in the assessment.
- In the selection process of the earthquake records for this assessment, the intention was to have suites which can embrace a wider range of sites with different seismic characteristics. Hence, for assessing a structure in a particular location, it is recommended to select hazard-compatible ground motions.
- As the index buildings were simulated in a three-dimensional environment, both components of the earthquake were applied concurrently. However, the directionality of the earthquake was not considered in this procedure and the components were implemented perpendicular to the axis of the structure. Therefore, the response of the structure may degrade as the components are applied at different directions. Several

studies have investigated the effect of directionality, their finding may improve the modelling approach.

- Two of the commonly used masonry infill panels, solid clay brick and hollow clay blocks, were simulated and calibrated based on available experimental data of the region under study. Having access to experimental observations of masonry material with other characteristics may result in different response and subsequently altered vulnerability.
- Although in case of infilled steel frames the shear failure of the surrounding frame does not occur frequently, however, the implemented infill's macro model (Crisafulli & Carr, 2007) cannot fully identify and distinguish this failure. Therefore, in cases for which the shear failure of the frame is expected, micro models should be implemented to fully capture this deficiency.

8.4. Final Remarks

In conclusion, despite the limitation and the future challenges outlined above, this research has shown the importance and sensitivity of detailed seismic fragility and vulnerability functions in both loss and life cycle cost assessment of low- to mid-rise infilled and bare steel frame structures. The methodology followed in this study can be implemented to assess a population of buildings with different qualities of construction, while having the same typology.

References

Abdi, F., Mirzaei, N., Shabani, E., 2013. Ground-motion scenarios consistent with PSH deaggregation for Tehran, capital city of Iran. Nat. Hazards Earth Syst. Sci. 13, 679–688.

Abrahamson, N.A., Silva, W.J., 1997. Empirical response spectral attenuation relationships for shallow crustal earthquakes. Seismol. Res. Lett. 68, 94–127.

Al-Chaar, G., Issa, M., Sweeney, S., 2002. Behavior of Masonry-Infilled Nonductile Reinforced Concrete Frames. J. Struct. Eng. 128, 1055–1063.

Al Mamun, A., Saatcioglu, M., 2017. Seismic fragility curves for reinforced concrete frame buildings in Canada designed after 1985. Can. J. Civ. Eng. 44, 558–568.

Alam, N., Alam, M.S., Tesfamariam, S., 2012. Buildings' seismic vulnerability assessment methods: A comparative study. Nat. Hazards 62, 405–424.

Albayrak, U., Ünlüoğl, E., Doğan, M., 2017. An Overview of the Modelling of Infill Walls in Framed Structures. Int. J. Struct. Civ. Eng. Res. 6, 24–29.

Ambraseys, N.N., Melville, C.P., 1982. A History of Persian Earthquakes. Cambridge Univ. Press 139–167.

Andisheh, K., Amiri, G.G., 2010. Evaluation of Iranian Code No.2800 for Seismic Resistant Design of Near Source Buildings Based on Real Record of Iran, in: International Conferences on Recent Advances in Geotechnical Earthquake Engineering and Soil Dynamics. Missouri University of Science and Technology Scholars' Mine, Missouri.

Andreaus, U., Cerone, M., D'Asdia, P., Iannozzi, F., 1985. A finite element model for the analysis of masonry structures under cyclic actions. Int. brick Mason.

Angel, R., Abrams, D., Shapiro, D., Uzarski, J., Webster, M., 1994. Behavior of reinforced concrete frames with masonry infills.

ANSI/AISC 360-10, 2010. Specification for Structural Steel Buildings. Chicago, Illinois.

Ariyaratana, C., Fahnestock, L.A., 2011. Evaluation of buckling-restrained braced frame seismic performance considering reserve strength. Eng. Struct. 33, 77–89.

ASCE/SEI 41-13, 2013. Seismic Evaluation and Retrofit of Existing Buildings. American Society of Civil Engineers, Reston, Virginia - United States of America.

ASCE/SEI 7-10, ASCE 7-16, 2013. Minimum Design Loads for Buildings and Other Structures. American Society of Civil Engineers, Reston, VA.

Aschheim, M., Gülkan, P., Sezen, H., Bruneau, M., Elnashai, A., Halling, M., Love, J., Rahnama, M., 2000. Performance of Buildings. Earthq. Spectra 16, 237–279.

Asgarian, B., Ordoubadi, B., 2016. Effects of structural uncertainties on seismic performance of steel moment resisting frames. J. Constr. Steel Res. 120, 132–142.

Asgarian, B., Sadrinezhad, A., Alanjari, P., 2010. Seismic performance evaluation of steel moment resisting frames through incremental dynamic analysis. J. Constr. Steel … 66, 178–190.

Asteris, P.G., 2008. Finite element micro-modeling of infilled frames. Electron. J. Struct. Eng. 8, 1–11.

Asteris, P.G., 2003. Lateral Stiffness of Brick Masonry Infilled Plane Frames. J. Struct. Eng. 129, 1071–1079.

Asteris, P.G., Kakaletsis, D.J., Chrysostomou, C.Z., Smyrou, E.E., 2011. Failure Modes of Infilled Frames. J. Struct. Eng. 11, 11–20.

ASTM C10-07, 2007. Standard Specification for Natural Cement.

ASTM C1314-10, 2010. Standard Test Method for Compressive Strength of Masonry Prisms. ASTM Int. 1–10.

ASTM E-2026, 1999. Standard Guide for the Estimation of Building Damageability in Earthquakes.

Astriana, L., Sangadji, S., Purwanto, E., Kristiawan, S.A., 2017. Assessing Seismic Performance of Moment Resisting Frame and Frame-shear Wall System Using Seismic Fragility Curve, in: Procedia Engineering. pp. 1069–1076.

ATC-13, 1985. Earthquake Damage Evaluation Data for California. Appl. Technol. Counc.

ATC-40, 1996. Seismic Evaluation and Retrofit of Concrete Buildings 1, 612.

ATC-58, 2012. Seismic Performance Assessment of Buildings - Volume 1 - Methodology - P-58. Federal_Emergency_Management_Agency, Redwood City, California.

Atlayan, O., Charney, F.A., 2014. Hybrid buckling-restrained braced frames. J. Constr. Steel Res. 96, 95–105.

Badpay, A., Arbabi, F., 2008. A Comparison of Seismic Performance and Vulnerability of Buckling Restrained and Conventional Steel Braced Frames. Response.

Baker, J.W., 2015. Code supplement to efficient analytical fragility function fitting using dynamic structural analysis. Earthq. Eng. Res. Inst. 31, 579–599.

Baker, J.W., 2007. Probabilistic structural response assessment using vector-valued intensity measures. Earthq. Eng. Struct. Dyn.

Bayraktar, A., Altunişik, A.C., Pehlivan, M., 2013. Performance and damages of reinforced concrete buildings during the October 23 and November 9, 2011 Van, Turkey, earthquakes. Soil Dyn. Earthq. Eng. 53, 49–72.

Bennett, R.M., Boyd, K.A., Flanagan, R.D., 1997. Compressive Properties of Structural Clay Tile Prisms. J. Struct. Eng. 123, 920–926.

Berberian, M., 2014. Earthquakes and coseismic surface faulting on the Iranian Plateau : a historical, social and physical approach.

Bertogg, M., Hitz, L., Schmid, E., 2002. Vulnerability Functions derived from loss data for insurance risk modelling: findings from recent earthquakese, in: 12th European Conference on Earthquake Engineering.

BHRC, 2007. Iranian code of practice for seismic resistant design of buildings, standard No. 2800 (4th edition). Building and Housing Research Center, Tehran - IRAN.

Biondini, F., Frangopol, D.M., 2016. Life-Cycle Performance of Deteriorating Structural

Systems under Uncertainty: Review. J. Struct. Eng. 142, F4016001.

Bommer, J.J., Aceved, A.B., 2004. The use of real earthquake accelerograms as input to dynamic analysis. J. Earthq. Eng. 8, 43–91.

Boore, D.M., Atkinson, G.M., 2008. Ground-motion prediction equations for the average horizontal component of PGA, PGV, and 5%-damped PSA at spectral periods between 0.01 s and 10.0 s. Earthq. Spectra 24, 99–138.

Boore, D.M., Joyner, W.B., Fumal, T.E., 1997. Equations for Estimating Horizontal Response Spectra and Peak Acceleration from Western North American Earthquakes: A Summary of Recent Work. Seismol. Res. Lett. 68, 128–153.

Braconi, A., Bursi, O.S., Fabbrocino, G., Salvatore, W., Tremblay, R., 2008. Seismic performance of a 3D full-scale high-ductility steel-concrete composite moment-resisting structure-Part I: Design and testing procedure. Earthq. Eng. Struct. Dyn. 37, 1609–1634.

Braconi, A., Salvatore, W., Tremblay, R., Bursi, O.S., 2007. Behaviour and modelling of partial-strength beam-to-column composite joints for seismic applications. Earthq. Eng. Struct. Dyn. 36, 142–161.

Braga, F., Manfredi, V., Masi, A., Salvatori, A., Vona, M., 2011. Performance of non-structural elements in RC buildings during the L'Aquila, 2009 earthquake. Bull. Earthq. Eng. 9, 307–324.

Brando, G., Rapone, D., Spacone, E., Barbosa, A., Olsen, M., Gillins, D., Soti, R., Varum, H., Arede, A., Vila-Pouca, N., Furtado, A., Oliveira, J., Rodrigues, H., Stavridis, A., Bose, S., Faggella, M., Gigliotti, R., Wood, R.L., 2015. Reconnaissance report on the 2015 Gorkha earthquake effects in Nepal. XVI Convegno Anidis.

Bruneau, M., Chang, S.E., Eguchi, R.T., Lee, G.C., O'Rourke, T.D., Reinhorn, A.M., Shinozuka, M., Tierney, K., Wallace, W.A., Von Winterfeldt, D., 2003. A Framework to Quantitatively Assess and Enhance the Seismic Resilience of Communities. Earthq. Spectra.

Brunesi, E., Nascimbene, R., Parisi, F., Augenti, N., 2015. Progressive collapse fragility of reinforced concrete framed structures through incremental dynamic analysis. Eng. Struct. 104, 65–79.

Brzev, S., Anderson, D.L., Mcewen, W., Sturgeon, G., 2009. HIGHLIGHTS OF THE SEISMIC DESIGN GUIDE FOR MASONRY, in: 11th Canadian Masonry Symposium. Toronto, Ontario.

Brzev, S., Scawthorn, C., Charleson, A.W., Allen, L., Greene, M., Jaiswal, K., Silva, V., 2013. GEM Building Taxonomy Version 2.0. GEM Tech. Rep. 02, 188.

BS EN 1998-3, 2005. Eurocode 8 : Design of structures for earthquake resistance - Part 3: Assessment and retrofitting of buildings. Brussels.

Buonopane, S.G., White, N., White, R.N.R.N., White, N., White, R.N.R.N., 1999. Pseudodynamic testing of masonry infilled reinforced concrete frame. J. Struct. Eng. 125, 578–589.

Calvi, G.M., Pinho, R., 2006. Development of seismic vulnerability assessment methodologies over the past 30 years. ISET J. {…} 43, 75–104.

Campbell, K.W., Bozorgnia, Y., 2008. NGA ground motion model for the geometric mean horizontal component of PGA, PGV, PGD and 5% damped linear elastic response spectra for periods ranging from 0.01 to 10 s. Earthq. Spectra 24, 139–171.

Campbell, K.W., Bozorgnia, Y., 2002. Mutually consistent near-source attenuation relations

for the horizontal and vertical components of PGA and acceleration response spectra. Bull. Seismol. Soc. Am. Submitt. 93, 314–331.

Cărăuşu, A., Vulpe, A., 1996. Fragility estimation for seismically isolated nuclear structures by high confidence low probability of failure values and bi-linear regression. Nucl. Eng. Des. 160, 287–297.

Cardone, D., Perrone, G., 2015. Developing fragility curves and loss functions for masonry infill walls. Earthq. Struct. 9, 257–279.

Carr, A.J., 2007. Ruaumoko.

Casotto, C., Silva, V., Crowley, H., Nascimbene, R., Pinho, R., 2015. Seismic fragility of Italian RC precast industrial structures. Eng. Struct. 94, 122–136.

Ceresa, P., Petrini, L., Pinho, R., 2007. Flexure-shear fiber beam-column elements for modeling frame structures under seismic loading - State of the art. J. Earthq. Eng. 11, 46–88.

Cherng, R.-H., 2001. Preliminary Study on the Fragility Curves for Steel Structures in Taipei. Earthq. Eng. Eng. Seismol. 3, 35–42.

Chiou, B.-J., Youngs, R.R., 2008. An NGA Model for the Average Horizontal Component of Peak Ground Motion and Response Spectra. Earthq. Spectra.

Chrysostomou, C., Gergely, P., Abel, J., 1990. Preliminary studies of the effects of degrading infill walls on the nonlinear seismic response of steel frames, in: The Fourth U.S. National Conference on Earthquake Engineering. pp. 229–238.

Chrysostomou, C.Z., Gergely, P., Abel, J.F., 2002. A six-strut model for nonlinear dynamic analysis of steel infilled frames. Int. J. Struct. Stab. Dyn. 02, 335–353.

Clough, R.W., Benuska, K.L., 1967. Nonlinear earthquake behavior of tall buildings. J. Eng. Mech. Div. 93, 129--146.

Colangelo, F., 2005. Pseudo-dynamic seismic response of reinforced concrete frames infilled with non-structural brick masonry. Earthq. Eng. Struct. Dyn. 34, 1219–1241.

Computers & Structures Inc., 2016. CSI ETABS v.2015. SAP2000 Ref. Man.

Correia, A.A., Virtuoso, F.B.E., 2006. Nonlinear analysis of space frames, in: III European Conference on Computational Mechanics. Springer Netherlands, Dordrecht, p. 107.

Cortés-Areizaga, G., López-Rodríguez, R., Saffar, A., 2006. Earthquake Induced Damage Estimation In Steel Buildings. Fourth LACCEI Int. Lat. Am. Caribb. Conf. Eng. Technol. 21–23.

Cosenza, E., Monti, G., 2009. Assessment and reduction of the vulnerability of existing reinforced concrete buildings. state Earthq. Eng. Res. Italy 51–110.

Crisafulli, F., Carr, A., 2007. Proposed macro-model for the analysis of infilled frame structures. Bull. New Zeal. Soc. Earthq. Eng.

Crisafulli, F.J., 1997. Seismic behaviour of reinforced concrete structures with masonry infills.

Crisafulli, F.J., Carr, A.J., Park, R., 2000. Analytical Modelling og infilled Frame Structures - A General Review. Bull. New Zeal. Soc. Earthq. Eng. 33, 30–47.

D'Aniello, M., La Manna Ambrosino, G., Portioli, F., Landolfo, R., 2012. The effect of different modelling approach on seismic analysis of steel concentric braced frames. 15th World Conf. Earthq. Eng.

D'Ayala, D., Meslem, A., Vamvatsikos, D., Porter, K., Rossetto, T., Crowley, H., Silva, V., 2015. Guidelines for Analytical Vulnerability Assessment of Low/Mid-Rise Buildings, GEM Technical Report.

D'Ayala, D., Worth, J., Riddle, O., 2009. Realistic shear capacity assessment of infill frames: Comparison of two numerical procedures. Eng. Struct. 31, 1745–1761.

D'Ayala, D.F., Meslem, A., Vamvatsikos, D., Porter, K.A., Rossetto, T., Crowley, H., Silva, V., 2014. Guidelines for analytical vulnerability assessment of low/mid-rise buildings - methodology, Vulnerability Global Component project.

Dawe, J.L., Seah, C.K., 1989a. Behaviour of masonry infilled steel frames. Can. J. Civ. Eng. 16, 865–876.

Dawe, J.L., Seah, C.K., 1989b. Out-of-plane resistance of concrete masonry infilled panels. Can. J. Civ. Eng. 16, 854–864.

Dawe, J.L., Seah, C.K., Liu, Y., 2001. A computer model for predicting infilled frame behaviour. Can. J. Civ. Eng. 28, 133–148.

De Luca, F., Vamvatsikos, D., Iervolino, I., 2013. Near-optimal piecewise linear fits of static pushover capacity curves for equivalent SDOF analysis. Earthq. Eng. Struct. Dyn. 42, 523–543.

Decanini, L., Fantin, G., 1986. Modelos simplificados de la mamposteria incluida en porticos. Caracteristicas de rigidez y resistencia lateral en estado limite. Jornadas Argentinas Ing. Estructural.

Deierlein, G.G., Krawinkler, H., Cornell, C.A., 2003. A framework for performance-based earthquake engineering, in: 2003 Pacific Conference on Earthquake Engineering. pp. 140–148.

Deierlein, G.G., Reinhorn, A.M., Willford, M.R., Charney, F.A., 2010. Nonlinear Structural Analysis For Seismic Design: A Guide for Practicing Engineers. Gaithersburg.

DesRoches, J.D., Padgett, J.E., 2012. Sensitivity Study of Design Parameters Used to Develop Bridge Specific Fragility Curves. 15th World Conf. Earthq. Eng.

DIN 1025-5, 1994. Hot rolled I-beams; medium flange I-beams, IPE-serie; dimensions, masses, sectional properties.

DIN EN 10025-1, 2004. Hot rolled products of structural steels— Part 1: General technical delivery conditions.

DIN EN 10210-1, 2006. Hot finished structural hollow sections of non-alloy and fine grain steels - Part 1: Technical delivery conditions.

Dolšek, M., Fajfar, P., 2008. The effect of masonry infills on the seismic response of a four-storey reinforced concrete frame — a deterministic assessment. Eng. Struct. 30, 1991–2001.

Dolšek, M., Fajfar, P., 2001. Soft storey effects in uniformly infilled reinforced concrete frames. J. Earthq. Eng. 5, 12.

Doudoumis, I., Mitsopoulou, E., 1986. Non-linear analysis of multistorey infilled frames for unilateral contact conditions, in: Proc., 8th European Conf. on Earthquake Engineering (EAEE). Istanbul, Turkey.

Eads, L., Miranda, E., Krawinkler, H., Lignos, D.G., 2013. An efficient method for estimating the collapse risk of structures in seismic regions. Earthq. Eng. Struct. Dyn. 42, 25–41.

El-Dakhakhni, W.W., 2004. Seismic retrofit of concrete-masonry-infilled steel frames with glass fiber-reinforced polymer laminates. J. Struct. Eng. 1343–1352.

El-Dakhakhni, W.W., 2002. Experimental and analytical seismic evaluation of concrete masonry-infilled steel frames retrofitted using GFRP laminates.

El-Dakhakhni, W.W., Elgaaly, M., Hamid, A.A., 2003. Three-Strut Model for Concrete Masonry-Infilled Steel Frames. J. Struct. Eng. 129, 177–185.

El-Dakhakhni, W.W., Hamid, A.A., Elgaaly, M., 2004. Strength and stiffness prediction of masonry infill panels. 13WCEE.

Elefante, L., Jalayer, F., Iervolino, I., Manfredi, G., 2010. Disaggregation-based response weighting scheme for seismic risk assessment of structures. Soil Dyn. Earthq. Eng. 30, 1513–1527.

Ellul, F., D'Ayala, D., 2012. Realistic FE models to enable push-over non linear analysis of masonry infilled frames. Open Constr. Build. Technol. J. 6, 213–235.

Ellul, F., D'Ayala, D., 2008. Push-over non linear analysis of infilled frames: realistic FE models of panels and contact. 14WCEE.

Erberik, M.A., 2008. Fragility-based assessment of typical mid-rise and low-rise RC buildings in Turkey. Eng. Struct. 30, 1360–1374.

Erdikt, M., Aydinoglu, N., Fahjan, Y., Sesetyan, K., Demircioglu, M., Siyahi, B., Durukal, E., Ozbey, C., Biro, Y., Akman, H., Yuzugullu, O., 2003. Earthquake risk assessment for Istanbul metropolitan area 2.

Faizian, M., Ishiyama, Y., 2004. Comparison of Seismic Codes of 1981 Japan (BSLJ), 2000 USA (IBC) and 1999 Iran (ICS), in: 13WCEE.

Fajfar, P., 2000. A Nonlinear Analysis Method for Performance-Based Seismic Design. Earthq. Spectra 16, 573–592.

Fajfar, P., Krawinkler, H., 2004. Performance-based seismic design concepts and implementation, Pacific Earthquake Engineering Research Center (PEER).

Fardis, M.N., 2009. Seismic design, assessment and retrofitting of concrete buildings: Based on EN-Eurocode8. Geotech. Geol. Earthq. Eng. 8, 1–735.

Fardis, M.N., 1996. Experimental and numerical investigations on the seismic response of RC infilled frames and recommendations for code provisions.

Fardis, M.N., Negro, P., Bousias, S.N., Colombo, A., 1999. Seismic design of open-storey infilled RC buildings. J. Earthq. Eng. 3, 173–197.

Farsangi, E.N., Rezvani, F.H., Talebi, M., Hashemi, S.A.H., 2014. Seismic Risk Analysis of Steel-MRFs by Means of Fragility Curves in High Seismic Zones. Adv. Struct. Eng. 17, 1227–1240.

FEMA-224, 1991. Seismic Vulnerabilityand Impact of Disruption of Lifelines in the Conterminous United States.

FEMA-227, 1992. A Benefit-Cost Model for the Seismic Rehabilitation of Buildings. Washington D.C.

FEMA-273, 1997. NEHRP guidelines for the seismic rehabilitation of buildings.

FEMA-306, 1998. Evaluation of earthquake damaged concrete and masonry wall buildings (ATC-43 Project).

FEMA-350, 2000. FEMA-350: Recommended seismic design criteria for new steel moment frame buildings.

FEMA-356, 2000. FEMA-356: Prestandard and Commentary for the Seismic Rehabilitation of Buildings. Rehabil. Requir. 1–518.

FEMA-P-58, 2012. Seismic Performance Assessment of Buildings - methodology.

FEMA P-1050, 2015. FEMA P-1050-1: NEHRP Seismic Provisions for New Buildings and Other Structures. Washington D.C.

FEMA P-695, 2009. FEMA P-695: Quantification of Building Seismic Performance Factors.

FEMA P-751, 2012. 2009 NEHRP Recommended Seismic Provisions: Design Examples. Washington, D.C.

Fernandez-Davila, I., Cominetti, S., F Cruz, E., 2000. Considering the Bi-Directional Effects and the Seismic Angle. 12WCEE.

Filippou, F., Popov, E., Bertero, V., 1983. Effects of Bond Deterioration on Hysteretic Behaviour of Reinforced Concrete Joints. Report to the National Science Foundation, Earthquake Engineering Research Center.

Fiore, a., Porco, F., Raffaele, D., Uva, G., 2012. About the influence of the infill panels over the collapse mechanisms actived under pushover analyses: Two case studies. Soil Dyn. Earthq. Eng. 39, 11–22.

Flanagan, R., Bennett, R., 1999. Bidirectional behavior of structural clay tile infilled frames. J. Struct. Eng. 125, 236–244.

Flanagan, R.D., 1994. Behavior of structural clay tile infilled frames. Oak Ridge, TN.

Flanagan, R.D., Bennett, R.M., 2001. In-Plane Analysis of Masonry Infill Materials. Pract. Period. Struct. Des. Constr. 6, 176–182.

Flanagan, R.D., Bennett, R.M., 1999. Arching of Masonry Infilled Frames: Comparison of Analytical Methods. Pract. Period. Struct. Des. Constr. 4, 105–110.

Flanagan, R.R.D., Jones, W.W.D., Bennett, R.R.M., 1991. Analytical modeling of masonry infilled steel frames.

Frangopol, B.D.M., Kong, J.S., Gharaibeh, E.S., 2001. Reliability -Based Life -Cycle Management. J. Comput. Civ. Eng. 27–34.

Furtado, A., Rodrigues, H., Arêde, A., Engineering, H.V.-P., 2015, U., 2015. Influence of the in plane and out-of-plane masonry infill walls' interaction in the structural response of RC buildings. Procedia Eng. 114, 722–729.

Ganjavi, B., Amiri, G.G., 2018. A COMPARATIVE STUDY OF OPTIMUM AND IRANIAN SEISMIC DESIGN FORCE DISTRIBUTIONS FOR STEEL MOMENT RESISTING BUILDINGS. Int. J. Optim. Civ. Eng. Int. J. Optim. Civ. Eng 8, 54.

Gardoni, P., Der Kiureghian, A., Mosalam, K.M., 2002. Probabilistic Capacity Models and Fragility Estimates for Reinforced Concrete Columns based on Experimental Observations. J. Eng. Mech. 128, 1024–1038.

Gehl, P., Douglas, J., Seyedi, D.M., 2015. Influence of the number of dynamic analyses on the accuracy of structural response estimates. Earthq. Spectra 31, 97–113.

Gergely, P., White, R., Zawilinski, D., 1993. The interaction of masonry infill and steel or concrete fames. Natl. Earthq. Conf.

Gholipour, Y., Bozorgnia, Y., Rahnama, M., Berberian, M., Shojataheri, J., 2008. Probabilistic Seismic Hazard Analysis Phase I- Greater Tehran Region Final Report. Fac. Eng. Univ. Tehran.

Giberson, M.F., 1967. The Response of Nonlinear Multi-story Structures Subjected to Earthquake Excitation. Calif. Inst. Technol. Pasadena, CA.

Gneyisi, E.M., Güneyisi, E.M.M., Gneyisi, E.M., Güneyisi, E.M.M., 2012. Seismic reliability of steel moment resisting framed buildings retro fi tted with buckling restrained braces. Earthq. Eng. Struct. Dyn. 41, 853–874.

Gomez, L., 2014. Seismic Fragility Analysis of Steel Moment-Resisting Frames (MRF) Designed in Canada in the 1960s , 1980s , and 2010.

Guéguen, P., Michel, C., Lecorre, L., 2007. A simplified approach for vulnerability assessment in moderate-to-low seismic hazard regions: Application to Grenoble (France). Bull. Earthq. Eng. 5, 467–490.

Güneyisi, E.M., Altay, G., 2008. Seismic fragility assessment of effectiveness of viscous dampers in R/C buildings under scenario earthquakes. Struct. Saf. 30, 461–480.

Hajjar, J., Leon, R., 1998. Seismic response of composite moment-resisting connections. II: Behavior. J. Struct. Eng. 877–885.

HAZUS-MH MR4, 2003. HAZUS-MH MR4 Technical Manual. Natl. Inst. Build. Sci. Fed. Emerg. Manag. Agency (NIBS FEMA) 712.

Helmut Krawinkler, G.D.P.K.S., 1998. Pros and cons of a pushover analysis of seismic performance evaluation. Eng. Struct. 20, PP.452-464.

Hill, M.P., Rossetto, T., 2008. Do Existing Damage Scales Meet The Needs Of Seismic Loss Estimation? 14th World Conf. Earthq. Eng. 6, 335–365.

Holmes, M., 1961. Steel frames with brickwork and concrete infilling. Civ. Eng. Inst. Technol. Bradford 19, 473–478.

Ibarra, L.F., Medina, R.A., Krawinkler, H., 2005. Hysteretic models that incorporate strength and stiffness deterioration. Earthq. Eng. Struct. Dyn. 34, 1489–1511.

Iervolino, I., Cornell, C.A., 2005. Record selection for nonlinear seismic analysis of structures. Earthq. Spectra 21, 685–713.

Ilki, A., Girgin, K., Barbat, A.H., 2007. Guidelines for seismic vulnerability reduction in the urban environment. LESSLOSS report No. Lessloss-2007/07 333.

Imashi, N., Massumi, A., 2011. A comparative study of the seismic provisions of Iranian seismic code (Standard No. 2800) and International Building Code 2003. Asian J. Civ. Eng. 12, 579–598.

INBC, 2013a. Iranian National Building Code (INBC), Part 6: Minimum Design Loads for Buildings (3rd edition). Tehran - IRAN.

INBC, 2013b. Iranian National Building Code (INBC), Part 10: Steel Structures (4th edition). Tehran - IRAN.

Ioannou, I., Borg, R., Novelli, V., Melo, J., Alexander, D., Verucci, E., Cahill, B., Rossetto, T., 2012. The 29th May 2012 Emilia Romagna Earthquake, EPICentre Field Report.

Jalayer, F., 2003. Direct probabilistic seismic analysis: implementing non-linear dynamic assessments. Stanford Univ.

Jalayer, F., Cornell, C.A., 2009. Alternative non-linear demand estimation methods for

probability-based seismic assessments. Earthq. Eng. Struct. Dyn. 38, 951–972.

Jalayer, F., Ebrahimian, H., Miano, A., Manfredi, G., Sezen, H., 2017. Analytical fragility assessment using unscaled ground motion records. Earthq. Eng. Struct. Dyn. 46, 2639–2663.

Jazany, R.A., Hajirasouliha, I., Farshchi, H., 2013. Influence of masonry infill on the seismic performance of concentrically braced frames. J. Constr. Steel Res. 88, 150–163.

JICA, 2000. The study on microzoning of the Greater Tehran Area in the I. R. of Iran, final report, Tehran, Iran.

Kappos, A., Pitilakis, K., Stylianidis, K., Morfidis, K., Asimakopoulos, D., 1995. Cost-benefit analysis for the seismic rehabilitation of buildings in Thessaloniki, based on a hybrid method of vulnerability assessment. Proc. 5th Int. Conf. Seism. Zo. Nice 1, 406–413.

Katsanos, E.I., Sextos, A.G., Manolis, G.D., 2010. Selection of earthquake ground motion records: A state-of-the-art review from a structural engineering perspective. Soil Dyn. Earthq. Eng.

Kaushik, H.B., Rai, D.C., Jain, S.K., 2006. Code Approaches to Seismic Design of Masonry-Infilled Reinforced ConcreteFrames: A State-of-the-Art Review. Earthq. Spectra 22, 961–983.

Kazantzi, a. K., Righiniotis, T.D., Chryssanthopoulos, M.K., 2011. A Simplified Fragility Methodology for Regular Steel MRFs. J. Earthq. Eng. 15, 390–403.

Kazantzi, A.K., Vamvatsikos, D., Lignos, D.G., 2014. Seismic performance of a steel moment-resisting frame subject to strength and ductility uncertainty. Eng. Struct. 78, 69–77.

Kazemi, H., Ghafory-ashtiany, M., Azarbakht, A., 2013. Effect of epsilon-based record selection on fragility curves of typical irregular steel frames with concrete shear walls in Mashhad city. Int. J. Adv. Struct. Eng. 5.

Kelly, T.E., Chambers, J.D., 2000. Analysis Procedures for Performanced Based Design. 12th World Conf. Earthq. Eng. 1–8.

Keyvani Boroujeni, A.R., Sadeghazar, M., 2008. Evaluation of Iranian seismic guidelines: Case study of special steel moment frames. Sci. Iran. 15, 50–55.

Kiani, A., Mansouri, B., Moghadam, A.S., 2016. Fragility curves for typical steel frames with semi-rigid saddle connections. J. Constr. Steel Res. 118, 231–242.

Kinali, K., Ellingwood, B.R., 2007. Seismic fragility assessment of steel frames for consequence-based engineering: A case study for Memphis, TN. Eng. Struct. 29, 1115–1127.

Klingner, R., Bertero, V., 1976. Infilled frames in earthquake-resistant construction.

Koutromanos, I., Stavridis, A., Shing, P.B., Willam, K., 2011. Numerical modeling of masonry-infilled RC frames subjected to seismic loads. Comput. Struct. 89, 1026–1037.

Krawinkler, H., Miranda, E., 2004. Performance-Based Earthquake Engineering, in: Earthquake Engineering from Engineering Seismology to Performance-Based Engineering. p. 976.

Kumar, S.R.S., Smitha, M.S., 2013. Steel–concrete composite flange plate connections: Cyclic performance and tests. J. Constr. Steel Res. 82, 216–222.

Kwon, O.S., Elnashai, A., 2006. The effect of material and ground motion uncertainty on the

seismic vulnerability curves of RC structure. Eng. Struct. 28, 289–303.

Lagaros, N.D., 2007. Life-cycle cost analysis of design practices for RC framed structures. Bull. Earthq. Eng. 5, 425–442.

Lagaros, N.D., Fragiadakis, M., Papadrakakis, M., Tsompanakis, Y., 2006. Structural optimization: A tool for evaluating seismic design procedures. Eng. Struct. 28, 1623–1633.

Lagaros, N.N.D.N., 2010. Multicomponent incremental dynamic analysis considering variable incident angle. Struct. Infrastruct. Eng. 6, 77–94.

Lallemant, D., Kiremidjian, A., Burton, H., 2015. Statistical procedures for developing earthquake damage fragility curves. Earthq. Eng. Struct. Dyn. 44, 1373–1389.

Lang, K., 2002. Seismic Vulnerability of Existing Buildings, Institute of Structural Engineering Swiss Federal Institute of Technology. Vdf, Hochschulverl. an der ETH.

Lang, K., Bachmann, H., 2004. On the Seismic Vulnerability of Existing Buildings: A Case Study of the City of Basel. Earthq. Spectra 20, 43–66.

Lantada, N., Irizarry, J., Barbat, A.H., Goula, X., Roca, A., Susagna, T., Pujades, L.G., 2009. Seismic hazard and risk scenarios for Barcelona, Spain, using the Risk-UE vulnerability index method. Bull. Earthq. Eng. 8, 201–229.

Lee, S.S., Lu, L.L., 1989. Cyclic tests of full scale composite joint subassemblages. J. Struct. Eng. 115, 1977–1998.

Leon, R.T., 1998. Analysis and design problems for PR composite frames subjected to seismic loads. Eng. Struct. 20, 364–371.

Leon, R.T., 1998. Composite connections. Prog. Struct. Eng. Mater. 1, 159–169.

Leon, R.T., 1990. Semi-rigid composite construction. J. Constr. Steel Res. 15, 99–120.

Leon, R.T., 1987. Behavior and Design of Semi-Rigid Composite Frames, Materials and Member Behavior.

Leuchars, J., Scrivener, J., 1976. Masonry infill panels subjected to cyclic in-plane loading. Bull. New Zeal. Natl. Soc. Earthq. Eng. 9, 122–131.

Li, Q., Ellingwood, B.R., 2008. Damage inspection and vulnerability analysis of existing buildings with steel moment-resisting frames. Eng. Struct. 30, 338–351.

Liauw, T.C., 1972. An Approximate Method of Analysis for Infilled Frames with or without Opening. Build. Sci. 7, 233–238.

Liauw, T.C., Kwan, K.H., 1985. Unified Plastic Analysis for Infilled Frames. J. Struct. Eng. 111, 1427–1448.

Liauw, T.C., Lee, S.W., 1977. On the behaviour and the analysis of multi-storey infilled frames subject to lateral loading. Proc. Instn Civ. Engrs 63, 641–656.

Liel, A.B., Lynch, K.P., 2012. Vulnerability of Reinforced-Concrete-Frame Buildings and Their Occupants in the 2009 L'Aquila, Italy, Earthquake. Nat. Hazards Rev. 13, 11–23.

Liu, J., Astaneh-Asl, A., 2000. Cyclic testing of simple connections including effects of slab. J. Struct. Eng. 32–39.

Liu, M., Wen, Y.K., Burns, S.A., 2004. Life cycle cost oriented seismic design optimization of steel moment frame structures with risk-taking preference. Eng. Struct. 26, 1407–1421.

Liu, Z., Zhang, Z., 2017. Artificial Neural Network based method for seismic fragility analysis of steel frames. KSCE J. Civ. Eng. 00, 1–10.

Lotfi, H.R., Shing, P.B., 1994. Interface Model Applied to Fracture of Masonry Structures. J. Struct. Eng. 120, 63–80.

Lotfi, H.R., Shing, P.B., 1991. An appraisal of smeared crack models for masonry shear wall analysis. Comput. Struct. 41, 413–425.

Lourenço-de-Oliveira, R., Vazeille, M., de Filippis, A.M.B., Failloux, A.B., 2004. Aedes aegypti in Brazil: Genetically differentiated populations with high susceptibility to dengue and yellow fever viruses. Trans. R. Soc. Trop. Med. Hyg. 98, 43–54.

Lourenço, P.B., 2002. Computations on historic masonry structures. Prog. Struct. Eng. Mater. 4, 301–319.

Lourenço, P.B., Rots, J.G., Blaauwendraad, J., 1998. Continuum Model for Masonry: Parameter Estimation and Validation. J. Struct. Eng. 124, 642–652.

Madan, A., Reinhorn, A.M., Mander, J.B., Valles, R.E., 1997. Modeling of masonry infill panels for structural analysis. J. Struct. Eng. 123, 1295–1302.

Mahen, M.R., Grove, W., 1990. the Manjil , Iran Earthquake of 20 June 1990 a Field Report By Eefit. Earthquake.

Mai, C., Konakli, K., Sudret, B., 2017. Seismic fragility curves for structures using non-parametric representations. Front. Struct. Civ. Eng. 11, 169–186.

Mainstone, R.J., 1971. On the stiffness and strenghts of infilled frames. Institue Civ. Eng. IV, 57–90.

Majd, M., Hosseini, M., Amini, A.M., Moein Amini, A., 2012. Developing Fragility Curves for Steel Building with X-Bracing by Nonlinear Time History Analyses, in: Proceedings of the 15WCEE, Lisbon,. 15 WCEE, Lisboa.

Mallick, D. V, Garg, R.P., 1971. Effect of openings on the lateral stiffness of infilled frames. ICE Proc. 49, 193–209.

Manafpour, A., 2003. The Bam, Iran Earthquake of 26 December 2003, Earthquake Engineering Field Investigation Team (EEFIT).

Martinelli, E., Lima, C., De Stefano, G., 2015. A simplified procedure for Nonlinear Static analysis of masonry infilled RC frames. Eng. Struct. 101, 591–608.

Mathiasson, A., Medina, R.R., 2014. Seismic Collapse Assessment of a 20-Story Steel Moment-Resisting Frame Structure. Building 4, 806–822.

McCrum, D.P., Amato, G., Suhail, R., 2016. Development of Seismic Fragility Functions for a Moment Resisting Reinforced Concrete Framed Structure. Open Constr. Build. Technol. J. 10, 42–51.

McGuire, R.K., 2004. Seismic Hazard and Risk Analysis, Earthquake Engineering Research Institute. Earthquake Engineering Research Institute.

Mehrabi, A.B., Shing, P.B., 2003. Seismic Analysis of Masonry-Infilled Reinforced Concrete Frames. TMS J. 81–94.

Mehrabi, A.B., Shing, P.B., 1997. Finite element modeling of masonry-infilled RC frames. J. Struct. Eng. 123, 604–613.

Mehrabi, A.B., Shing, P.B., Schuller, M.P., Noland, J.L., 1996. Experimental evaluation of masonry-infilled. J. Struct. Eng. 122, 228–237.

Mehrabian, A., Haldar, A., 2005. Some lessons learned from post-earthquake damage survey of structures in Bam, Iran earthquake of 2003. Struct. Surv. 23, 180–192.

Menegotto, M., Pinto, P.E., 1973. Method of analysis of cyclically loaded RC plane frames including changes in geometry and non-elastic behavior of elements under normal force and bending. Prelim. Rep. IABSE 13.

Milutinovic, Z. V, Trendafiloski, G.S., 2003. WP4: Vulnerability of Current Buildings, in: RISK-UE Project Handbook. p. 111.

Mitropoulou, C.C., Lagaros, N.D., Papadrakakis, M., 2011. Life-cycle cost assessment of optimally designed reinforced concrete buildings under seismic actions. Reliab. Eng. Syst. Saf. 96, 1311–1331.

Miyajima, M., Fallahi, A., Sadeghi, A., Ghanbari, E., 2012. Site investigation of the Ahar-Varzeghan earthquake in NW Iran of August 11 , 2012.

Moehle, J., Deierlein, G.G., 2004. A framework methodology for performance-based earthquake engineering, in: 13th World Conference on Earthquake Engineering. pp. 3812–3814.

Moghaddam, H., Hajirasouliha, I., Doostan, A., 2005. Optimum seismic design of concentrically braced steel frames: Concepts and design procedures. J. Constr. Steel Res. 61, 151–166.

Moghaddam, H.A., 2004. Lateral Load Behavior of Masonry Infilled Steel Frames with Repair and Retrofit. J. Struct. Eng. 130, 56–63.

Moghaddam, H.A., Dowling, P.J., 1987. The state of the art in infilled frames. ESEE Res. Rep., Imp. Coll. London, Civ. Eng. Dep. London, Engl. 87.

Mohebkhah, A., Tasnimi, a. a., Moghadam, H. a., 2008. Nonlinear analysis of masonry-infilled steel frames with openings using discrete element method. J. Constr. Steel Res. 64, 1463–1472.

Mohebkhah, A., Tasnimi, A., 2012. Distinct Element Modeling of Masonry-Infilled Steel Frames with Openings. Open Constr. Build. Technol. J. 6, 42–49.

Mohebkhah, A., Tasnimi, A., Moghaddam, H.A., 2007. A Modified Three-Strut (MTS) Model for Masonry-Infilled Steel Frames with Openings. J. Seismol. Earthq. Eng. 9.

Mohyeddin-Kermani, A., Goldsworthy, H., Gad, E., 2008. The Behaviour of RC Frames with Masonry Infill in Wenchuan Earthquake, aees.org.au.

Mohyeddin, A., Dorji, S., Gad, E.F., Goldsworthy, H.M., 2017. Inherent limitations and alternative to conventional equivalent strut models for masonry infill-frames. Eng. Struct. 141, 666–675.

Mohyeddin, A., Goldsworthy, H.M., Gad, E.F., 2013. FE modelling of RC frames with masonry infill panels under in-plane and out-of-plane loading. Eng. Struct. 51, 73–87.

Molina, S., Lang, D.H.H., Lindholm, C.D.D., 2010. SELENA - An open-source tool for seismic risk and loss assessment using a logic tree computation procedure. Comput. Geosci. 36, 257–269.

Molina, S., Lindholm, C., 2005. A logic tree extension of the capacity spectrum: Method developed to estimate seismic risk in Oslo, Norway. J. Earthq. Eng. 9, 877–897.

Moretti, M.L., Papatheocharis, T., Perdikaris, P.C., 2014. Design of Reinforced Concrete Infilled Frames. J. Struct. Eng. 140, 04014062.

Mosalam, K., Günay, M., 2012. Behavior and modeling of reinforced concrete frames with unreinforced masonry infill walls. Struct. Eng. Geomech. Oxford, UK.

Mosalam, K., White, R., Ayala, G., 1998. Response of infilled frames using pseudo-dynamic experimentation. Earthq. Eng. Struct. Dyn. 608, 589–608.

Mosalam, K.M., White, N., Gergely, P., White, R.N., 1997. Static response of infilled frames using quasi-static experimentation. J. Struct. Eng. 123, 1462–1469.

Murty, C., Nagar, A., 1996. Effect of brittle masonry infills on displacement and ductility demand of moment resisting frames. Proc. Elev. world Conf. Earthq. Eng. Acapulco, Mex.

Murty, C.V.R., Jain, S.K., 2000. Beneficial influence of masonry infill walls on seismic performance of rc frame buildings, in: 12WCEE. pp. 1–6.

Muto, M., Krishnan, S., 2011. Hope for the best, prepare for the worst: Response of tall steel buildings to the ShakeOut Scenario earthquake. Earthq. Spectra 27, 375–398.

Mwafy, A.M.A.M., Elnashai, A.S.A.A.S., 2001. Static pushover versus dynamic collapse analysis of RC buildings. Eng. Struct. 23, 407–424.

Naeim, F., Boppana, R.R., 2000. Chapter 8 Seismic Design of Floor Diaphragms. Seism. Des. Handb. 373–408.

Nazri, F.M., Saruddin, S.N.A., 2015. Seismic Fragility Curves for Steel and Reinforced Concrete Frames Based on Near-Field and Far-Field Ground Motion Records. Arab. J. Sci. Eng. 40, 2301–2307.

NBC-201, 1994. Mandatory Rules of Thumb - Reinforced Concrete Buildings with Masonry Infill.

Negro, P., Verzeletti, G., 1996. Effect of infills on the global behaviour of RC frames: energy considerations from pseudodynamic tests. Earthq. Eng. Struct. Dyn. 25, 753–773.

Nogueiro, P., Silva, L., Bento, R., Simões, R., 2005. Numerical implementation and calibration of a hysteretic model with pinching for the cyclic response of steel and composite joints.

Nwofor, T., 2012. Numerical micro-modeling of masonry in filled frames. Arch. Appl. Sci. Res. 4, 764–771.

Papaioannou, C., 2004. Technical Report Research Program SRM-LIFE, Seismic Hazard Scenarios: Probabilistic Analysis of Seismic Hazard. Thessaloniki.

Papia, M., Cavaleri, L., Fossetti, M., 2003. Infilled frames: Developments in the evaluation of the stiffening effect of infills. Struct. Eng. Mech. 16, 675–693.

Park, J., Kim, J., 2010. Fragility analysis of steel moment frames with various seismic connections subjected to sudden loss of a column. Eng. Struct. 32, 1547–1555.

Park, S.H., Choi, S.M., Kim, Y.S., Park, Y.W., Kim, J.H., 2010. Hysteresis behavior of concrete filled square steel tube column-to-beam partially restrained composite connections. J. Constr. Steel Res. 66, 943–953.

Paulay, T., Priestley, M., 1992. Seismic Design of Reinforced Concrete and Masonry Buildings. John Wiley & Sons, Inc., New York, NY, USA.

Pei, S., van de Lindt, J.W., 2009. Methodology for earthquake-induced loss estimation: An application to woodframe buildings. Struct. Saf. 31, 31–42.

Personeni, S., Pilato, M., 2008. NUMERICAL INVESTIGATIONS ON THE SEISMIC

RESPONSE OF MASONRY INFILLED STEEL FRAMES. 14WCEE.

Peruš, I., Fajfar, P., Dolšek, M., 2008. Simplified nonlinear seismic assessment of structures using approximate Sdof-Ida curves, in: The 14th World Conference on Earthquake Engineering.

Petruzzelli, F., Della Corte, G., Iervolino, I., 2012. Seismic Risk Assessment of an Industrial Steel Building Part 1: Modelling and Analysis. 15WCEE.

Pitilakis, K., 2010. Systemic Seismic Vulnerability and Risk Analysis for Buildings, Lifeline Networks and Infrastructures Safety Gain.

Pitilakis, K., Franchin, P., Khazai, B., Wenzel, H., 2014. SYNER-G: Systemic seismic vulnerability and risk assessment of complex urban, utility, lifeline systems and critical facilities: Methodology and Applications. Geotech. Geol. Earthq. Eng., Geotechnical, Geological and Earthquake Engineering 31, 408.

Polyakov, S. V, 1956. Masonry in framed buildings. National Lending Library for Science and Technology, Boston Spa, Yorkshire, UK.

Porter, K., 2017. A Beginner's guide to fragility, vulnerability, and risk, University of Colorado Boulder.

Porter, K., Farokhnia, K., Cho, I., Grant, D., Jaiswal, K., Wald, D., D'Ayala, D., Meslem, A., So, E., Kiremidjian, A., Noh, H., 2012. Global vulnerability estimation methods for the Global Earthquake Model. Proc. 15th World Conf. Earthq. Eng. - WCEE 9.

Porter, K.A., 2003. An Overview of PEER's Performance-Based Earthquake Engineering Methodology. 9th Int. Conf. Appl. Stat. Probab. Civ. Eng. 273, 973–980.

Rackwitz, R., 2006. The effect of discounting, different mortality reduction schemes and predictive cohort life tables on risk acceptability criteria. Reliab. Eng. Syst. Saf. 91, 469–484.

Rassati, G.A., Leon, R.T., Noe, S., 2004. Component Modeling of Partially Restrained Composite Joints under Cyclic and Dynamic Loading. J. Struct. Eng. 130, 343–351.

Retamales, R., Davies, R., 2013. Experimental Seismic Fragility of Cold-Formed Steel Framed Gypsum Partition Walls. J. Struct. J. Struct. Eng. 139, 1285–1293.

Reyes-Salazar, A., López-Barraza, A., López-López, A., Haldar, A., Reyes-Salazar, A., 2008. Multi-Component Seismic Response Analysis – A Critical Review Multi-Component Seismic Response Analysis. J. Earthq. Eng. 12, 779–799.

Ricci, P., de Luca, F., Verderame, G.M., 2011. 6th April 2009 L'Aquila earthquake, Italy: Reinforced concrete building performance. Bull. Earthq. Eng. 9, 285–305.

Rigato, A.B., Medina, R.A., 2007. Influence of angle of incidence on seismic demands for inelastic single-storey structures subjected to bi-directional ground motions. Eng. Struct. 29, 2593–2601.

Robinson, D., Gray, D., Ghasemi, H., Horspool, N., 2014. EQRM : Geoscience Australia' s Earthquake Risk Model. Tech. Man.

Roca, A., Goula, X., Susagna, T., Chávez, J., González, M., Reinoso, E., 2006. A simplified method for vulnerability assessment of dwelling buildings and estimation of damage scenarios in catalonia, Spain. Bull. Earthq. Eng. 4, 141–158.

Rodrigues, H., Varum, H., Costa, A., 2010. Simplified macro-model for infill masonry panels. J. Earthq. Eng. 14, 390–416.

Rossetto, T., D'Ayala, D., Ioannou, I., Meslem, A., 2014a. Evaluation of Existing Fragility Curves. Springer, Dordrecht, pp. 47–93.

Rossetto, T., Elnashai, A., 2003. Derivation of vulnerability functions for European-type RC structures based on observational data. Eng. Struct. 25, 1241–1263.

Rossetto, T., Elnashai, A.S., 2005. A new analytical procedure for the derivation of displacement-based vulnerability curves for populations of RC structures. Eng. Struct. 27, 397–409.

Rossetto, T., Gehl, P., Minas, S., Galasso, C., Duffour, P., Douglas, J., Cook, O., 2016. FRACAS: A capacity spectrum approach for seismic fragility assessment including record-to-record variability. Eng. Struct. 125, 337–348.

Rossetto, T., Ioannou, I., Grant, D., Maqsood, T., 2014b. Guidelines for the empirical vulnerability assessment. GEM Tech. Rep. 08, 140.

Sadigh, K., Chang, C.-Y., Egan, J.A., Makdisi, F., Youngs, R.R., 1997. Attenuation Relationships for Shallow Crustal Earthquakes Based on California Strong Motion Data. Seismol. Res. Lett. 68, 180–189.

Salawdeh, S., Goggins, J., 2013. Numerical simulation for steel brace members incorporating a fatigue model. Eng. Struct. 46, 332–349.

Sanchez-Silva, M., Klutke, G.-A., Rosowsky, D. V., 2011. Life-cycle performance of structures subject to multiple deterioration mechanisms. Struct. Saf. 33, 206–217.

Saneinejad, A., Hobbs, B., 1995. Inelastic design of infilled frames. J. Struct. Eng. 121, 634–650.

Sarokolayi, L.K., Faghihmaleki, H., Gholampour, S., 2013. Fragility Curve Assessment of Collapse and Yielding Limit State for Steel Buildings with X-Brace. Adv. Civ. Environ. Eng. 01, 136–145.

Sarokolayi, L.K.L.K., Faghihmaleki, H., Gholampour, S., 2013. Fragility Curve Assessment of Collapse and Yielding Limit State for Steel Buildings with X-Brace [WWW Document]. Adv. Civ. Environ. Eng.

Sawires, R., Peláez, J.A., Fat-Helbary, R.E., Ibrahim, H.A., 2015. An earthquake catalogue (2200 b.c. to 2013) for seismotectonic and seismic hazard assessment studies in Egypt, in: Earthquakes and Their Impact on Society. Springer International Publishing, Cham, pp. 97–136.

Schotanus, M.I.J., Franchin, P., Lupoi, A., Pinto, P.E., 2004. Seismic fragility analysis of 3D structures. Struct. Saf. 26, 421–441.

SCI, 2016. Selected Findings of the 2016 National Population and Housing Census.

SEAOC, 1995. Performance Based Seismic Engineering of Buildings. Vision 2000. California.

SeismoSoft, 2014. SeismoStruct.

Shing, P.B., Mehrabi, A.B., 2002. Behaviour and analysis of masonry-infilled frames. Prog. Struct. Eng. Mater. 4, 320–331.

Shinozuka, M., Feng, M.M., Lee, J., Naganuma, T., 2000. Statistical Analysis of Fragility Curves. J. Eng. … 126, 1224–1231.

Shome, N., 1999. Probabilistic seismic demand analysis of nonlinear structures. Ph.D. Diss. Stanford Univ.

Shome, N., Cornell, C.A., Bazzurro, P., Carballo, J.E., 1998. Earthquakes, records, and nonlinear responses. Earthq. Spectra 14, 469–500.

Siamak, S., 2013. Influence of masonry infill walls and other building charactristics on seismic collapse of concrete frame building. PhD Propos.

Silva, V., Crowley, H., Pinho, R., Varum, H., 2013. Extending displacement-based earthquake loss assessment (DBELA) for the computation of fragility curves. Eng. Struct. 56, 343–356.

Silva, V., Varum, H., Crowley, H., Sousa, R., Pinho, R., Varum, H., Pinho, R., Sousa, R., 2014. Evaluation of analytical methodologies used to derive vulnerability functions. Earthq. Eng. Struct. Dyn. 43, 181–204.

Smerzini, C., Paolucci, R., 2013. SIMBAD: a database with Selected Input Motions for displacement Based Assessment and Design - 3rd release. Report of DPC - ReLUIS 2020-2013 Research Project.

Smyrou, E., Blandon, C., Antoniou, S., Pinho, R., Crisafulli, F.J., 2011. Implementation and verification of a masonry panel model for nonlinear dynamic analysis of infilled RC frames. Bull. Earthq. Eng. 9, 1519–1534.

Song, J., Ellingwood, B.R., 1999. Seismic Reliability of Special Moment Steel Frames with Welded Connections: II. J. Struct. Eng. 125, 372–384.

Stafford-Smith, B., 1966. Behaviour of square infilled frames. J. Struct. Div. 92, 381–403.

Stafford-Smith, B., 1962. Lateral stiffness of infilled frames. J. Struct. Div. 88, 183–199.

Stafford-Smith, B., Carter, C., Smith, B.S., 1969. A method of analysis for infilled frames. Struct. Eng. 31–48.

Stafford-Smith, B., Riddington, J.R., 1978. The design of masonry infilled steel frames for bracing structures. Struct. Eng. 56, 1–7.

Stavridis, A., Koutromanos, I., Shing, P.B., 2012. Shake-table tests of a three-story reinforced concrete frame with masonry infill walls. Earthq. Eng. Struct. Dyn. 41, 1089–1108.

Stavridis, A., Shing, P.B., 2010. Finite-Element Modeling of Nonlinear Behavior of Masonry-Infilled RC Frames. J. Struct. Eng. 136, 285–296.

Strasser, F.O., Bommer, J.J., Şeşetyan, K., Erdik, M., Çağnan, Z., Irizarry, J., Goula, X., Lucantoni, A., Sabetta, F., Bal, I.E., Crowley, H., Lindholm, C., 2008. A comparative study of European earthquake loss estimation tools for a scenario in Istanbul, in: Journal of Earthquake Engineering. pp. 246–256.

Sucuoğlu, H., Yazgan, U., Yakut, A., 2007. A screening procedure for seismic risk assessment in urban building stocks. Earthq. Spectra 23, 441–458.

Tasnimi, a. a., Mohebkhah, a., 2011. Investigation on the behavior of brick-infilled steel frames with openings, experimental and analytical approaches. Eng. Struct. 33, 968–980.

Tavakoli, B., Ghafory-Ashtiany, M., Tavakoli, B., Ghafory-Ashtiany, M., 1999. Seismic hazard assessment of Iran. Ann. Geophys. 42.

Tirca, L., Serban, O., Wang, M.Z., Di Modica, D., 2013. Incremental Dynamic Analysis of Existing Steel Braced Frame Buildings in Moderate Seismic Zones, in: Structures Congress 2013. American Society of Civil Engineers, Reston, VA, pp. 2298–2309.

Tjhin, T., Aschheim, M., Hernández-Montes, E., 2006. Observations on the Reliability of Alternative Multiple-Mode Pushover Analysis Methods. J. Struct. Eng. 132, 471–477.

TMD, 2017. Atlas of Tehran Metropolis.

Tong, X., Hajjar, J.F., Schultz, A.E., Shield, C.K., 2005. Cyclic behavior of steel frame structures with composite reinforced concrete infill walls and partially-restrained connections. J. Constr. Steel Res. 61, 531–552.

Uma, S., Bradley, B.A., 2010. Displacement-based fragility functions for New Zealand buildings subject to ground motion hazard. GNS Sci.

Vamvatsikos, D., Cornell, C.A.C., 2002. Incremental dynamic analysis. Earthq. Eng. … 31, 523–553.

Vasdravellis, G., Valente, M., Castiglioni, C.A., 2009. Behavior of exterior partial-strength composite beam-to-column connections: Experimental study and numerical simulations. J. Constr. Steel Res. 65, 23–35.

Vatansever, C., Yardimci, N., 2010. Cyclic behavior and numerical modelling of a semi-rigid frame. Steel Constr. 3, 128–133.

Ventura, C.E., Finn, W.. L., Onur, T., Blanquera, A., Rezai, M., 2005. Regional seismic risk in British Columbia — classification of buildings and development of damage probability functions. Can. J. Civ. Eng. 32, 372–387.

Vicente, R., Parodi, S., Lagomarsino, S., Varum, H., Mendes da Silva, J.A.R., 2008. Seismic Vulnerability Assessment Damage Scenarios and Loss Estimation. Case study of the old city centre of Coimbra, Portugal, in: The 14th World Conference on Earthquake Engineering.

Wallace, B.J., Krawinkler, H., 1985. Small-scale model experimentation on R/C Assemblies, Report - Stanford University, John A. Blume Earthquake Engineering Center.

Wang, J.P., Taheri, H., 2014. Seismic Hazard Assessment of the Tehran Region. Nat. Hazards Rev. 15, 121–127.

Warszawski, A., Gluck, J., Segal, D., 1996. Economic Evaluation of Design Codes—Case of Seismic Design. J. Struct. Eng. 122, 1400–1408.

Wen, Y.K., Kang, Y.J., 2001. Minimum Building Life-Cycle Cost Design Criteria. II: Applications. J. Struct. Eng. 127, 338–346.

Whitman, R., 1973. Damage probability matrices for prototype buildings. Struct. Publ.

Whitney, S., Anderson, B.G., Cohen, E., 1955. Design of Blast Resistant Construction for Atomic Explosions *. J. Am. Concr. Inst.

Wibowo, A., Kafle, B., Kermani, A.M.A., Lam, N.T.K.N., Wilson, J.L., Gad, E.F., 2008. Damage in the 2008 China Earthquake.

Wood, R.H., 1978. Plasticity, composite action and collapse design of unreinforced shear wall panels in frames. Proc. Instn Civ. Engrs 65, 381–411.

Yamazaki, F., Murao, O., 2000. Vulnerability Functions for Japanese Buildings based on Damage Data due to the 1995 Kobe Earthquake. Implic. Recent Earthquakes Seism. Risk 91–102.

Yekrangnia, M., Eghbali, M., Seyri, H., Panahi, M., Zanganeh, S.Y., Beyti, M., Hayatgheybi, D.S.V., Nazarpour, M., Amiri, G.G., 2017. A preliminary report on school buildings performance during M 7.3 Ezgeleh, Iran earthquake of Participants Project Team Steering Committee Advisory Committee.

Yorulmaz, M., Sozen, M.A., 1968. Behavior of single-story reinforced concrete frames with

filler walls. Tech. Report, Struct. Res. Ser. no.337, Univ. Illinois Urbana.

Yoshimura, K., Kuroki, M., 1999. Damage to building structures caused by the 1999 Chi-chi earthquake in Taiwan. Reports Fac. Eng. Oita Univ. 40, 32–39.

Yuen, T.Y.P., Kuang, J.S., Ali, B.S.M., 2016. Assessing the effect of bi-directional loading on nonlinear static and dynamic behaviour of masonry-infilled frames with openings. Bull. Earthq. Eng. 14, 1721–1755.

Yuen, Y.P.P., Kuang, J.S.S., 2015. Nonlinear seismic responses and lateral force transfer mechanisms of RC frames with different infill configurations. Eng. Struct. 91, 125–140.

Zahrai, S.M., Heidarzadeh, M., 2004. Seismic performance of existing buildings during the 2003 bam earthquake, in: 13th World Conference on Earthquake Engineering.

Zarnic, R., 1997. Masonry infilled frames as an effective structural sub-assemblage, in: International Workshop on Seismic Design Methodologies for the Next Generation of Codes. Slovenia, pp. 335–346.

Zarnic, R., Tomazevic, M., 1988. An Experimentally Obtained Method for Evaluation of the Behaviour of Masonry Infilled R/C Frames, in: 9WCEE. p. 6.

Appendix A – Numerical Modelling of the Infill-Frame

Summary of Findings

Following is a summary of important points obtained by reviewing the studies conducted on modelling the infilled frame structures:

a) Great number of physical experimental studies on infilled frames indicate that the structures with the infill have a stiffness 4 to 20 times greater than the one of the surrounding bare frame. Moreover, the presence of infill influences the overall strength, ductility and mode of failure when subjected to lateral loads. (FEMA-306, 1998; Moghaddam & Dowling, 1987; Stafford-Smith, 1966; Wood, 1978)

b) If the infill is properly designed, it can be beneficial by strengthening the existing structure and improving their earthquake resistance. On the contrary, the frame-infill interaction can induce brittle shear failures of the surrounding columns and cause short-column phenomena. Moreover, the infill can over-strengthen the upper storeys and induce soft storey. Consequently, their effect should not be overlooked. (Shing & Mehrabi, 2002)

c) The infilled frame structures cannot be modelled as elasto-plastic systems, due to the stiffness and strength degradation occurring under cyclic loading. This is important especially in case of short period structures such as infilled frames, where the energy dissipation capacity and shape of the hysteresis loops have strong influence on the overall response.

d) With all the advancements in 3D and multilevel structural analysis techniques and evolution of seismic design method, considering the effect of infill in the analysis and design is possible. (Crisafulli et al., 2000; D'Ayala et al., 2009; Ellul & D'Ayala, 2008; Mohebkhah & Tasnimi, 2012)

e) The most challenging part of the simulation is to determine the type of interaction between infill and the frame. This has a major effect on structural behaviour and load-resisting mechanism. (Dawe et al., 2001; Shing & Mehrabi, 2002)

f) Micro models take into consideration the local effects of each element separately and in great details. Hence, they are generally used for detailed analysis and allow interpretation of the behaviour at local level. Thus, the cracking pattern, the ultimate load and the collapse mechanism can be obtained with high accuracy. (Nwofor, 2012)

g) In case of micro models, issues such as high computational effort and large number of parameters involved make them unsuitable for practical purposes such as the analysis of multi-storey, multi-bay framed structures in design offices. (Mohebkhah *et al.*, 2007)

h) Macro models are much simplified in comparison to the micro ones, while it has been proven that they are able to represent the global behaviour of the infill panels and their influence on the structural response. The macro technique is mainly based on a physical understanding of the behaviour of the infill panel. (Crisafulli *et al.*, 2000; Rodrigues *et al.*, 2010)

i) Majority of analytical models proposed so far, can only focus on one type of failure mechanism (e.g. in-plane and out-of-plane) and are not universally applicable to all infilled structures.

j) The equivalent diagonal strut model is considered as an acceptable rational way to describe the influence of masonry panel under lateral loading, as it gives an adequate estimation of the stiffness of the infilled frame and the axial forces induced in the surrounding frame. (Crisafulli, 1997; Holmes, 1961; Stafford-Smith, 1962; Zarnic & Tomazevic, 1988)

k) The main uncertainties in the equivalent diagonal models are the area of the struts and their strength.

l) The diagonal struts can only account for compression or tension and simulate the diagonal crack propagation. Diagonal struts are not capable of predicting horizontal shear sliding and the local failure due to interaction of frame element and the masonry panel. (Ellul & D'Ayala, 2012)

m) In case of cyclic and dynamic loading, using only one diagonal compressive strut and one tensile strut does not represent the internal forces induced in members and at least two diagonal struts must be used. (Crisafulli, 1997)

n) Although one diagonal strut results in acceptable values for stiffness and axial forces induced in the frame members, due to lateral load, it underestimates the bending moments and is not capable of estimating the horizontal shear sliding of the masonry panel.

o) While flexural failure is more common, the shear failure can be significant as the structure losses its gravity load capacity as well as its lateral capacity. As most infilled frames are designed only to resist gravity loads, the stiffening effect of infill, subjects

the frame elements to increased concentration of lateral force. For weak frames, shear failure of columns prevents a more robust and ductile load-resisting mechanism to be developed. (Mehrabi *et al.*, 1996)

p) Unreinforced masonry infills, which are usually brittle to semi brittle, do not have an acceptable response during an earthquake and so they suffer structural and non-structural damages in forms of minor cracks, crushing and complete collapse. Such behaviour is explained by the deterioration of stiffness, strength and energy dissipation capacity due to brittle failure of the masonry walls. (Shing & Mehrabi, 2002)

q) Different types of masonry units and mortars are used around the world, with a wide range of geometric and mechanical properties. Therefore, the resultant masonry material presents a large variation in its characteristics and distinct behaviour. For this reason, it is difficult to calibrate analytical models or empirical expressions that are valid in a general sense.

r) The compression strength of masonry units plays an important role, as other mechanical properties of the masonry can be related to it (e.g. Modulus of elasticity).

s) Strength of the mortar joint is also a dominant factor. A better quality of constitutive material will result in a stronger masonry, but not necessarily an increase in the lateral strength of infilled frame. This is true because if the masonry panel becomes stronger compared to its surrounding frame, premature failure of the frame members may occur and the strength of the system can be significantly reduced. (Dawe et al., 2001; Mehrabi & Shing, 1997)

t) The compression and shear strength of masonry infill panels depend on the properties of its component bricks and mortar. In order to obtain adequate shear bond strength, the hydration conditions at the mortar-brick interface, the characteristics of brick surface and the compressive strength of mortar should be controlled.

u) The cyclic behaviour of masonry subjected to shear is mainly controlled by the behaviour of the mortar joints.

v) The presence of masonry infill can have a significant influence to the energy dissipation capacity of the structural system (Mallick & Garg, 1971). This is mainly due to the contribution of inelastic behaviour of masonry panels to the inelastic behaviour of its surrounding frame and the friction at the panel-frame interaction.

w) If inelastic effects are brittle in nature (e.g. cracking of infill, bond slip failure in frame, or shear failure in frame members), the drop in strength and stiffness under repeated loading may be large and result in low energy dissipation capacity. (Asteris et al., 2011; El-Dakhakhni, 2004; Murty & Jain, 2000)

x) During intense cyclic loadings such as earthquake, cracks propagate on the diagonals of the infill (cross), however due to the restriction of the surrounding frame and the friction inside the cracks, the infill is able to withstand the lateral loads until full collapse.

y) The infill passes its elastic limit due to propagation of cracks. At this stage the contact length between the frame and the infill panel starts to decrease as the lateral and consequently axial displacement increases, thus affecting the area of equivalent strut. Therefore, the width of the equivalent strut should be reduced as loading and damage progress. (Crisafulli, 1997)

z) The openings influence the lateral stiffness (about 60–70%) and strength (about 45%) of the infill panel. (Asteris, 2003; Mallick & Garg, 1971; Tasnimi & Mohebkhah, 2011)

aa) The thickness of the infill masonry can be taken as the summation of the masonry unit thickness and total plaster thickness (Binici *et al.*, 2007). While an equivalent modulus of elasticity (E_{me}) approach can be applied to account for the plaster effect.

$$E_m = \frac{E_m t_m + E_p t_p}{t_m + t_p}$$

bb) Out of plane failure of such masonry infills can cause casualty and economic losses as the infill tends to fall out of the frame plane due to the perpendicular components of the earthquake excitation. However, this failure is mostly restrained by friction at the interface and it is unlikely due to the arching mechanism. (Dawe & Seah, 1989b)

Characteristics of the Implemented Masonry Infill-Frame Model

In order to consider all the points mentioned in the previous section, the numerical models discussed in the lecturer review have been compared based on accuracy, validity, availability and feasibility. Accordingly, for this study a macro model proposed by Crisafulli (1997) is adopted for simulating the masonry infills. This does not necessarily indicate that Crisafulli's model is the best option, however for the time being is the most complete and accessible model among the studied one.

In Crisafulli's (1997) model, the panel element accounts separately the compression and shear behaviour of the masonry infill using two parallel struts and a shear spring in each direction. This double-strut model is accurate enough to consider the lateral stiffness and the strength of the masonry, particularly when a shear failure along mortar joints or diagonal tension failure is expected. Furthermore, the model is easy to apply for analysing large infilled frame structures, while being less complicated and time consuming compared to the triple-strut models (e.g. Chrysostomou *et al.*, 2002). A drawback of the model is not being able to predict

properly the bending moment and shear forces in the surrounding frame, since the panel is connected to the beam-column joints of the frame.

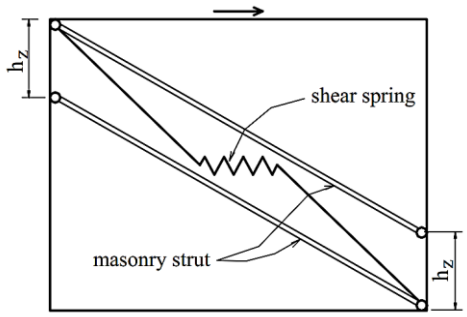

Figure A.1 - Arrangement of the active struts and shear spring of Crisafulli (1997) model

In this model the response of the axial struts is represented by a hysteresis stress-strain relationship, which consists of seven hysteresis rules in order to consider different behaviours for loading, unloading and reloading. Therefore, the axial force and axial displacement of struts are related to the stress and strain of the masonry unit.

Figure A.2 - Hysteresis curve and compressive diagonal strut for masonry infill (Crisafulli, 1997)

The hysteresis response of the shear spring follows an elasto-plastic rule with variable shear strength. This shear strength variation is controlled by a shear-friction mechanism. Hence, the shear strength is calculated considering two different stages; first, the elastic response, which happens before reaching the bond-shear strength, and secondly, the sliding, in which the strength depends on the compressive force of the struts. To avoid large shear values in the sliding stage, the shear strength is limited due to high axial forces in the struts. Moreover, the shear stiffness is assumed to be a fracture (varies between 50% to 75%) of the total stiffness of the masonry strut.

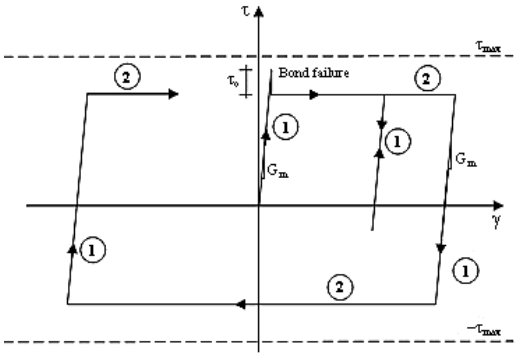

Figure A.3 - Analytical response for cyclic shear response of mortar joints (Crisafulli, 1997)

In order to account for the cracking of the masonry infill and the reduction of the contact length between the panel and the frame, the area of the equivalent strut (A_{ms}) reduces as a function of axial displacement. It should be noted that there is insufficient information to estimate the practical values for this variation and according to empirical result, the width strut, can decrease between 20% to 50% (Crisafulli & Carr, 2007; Decanini & Fantin, 1986). The model also considers the local contact effects of the cracked material, the effect of the small inner cycles and the tensile behaviour of masonry.

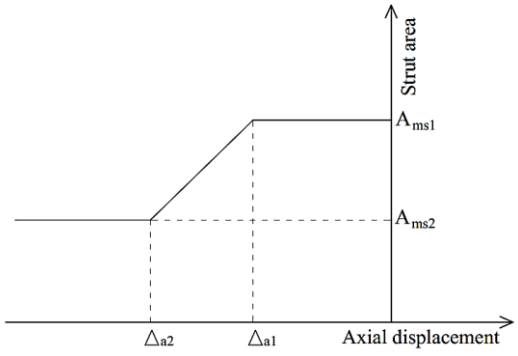

Figure A.4 - Variation of strut area as function of axial displacement

The model assumes that when no previous compression has taken place, the stress-strain relationship in tension is linearly elastic until the tensile strength is reached. At this point a brittle failure occurs and no tensile stress can be resisted in further cycles. A tensile softening has also been considered in the model. In case of previous compressive strain, due to degradation of tensile strength and elastic modulus, the tensile strength is assumed to be zero when the plastic strain (ε_{pl}) exceeds the magnitude of strain at maximum compressive strength.

The features of Crisafulli's model can be summarised as follows:

- Model is able to simulate the *Diagonal tension failure* of the masonry units, as a result of combination of compressive and shear stresses in the masonry,
- The model is capable of representing the hysteretic axial behaviour of masonry,
- Envelope in compression is defined with the Sargin *et al.* (1971) equation originally proposed for concrete,
- Model is capable of considering the effect of local phenomena due to introduction of nodes which represent the contact length between the frame and infill panel,
- The user can control the variation of the stiffness and the axial strength of the masonry strut,
- The unloading-reloading curves are represented with a general expression, which pass through two predefined points where the slope of the curve is also imposed,
- The model is capable of considering the contact effect in the cracked material,
- Due to large number of inputs, the model is capable to represent a wide range of fragile masonry material,
- As the model is able to keep information regarding previous loading history, it is ideal to represent properly the dynamic response under earthquake induced actions,
- The shear behaviour is represented according to a bond-friction model,
- The shear response of mortar joints are assumed to be linear elastic, while the shear strength has not been reached. Unloading and reloading are also in the elastic range.
- The bond-friction model accounts for the de-bonding of mortar joints and the variation of the shear strength depending on the axial stress level.

The following graphs illustrate the validity tests conducted using Crisafulli's model on infilled framed structures. It is evident that the model is capable of simulating the actual behaviour of masonry infilled frames to high extents.

Negro *et al.* 1996
A full-scale, four-storey building, [pseudo-dynamic loading] (ELSA+ISPRA)

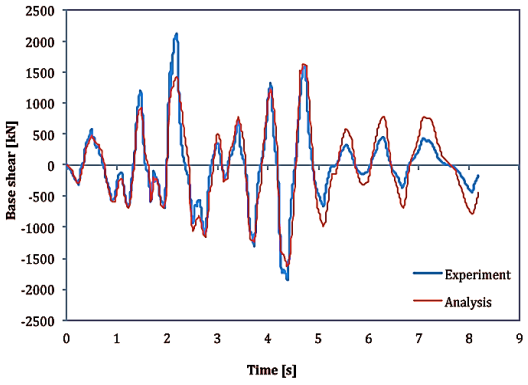

Crisafulli 1997
One storey, single bay infilled RC frame [pseudo-static cyclic load]

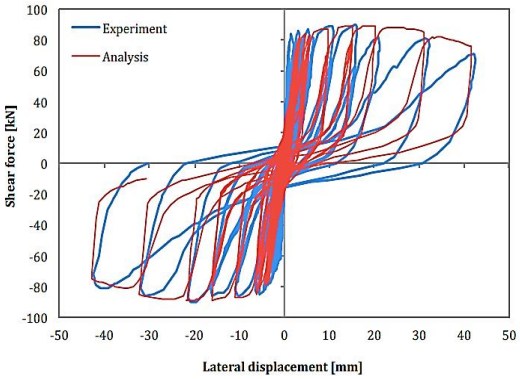

Colangelo *et al.* 1999
One storey, single bay infilled RC frame, [pseudo-dynamic loading]

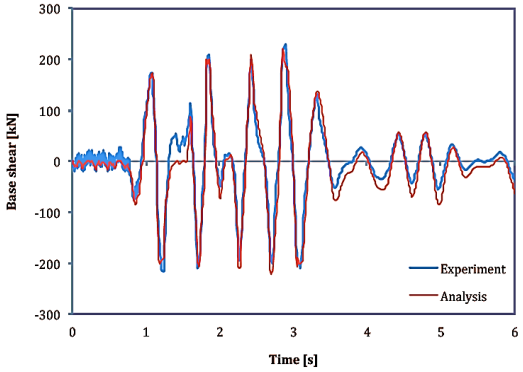

Pinto *et al.* 1999
A full-scale four storey 2D infilled RC frame with opening, [pseudo-dynamic loading] (ICONS)

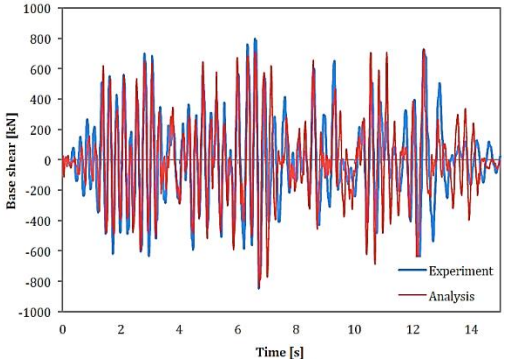

Figure A.5 - Validation of Crisafulli's model with experimental results presented in literature

It's important to note that this model only accounts for the most common modes of failure, since a model that can account for all types of masonry failure would not be practical due to the high level of complexity and uncertainty involved. Furthermore, the strength and stiffness of the infills are introduced after the application of the initial loads, therefore the panels do not bear gravity load. This is mainly because the vertical load is usually absorbed by the surrounding frame, which is erected first.

Calibration of the Infill-Frame Model

The following graphs illustrate the results obtained from the calibration of the Crisafulli model, following the experimental results of Tasnimi and Mohebkhah (2011) on a solid infilled steel frame. Only the most influential parameters are presented in this section. Tables A1 and A2 indicate the influence of each parameter on the general behaviour of the structure.

Table A.1 - Strut curve parameters. Employed in the definition of the masonry strut hysteresis model.

Properties	**Effect on Structural Behaviour**
Initial Young Modulus (E_m)	Mainly effect the strength of the final cycles
Compressive Strength (f_m)	Effects the overall strength of all cycles
Tensile Strength (f_t)	Minor effect
Strain at Maximum Stress ($\mathcal{E}_m$)	Great effect on the hysteresis curve slope and stiffness
Ultimate Strain ($\mathcal{E}_u$)	Significant effect on the later cycles (after the ones effected by $\mathcal{E}_1$ and $\mathcal{E}_1$)
Closing Strain ($\mathcal{E}_{cl}$)	Minor effect, in most cases very small values were the best chose.
Strut area reduction strain ($\mathcal{E}_1$)	These two parameters effect the initial stiffness and strength of the first cycles. Larger values result in stepper initial slope and higher stiffness.
Residual strut area strain ($\mathcal{E}_2$)	
Starting unload. stiffness factor (γ_{un})	Minor or no effect
Strain reloading factor (α_{re})	Minor or no effect
Strain inflection factor (α_{ch})	-
Complete unloading strain factor (β_a)	-
Stress inflection factor (β_{ch})	-
Zero stress stiffness factor (γ_{plu})	-
Reloading stiffness factor (γ_{pr})	Minor effect on the unloading curve's shape
Plastic unloading stiffness factor (e_{x1})	-
Repeated cycle strain factor (e_{x2})	-

Table A.2 - Inelastic infill panel element properties

Properties	**Definition**	**Effect on Structural Behaviour**
Infill panel thickness (t_i)	Width of the panel brick alone or including plaster	No effect, as the thickness is evaluated through the give A1
Out-of-plane failure drift	Defined as a percentage of storey height	-
Strut Area 1 (*A1*)	Product of panel thickness (t_i) and equivalent width of strut (b_w)	Effects mainly the strength
Strut Area 2 (*A2*)	Accounts for the area reduction due to cracking of infill	Effects mainly the strength
Equivalent contact length (h_Z)	Accounting for the contact length between frame and infill panel (Stafford-Smith 1966) $0.5\pi\lambda^{-1}$	Effects the stiffness and strength
Horizontal offsets (X_{oi})	Representing the reduction due to the depth of column	Minor effect (case sensitive)
Vertical offsets (Y_{oi})	Representing the reduction due to the depth of beam	Minor effect (case sensitive)
Proportion of stiffness assigned to shear (γ_s)	Proportion of the panel stiffness (computed by program) that should be assigned to the shear spring (typical: 0.2 to 0.6)	Effects the stiffness of the returning curve, and strength of the initial cycles. No effect on initial stiffness.

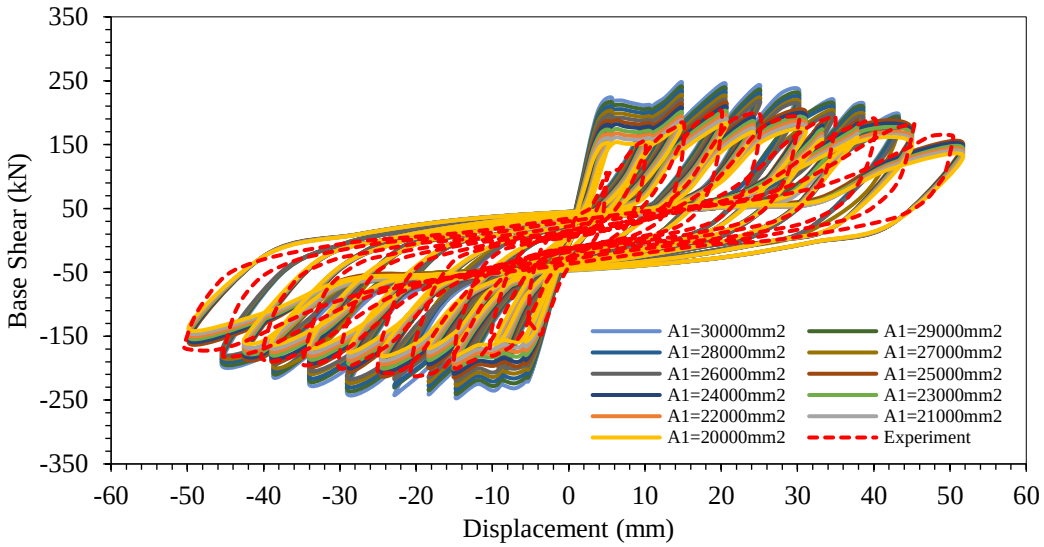

Figure A.6 - Sensitivity of infilled steel frame model to strut area 1 - A1 (mm^2)

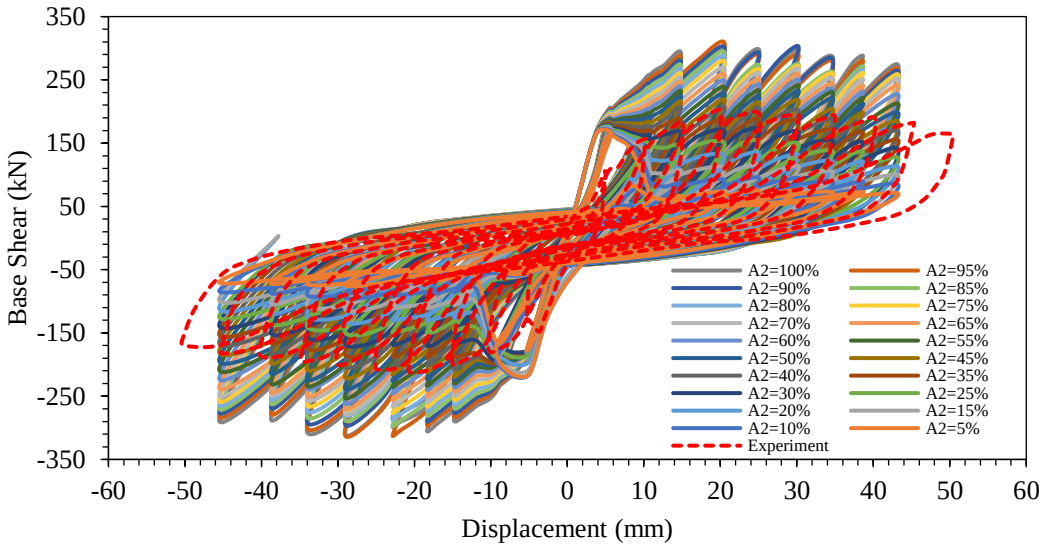

Figure A.7 - Sensitivity of infilled steel frame model to strut area 2 - A2 (%)

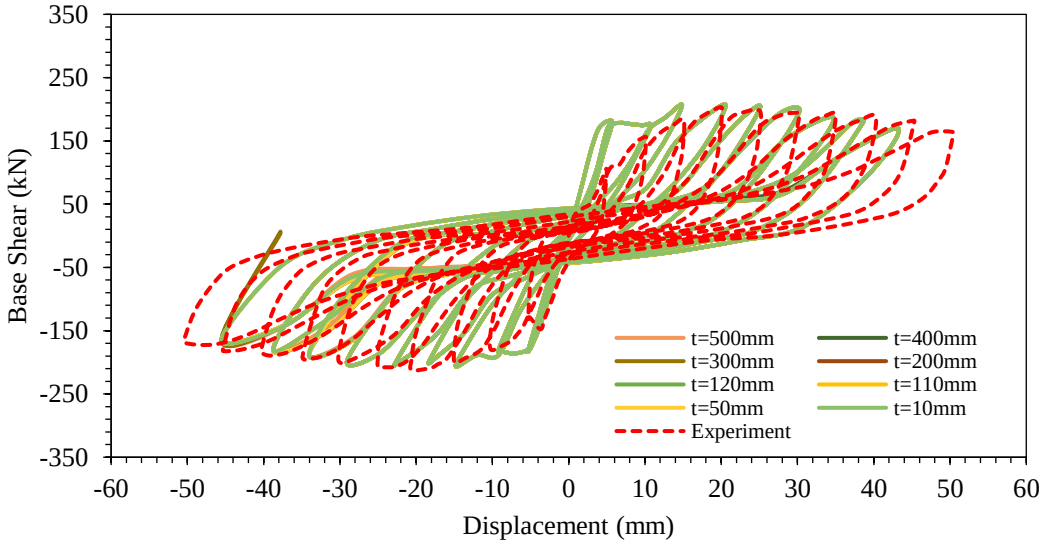

Figure A.8 - Sensitivity of infilled steel frame model to panel thickness - t (mm)

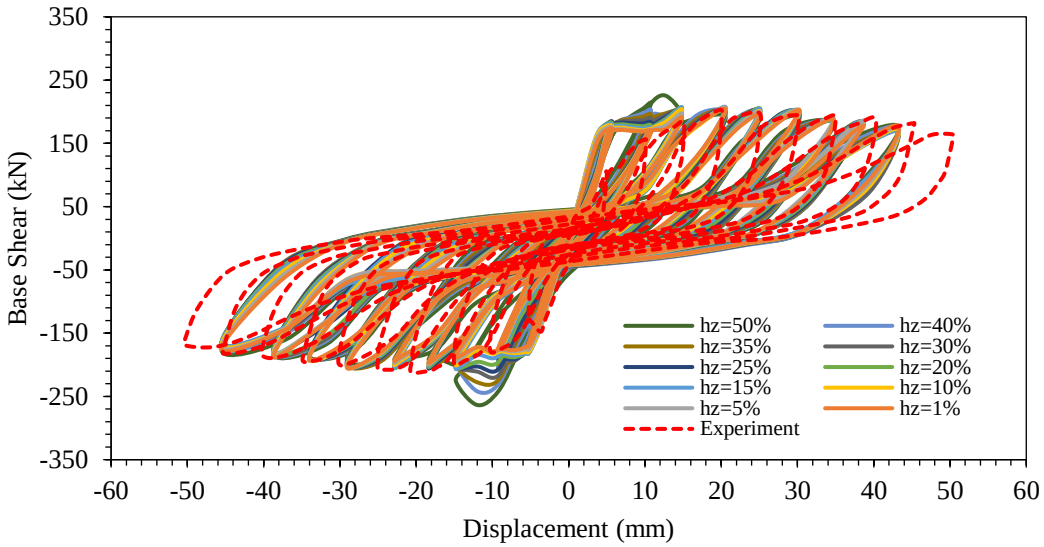

Figure A.9 - Sensitivity of infilled steel frame model to equivalent contact length - hz (%)

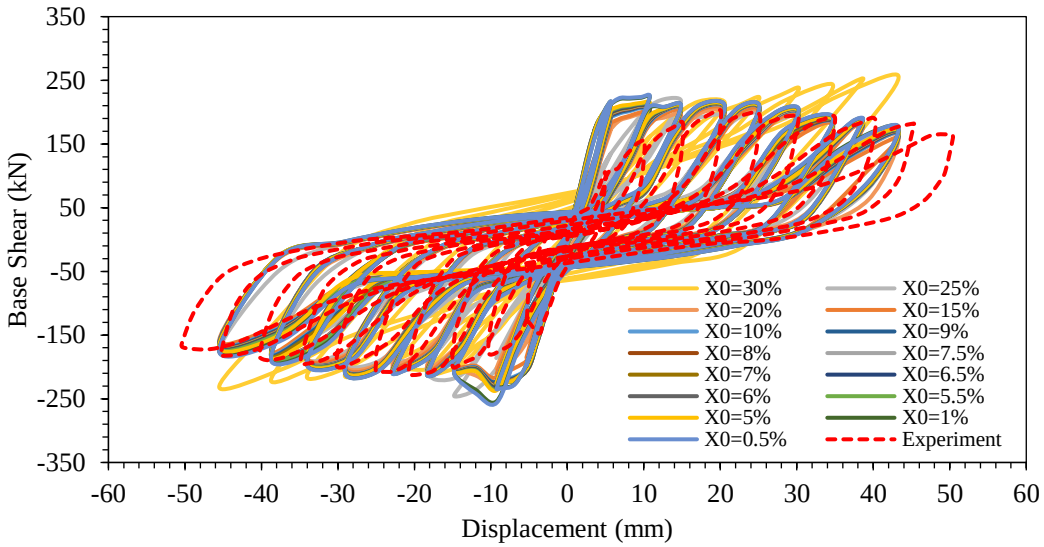

Figure A.10 - Sensitivity of infilled steel frame model to horizontal offset - X0 (%)

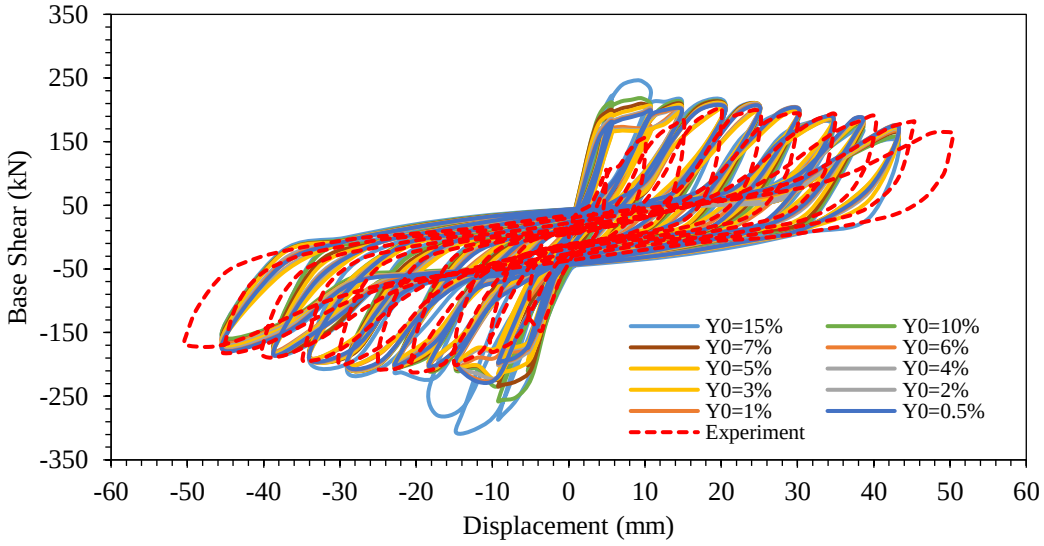

Figure A.11 - Sensitivity of infilled steel frame model to vertical offset - Y0 (%)

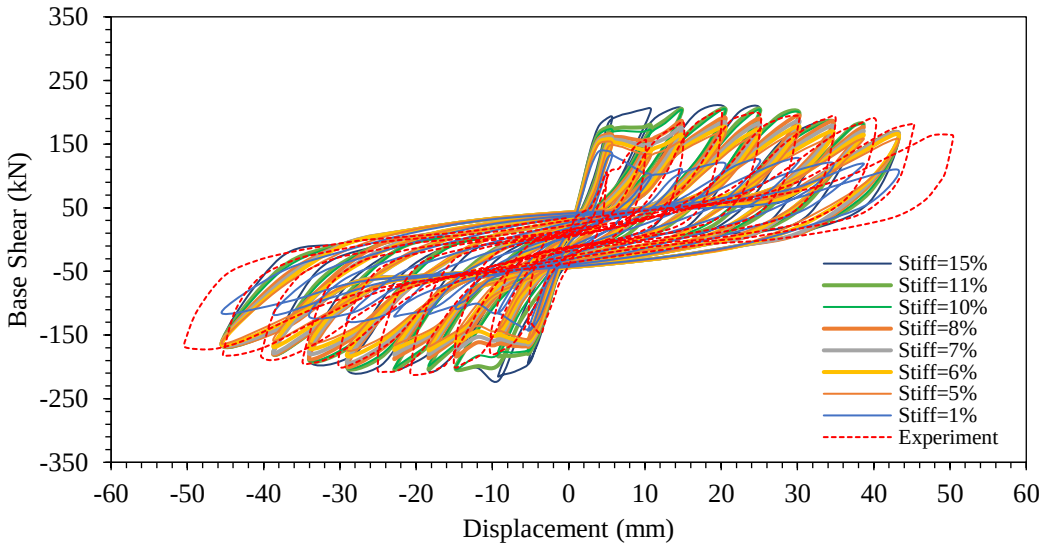

Figure A.12 - Sensitivity of infilled steel frame model to proportion of stiffness assigned to shear

Appendix B – Characteristics of Applied Ground Motions

The characteristics of the ground motions utilised for each of the nonlinear static and dynamic analysis are presented here.

SIMBAD (3rd version) set of ground motions (Smerzini et al., 2014)

Ref.	ID	Earthquake Name	M_w	Fault Mechanism	Epicentral Distance (km)	PGA X (m/s^2)	PGA Y (m/s^2)	Site Class
1	20	W Tottori Prefecture	6.6	strike-slip	11.8	6.0	6.1	B
2	21	W Tottori Prefecture	6.6	strike-slip	12.8	5.6	7.1	B
3	22	W Tottori Prefecture	6.6	strike-slip	19.0	2.7	1.5	B
4	23	W Tottori Prefecture	6.6	strike-slip	25.5	3.3	4.9	C
5	25	Shimane Hiroshima Border	5.1	strike-slip	6.8	3.9	2.7	C
6	32	N Miyagi Prefecture	5.5	reverse	18.1	2.7	1.6	D
7	39	Mid Niigata Prefecture	6.6	reverse	7.0	12.9	11.5	C
8	40	Mid Niigata Prefecture	6.6	reverse	11.1	4.0	5.2	C
9	41	Mid Niigata Prefecture	6.6	reverse	16.4	3.7	4.7	C
10	42	Mid Niigata Prefecture	6.6	reverse	21.3	8.5	16.8	B
11	43	Mid Niigata Prefecture	6.6	reverse	28.8	3.4	3.4	C
12	45	Mid Niigata Prefecture	6.3	reverse	9.0	5.1	5.2	C
13	46	Mid Niigata Prefecture	6.3	reverse	16.5	3.2	2.2	C
14	47	Rumoi	5.7	reverse	8.1	11.3	5.3	B
15	48	Rumoi	5.7	reverse	13.3	2.7	1.8	C
16	50	Nw Off Kyushu	6.6	strike-slip	20.3	2.6	1.9	C
17	51	Nw Off Kyushu	6.6	strike-slip	26.0	2.4	2.8	C
18	56	Honshu	5.9	reverse	13.9	3.9	4.6	B
19	60	Kyushu	5.7	normal	5.8	2.8	3.9	C
20	61	Kyushu	5.7	normal	17.2	3.6	2.2	B
21	68	Nw Kagoshima Prefecture	6.1	strike-slip	12.1	5.5	7.6	B
22	69	Nw Kagoshima Prefecture	6.1	strike-slip	12.2	4.9	4.2	B
23	71	Nw Kagoshima Prefecture	6.1	strike-slip	19.7	2.2	2.1	C
24	81	Nw Kagoshima Prefecture	6.0	strike-slip	15.4	3.1	3.1	C
25	82	Nw Kagoshima Prefecture	6.0	strike-slip	16.2	4.2	7.1	B
26	83	Nw Kagoshima Prefecture	6.0	strike-slip	15.7	8.9	9.0	B
27	87	Yamaguchi Prefecture	5.8	strike-slip	10.1	3.0	4.3	C
28	102	Bam	6.6	strike-slip	10.2	7.8	6.2	B
29	107	Anza	5.2	strike-slip	14.2	2.7	3.1	B

Ref.	ID	Earthquake Name	M_w	Fault Mechanism	Epicentral Distance (km)	PGA X (m/s^2)	PGA Y (m/s^2)	Site Class
30	108	Anza	5.2	strike-slip	18.2	5.5	5.0	B
31	112	South Iceland	6.5	strike-slip	14.6	2.1	4.7	B
32	113	South Iceland	6.5	strike-slip	5.3	3.1	3.4	A
33	115	South Iceland	6.5	strike-slip	17.4	3.7	2.4	B
34	117	South Iceland	6.4	strike-slip	12.2	3.3	3.9	B
35	121	South Iceland	6.4	strike-slip	11.1	4.3	6.9	B
36	136	Off Noto Peninsula	6.7	reverse	6.6	8.4	7.2	B
37	137	Off Noto Peninsula	6.7	reverse	19.0	7.8	4.7	D
38	138	Off Noto Peninsula	6.7	reverse	27.2	3.9	5.2	B
39	139	Southern Iwate Prefecture	6.9	reverse	23.1	2.9	2.2	B
40	140	Southern Iwate Prefecture	6.9	reverse	18.8	3.6	3.7	B
41	141	Southern Iwate Prefecture	6.9	reverse	26.9	2.2	1.5	C
42	142	S Suruga Bay	6.2	reverse	26.7	2.9	2.1	C
43	143	S Suruga Bay	6.2	reverse	28.1	2.3	1.7	D
44	144	S Suruga Bay	6.2	reverse	22.5	3.0	3.1	B
45	145	S Suruga Bay	6.2	reverse	18.5	2.9	3.1	C
46	146	S Suruga Bay	6.2	reverse	25.4	4.1	2.5	B
47	150	N Mie Prefecture	5.0	reverse	12.0	3.2	2.5	C
48	153	Southern Iwate Prefecture	5.5	reverse	9.5	2.7	2.7	B
49	154	Off S Niigata Prefecture	6.6	reverse	24.8	2.4	2.0	C
50	155	Off S Niigata Prefecture	6.6	reverse	21.3	5.1	6.7	C
51	157	Mid Niigata Prefecture	5.8	reverse	23.3	3.6	2.3	C
52	158	Mid Niigata Prefecture	5.8	reverse	9.0	3.9	5.2	C
53	159	App. Umbro-Marchigiano	5.4	normal	10.6	3.1	5.2	E
54	165	L'Aquila Mainshock	6.3	normal	4.6	3.9	4.3	B
55	166	L'Aquila Mainshock	6.3	normal	4.4	4.4	4.8	B
56	167	L'Aquila Mainshock	6.3	normal	5.7	3.2	3.5	B
57	168	L'Aquila Mainshock	6.3	normal	4.9	6.4	5.4	B
58	184	L'Aquila Aftershock	5.6	normal	16.8	2.8	2.5	B
59	208	Duzce	7.1	strike-slip	27.2	4.9	8.9	B
60	209	Bingol	6.3	strike-slip	11.8	2.9	5.1	B
61	211	Izmit_Aftershock	5.6	normal	11.2	3.2	2.0	B
62	213	Parkfield	6.0	strike-slip	14.2	2.4	2.3	C
63	214	Parkfield	6.0	strike-slip	8.2	2.4	2.4	B
64	215	Parkfield	6.0	strike-slip	7.8	2.9	2.9	B
65	216	Parkfield	6.0	strike-slip	7.1	2.4	1.9	A
66	217	Olfus	6.3	strike-slip	8.9	6.6	4.7	A
67	218	Olfus	6.3	strike-slip	8.3	5.3	3.3	A
68	219	Olfus	6.3	strike-slip	8.0	5.0	2.1	A
69	220	E Off Izu Peninsula	5.6	strike-slip	24.3	2.1	1.0	B
70	221	E Off Izu Peninsula	5.6	strike-slip	8.9	3.1	1.3	C
71	241	Western Fukushima Pref	5.6	reverse	11.0	2.1	1.5	B
72	248	Northern Nagano Pref	5.4	strike-slip	21.4	2.1	1.0	C
73	251	Eastern Fukushima Pref	5.9	strike-slip	24.7	2.2	1.9	C
74	258	E Off Fukushima Pref	5.1	normal	18.1	3.7	2.5	B
75	264	Northern Gifu Pref	5.1	reverse	12.0	2.5	2.4	B
76	272	Mid Niigata Pref	6.2	reverse	20.7	2.5	2.8	B
77	274	Mid Niigata Pref	6.2	reverse	6.0	6.8	5.3	B
78	285	Mt Fuji Region	5.9	strike-slip	12.8	9.8	5.0	B
79	286	Mt Fuji Region	5.9	strike-slip	19.8	2.4	1.6	B
80	289	Northern Ibaraki Pref	5.8	normal	29.4	5.5	3.5	C
81	304	Loma Prieta	6.9	oblique	18.8	5.8	9.5	B
82	306	Hyogo - Ken Nanbu	6.9	strike-slip	16.6	6.2	8.2	C

Ref.	ID	Earthquake Name	M_w	Fault Mechanism	Epicentral Distance (km)	PGA X (m/s^2)	PGA Y (m/s^2)	Site Class
83	307	Duzce	7.1	strike-slip	36.1	8.1	7.4	C
84	308	Duzce	7.1	strike-slip	32.3	2.5	1.2	C
85	311	Emilia_Pianura_Padana	6.1	reverse	13.4	2.6	2.6	C
86	312	Emilia_Pianura_Padana	6.0	reverse	3.6	2.2	2.9	C
87	316	Emilia_Pianura_Padana	6.0	reverse	16.0	2.1	2.4	C
88	317	Emilia_Pianura_Padana	6.0	reverse	16.4	2.4	1.7	C
89	319	Emilia_Pianura_Padana	6.0	reverse	21.3	2.2	2.9	C
90	329	Darfield	7.1	strike-slip	9.1	5.0	4.7	C*
91	330	Darfield	7.1	strike-slip	13.3	2.3	2.5	C*
92	331	Darfield	7.1	strike-slip	17.8	4.5	4.3	C*
93	333	Darfield	7.1	strike-slip	17.0	3.0	3.5	C*
94	335	Darfield	7.1	strike-slip	23.6	2.7	1.8	C*
95	337	Christchurch	6.2	reverse	2.3	14.2	11.5	B*
96	338	Christchurch	6.2	reverse	24.9	2.1	1.9	D*
97	339	Christchurch	6.2	reverse	1.5	8.2	9.2	A*
98	340	Christchurch	6.2	reverse	14.4	2.1	1.9	C*
99	341	Christchurch	6.2	reverse	13.7	2.9	2.5	C*
100	347	Christchurch	5.5	reverse	4.1	5.2	5.4	B*
101	348	Christchurch	5.5	reverse	23.6	2.1	1.0	D*
102	349	Christchurch	5.5	reverse	5.5	4.9	4.4	A*
103	350	Christchurch	5.5	reverse	9.9	2.5	1.8	C*
104	355	Christchurch	5.6	reverse	7.4	6.2	7.2	B*
105	357	Christchurch	5.6	reverse	8.4	5.4	3.4	A*
106	358	Christchurch	5.6	reverse	8.2	2.3	2.2	C*
107	376	Christchurch	5.3	reverse	4.9	3.5	5.2	B*
108	384	Christchurch	6.0	reverse	3.2	6.4	10.5	B*
109	386	Christchurch	6.0	reverse	5.1	5.9	5.5	A*
110	395	Christchurch	5.2	reverse	15.0	2.7	2.4	B*
111	404	Christchurch	5.2	reverse	6.8	2.8	2.3	C*
112	410	Athens_Mainshock	6.0	strike-slip	13.9	3.2	3.1	B*
113	412	Hector Mine	7.1	strike-slip	28.6	3.3	2.6	B
114	419	Umbria-Marche 1st Shock	5.7	normal	2.8	2.8	3.3	D
115	422	Friuli 1st Shock	6.4	reverse	21.7	3.1	3.4	B
116	424	Friuli 2nd Shock	5.6	reverse	26.2	2.3	1.3	B
117	425	Friuli 2nd Shock	5.6	reverse	15.0	2.9	3.2	B
118	427	Friuli 3rd Shock	5.9	reverse	17.3	2.1	2.6	B
119	429	Friuli 4th Shock	5.9	reverse	16.8	3.3	3.4	B
120	431	Dinar	6.4	normal	0.5	3.2	2.7	C
121	432	Parkfield	6.0	strike-slip	19.5	3.5	2.2	B
122	433	Parkfield	6.0	strike-slip	3.0	3.6	3.8	B
123	434	Parkfield	6.0	strike-slip	12.5	5.6	5.0	B
124	436	Parkfield	6.0	strike-slip	4.0	6.7	4.1	B
125	439	Parkfield	6.0	strike-slip	7.0	5.4	4.9	B
126	440	Gazli	6.7	reverse	12.8	7.0	6.0	B
127	441	Tabas	7.1	reverse	20.6	4.0	3.2	B
128	442	Imperial Valley	6.5	strike-slip	2.3	3.2	2.5	C
129	444	Imperial Valley	6.5	strike-slip	19.3	2.9	3.1	C
130	445	Imperial Valley	6.5	strike-slip	27.0	3.5	4.8	C
131	446	Imperial Valley	6.5	strike-slip	27.7	3.7	5.1	C
132	447	Imperial Valley	6.5	strike-slip	27.4	4.3	4.0	C
133	450	Loma Prieta	6.9	oblique	9.3	4.3	5.2	C
134	451	Loma Prieta	6.9	oblique	7.1	4.7	6.3	B
135	452	Loma Prieta	6.9	oblique	28.6	4.6	4.0	A
136	453	Loma Prieta	6.9	oblique	29.7	3.2	3.6	C
137	454	Loma Prieta	6.9	oblique	28.8	3.5	3.2	B
138	455	Loma Prieta	6.9	oblique	16.4	3.9	4.4	B

Ref.	ID	Earthquake Name	M_w	Fault Mechanism	Epicentral Distance (km)	PGA X (m/s^2)	PGA Y (m/s^2)	Site Class
139	456	Loma Prieta	6.9	oblique	27.6	3.2	5.0	B
140	457	Landers	7.3	strike-slip	13.1	2.8	2.7	B
141	458	Northridge	6.7	reverse	11.0	3.4	3.0	C
142	459	Northridge	6.7	reverse	20.2	2.5	2.2	C
143	460	Northridge	6.7	reverse	23.6	2.3	3.5	C
144	461	Northridge	6.7	reverse	20.3	5.7	5.8	C
145	462	Northridge	6.7	reverse	5.4	17.4	9.7	C
146	463	Northridge	6.7	reverse	18.6	2.7	4.6	B
147	464	Northridge	6.7	reverse	14.7	2.8	2.3	B
148	465	Erzincan	6.6	strike-slip	9.0	4.9	5.1	C
149	466	Duzce	7.1	strike-slip	5.3	5.1	4.1	C
150	467	Kozani_Mainshock	6.5	strike-slip	16.7	2.0	1.4	A

ATC-63 far-field set of ground motion records (FEMA-P695)

Ref.	ID	Earthquake Name	M_w	Fault Mechanism	Epicentral Distance (km)	PGA_ X (m/s^2)	PGA_ Y (m/s^2)	Site Class
1	68	San_Fernando	6.6	Reverse	22.8	2.1	1.7	D
3	125	Friuli-Italy-01	6.5	Reverse	15.8	3.4	3.1	C
5	169	Imperial_Valley-06	6.5	Strike-Slip	22.0	2.3	3.4	D
7	174	Imperial_Valley-06	6.5	Strike-Slip	12.4	3.6	3.7	D
9	721	Superstition_Hills-02	6.5	Strike-Slip	18.2	3.5	2.5	D
11	725	Superstition_Hills-02	6.5	Strike-Slip	11.2	4.4	2.9	D
13	752	Loma_Prieta	6.9	Reverse-Oblique	15.2	5.2	4.3	D
15	767	Loma_Prieta	6.9	Reverse-Oblique	12.8	5.4	3.6	D
17	829	Cape_Mendocino	7.0	Reverse	14.3	3.8	5.4	D
19	900	Landers	7.3	Strike-Slip	23.6	2.4	1.5	D
21	953	Northridge-01	6.7	Reverse	17.1	4.1	5.1	D
23	960	Northridge-01	6.7	Reverse	12.4	4.0	4.7	D
25	1111	Kobe-Japan	6.9	Strike-Slip	7.1	5.0	4.9	C
27	1116	Kobe-Japan	6.9	Strike-Slip	19.1	2.4	2.1	D
29	1148	Kocaeli-Turkey	7.5	Strike-Slip	13.5	2.1	1.5	C
31	1158	Kocaeli-Turkey	7.5	Strike-Slip	15.4	3.1	3.5	D
33	1244	Chi-Chi-Taiwan	7.6	Reverse-Oblique	10.0	3.5	4.3	D
35	1602	Duzce-Turkey	7.1	Strike-Slip	12.0	7.1	8.1	D
37	1787	Hector_Mine	7.1	Strike-Slip	11.7	2.6	3.1	C
12	848	Lander	7.3	Strike-slip	82.1	4.1	3.0	D
15	1633	Manjil, Iran	7.4	Strike-slip	40.4	5.0	4.5	C
20	1485	Chi-Chi, Taiwan	7.6	Thrust	77.5	5.0	3.8	C

Appendix C – Fragility Functions of the Index Buildings

2 Storey - 2 Bay (X-dir) & 1 Bay (Y-dir)

2Storey-S-SGF-Bare

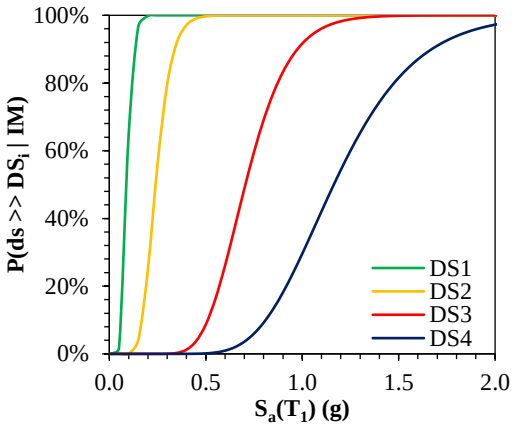

2Storey-S-MRF-Bare

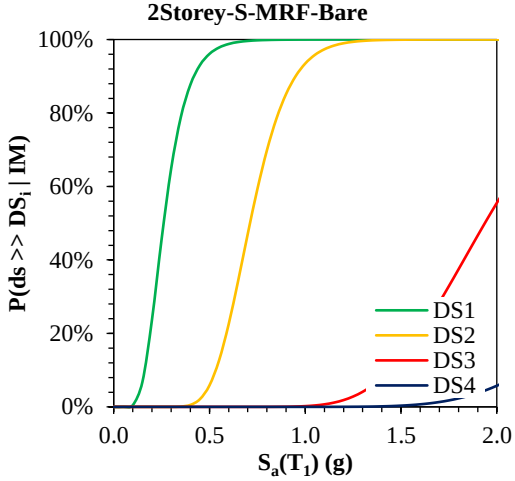

2Storey-S-SGF-Infill HCB

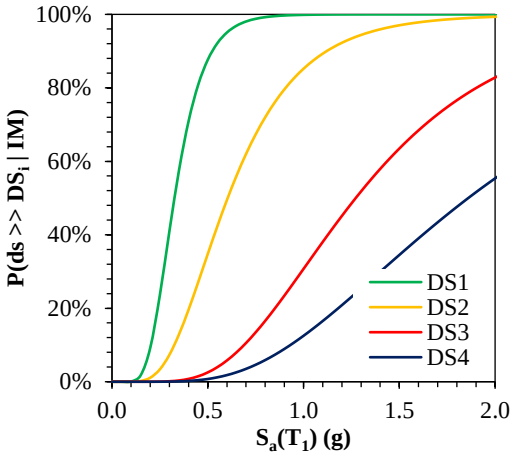

2Storey-S-MRF-Infill HCB

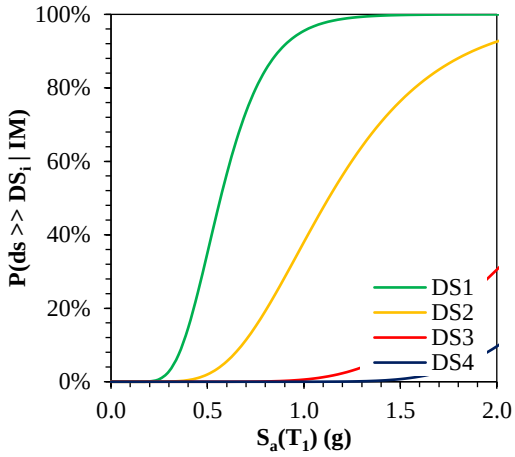

2Storey-S-SGF-Infill SCB

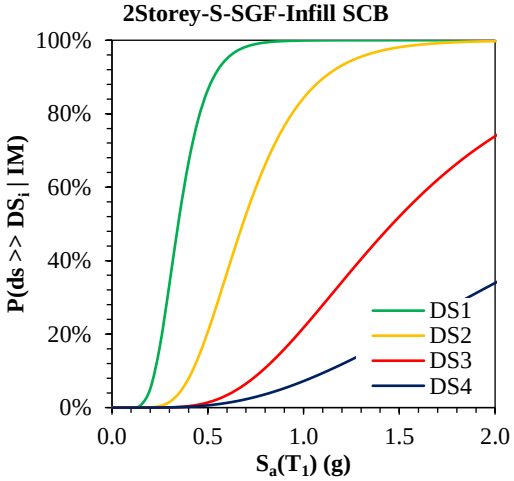

2Storey-S-MRF-Infill SCB

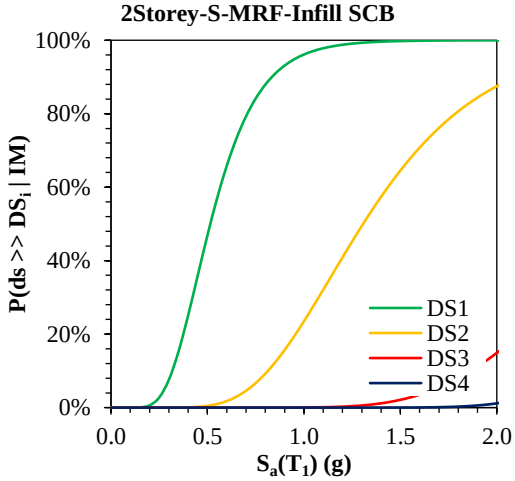

	DS1 - Slight		DS2 - Moderate		DS3 - Extensive		DS4 - Complete		Avg.
	μ	β	μ	β	μ	β	μ	β	β_{Avg}
2Storey-S-SGF-Bare	0.09	0.278	0.24	0.269	0.71	0.253	1.16	0.282	0.271
2Storey-S-SGF-Infill HCB	0.33	0.369	0.60	0.482	1.27	0.478	1.86	0.540	0.467
2Storey-S-SGF-Infill SCB	0.35	0.335	0.68	0.379	1.46	0.488	2.63	0.663	0.466
2Storey-S-MRF-Bare	0.26	0.370	0.71	0.225	1.94	0.230	2.97	0.252	0.269
2Storey-S-MRF-Infill HCB	0.57	0.333	1.13	0.396	2.38	0.344	2.77	0.251	0.331
2Storey-S-MRF-Infill SCB	0.51	0.376	1.31	0.370	2.71	0.290	3.18	0.204	0.310

2 Storey - 4 Bay (X-dir) & 3 Bay (Y-dir)

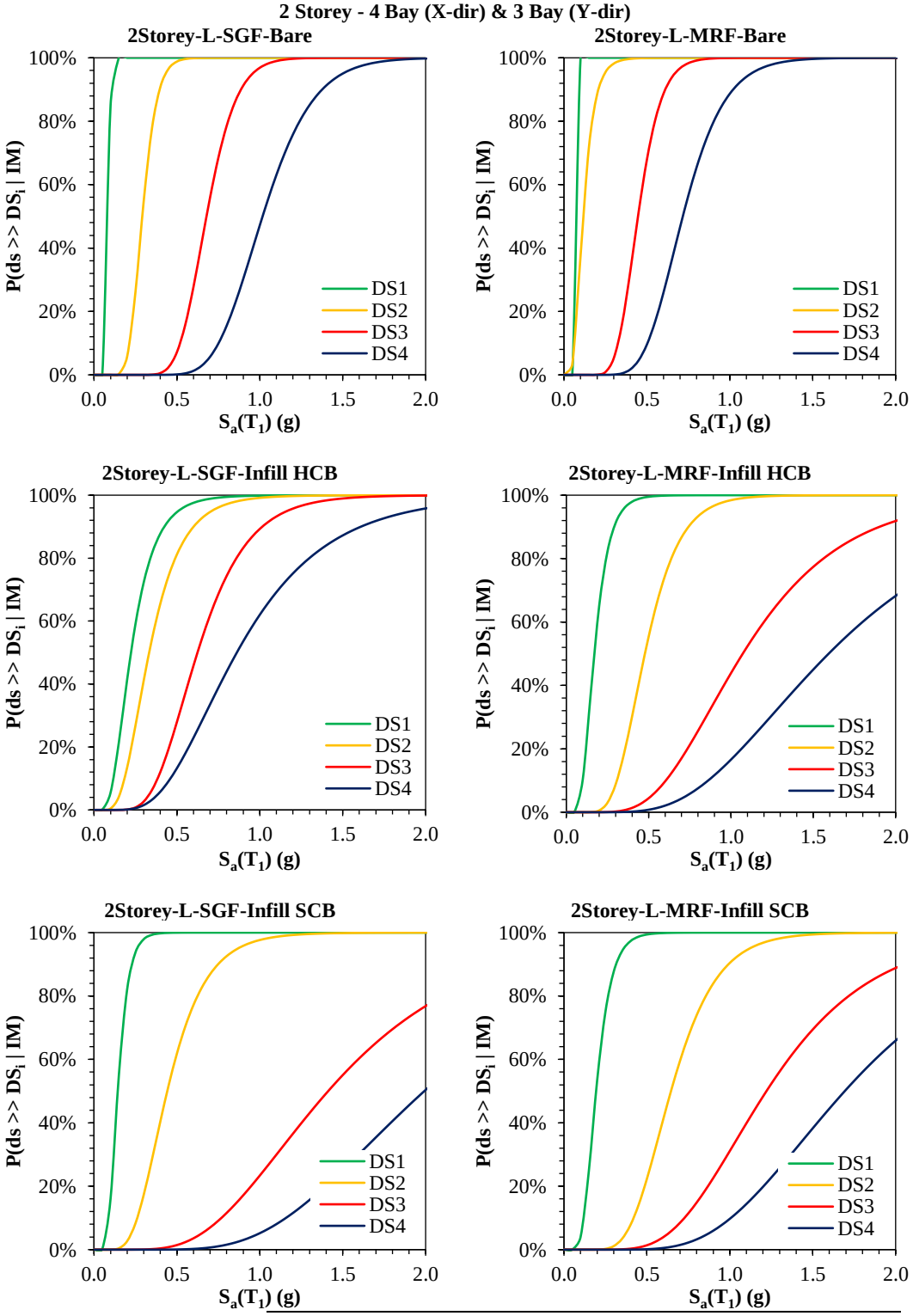

	DS1 - Slight		DS2 - Moderate		DS3 - Extensive		DS4 - Complete		Avg.
	μ	β	μ	β	μ	β	μ	β	β_{Avg}
2Storey-L-SGF-Bare	0.09	0.120	0.29	0.239	0.68	0.208	1.02	0.236	0.201
2Storey-L-SGF-Infill HCB	0.22	0.502	0.33	0.461	0.62	0.379	0.86	0.488	0.457
2Storey-L-SGF-Infill SCB	0.14	0.363	0.44	0.411	1.41	0.475	1.99	0.424	0.418
2Storey-L-MRF-Bare	0.07	0.008	0.12	0.457	0.45	0.245	0.72	0.275	0.246
2Storey-L-MRF-Infill HCB	0.17	0.419	0.48	0.344	1.07	0.447	1.59	0.480	0.422
2Storey-L-MRF-Infill SCB	0.19	0.377	0.65	0.335	1.22	0.405	1.69	0.406	0.381

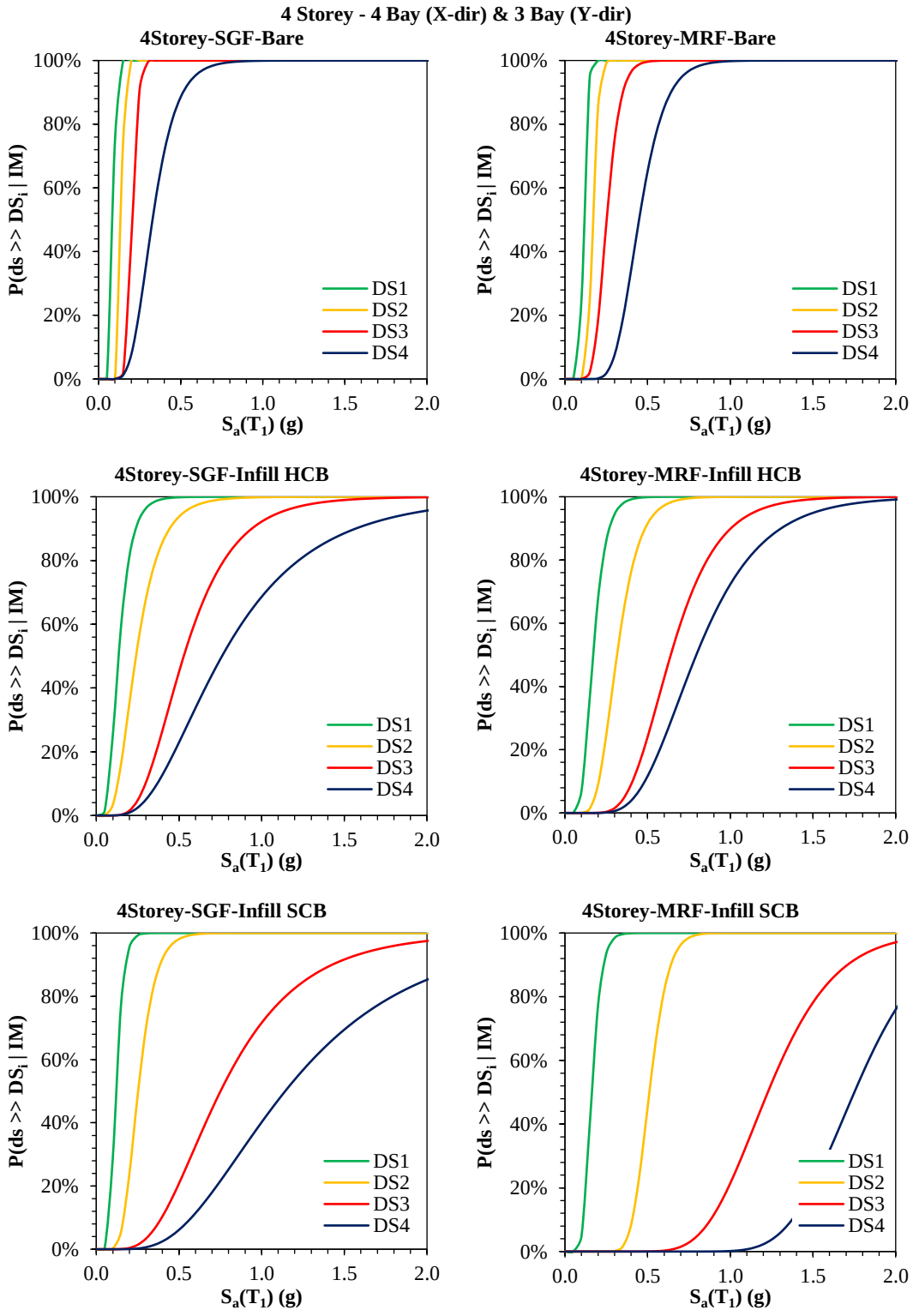

	DS1 - Slight		DS2 - Moderate		DS3 - Extensive		DS4 - Complete		Avg.
	μ	β	μ	β	μ	β	μ	β	β_{Avg}
4Storey-SGF-Bare	0.09	0.098	0.14	0.068	0.20	0.151	0.33	0.350	0.167
4Storey-SGF-Infill HCB	0.13	0.446	0.24	0.478	0.53	0.449	0.76	0.565	0.485
4Storey-SGF-Infill SCB	0.12	0.309	0.25	0.329	0.75	0.501	1.14	0.535	0.418
4Storey-MRF-Bare	0.11	0.175	0.17	0.167	0.25	0.257	0.45	0.279	0.220
4Storey-MRF-Infill HCB	0.17	0.357	0.31	0.337	0.64	0.351	0.79	0.389	0.358
4Storey-MRF-Infill SCB	0.16	0.288	0.51	0.177	1.23	0.258	1.75	0.189	0.228

6 Storey - 4 Bay (X-dir) & 3 Bay (Y-dir)

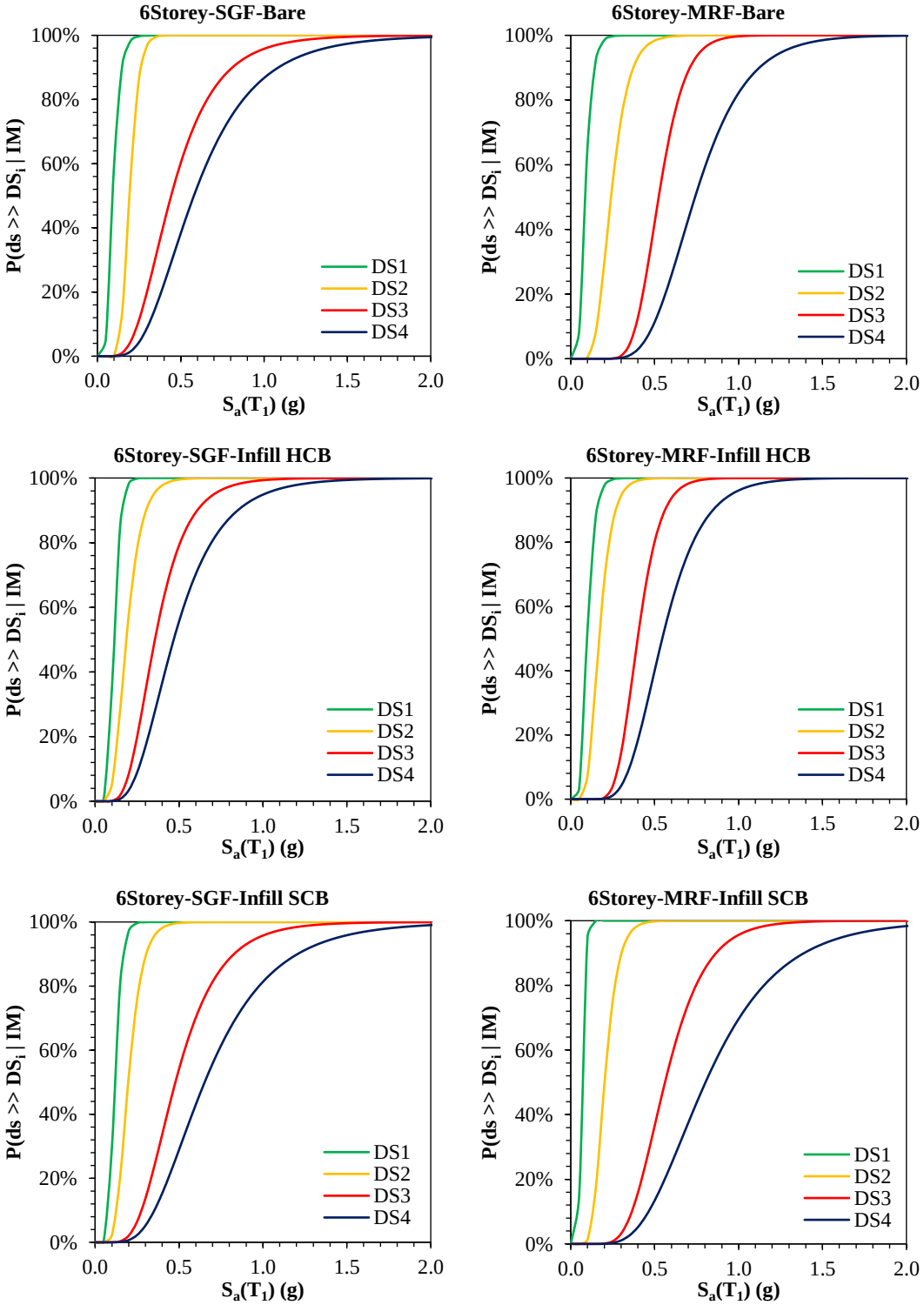

	DS1 - Slight		DS2 - Moderate		DS3 - Extensive		DS4 - Complete		Avg.
	μ	β	μ	β	μ	β	μ	β	β_{Avg}
6Storey-SGF-Bare	0.09	0.370	0.19	0.235	0.44	0.472	0.58	0.491	0.392
6Storey-SGF-Infill HCB	0.11	0.279	0.19	0.383	0.36	0.418	0.47	0.465	0.386
6Storey-SGF-Infill SCB	0.12	0.285	0.20	0.339	0.48	0.427	0.65	0.479	0.382
6Storey-MRF-Bare	0.09	0.391	0.24	0.344	0.52	0.237	0.74	0.325	0.324
6Storey-MRF-Infill HCB	0.10	0.363	0.17	0.361	0.40	0.267	0.55	0.344	0.334
6Storey-MRF-Infill SCB	0.07	0.258	0.20	0.318	0.56	0.338	0.80	0.429	0.336

8 Storey - 4 Bay (X-dir) & 3 Bay (Y-dir)

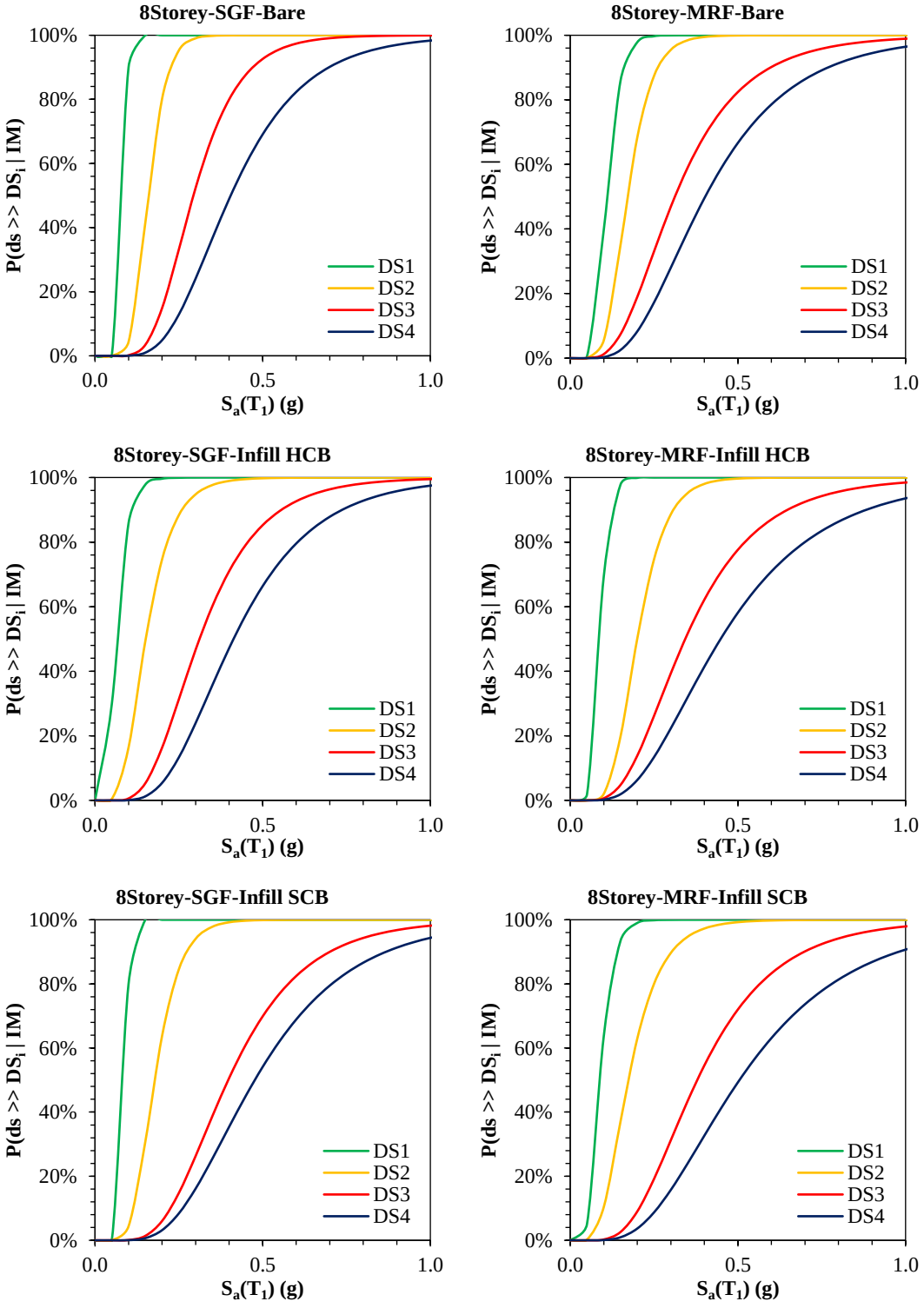

	DS1 - Slight		DS2 - Moderate		DS3 - Extensive		DS4 - Complete		Avg.
	μ	β	μ	β	μ	β	μ	β	β_{Avg}
8Storey-SGF-Bare	0.09	0.113	0.16	0.271	0.29	0.368	0.40	0.425	0.294
8Storey-SGF-Infill HCB	0.06	0.432	0.15	0.422	0.31	0.452	0.41	0.452	0.439
8Storey-SGF-Infill SCB	0.09	0.102	0.18	0.336	0.40	0.442	0.48	0.468	0.337
8Storey-MRF-Bare	0.11	0.303	0.17	0.334	0.31	0.506	0.40	0.504	0.412
8Storey-MRF-Infill HCB	0.09	0.268	0.20	0.337	0.34	0.496	0.45	0.528	0.408
8Storey-MRF-Infill SCB	0.09	0.349	0.17	0.436	0.38	0.477	0.50	0.517	0.445

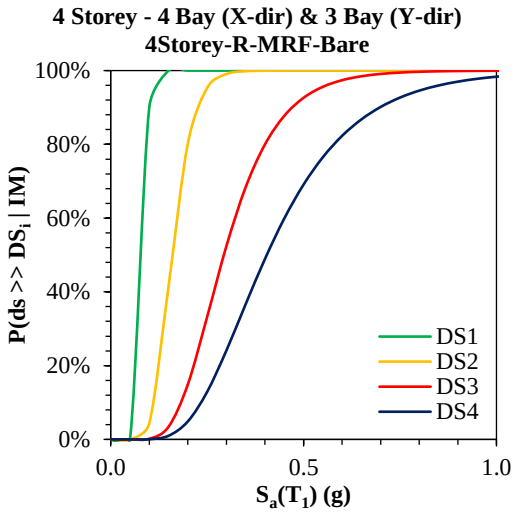

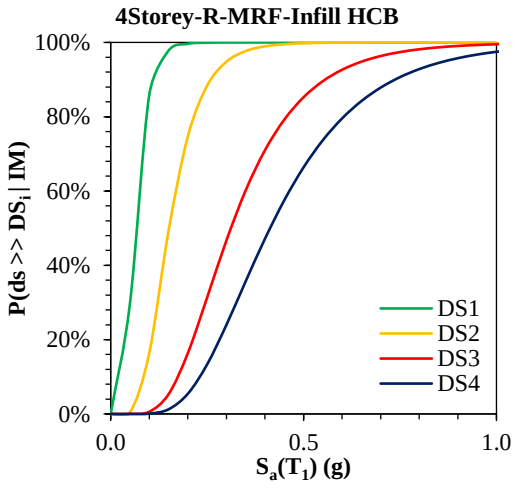

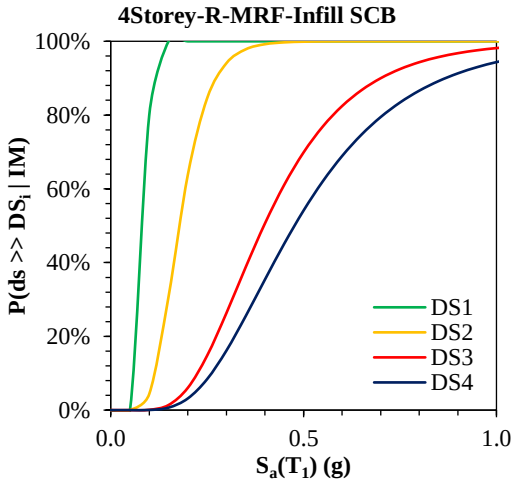

	DS1 - Slight		DS2 - Moderate		DS3 - Extensive		DS4 - Complete		Avg.
	μ	β	μ	β	μ	β	μ	β	β_{Avg}
4Storey-R-MRF-Bare	0.08	0.201	0.25	0.354	0.34	0.326	0.58	0.257	0.285
4Storey-R-MRF-Infill HCB	0.25	0.528	0.47	0.519	0.91	0.628	1.14	0.677	0.588
4Storey-R-MRF-Infill SCB	0.25	0.336	0.63	0.375	1.09	0.532	1.61	0.553	0.449

No.	Reference	HAZUS Category	Total Height (m)	Fundamental Period of Vibration, T_1(s)
1	2 Storey - L -MRF - Bare	S1H Low-Rise	7.00	0.78
2	2 Storey - L -SGF - Bare	S1L Low-Rise	7.00	0.80
3	2 Storey - L -MRF - Infill SCB	S5H Low-Rise	7.00	0.30
4	2 Storey - L -SGF - Infill SCB	S5L Low-Rise	7.00	0.32
5	2 Storey - L -MRF - Infill HCB	S5H Low-Rise	7.00	0.30
6	2 Storey - L -SGF - Infill HCB	S5L Low-Rise	7.00	0.32
7	2 Storey - S - MRF - Bare	S1H Low-Rise	7.00	0.40
8	2 Storey - S - SGF - Bare	S1L Low-Rise	7.00	0.68
9	2 Storey - S - MRF - Infill SCB	S5H Low-Rise	7.00	0.24
10	2 Storey - S - SGF - Infill SCB	S5L Low-Rise	7.00	0.27
11	2 Storey - S - MRF - Infill HCB	S5H Low-Rise	7.00	0.21
12	2 Storey - S - SGF - Infill HCB	S5L Low-Rise	7.00	0.25
13	4 Storey - MRF - Bare	S1H Mid-Rise	14.00	1.46
14	4 Storey - SGF - Bare	S1L Mid-Rise	14.00	1.84
15	4 Storey - MRF - Infill SCB	S5H Mid-Rise	14.00	0.68
16	4 Storey - SGF - Infill SCB	S5L Mid-Rise	14.00	0.72
17	4 Storey - MRF - Infill HCB	S5H Mid-Rise	14.00	0.70
18	4 Storey - SGF - Infill HCB	S5L Mid-Rise	14.00	0.74
19	4 Storey - R - MRF - Bare	S1+S2M Mid-Rise	12.58	1.33
20	4 Storey - R - MRF - Infill SCB	S5M Mid-Rise	12.58	0.41
21	4 Storey - R - MRF - Infill HCB	S5M Mid-Rise	12.58	0.44
22	6 Storey - MRF - Bare	S1H Mid-Rise	21.00	1.96
23	6 Storey - SGF - Bare	S1L Mid-Rise	21.00	2.70
24	6 Storey - MRF - Infill SCB	S5H Mid-Rise	21.00	0.98
25	6 Storey - SGF - Infill SCB	S5L Mid-Rise	21.00	1.02
26	6 Storey - MRF - Infill HCB	S5H Mid-Rise	21.00	0.96
27	6 Storey - SGF - Infill HCB	S5L Mid-Rise	21.00	1.00
28	8 Storey - MRF - Bare	S1H High-Rise	28.00	3.50
29	8 Storey - SGF - Bare	S1L High-Rise	28.00	3.60
30	8 Storey - MRF - Infill SCB	S5H High-Rise	28.00	1.40
31	8 Storey - SGF - Infill SCB	S5L High-Rise	28.00	1.36
32	8 Storey - MRF - Infill HCB	S5H High-Rise	28.00	1.38
33	8 Storey - SGF - Infill HCB	S5L High-Rise	28.00	1.34